DOE/ER/75782--T1

THE UNIVERSITY OF
ARIZONA
TUCSON ARIZONA

Final Report

DOE Initiation Grant
DE-FG03-92ER75782

PIs: B. D. Ganapol and D. E. Kornreich
Department of Nuclear Engineering
University of Arizona

Analytical Three-Dimensional Neutron Transport Benchmarks for Verification of Nuclear Engineering Codes

DISTRIBUTION OF THIS DOCUMENT IS UNLIMITED

PROCESSED FROM BEST AVAILABLE COPY

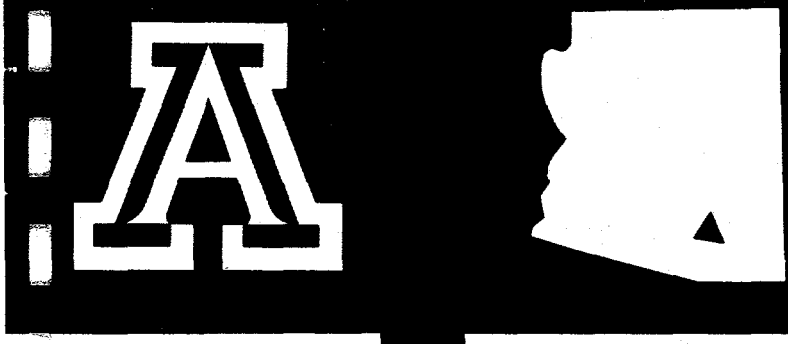

MASTER

ENGINEERING EXPERIMENT STATION
COLLEGE OF ENGINEERING AND MINES
THE UNIVERSITY OF ARIZONA
TUCSON, ARIZONA 85721

DISCLAIMER

Portions of this document may be illegible in electronic image products. Images are produced from the best available original document.

Final Report

DOE Initiation Grant
DE-FG03-92ER75782

PIs: B. D. Ganapol and D. E. Kornreich
Department of Nuclear Engineering
University of Arizona

Analytical Three-Dimensional Neutron Transport Benchmarks for Verification of Nuclear Engineering Codes

DISCLAIMER

This report was prepared as an account of work sponsored by an agency of the United States Government. Neither the United States Government nor any agency thereof, nor any of their employees, makes any warranty, express or implied, or assumes any legal liability or responsibility for the accuracy, completeness, or usefulness of any information, apparatus, product, or process disclosed, or represents that its use would not infringe privately owned rights. Reference herein to any specific commercial product, process, or service by trade name, trademark, manufacturer, or otherwise does not necessarily constitute or imply its endorsement, recommendation, or favoring by the United States Government or any agency thereof. The views and opinions of authors expressed herein do not necessarily state or reflect those of the United States Government or any agency thereof.

EXECUTIVE SUMMARY

The development of a suite of sophisticated benchmarks for nuclear engineering applications was begun under DOE Initiation Grant DE-FG03-92ER75782. Because of the requirement of accountability and quality control in the scientific world, a demand for high-quality analytical benchmark calculations has arisen in the neutron transport community. The intent of these benchmarks is to provide a numerical standard to which production neutron transport codes may be compared in order to verify proper operation. The overall investigation as modified in the second year renewal application includes the following three primary tasks:

Task I. Two Dimensional Neutron Transport
- A. Single Medium Searchlight Problem (SLP)
- B. Two-Adjacent Half-Space SLP

Task II. Three-Dimensional Neutron Transport
- A. Point Source in Arbitrary Geometry
- B. Single Medium SLP
- C. Two-Adjacent Half-Space SLP

Task III. Code Verification
- A. Deterministic Codes
- B. Probabilistic Codes

A complete analysis of the single medium SLP (Task 1.A) has been completed and has been published in the literature. The material in this report describes the theory and numerical implementation of the solutions in detail for the primary tasks listed above. The analysis begins by considering the suite of analytical benchmarks in infinite isotropically scattering media. The historically significant infinite medium problems are presented to provide a foundation upon which a more sophisticated analysis may be built. In the analysis of the infinite medium, for the first time, the monodirectional point source solution, or the so-called Green's function, has been obtained (Task II.A). The relationship between this fundamental solution and all other solutions in infinite isotropically scattering media is specified and thoroughly investigated. The final case treated is for the anisotropic infinite line source in an infinite medium. This source is examined because the numerical methods associated with its evaluation are similar to those that must be used to obtain numerical results for the three-dimensional SLP in the next task.

The three-dimensional SLP for an isotropically scattering half-space (Task II.B) is investigated and employs similar numerical and mathematical techniques as used to obtain solutions for the infinite medium problems. The fundamental numerical techniques include quadrature, series summation, convergence acceleration, and root location leading to higher level packages for numerical Fourier and Laplace transform inversion. Numerical solutions for the three-dimensional searchlight problem (canted beam) are presented for both the surface and interior of a half-space. Although benchmark-quality results are presented, they are obtained at great computational expense, calling for the use of massively parallel computation for future implementation. The theory for Tasks I.B and II.C has been set forth in a paper which is now in preparation. The numerical implementation is expected to follow along the lines of the single medium SLP. Several code verifications (Tasks III.A and III.B) have been performed and are continuing. The analytical results generated under this grant have been compared to the deterministic DANTSYS code series and the probabilistic code MCNP, both of which have been developed and are maintained at Los Alamos National Laboratory. Also, a comparison with the SMARTEPANTS code developed at the University of Arizona has been published. Additional comparisons will be presented in an article to be submitted to a nuclear engineering journal.

The primary aim of the proposed investigation was to provide a suite of comprehensive two- and three-dimensional analytical benchmarks for neutron transport theory applications. This objective has been achieved. The suite of benchmarks in infinite media and the three-dimensional SLP are a relatively comprehensive set of one-group benchmarks for isotropically scattering media. Because of time and resource limitations, the extensions of the benchmarks to include multi-group and anisotropic scattering are not included here. Presently, however, enormous advances in the solution for the planar Green's function in an anisotropically scattering medium have been made and will eventually be implemented in the two- and three-dimensional solutions considered under this grant. Of particular note in this work are the numerical results for the three-dimensional SLP, which have never before been presented. The results presented were made possible only because of the tremendous advances in computing power that have occurred during the past decade. These advances show no signs of slowing, and as computing power increases, we should be able to treat more comprehensive benchmarks. Based on the work completed under this grant, we

will, therefore, be able to continue to serve the neutron transport community by providing more complicated benchmarks in the future.

CONFERENCE PROCEEDINGS:

"Analytical Two-Dimensional Neutron Transport Benchmark: The Searchlight Problem," B. D. Ganapol and D. W. Nigg, *Trans. Am. Nuc. Soc.*, **64**, 276 (1991).

"The Searchlight Problem for Neutrons in a Semi-Infinite Medium," B. D. Ganapol, D. W. Nigg, S. N. Jahshan, and C. A. Wemple, M & C Topical, Karlsruhe Germany (1993).

"A Three-Dimensional Neutron Transport Benchmark Solution," B. D. Ganapol and D. E. Kornreich, *Trans. Am. Nucl. Soc.*, **68**, 215 (1993).

"A Three-Dimensional Neutron Transport Benchmark Solution," B. D. Ganapol, D. E. Kornreich, and J. A. Dahl, International Conference on Reactor Physics and Reactor Computation, Tel Aviv, Israel, 70 (1994).

"Numerical Treatment of the One-Group Half-Space Problem with Anisotropic Scattering," M. A. Alani and B. D. Ganapol, *Trans. Am. Nucl. Soc.*, **70**, 146 (1994).

"A Two-Dimensional One-Group Transport Benchmark in Infinite Cylindrical Geometry," D. E. Kornreich and B. D. Ganapol, *Trans. Am. Nucl. Soc.*, **71**, 214 (1994).

"Two-Dimensional One-Group Neutron Transport in Transverse Cylindrical Coordinates," D. E. Kornreich and B. D. Ganapol, International Conference on Mathematics and Computations, Reactor Physics, and Environmental Analysis, Portland, Oregon, **2**, 1223 (1995).

"Isotropic Finite Surface Sources in an Infinite Medium," D. E. Kornreich and B. D. Ganapol, *Trans. Am. Nucl. Soc.*, **73**, 186 (1995).

"Angular Green's Function Flux in an Infinite Medium with Anisotropic Scattering," M. A. Alani and B. D. Ganapol, *Trans. Am. Nucl. Soc.*, **73**, 188 (1995).

JOURNAL ARTICLES:

"Equivalence of the Single- and Double-Integral Formulation for a Multidimensional Semi-Infinite Medium," B. D. Ganapol, *J. Quant. Spectrosc. Radiat. Transfer*, **50**, 551 (1993).

"The Searchlight Problem for Neutrons in a Semi-Infinite Medium," B. D. Ganapol, et al., *Nuclear Science and Engineering*, **118**, 38 (1994).

"A 3-D Neutron Transport Benchmark Solution," B. D. Ganapol and D. E. Kornreich, *Transport Theory and Statistical Physics*, **24**, 89 (1995).

"The Suite of Analytical Benchmarks for Neutral Particle Transport in Infinite Isotropically Scattering Media," D. E. Kornreich and B. D. Ganapol, to be published in *Nuclear Science and Engineering* (1996).

"Numerical Evaluation of the Three-Dimensional Searchlight Problem," D. E. Kornreich and B. D. Ganapol, to be submitted to *Nuclear Science and Engineering*.

C:\OFFICE\WP\WIN\WPDOCS\GANAPOL\DOEFINAL.RPT

The balance of this report consists of the dissertation of Drew E. Kornreich.

MULTI-DIMENSIONAL ANALYTICAL BENCHMARKS FOR NEUTRAL PARTICLE TRANSPORT

by

Drew Edward Kornreich

A Dissertation Submitted to the Faculty of the

DEPARTMENT OF NUCLEAR AND ENERGY ENGINEERING

In Partial Fulfillment of the Requirements

For the Degree of

DOCTOR OF PHILOSOPHY

WITH A MAJOR IN NUCLEAR ENGINEERING

In the Graduate College

THE UNIVERSITY OF ARIZONA

1995

ACKNOWLEDGMENTS

I would like to express great thanks and appreciation to Dr. Ganapol for his extreme patience and unending support. It has been a joy to work with one who is so gifted as a teacher and as a researcher. His abilities in these areas are a model for those like myself who wish to follow in such pursuits.

I would also like to thank Drs. Robert Seale, John Williams, David Hetrick, and Barry Ganapol for allowing me to teach various classes for and with them. The experiences gained in the classroom were as great at the front as in the desk.

This research was partially performed under appointment to the *Nuclear Engineering and Health Physics Fellowship* program administered by Oak Ridge Associated Universities for the United States Department of Energy. Their support provided a strong financial base on which this work was built. Other support was provided by the DOE Initiation Grant DE-FG03-92ER75782.

TABLE OF CONTENTS

LIST OF TABLES

LIST OF ILLUSTRATIONS

ABSTRACT

The linear Boltzmann equation for the transport of neutral particles is investigated with the objective of generating benchmark-quality calculations for homogeneous infinite and semi-infinite media. In all cases, the problems are stationary, of one energy group, and the scattering is isotropic. In the transport problems considered, the scalar flux is generally the quantity of interest. The scalar flux will have one-, two-, or three-dimensional variation, based on the nature of the medium and source. The solutions are obtained through the use of Fourier and Laplace transform methods. For the multi-dimensional problems, the transformed transport equation is formulated in a form that can be related to a one-dimensional pseudo problem, thus providing some analytical leverage for the inversions. The numerical inversions use standard numerical techniques such as Gauss-Legendre quadrature, summation of infinite series, and Euler-Knopp acceleration.

Consideration of the suite of benchmarks in infinite homogeneous media begins with the standard one-dimensional problems: an isotropic point source, an isotropic planar source, and an isotropic infinite line source. The physical and mathematical relationships between these source configurations is investigated. The progression of complexity then leads to multi-dimensional problems with sources which also emit particles isotropically: the finite line source, the disk source, and the rectangular source. It is noted that a finite isotropic disk will have a two-dimensional variation in the scalar flux and a finite rectangular source will have a three-dimensional variation in the scalar flux. Next, sources which emit particles anisotropically are considered. The most basic such source is the point-beam, or Green's function source. The Green's function source holds an interesting place in the suite of infinite medium benchmarks as it is the most fundamental of sources yet may be constructed from the isotropic point source solution. Finally, the anisotropic

plane and anisotropically emitting infinite line sources are considered. Many of the mathematical techniques used to generate results for the anisotropic line are of use in the three-dimensional searchlight problem. Thus, a firm theoretical and numerical basis is established for benchmarks which are most appropriate in infinite homogenous media.

Attention is then turned to a homogeneous semi-infinite medium. The final problem which is investigated is the three-dimensional searchlight problem for a half-space. The primary feature is a canted incident beam at the center of the free surface. For the three-dimensional problem, the surface scalar flux and current are obtained, and the interior scalar flux is obtained with significant additional computational effort.

CHAPTER 1: INTRODUCTION

The physical world contains many phenomena and processes for which it is desirable and possible to create simplified computational models. These models are based on physical laws and require mathematical agility to make the necessary simplifications so that both theoretical and numerical results may be obtained in a reasonable time while maintaining the relevant physical features. One area of interest in such computations is called "analytical benchmarking." The investigation presented here will consider several benchmarks for nuclear engineering and radiative transfer applications. The benchmarks are limited to those which consider neutral particle transport.

1.A. The Growth of Computational Power and Benchmarking

The world of analytical benchmarking has undergone many changes since the middle of this century. When the effort to construct nuclear weapons during the second World War was initiated, the available computational facilities were limited to rooms full of people operating the "supercomputers" of the time - simple adding machines. The emphasis was therefore on deriving relatively simple mathematical expressions to describe physical phenomena. These expressions often contained integral and/or differential operators. Because it was a significant task to obtain the value of something as simple as a sine function (i.e. the Taylor series form of the sine function would be calculated on the adding machines), theorists would often be satisfied with symbolic mathematical expressions rather than numerical evaluations. Their analyses would involve the asymptotic behavior of the functions and operators both near to and far from sources and

boundaries. Whatever simplifications, assumptions, or manipulations a theorist could perform to formulate the mathematical expressions in simple forms were greatly appreciated. This provided the groundwork for the field of analytical benchmarking, a field which was rich in the mathematics of operational calculus.

During the past ten years, the computer world has seen astronomical advancements in the speed, storage, and memory capabilities of desktop personal computers and workstations so that the companies who make supercomputers are currently challenged by a product accessible to individuals. Researchers can now run computationally-intensive Monte Carlo codes overnight on a personal computer and obtain the same result requiring three or four hours on a supercomputer. With the recent interest in parallel processing, several central processing units (CPUs) can be linked together with calculations performed in tandem as opposed to sequentially so that calculational times may be further reduced. As a consequence of advances in the computing environment, advances in numerical analysis have also been made. Highly accurate numerical integration techniques, differentiation schemes, matrix inverters, series evaluators, root locators, etc. have all been developed to assist the numerical analyst to evaluate mathematical expressions. Thus, some emphasis has shifted from pure mathematical analysis to a combination of applied mathematics and numerics.

The recent increases in computing power have allowed researchers to create complicated codes to model physical systems. With the creation of any code comes debugging, validation, and ultimately (if possible) verification. Before a code can be used to model complicated systems, the developers must be confident that the code is operating properly. They can gain this confidence by comparing the results of the calculation to experimental data; however, this validation is not always readily available, and even then experimental error is a significant concern. Validating a code ensures that it is not violating any physical laws. Validation does not ensure that the code produces the correct result or

that the numerical methods are being used properly - this falls under "code verification." Unfortunately, the only means of verifying a code is to compare it with the "correct" answer. Verification of a code pertains to the numerical methods used, and does not ensure the accuracy of the physical model upon which the code is based. Ideally, confirmation that the code provides physically realistic results and operates properly is obtained through both verification and validation. The code developer who desires to verify a code's proper operation must have a standard, or benchmark, with which to compare the code. When this benchmark concerns a relatively simple physical problem and obtains results through mathematical expression, it is called an "analytical benchmark."

1.B. Definition of an Analytical Benchmark

The term "analytical benchmark" often creates some confusion. If taken in the strictest sense, the only true analytical benchmarks are those where a mathematically closed-form solution involving known functions is available (e.g. the solution for the uncollided flux from an isotropic point source in an infinite medium). If there are derivatives or integrals which must be numerically evaluated, then there will always be some numerical uncertainty in the solution. However, an analytic expression can be thought of as an expression that contains integrals which must be evaluated. An analytic benchmark consists of a numerical evaluation of an analytic expression as opposed to a numerical benchmark, which may consist of testing a code by considering numerically limiting cases. Generally, analytical benchmarks are used to test codes which use Monte Carlo or discrete numerical methods. In the former, an analytical benchmark may test the applicability of a limited statistical sampling of particles, and in the latter a benchmark may test the effects of spatial discretization and angular binning on the calculated results. In these methods, approximations are made to the statistical nature of the problem (Monte

Carlo methods) or the mathematics is reformulated using a discretized numerical method (discrete ordinates methods), and these approximate formulations describing particle transport are then coded in an algorithm. For analytical benchmarks, the error in the physical parameters is not considered. Numerical approximations occur in the evaluation of mathematical expressions such as integrals or infinite series. In principle, an analytical benchmark can provide any desired accuracy at the expense of computational time, and in practice an analytical benchmark provides a numerical test with firm control over the desired error.

1.C. Analytical Benchmarks and Nuclear Engineering

One of the areas that has been and continues to be important in the fields of nuclear engineering and radiative transfer is development of computer codes to model the flow and distribution of particles in a medium. Codes which have found the greatest use are discrete ordinates or Monte Carlo methods. In the former, "the numerical description of the transport of neutral particles involves discretization of the independent variables of the transport equation" [O'Dell and Alcouffe]. Spatial and angular discretizations imply that the respective differential operators are discretized, and these discretizations result in an algebraic set of equations. The set of equations can then be solved iteratively. Because of the implicit levels of discretization involved, multiple levels of iteration are required (i.e. inner iteration for the spatial variables and outer iteration for energy). Monte Carlo codes are very simple with respect to the underlying mathematics as their primary constituent is a random number generator. In such codes, particles are given a source location from which they travel in a random direction, have a collision at a random distance from the source (with consideration of material properties and boundaries), are absorbed or scattered based on a random sampling, etc. Many particle histories are required to obtain statistically

reliable answers. In short, Monte Carlo methods, while exceedingly simple, require substantial computational effort to obtain a reliable numerical result.

With the development of a code comes the need for testing the code against reliable benchmarks. This implies that a production code must also be able to solve the simple problems. As the large codes evolve and are able to model more complex systems so must the available benchmarks become more comprehensive. Analytical benchmarks will always involve simpler problems relative to those considered by the comprehensive production codes; however, the standards for what constitutes a benchmark should remain constant. The suite of benchmarks to be considered in this work involve three primary simplifications or assumptions: one energy group; time-independence; and infinite/semi-infinite homogeneous media.

1.D. The "Big Picture"

When referring to a suite of benchmarks one assumes a specific commonality among the individual benchmarks in that suite. In this case, the common characteristic of the benchmarks is the medium of interest, that is, an infinite homogeneous medium which scatters particles isotropically. The specific benchmarks are therefore defined primarily by the type of source in an infinite medium. As will be seen, all fundamental benchmarks are related to each another.

1.D.1. The Intuitive "Big Picture."

The most basic physical source type is a point source which emits in a specific direction. Physically, all other types of sources may be constructed from this source, which is distributionally singular in both space and direction. Because all other sources may be constructed from this point-beam source, it is referred to as the "Green's function"

source. By integrating the scalar flux from this source over the unit sphere, the flux from an isotropic point source is obtained. Integration over an infinite line or an infinite plane yields the scalar flux from an anisotropically emitting line source or anisotropic planar source, respectively. Integration of the anisotropically emitting line and planar sources' scalar fluxes over the unit sphere produces fluxes from infinite isotropic line and plane sources. These infinite isotropic line and plane sources could also have been modeled by integrating the scalar flux from the isotropic point source over an infinite line or over a plane. Such a relational scheme is pictorially presented in Fig. 1.1.

1.D.2. The Constructive "Big Picture."

When sources are usually described, we consider how a source is physically constructed; conversely, when the descriptions are mathematical, considerations turn toward mathematical tractability. The scheme established for the intuitive "big picture" is not the same as the one for the construction. The fluxes from the anisotropic sources are mathematically constructed from the Green's function source, and these in turn may be integrated over source angle to create isotropic sources. However, it will be shown that the scalar flux from the Green's function source may be mathematically constructed from the isotropic point source solution. Thus, the most basic source in the mathematical construction is the isotropic point source. From the isotropic point source all the anisotropic sources may be constructed as shown. Also, by integrating the isotropic point source solution over a finite length one can create a general finite curvilinear source. If the path is a finite line then a finite line source results. If the path is an infinite line the infinite isotropic line source will result. Integrating the isotropic point source solution over a finite area yields the scalar flux from a finite isotropic area source. If this area is a circle or rectangle then the isotropic disk and rectangular sources result. If this area is infinite the isotropic plane source is the result. Likewise, integration over a volume produces a

volumetric source. Therefore, any source in an infinite medium may be mathematically constructed from the solution to the isotropic point source. This constructive scheme is presented in Fig. 1.2.

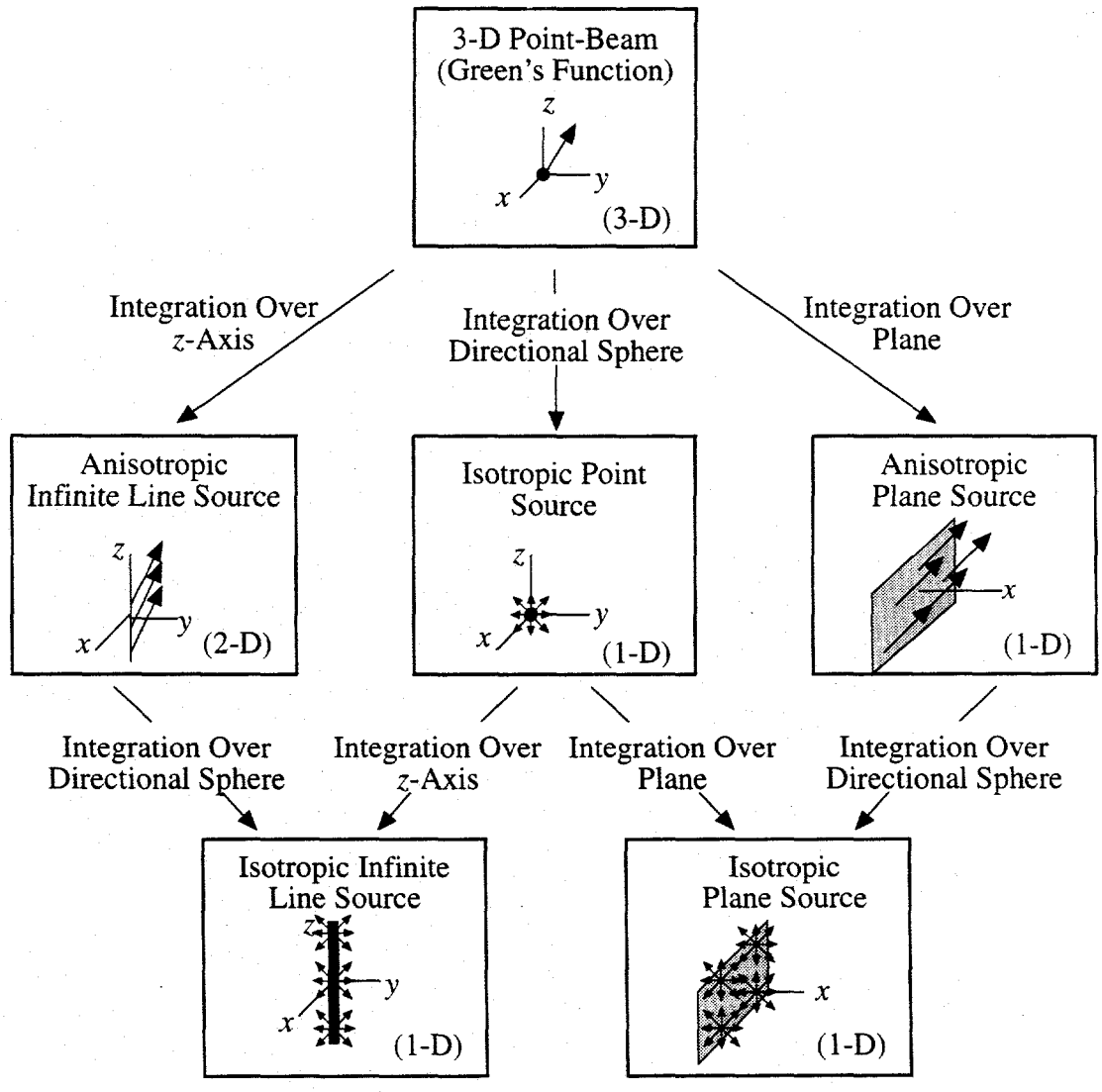

Fig. 1.1. The intuitive "big picture" of sources in an infinite homogeneous medium.

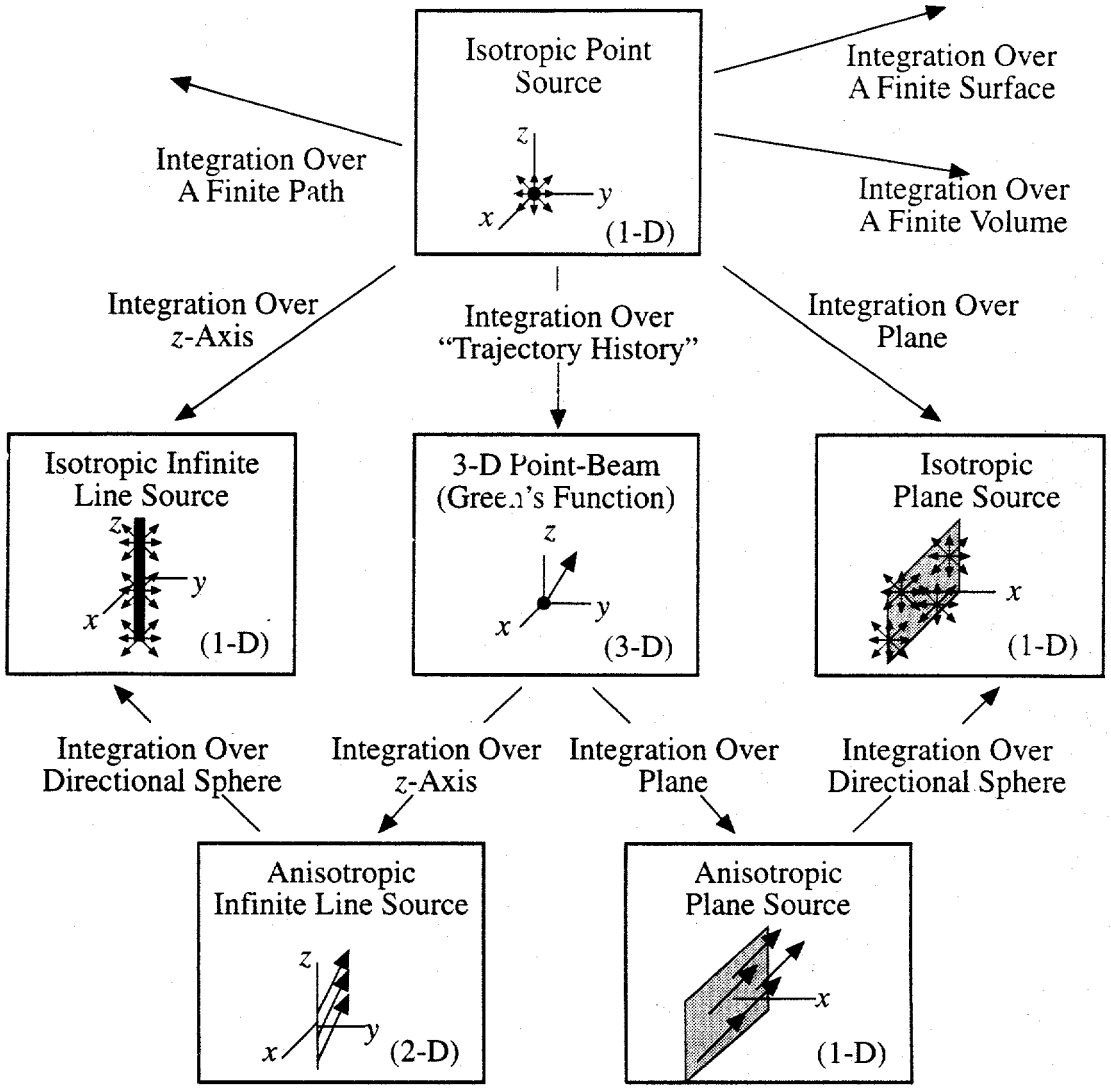

Fig. 1.2. The constructive "big picture" of sources in an infinite homogeneous medium.

1.E. Previous Work and Literature Review for Infinite Media Problems

For one-group neutron transport theory in one dimension, several powerful analytical techniques have been developed to solve the neutron transport equation including singular eigenfunction expansion, Wiener-Hopf factorization, and Fourier and Laplace transform methods. The literature regarding one-dimensional problems is extensive. Some

1.F. Extensions of the Available Benchmarks in Infinite Media

With the basis of infinite medium benchmarks provided by much previous work, we now turn attention to extending the available benchmarks in infinite media. As discussed previously, the scalar flux from the Green's function source may be mathematically constructed from the solution to the isotropic point source solution. If the Green's function source is at the center of the infinite medium and emits along the z-axis, the resulting scalar flux will have two-dimensional variation in cylindrical coordinates. However, by rotating and translating the source, the resulting scalar flux appears to be three-dimensional in Cartesian coordinates (see Fig. 1.3).

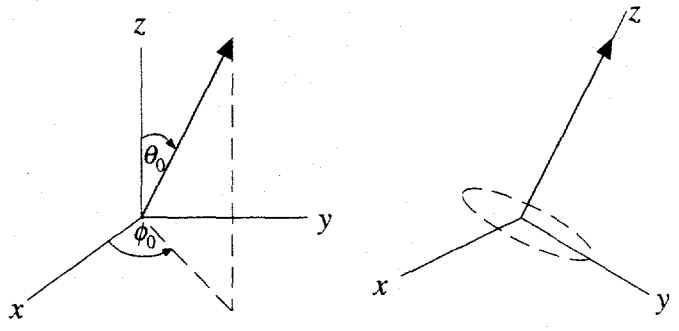

Fig. 1.3. Two- and three-dimensional orientations of the Green's function source.

Therefore, given a Green's function source of arbitrary position and orientation two-dimensional mathematical techniques may be used to determine the scalar flux which nevertheless has a three-dimensional variation. The solution method involves a double Fourier transform in the transverse plane and a single Fourier transform in the longitudinal dimension. Equivalence to a pseudo problem is obtained and then inversions are considered. No publication has been found which has considered the symmetry of the two-dimensional case to generate a pseudo three-dimensional solution as will be done in this work.

With the isotropic point source solution, it is now possible to construct solutions for a host of other sources. Using methods and formulations similar to those obtained for the Green's function, the scalar fluxes from finite isotropic line, disk, and rectangular sources will also be provided. These are some of the less complicated finite sources. The resultant scalar fluxes from the finite isotropic line and disk sources will have two-dimensional spatial variation; however, the rectangular source generates a three-dimensional scalar flux.

There are particular motivations for considering these finite isotropic sources. By a suitable choice of source locations, a three-dimensional geometrical source configuration can be designed to yield a valuable assessment of the accuracy of a three-dimensional transport algorithm in specific situations. However, beyond code comparisons, one possible application is in the field of radiation oncology where radioactive seeds are implanted in a specific configuration to deposit the maximum dose to a particular location so that cancerous tissue may be most efficiently destroyed. Although the analyses of these sources are supposedly for neutrons, it is equally applicable to gamma particles (assuming isotropic scattering) and therefore is appropriate for the determination of how well a Monte Carlo code predicts the dose at a point resulting from a complicated seed implant configuration.

Once the one-dimensional sources (isotropic point, isotropic line, isotropic plane, and anisotropic plane) and the two-dimensional (mathematically speaking) Green's function source have been considered, the last type of source in Figs. 1.1 and 1.2 to be considered is the infinite anisotropic line source. As this line source is infinite in the longitudinal dimension, the resultant scalar flux has a two-dimensional variation; however, the variation is in the transverse plane or in polar coordinates (r,θ). Again, the solution is obtained by taking a two-dimensional Fourier transform of the transport equation and then inverting. The mathematics used in the analysis of this problem lead directly to those used for the

searchlight problem considered in the penultimate chapter. The next step in complexity of benchmarks comes from considering more complicated geometries such as a semi-infinite medium.

1.G. An Extension to Semi-Infinite Geometry

In attempting to establish more comprehensive benchmarks, the next level of difficulty for monoenergetic, homogeneous medium, isotropic scattering problems is the consideration of a semi-infinite medium. Full consideration will be given to the searchlight problem since three-dimensional results have never before been published.

One of the basic transport problems for semi-infinite media is the searchlight problem originally proposed by Chandrasekhar [1958] in the radiative transfer context. In the searchlight problem, incident radiation impinges on a free surface at a point, and the resultant interior and surface fluxes and surface current are to be determined. To date only one-group problems have been considered for a homogeneous isotropically scattering medium. As with other problems considered here, the searchlight problem has been shown to be a variant of a one-dimensional pseudo problem which facilitates its solution [Williams, 1982 and Rybicki, 1971]. Numerical analyses of this problem have been considered by Siewert and Dunn [1983, 1985, 1989] where the F_N method was applied to determine the flux from a normal beam incident on a finite slab. As mentioned above, Elliott considered an isotropic point source at the surface of a half-space but, as would be expected from a paper of that era (1955), no numerical results were presented due to the lack of computational power. Recently, numerical results for the searchlight problem for a half-space have been provided by Ganapol and Nigg (1991) and Ganapol, *et al.* (1994) for the case of the normal beam. When the beam is directed normal to the surface, the resultant flux is two-dimensional resulting in a significant numerical advantage. However, if the

beam is canted, the resultant flux is three-dimensional. Such a case will be considered here. It will be shown that the analytical expressions, while complex, lend themselves to numerical evaluation.

Like the analysis in Figs. 1.1 and 1.2, one can consider a similar hierarchy of problems for a half-space. The searchlight problem would be analogous to the Green's function source, an isotropic point source on the surface or in the medium would correspond to the isotropic point source in an infinite medium, and similar planar and linear sources could also be derived. Results for an isotropic point source and isotropic disk source on the surface are presented in Ganapol, *et al.* (1994). Ganapol's Benchmark Book also considered the planar sources on the surface of the half-space. To date, no one has considered an isotropic or anisotropic line source on the surface of the half-space. However, Williams (1982) did consider a line source perpendicular to the free surface extending into the medium.

1.H. Benchmarks as a Pedagogical Tool

The use of benchmarks for testing production codes is obvious; however, because benchmarks consider simplified problems that students may encounter in their study of particle motion, they are also useful as a pedagogical tool. Students generally are given problems which can be solved analytically with paper and pen, and a natural extension of their education is to consider slightly more intricate problems which require non-trivial computation. Analytical benchmarks have and will continue to provide students with a bridge between a physical problem statement, the associated engineering mathematics and operational calculus, and the numerical techniques which must be employed for solving such problems.

Also, because computers are becoming faster, in the future the Monte Carlo codes most likely will become an industry standard. Assuming that a Monte Carlo code could follow an infinite number of histories, then it is presumed that it could describe the physics of any given problem to any desired error. The faster computers become, the more the Monte Carlo codes will be able to provide this impossible service in a reasonable time. Thus, the market for benchmarks as a teaching aid will increase.

CHAPTER 2: FUNDAMENTAL PROBLEMS IN AN INFINITE MEDIUM

The relative difficulty of solving transport problems often hinges on the geometry in which the problem is set. Generally, the simplest problems (in the suite of one-group time-independent problems) are those where the medium scatters particles isotropically and the scalar flux varies in only one spatial dimension. Case, DeHoffmann, and Placzek, in their monumental work "Introduction to the Theory of Neutron Diffusion," led the way regarding the mathematical and numerical solutions to one-dimensional problems. The primary source configurations considered in this monograph were the isotropic point source and isotropic and anisotropic plane sources in infinite homogeneous media. For completeness and because of their fundamental nature, these problems will again be considered in this work. The numerical evaluation of the expressions found in this chapter follow the methods used in Ganapol's Benchmark Book. The construction of Fig. 1.2 begins by considering the isotropic point source in an infinite medium (see Fig. 1.2a).

2.A. The Isotropic Point Source in an Infinite Medium

Generating the integral form of the transport equation is a standard procedure in transport theory. It may be obtained by following the particle along its trajectory. When a homogeneous medium is assumed, the integral form of the transport equation for an isotropic point source of strength $4\pi S_0$ at the center of an infinite medium is [Davison]

$$\rho(\vec{r}) = \frac{c}{4\pi} \int_V dV' \, \rho(\vec{r}\,') \, \frac{e^{-|\vec{r}-\vec{r}\,'|}}{|\vec{r} - \vec{r}\,'|^2} + S_0 \frac{e^{-r}}{r^2} \, , \tag{2.1}$$

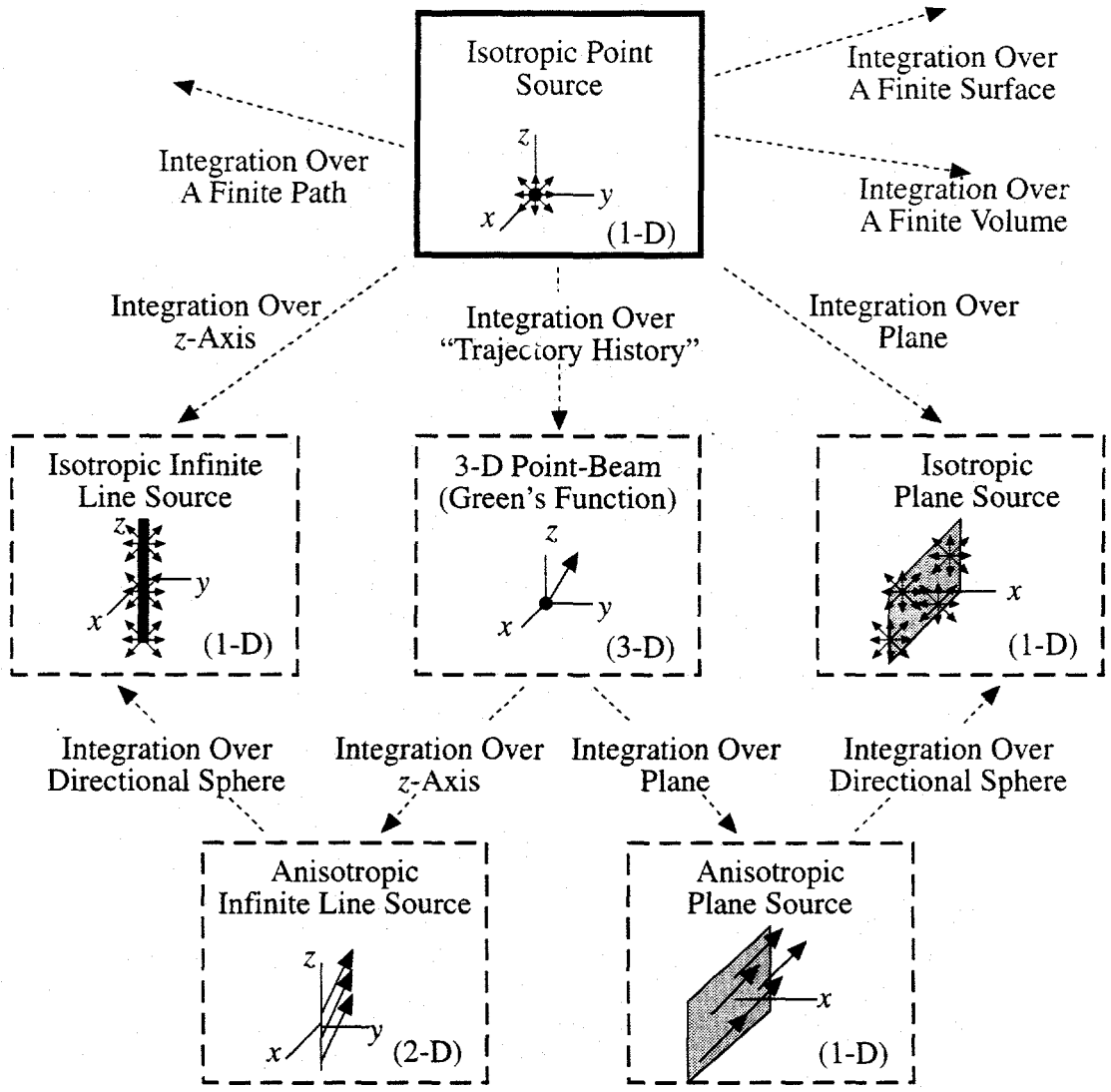

Fig. 1.2a. The first step in constructing the suite of infinite medium benchmarks - the isotropic point source.

where $\rho(\vec{r})$ is the scalar flux at a general position $\vec{r}$, c is the mean number of secondary particles per collision, and the integration is over all space V. Note that the part of the integrand which contains the term e^{-r}/r^2 serves as a Green's function for an arbitrary spatial distribution of sources given by $\rho(\vec{r}')$. Given that the point source at the center is the only source of particles in the medium, the isotropic nature of the source dictates that the variation in the scalar flux will only be a function of radial distance from the origin - i.e. the

problem is spherically symmetric. A three-dimensional Fourier transform is now applied to Eq. (2.1). The transform pair is defined as

$$\bar{\rho}(\vec{p}) \equiv \int_V dV\, e^{i\vec{p}\cdot\vec{r}}\, \rho(\vec{r}) \tag{2.2a}$$

$$\rho(\vec{r}) \equiv \frac{1}{(2\pi)^3} \int_{\vec{p}} d\vec{p}\, e^{-i\vec{p}\cdot\vec{r}}\, \bar{\rho}(\vec{p}) \ . \tag{2.2b}$$

Applying the transform to the source term in Eq. (2.1) produces

$$\bar{\rho}_S(\vec{p}) = S_0 \int_V dV\, e^{i\vec{p}\cdot\vec{r}}\, \frac{e^{-r}}{r^2} \ . \tag{2.3}$$

Note that the dot product of the transform vector and the spatial vector is $\vec{p}\cdot\vec{r} = pr\mu$, where μ is the cosine of the angle between the two vectors. Given that the spatial triple integral in spherical coordinates has the form

$$\int_V dV\, (\bullet) = \int_0^\infty dr\, r^2 \int_{4\pi} d\mu\, d\phi\, (\bullet) \ , \tag{2.4a}$$

where the integral over $\vec{\Omega}$ is over the standard solid angle, the transformed source term becomes

$$\bar{\rho}_S(\vec{p}) \ = \ S_0 \int_0^\infty dr\, e^{-r} \int_{-1}^{1} d\mu\, e^{ipr\mu} \int_0^{2\pi} d\phi \ = \ 2\pi S_0 \int_{-1}^{1} \frac{d\mu}{1 - ip\mu} \ , \tag{2.4b}$$

which upon evaluation becomes

$$\bar{\rho}_S(\vec{p}) = 4\pi S_0 \frac{\tan^{-1} p}{p} \ . \tag{2.4c}$$

The first integral term in Eq. (2.1) is now considered. Given the three dimensional convolution

$$U(\vec{r})^{*}V(\vec{r}) = \int_V d\vec{r}\,'\, U(\vec{r}\,')\; V(\vec{r}\,' - \vec{r}) \quad , \tag{2.5a}$$

it then the follows that

$$\mathcal{F}_{\vec{p}}\left\{ U(\vec{r})^{*}V(\vec{r}) \right\} = \mathcal{F}_{\vec{p}}\left\{ U(\vec{r}) \right\}\; \mathcal{F}_{\vec{p}}\left\{ V(\vec{r}) \right\} \quad . \tag{2.5b}$$

Noting that the integral term is of the form of a convolution, i.e.

$$\rho_I(\vec{r}) = \int_V dV'\; \rho(\vec{r}\,')\; f\left(\vec{r} - \vec{r}\,'\right) \quad , \tag{2.6}$$

it may be seen that

$$\mathcal{F}_{\vec{p}}\left\{ \rho_I(\vec{r}) \right\} = \bar{\rho}(\vec{p})\; \mathcal{F}_{\vec{p}}\left\{ f\left(\vec{r} - \vec{r}\,'\right) \right\} \quad . \tag{2.7}$$

However, the function $f(r)$ is the same as the function from the source term (with different preceding constants). Thus

$$\mathcal{F}_{\vec{p}}\left\{ \rho_I(\vec{r}) \right\} = \frac{c}{4\pi}\,\bar{\rho}(\vec{p})\; 4\pi\,\frac{\tan^{-1}p}{p} \quad . \tag{2.8}$$

Upon combining Eqs. (2.4c) and (2.8), we have for the transformed scalar flux from an isotropic point source

$$\bar{\rho}(\vec{p}) = 4\pi S_0\,\frac{\tan^{-1}p}{p} + c\,\bar{\rho}(\vec{p})\,\frac{\tan^{-1}p}{p} \quad , \tag{2.9a}$$

or

$$\bar{\rho}(\vec{p}) = 4\pi S_0\,\frac{L(p)}{1 - cL(p)} \quad , \tag{2.9b}$$

where $L(p)$ has been defined as $(\tan^{-1}p)/p$. The scalar flux is now obtained by inversion as

$$\rho(\vec{r}) = \frac{S_0}{2\pi^2}\int_{\vec{p}} d\vec{p}\; e^{-i\vec{p}\cdot\vec{r}}\;\frac{L(p)}{1 - cL(p)} \quad , \tag{2.10a}$$

or

$$\rho(\vec{r}) = \frac{S_0}{2\pi^2} \int_0^\infty dp\ p^2\ \frac{L(p)}{1 - cL(p)} \int_{-1}^{1} d\mu \int_0^{2\pi} d\phi\ e^{-ipr\mu} \quad . \tag{2.10b}$$

Evaluating the angular integrals and noting the solution is only a function of r yields

$$\rho(r) = \frac{2S_0}{\pi r} \int_0^\infty dp\ p\ \frac{L(p)}{1 - cL(p)} \sin(pr) \quad , \tag{2.11}$$

or if the source strength is normalized with respect to the unit sphere ($S_0 = 1/4\pi$)

$$\rho(r) = \frac{1}{2\pi^2 r} \int_0^\infty dp\ p\ f(p)\ \sin(pr) \quad , \tag{2.12a}$$

where

$$f(p) = \frac{L(p)}{1 - cL(p)} \quad . \tag{2.12b}$$

The numerical evaluation of Eq. (2.12a) is relatively simple except that the range of integration is over a semi-infinite interval and the integrand oscillates, which is not amenable to numerical methods. Therefore the integration must be truncated at some point. The simplest method for evaluating the integral is to reformulate the semi-infinite integrals as an infinite series of integrals over a finite interval. The finite intervals are defined as the zeroes of the sine function so that the value of the integrands will be zero at the endpoints. The individual integrals are evaluated and the convergence of the series is accelerated by an Euler-Knopp transformation [Press, *et al.*], which is intended to accelerate an oscillating series. When the series is converged to a desired relative error, the evaluation is considered complete.

Fig. 2.1 displays the results of such an evaluation. The flux converges to a $1/4\pi r^2$ (see Appendix A) variation near the source and the scalar flux increases as the absorption decreases at any given position. Also for c close to zero the scalar flux varies as $e^{-r}/4\pi r^2$,

as expected per Eq. (2.1). The scalar flux for highly scattering media quickly approaches the asymptotic scalar flux in the diffusive limit ($\phi_{as} \sim e^{-r/v_0}/4\pi r$) at large r. The scalar flux is within 1% of the diffusive value at 6 mfp and 4 mfp for $c = 0.9$ and 0.9999, respectively.

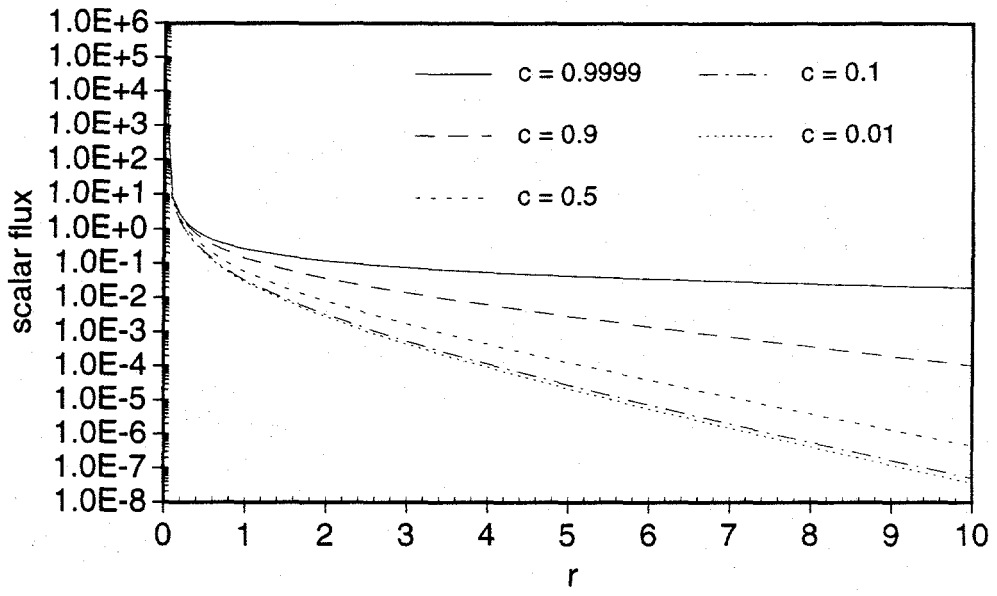

Fig. 2.1. The scalar flux from an isotropic point source as a function of position for several values of c.

2.B. The Isotropic Plane Source in an Infinite Medium

Like the isotropic point source solution, the isotropic planar source solution is one dimensional with respect to position. The point source solution may be used as a Green's function for the construction of any shape of source that emits particles isotropically. The solution which contains a plane source at the center of an isotropic homogeneous medium may be created by integrating the solution from the isotropic point source in the same medium over an infinite plane [Davison]. That is,

$$\phi_{pl}(x) = 2\pi \int_0^\infty dr\ r\ \rho(r') \quad , \tag{2.13}$$

where $r'^2 = r^2 + x^2$ (see Fig. 2.2). This constructive step is shown in Fig. 1.2b.

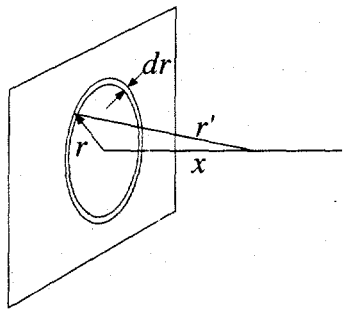

Fig. 2.2. Schematic for integrating the point source solution over the plane.

Inserting the expression for the point source solution yields

$$\phi_{pl}(x) = \frac{1}{\pi} \int_0^\infty dr\ \frac{r}{\left(r^2 + x^2\right)^{1/2}} \int_0^\infty dk\ k\ f(k)\ \sin\left[k\left(r^2 + x^2\right)^{1/2}\right] \quad , \tag{2.14a}$$

which upon the change of variable $u^2 = r^2 + x^2$ becomes

$$\phi_{pl}(x) = \frac{1}{\pi} \int_0^\infty dk\ k\ f(k) \int_{|x|}^\infty du\ \sin(ku) \quad . \tag{2.14b}$$

The u integral may be evaluated as

$$\int_{|x|}^\infty du\ \sin(ku) = \frac{1}{k} \cos(kx) \quad ,$$

in the Cesaro sense. That is, considering k constant in the limit above, it is seen that the frequency of the cosine becomes infinite (when $u \to \infty$), and as the cosine is a purely oscillating function whose value is bounded by $\pm$ 1, in the limit of a large frequency the

function takes on its average value, which is zero. Thus, the scalar flux from an infinite planar source is seen to be

$$\phi_{pl}(x) = \frac{1}{\pi}\int_0^\infty dk\, f(k)\, \cos(kx) \quad . \tag{2.15}$$

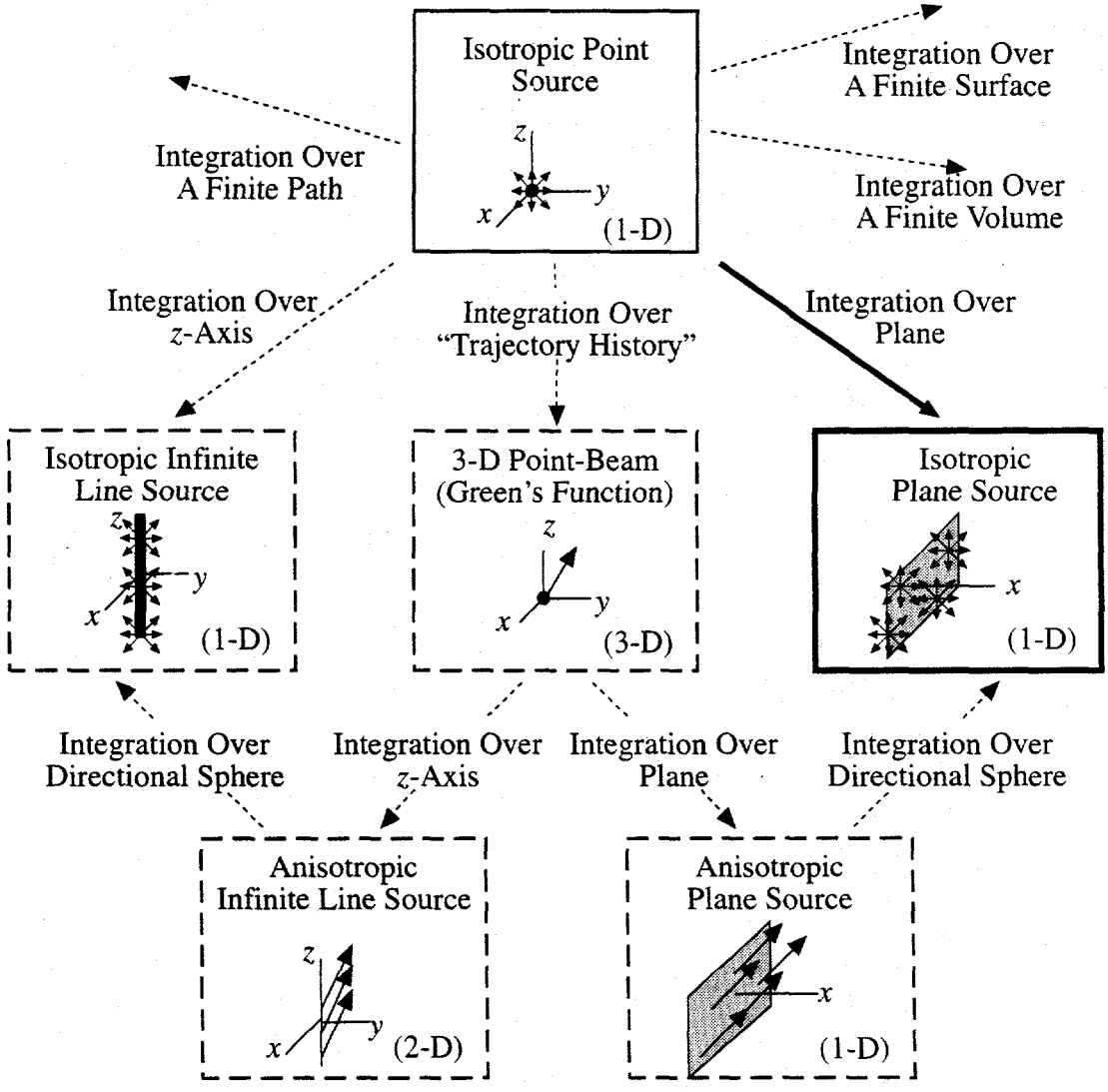

Fig. 1.2b. The second step in constructing the suite of infinite medium benchmarks - the isotropic plane source.

Note that the isotropic point source solution may be recovered by [Davison]

$$\rho(r) = -\frac{1}{2\pi r}\left[\frac{\partial \phi_{pl}(x)}{\partial x}\right]_{x=r} .$$

By numerically evaluating Eq. (2.15) using the techniques discussed previously, the scalar flux as a function of position may be obtained as shown in Fig. 2.3. Note that as a conservative medium ($c = 1$) is approached, the scalar flux becomes spatially uniform but its value becomes increasingly larger (approaching infinity). When no neutrons are lost in the system, a constant flux distribution is established in the medium, and as there is an infinite supply of particles in the planar source, the scalar flux becomes increasingly larger and the medium becomes more conservative. As with the point source, the scalar flux in highly scattering media approaches the diffusive limit ($\phi_{as} \sim A_0(\nu_0)e^{-z/\nu_0}$) at large z. For $c = 0.9$ the relative difference is within 1% at 3 mfp, and for $c = 0.9999$ this occurs at less than 1 mfp.

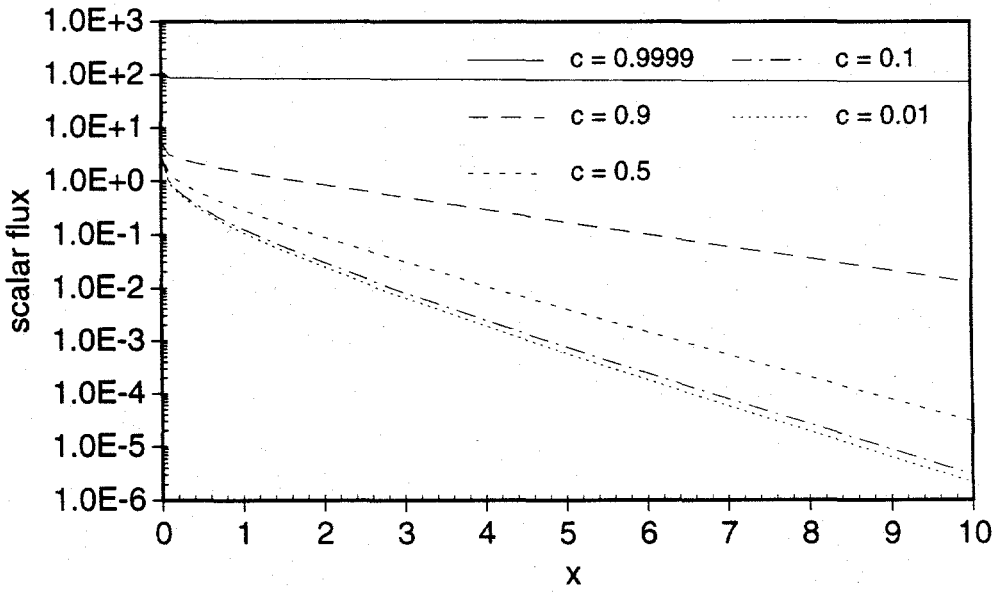

Fig. 2.3. The scalar flux from an isotropic plane source as a function of position for several values of c.

2.C. The Isotropic Line Source in an Infinite Medium

Again, the point source solution may be used as a Green's function to construct the problem which contains a line source at the center of an isotropically scattering homogeneous medium. This is done by integrating the solution from an isotropic point source over an infinite line:

$$\phi_l(r) = \int_{-\infty}^{\infty} dx\ \rho(r') \quad , \tag{2.16}$$

where $r'^2 = r^2 + x^2$ (the pictorial representation would be similar to that seen for Fig. 2.2). This part of the construction of Fig. 1.2 is shown in Fig. 1.2c.

As with the plane source, we insert the expression for the point source solution and make the change of variable $u^2 = r^2 + x^2$ so that

$$\phi_l(r) = \frac{1}{\pi^2} \int_0^{\infty} dk\ k\ f(k) \int_{|r|}^{\infty} \frac{du}{\left(u^2 - x^2\right)^{1/2}} \sin(ku) \quad . \tag{2.17}$$

The u integral can be evaluated as $\frac{\pi}{2} J_0(kr)$, leaving for the scalar flux from an infinite isotropic line source

$$\phi_l(r) = \frac{1}{2\pi} \int_0^{\infty} dk\ k\ f(k)\ J_0(kr) \quad . \tag{2.18}$$

This integral is converted into an infinite series of integrals over a finite interval; however, in this case, the individual integrals will have limits of integration equal to the zeroes of $J_0(u)$. The scalar flux from the isotropic infinite line source is displayed in Fig. 2.4. The scalar flux asymptotically approaches $1/4r$ near the source as given in App. A.

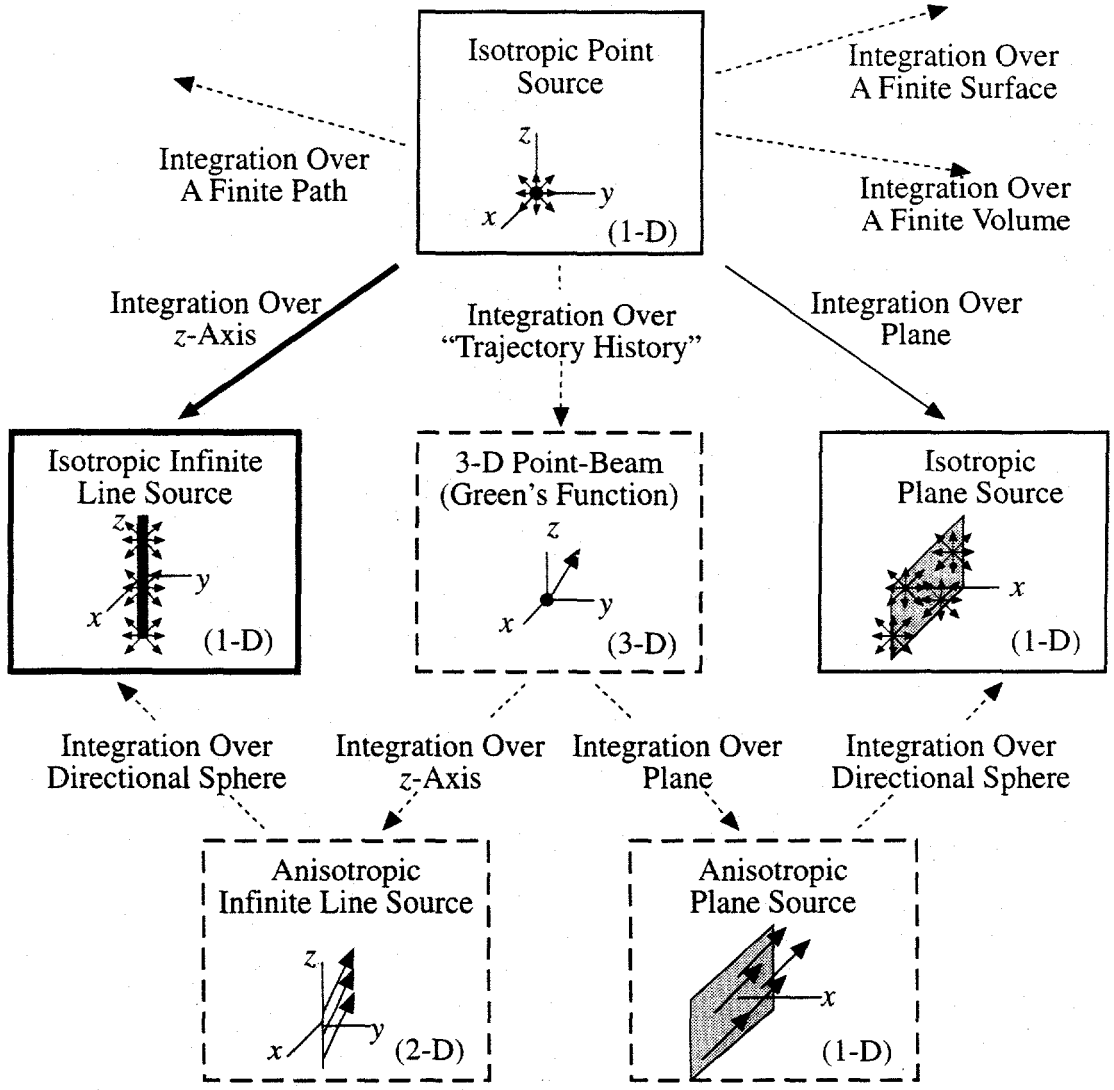

Fig. 1.2c. The third step in constructing the suite of infinite medium benchmarks - the isotropic line source.

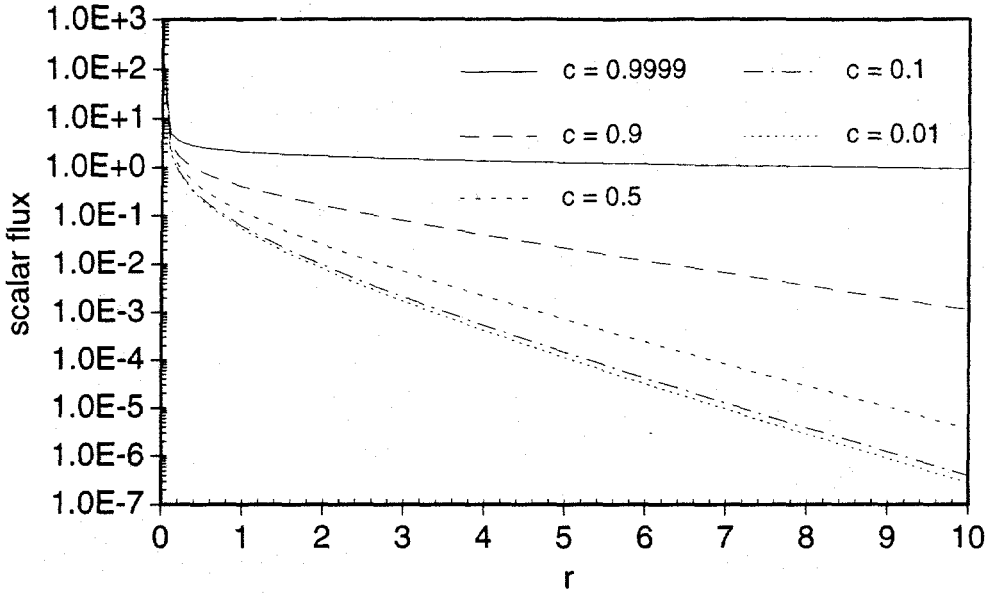

Fig. 2.4. The scalar flux from an isotropic infinite line source as a function of position for several values of *c*.

Clearly, a wide variety of problems in infinite media can be treated. Different isotropic sources may be constructed so that the variation in the scalar flux is one dimensional; however, except for the point source all the sources seen thus far are infinite in one or more dimension. As the isotropic point source solution was integrated to obtain the sources discussed thus far, so too can it be integrated to produce finite sources. This may include shell, surface, or volumetric sources. The latter two kinds of sources will be examined next. Again, the theme which connects the sources to this point is that they all emit particles isotropically.

CHAPTER 3: EXTENSIONS OF THE ISOTROPIC POINT SOURCE SOLUTION

With the solution for the isotropic point source, it is theoretically possible to generate the solution for a source of any shape or size in an infinite homogeneous medium via integration. This will produce integral equations which require two or three embedded integral evaluations, depending on the complexity of the source desired. Three of the more simple sources are finite line, disk, and rectangular sources. The consideration of these finite sources adds two more pieces toward the completion of Fig. 1.2; the additional arrows are indicated on Fig. 1.2d shown below. The isotropic point source solution is then used further to generate a volumetric source.

An alternative expression for the scalar flux from an isotropic point source will be used in the derivation of the scalar fluxes from these finite sources. Eqs. (2.12), with a change of variable and contour, and extracting the pole contribution, can be shown to be [Case, DeHoffmann, and Placzek]

$$\phi_i(r) = \frac{1}{4\pi r}\left[\frac{\partial k_0^2}{\partial c}\, e^{-k_0 r} + \int_0^1 \frac{d\mu}{\mu^2}\, e^{-r/\mu}\, g(c,\mu)\right] , \tag{3.1a}$$

where

$$g(c,\mu) \equiv \left[\left(1 - c\mu \tanh^{-1}\mu\right)^2 + \left(\frac{\pi}{2} c\mu\right)^2\right]^{-1} , \tag{3.1b}$$

$$\frac{\partial k_0^2}{\partial c} = \frac{2k_0^2(k_0^2 - 1)}{c(1 - c - k_0^2)} , \tag{3.1c}$$

and k_0 satisfies the familiar dispersion relation

$$1 - \frac{c}{k_0} \tanh^{-1}(k_0) = 0 . \tag{3.1d}$$

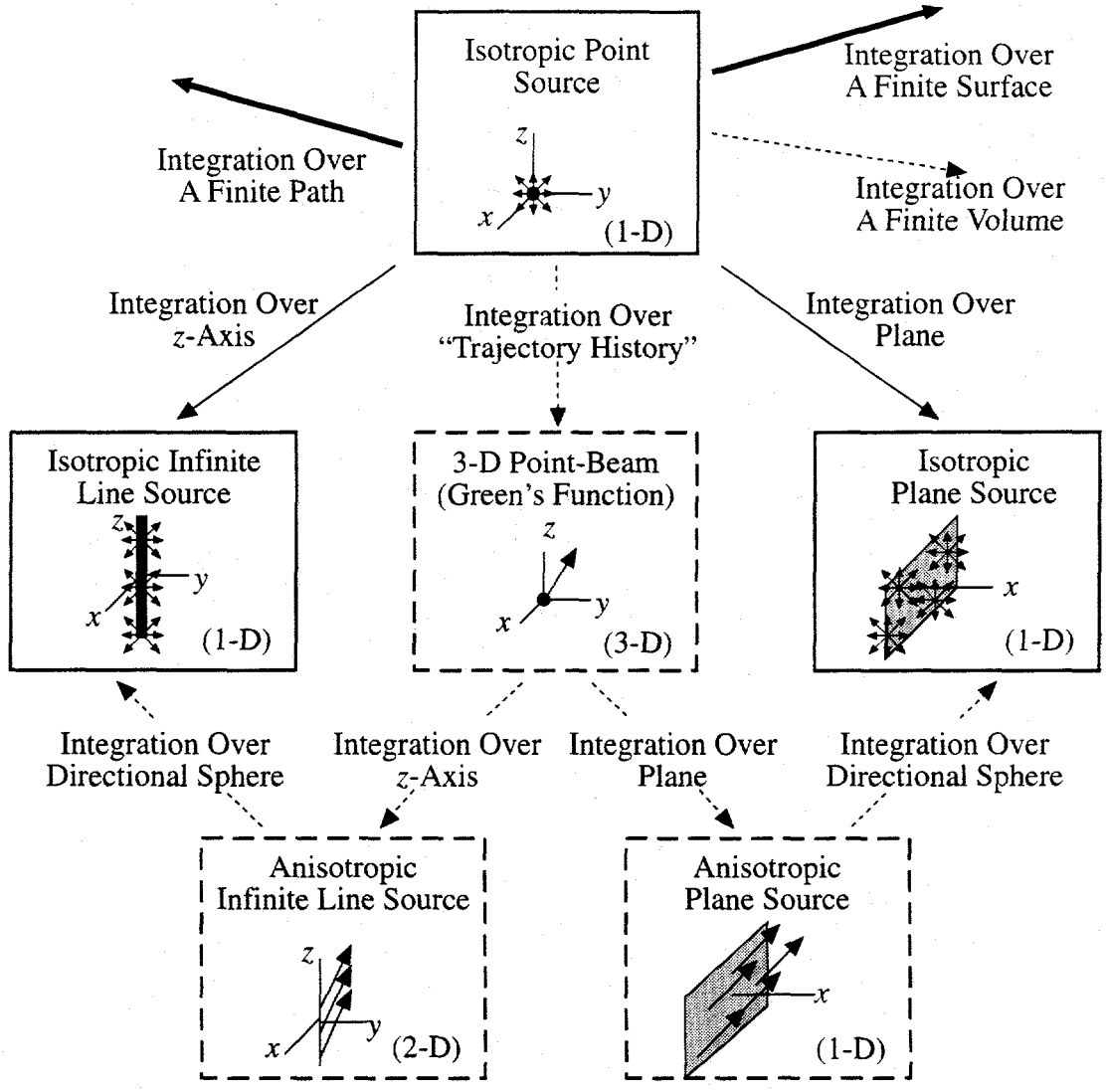

Fig. 1.2d. The fourth and fifth steps in constructing the suite of infinite medium benchmarks - finite line and surface sources.

3.A. Finite Isotropic Line Sources

Beginning with the scalar flux from an isotropic point source at the center of an infinite medium, the flux from an isotropic line source is obtained by integrating the isotropic point source solution over a finite length as (see Fig. 3.1)

$$\Psi_l(z,\rho) = \int_{-z_0}^{z_0} dz'\ \phi_l(z',\rho) \quad . \tag{3.2}$$

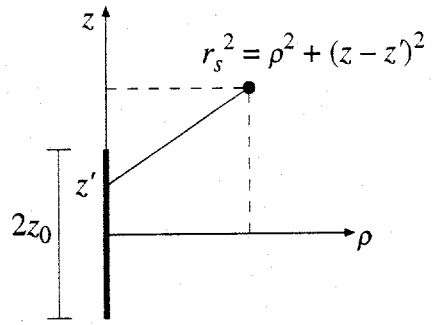

Fig. 3.1 Finite isotropic line source construction.

Upon substitution of the scalar flux from an isotropic point source, it is seen that

$$\Psi_l(z,\rho) = \int_{-z_0}^{z_0} dz'\ \frac{1}{4\pi r'}\left[\frac{\partial k_0^2}{\partial c}\, e^{-k_0 r'} + \int_0^1 \frac{d\mu}{\mu^2}\, e^{-r'/\mu}\, g(c,\mu)\right] , \tag{3.3a}$$

which can be written as

$$\Psi_l(z,\rho) = \frac{2z_0}{4\pi}\left[\frac{\partial k_0^2}{\partial c}\, \chi_l\left(z,\rho;k_0\right) + \int_0^1 \frac{d\mu}{\mu^2}\, \chi_l\left(z,\rho;\frac{1}{\mu}\right) g(c,\mu)\right] \tag{3.3b}$$

where

$$\chi_l(z,\rho;a) = \frac{1}{2z_0}\int_{-z_0}^{z_0} d\omega\ \frac{e^{-a(\rho^2+(z-\omega)^2)^{1/2}}}{\left[\rho^2 + (z-\omega)^2\right]^{1/2}} \quad .$$

Making the change of variable $\omega = z_0 - 2z\omega'$ yields (upon dropping the primes)

$$\chi_l(z,\rho;a) = \int_0^1 d\omega\ \frac{e^{-a(\rho^2+(z-z_0+2z_0\omega)^2)^{1/2}}}{\left[\rho^2 + (z - z_0 + 2z_0\omega)^2\right]^{1/2}} \quad . \tag{3.3c}$$

Noting the form of the denominator, it is evident that a singularity will occur in the integrand when $\rho = 0$ and $\omega = (z_0 - z)/2z_0$. Clearly, when $|z| > z_0$, the value of ω which causes a singularity is negative and thus beyond the range of integration; therefore, when $|z| > z_0$ there is no singularity in $\chi_l(z,0;a)$. When $\rho = 0$ and $|z| \leq z_0$, that is when the spatial point lies on the source, the value of ω which creates the singularity in the integrand is in the range [0,0.5] and will therefore create a singularity in the range of integration. Thus, special treatment of $\chi_l(z,\rho;a)$ must be made for a certain range of z, in this case for $|z| \leq z_0$ and $\rho = 0$ (on the source).

3.A.1. Scalar Flux for $|z| > z_0$.

As there will be no singularity in the integrand of $\chi_l(z,\rho;a)$ for $|z| > z_0$, the only modification of Eq. (3.2c) will be to make the integral more numerically tractable by subtracting 1 from $g(c,\mu)$ to counter the μ^2 in the denominator of the double integral term. Thus,

$$\Psi_l(z,\rho) = \frac{2z_0}{4\pi}\left\{\frac{\partial k_0^2}{\partial c}\,\chi_l\left(z,\rho;k_0\right) + \int_0^1 \frac{d\mu}{\mu^2}\,\chi_l\left(z,\rho;\frac{1}{\mu}\right)\,[g(c,\mu) - 1] + Q_g\right\}, \qquad (3.4a)$$

where

$$Q_g = \int_0^1 \frac{d\mu}{\mu^2}\int_0^1 d\omega\,\frac{e^{-(1/\mu)(\rho^2+(z-z_0+2z_0\omega)^2)^{1/2}}}{\left[\rho^2 + (z - z_0 + 2z_0\omega)^2\right]^{1/2}},$$

which by evaluating the μ integral may be shown to be

$$Q_g = \int_0^1 d\omega\,\frac{e^{-(\rho^2+(z-z_0+2z_0\omega)^2)^{1/2}}}{\rho^2 + (z - z_0 + 2z_0\omega)^2}. \qquad (3.4b)$$

3.A.2. Scalar Flux for $|z| \leq z_0$.

As with the case for $|z| > z_0$, the expression for the scalar flux is modified as in Eqs. (3.4). However, now there will be a singularity in the integrand of Q_g for $\rho = 0$. This singularity is extracted by subtracting $e^{-\rho}$ from the numerator (which makes the numerator zero when $\rho = 0$ and the value of ω at the singularity is reached). Thus,

$$Q_g = \int_0^1 d\omega \, \frac{e^{-(\rho^2+(z-z_0+2z_0\omega)^2)^{1/2}} - e^{-\rho}}{\rho^2 + (z - z_0 + 2z_0\omega)^2} + Q_0 \ , \tag{3.5a}$$

where

$$Q_0 = e^{-\rho} \int_0^1 \frac{d\omega}{\rho^2 + (z - z_0 + 2z_0\omega)^2} \ . \tag{3.5b}$$

An appropriate change of variable and evaluation of the above integral shows that it is an inverse tangent function,

$$Q_0 = \frac{e^{-\rho}}{2z_0\rho}\left[\tan^{-1}\left(\frac{z + z_0}{\rho}\right) + \tan^{-1}\left(\frac{z_0 - z}{\rho}\right)\right] \ . \tag{3.5c}$$

The other integral which must be specially treated with respect to singularities is $\chi_l(z,\rho;a)$. Again, there will be a singularity in the integrand when ρ is zero (or the scalar flux is evaluated on the source). Thus, following the above procedure Eq. (3.3c) is rewritten as

$$\chi_l(z,\rho;a) = \int_0^1 d\omega \, \frac{e^{-a(\rho^2+(z-z_0+2z_0\omega)^2)^{1/2}} - e^{-a\rho}}{\left[\rho^2 + (z - z_0 + 2z_0\omega)^2\right]^{1/2}} + e^{-a\rho} Q_1 \ , \tag{3.6a}$$

where

$$Q_1 = \int_0^1 \frac{d\omega}{\left[\rho^2 + (z - z_0 + 2z_0\omega)^2\right]^{1/2}} \ , \tag{3.6b}$$

which may be evaluated as

$$Q_1 = \frac{1}{2z_0} \ln\left\{\left[\left(\frac{z + z_0}{\rho}\right)^2 + 1\right]^{1/2} + \frac{z + z_0}{\rho}\right\} +$$

$$+ \frac{1}{2z_0} \ln\left\{\left[\left(\frac{z - z_0}{\rho}\right)^2 + 1\right]^{1/2} + \frac{z - z_0}{\rho}\right\} . \qquad (3.6c)$$

Now the singularities have been extracted. As evident in Eq. (3.6c), if $\rho = 0$ there will be a logarithmic singularity, so the flux still can not be evaluated on the source (nor will this ever be possible). However, the integrals will be much easier to evaluate near the source now that the singularity is expressed apart from the integral terms.

3.B. Finite Isotropic Disk Sources

The isotropic disk source is constructed by integrating the integral form for the scalar flux from an isotropic point source over the surface of a disk as shown in Fig. 3.2. It is assumed that the disk lies in the transverse (x-y) plane and is centered at the origin. Thus, the form for the scalar flux from an isotropic finite disk is given by

$$\Psi_d(z,\rho) = \frac{1}{4\pi}\left[\frac{\partial k_0^2}{\partial c}\chi_d\left(z,\rho;k_0\right) + \int_0^1 \frac{d\mu}{\mu^2}\chi_d\left(z,\rho;\frac{1}{\mu}\right) g(c,\mu)\right] , \qquad (3.7a)$$

where the integrals over the surface of the source disk have been included in the function

$$\chi_d(z,\rho;a) = R_0^2 \int_0^{2\pi} d\theta \int_0^1 d\omega\, \omega \frac{e^{-ar}}{r} , \qquad (3.7b)$$

$r^2 = \rho^2 + z^2 + R_0^2\omega^2 - 2\rho\omega R_0\cos\theta$, and R_0 is the radius of the source disk.

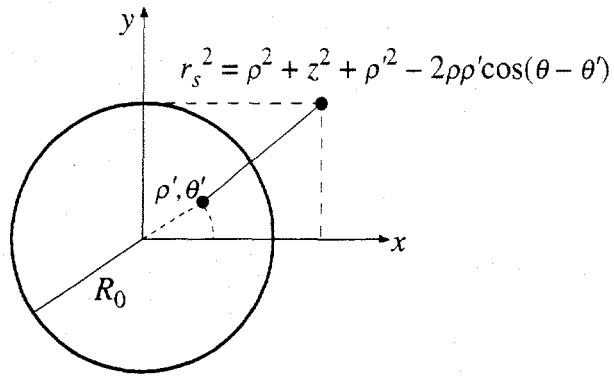

Fig. 3.2. Construction of a finite disk source.

As with the other sources, the treatment for points that lie within the source area will be different than the treatment for those points outside the source area. When z is near zero and ρ is less than R_0, the spatial point lies very near the source, and the singularity at $\rho = 0$ will manifest itself as a zero in the denominator of the ω integral at some point as it spans the range [0,1].

3.B.1. Scalar Flux for $\rho > R_0$.

For this case, no singularity will be found in the ω integral. As usual, the μ integral is made more numerically tractable by defining

$$T_g = \int_0^1 \frac{d\mu}{\mu^2}\, \chi_d\left(z,\rho;\frac{1}{\mu}\right)\, g(c,\mu) = \int_0^1 \frac{d\mu}{\mu^2}\, \chi_d\left(z,\rho;\frac{1}{\mu}\right)\, [g(c,\mu) - 1] + T_{g2}\ , \qquad (3.8a)$$

with

$$T_{g2} = R_0^2 \int_0^{2\pi} d\theta \int_0^1 d\omega\ \omega\ \frac{e^{-r}}{r^2}\ . \qquad (3.8b)$$

3.B.2. Scalar Flux for $\rho \le R_0$.

When $\rho \le R_0$, care must be taken with respect to the singularity in χ_d. As before, the μ integral is reformulated by defining

$$T_g = \int_0^1 \frac{d\mu}{\mu^2}\,\chi_d\left(z,\rho;\frac{1}{\mu}\right)\,g(c,\mu) = \int_0^1 \frac{d\mu}{\mu^2}\,\chi_d\left(z,\rho;\frac{1}{\mu}\right)\,[g(c,\mu) - 1] + T_{g2}\ , \qquad (3.9a)$$

and

$$T_{g2} = R_0^2 \int_0^{2\pi} d\theta \int_0^1 d\omega\ \omega\ \frac{e^{-r}}{r^2}\ . \qquad (3.9b)$$

T_{g2} is now written as

$$T_{g2} = R_0^2 \int_0^{2\pi} d\theta \int_0^1 d\omega\ \omega\ \frac{e^{-r} - e^{-z}}{r^2} + T_{g2z}\ , \qquad (3.10a)$$

where

$$T_{g2z} = R_0^2\, e^{-z} \int_0^{2\pi} d\theta \int_0^1 \frac{d\omega\ \omega}{r^2}\ . \qquad (3.10b)$$

Using the following two formulas (Gradshteyn and Ryzhik)

$$\int_0^{2\pi} \frac{d\theta}{a + b\cos\theta} = \frac{2\pi}{(a^2 - b^2)^{1/2}}\ ,\quad a > b\ ,$$

$$\int \frac{dx}{(a + bx + cx^2)^{1/2}} = \frac{1}{c^{1/2}} \ln\left\{2\left[c(a + bx + cx^2)\right]^{1/2} + 2cx + b\right\}\ ,\quad c > 0\ ,$$

T_{g2z} may be shown to be

$$T_{g2z} = \pi e^{-z} \ln\left\{\frac{\left[(\rho^2 + z^2 + R_0^2)^2 - 4\rho^2 R_0^2\right]^{1/2} + z^2 + R_0^2 - \rho^2}{2z^2}\right\}\ . \qquad (3.10c)$$

Thus, any numerical difficulties which may be caused by the μ^2 in the denominator have been mitigated.

The singularity in χ_d will now be analyzed. As mentioned, there will be a zero in the denominator at $z = 0$ if $\rho \leq R_0$ as the point will lie on the source. When z is small and $\rho \leq R_0$ the integral is nearly singular. As with the finite line source, the singularity is extracted by subtracting the appropriate quantity from the numerator as

$$\chi_d(z,\rho;a) = R_0^2 \int_0^{2\pi} d\theta \int_0^1 d\omega\, \omega \frac{e^{-ar} - e^{-az}}{r} + e^{-az} I_z \ , \tag{3.11a}$$

where

$$I_z = R_0^2 \int_0^{2\pi} d\theta \int_0^1 \frac{d\omega\, \omega}{r} \ . \tag{3.11b}$$

The ω integral may be evaluated by noting that

$$\int_0^1 \frac{x\, dx}{\left(ax^2 + bx + c\right)^{1/2}} = \frac{(a + b + c)^{1/2}}{a} - \frac{c^{1/2}}{a} -$$

$$- \frac{b}{2a^{3/2}} \ln\left[\frac{2a + b + 2a^{1/2}\,(a + b + c)^{1/2}}{b + 2(ac)^{1/2}}\right] ,$$

so that after some simplification

$$I_z = \int_0^{2\pi} d\theta \left\{ s + \rho\cos\theta \ln\left[\frac{R_0 - \rho\cos\theta + s}{\left(\rho^2 + z^2\right)^{1/2} - \rho\cos\theta}\right]\right\} - 2\pi\left(\rho^2 + z^2\right)^{1/2} , \tag{3.11c}$$

where $s = \left(\rho^2 + z^2 + R_0^2 - 2\rho R_0\cos\theta\right)^{1/2}$. Applying the above analysis to the first μ integral in Eq. (3.9a) and extracting the singularity in χ_d yields

$$T_{g1} = R_0^2 \int_0^1 \frac{d\mu}{\mu^2} \left[g(c,\mu) - 1\right] \int_0^{2\pi} d\theta \int_0^1 d\omega\, \omega\, \frac{e^{-r/\mu} - e^{-z/\mu}}{r} + T_{g1z} \ , \qquad (3.12a)$$

with

$$T_{g1z} = I_z \int_0^1 \frac{d\mu}{\mu^2} e^{-z/\mu} \left[g(c,\mu) - 1\right] \ . \qquad (3.12b)$$

Thus, the singularity in χ_d has been extracted, and the μ integrals have been placed in numerically convenient forms.

3.C. Finite Isotropic Rectangular Sources

As usual, using the isotropic point source solution as a Green's function and integrating over a rectangular area, one can construct the scalar flux from such an isotropic rectangular source. The parameters in this case are shown in Fig. 3.3. It is assumed that the rectangle lies in the transverse (x-y) plane and is centered at the origin. Note that the scalar flux from this source will be symmetric about all three axes; however, the solution will vary in all three spatial dimensions. Where the finite line and disk sources are in convenient reference frames such that the spatial variation is two-dimensional when examined in cylindrical coordinates, the rectangular source can not be placed in such a convenient reference frame. The form for the scalar flux from an isotropic rectangular source is given by

$$\Psi_r(x,y,z) = \frac{1}{4\pi}\left[\frac{\partial k_0^2}{\partial c}\, \chi_r\left(x,y,z;k_0\right) + \int_0^1 \frac{d\mu}{\mu^2}\, \chi_r\left(x,y,z;\frac{1}{\mu}\right) g(c,\mu)\right] \ , \qquad (3.13a)$$

where the integrals over the surface of the source have been included in the function

$$\chi_r(x,y,z;s) = \int_{-a_0}^{a_0} dx' \int_{-b_0}^{b_0} dy' \frac{e^{-sr}}{r} , \tag{3.13b}$$

and $r^2 = (x - x')^2 + (y - y')^2 + z^2$. With the changes of variable $u = (x' + a_0)/2a_0$ and $v = (y' + b_0)/2b_0$ Eq. (3.13b) becomes

$$\chi_r(x,y,z;s) = 4a_0b_0 \int_0^1 du \int_0^1 dv \frac{e^{-sr}}{r} , \tag{3.13c}$$

where $r^2 = (x + a_0 - 2a_0u)^2 + (y + b_0 - 2b_0v)^2 + z^2$.

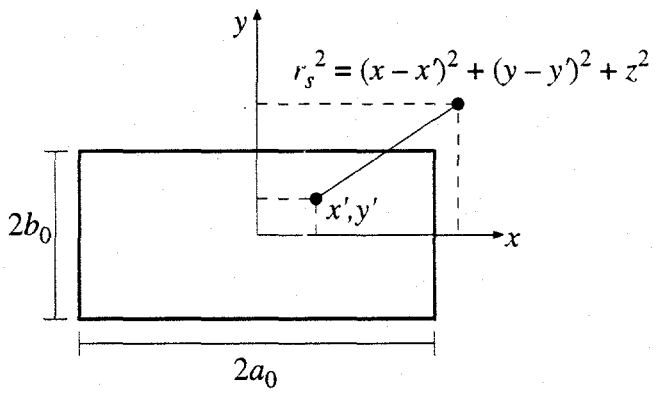

Fig. 3.3. Construction of a finite rectangular source.

As usual, when z is near zero and the point (x,y) lies within the rectangular range of the source there will be a near singularity in the integrand of χ_r as a zero in the denominator; therefore, the problem will be treated differently for these cases.

3.C.1. Scalar Flux for $|x| > a_0$ and $|y| > b_0$.

As usual, there are no true singularities if the point lies outside the source region; however, it is still desirable to place the μ integral in a numerically convenient form by subtracting 1 from $g(c,\mu)$ as this is its value at $\mu = 0$. Thus,

$$\Psi_r(x,y,z) = \frac{a_0 b_0}{\pi}\left\{\frac{\partial k_0^2}{\partial c}\chi_r\left(x,y,z;k_0\right) + \int_0^1 \frac{d\mu}{\mu^2}\,\chi_r\left(x,y,z;\frac{1}{\mu}\right)[g(c,\mu)-1]\right\} + T_{g2}\,, \qquad (3.14a)$$

where

$$T_{g2} = \int_0^1 du \int_0^1 dv\,\frac{e^{-r}}{r^2}\,. \qquad (3.14b)$$

3.C.2. Scalar Flux for $|x| \le a_0$ and $|y| \le b_0$.

With the possibility of a singularity present for the functions $\chi_r(x,y,z;s)$, there is also one for T_{g2} when the edit point is in the region of the source. Therefore, the singularity is extracted by subtracting and adding e^{-z} to the numerator in Eq. (3.14b) as

$$T_{g2} = \int_0^1 du \int_0^1 dv\,\frac{e^{-r} - e^{-z}}{r^2} + e^{-z}T_{g2z}\,, \qquad (3.15a)$$

where

$$T_{g2z} = \int_0^1 du \int_0^1 \frac{dv}{r^2}\,. \qquad (3.15b)$$

Either the u or v integral can be evaluated analytically. This yields (when the v integral is evaluated)

$$T_{g2z} = \frac{1}{2b_0}\int_0^1 \frac{du}{p}\left[\tan^{-1}\left(\frac{y + b_0}{p}\right) - \tan^{-1}\left(\frac{y - b_0}{p}\right)\right]\,, \qquad (3.16)$$

where $p^2 = (x + a_0 - 2a_0u)^2 + z^2$. In a similar fashion, the singularity in χ_r is extracted by subtracting and adding e^{-sz} to the numerator of the kernel, which produces

$$\chi_r(x,y,z;s) = 4a_0b_0 \int_0^1 du \int_0^1 dv \, \frac{e^{-sr} - e^{-sz}}{r} + e^{-sz} I_z \ , \tag{3.17}$$

with

$$I_z = \int_0^1 du \int_0^1 \frac{dv}{r} \ . \tag{3.18a}$$

As with the term T_{g2z}, the inner integral may be evaluated so that I_z becomes

$$I_z = \frac{1}{2b_0} \int_0^1 du \, \ln \left\{ \frac{\left[1 + \left(\frac{y + b_0}{p} \right)^2 \right]^{1/2} + \frac{y + b_0}{p}}{\left[1 + \left(\frac{y - b_0}{p} \right)^2 \right]^{1/2} + \frac{y - b_0}{p}} \right\} \ , \tag{3.18b}$$

and p is specified above. The term involving the μ integral and χ_r (T_{g1}) has the singularity extracted from the kernel (T_{g1z}) in the same fashion and with the same relative equations as with the isotropic disk source [see Eqs. (3.12)].

3.D. Results for the Finite Isotropic Line and Surface Sources

The numerical evaluation of the integral expressions for the scalar flux from a source requires the ability to accurately integrate functions and to properly describe the source geometry and the edit points at which the scalar flux is to be evaluated. Only basic results from the numerical evaluations of the expressions for the scalar flux from these sources will now be provided. The presentation begins with a discussion of the numerical methods used in an algorithm to generate results.

3.D.1. Numerical Methods.

The numerical methods involved in the evaluation of the scalar flux from these sources are primarily associated with the evaluation of integrals. One of the most common yet advanced means of evaluating an integral is Gauss-Legendre quadrature [Press, *et al.*]. Two variants of this integration method are used by the computer algorithm which generates the results.

3.D.1.a. Iterative Gauss-Legendre Quadrature. The iterative Gauss-Legendre quadrature routine is a relatively simple method used to calculate the value of an integral. Given a function $f(u)$, a desired relative error *error*, an initial Gauss-Legendre quadrature order N_0, an interval by which the Gauss-Legendre quadrature order is incremented N_{int}, and the limits of integration, the routine will return the value of an integral *ans*. The value of the integral is calculated at the initial quadrature order N_0 then it is recalculated at successively higher quadrature orders given by $N_0 + jN_{int}$. The relative error *relerr* for consecutive values of the integral is calculated, and only if three successive values of *relerr* are less than *error* the value is considered converged. If this does not occur before a maximum quadrature order N_{max} is reached, the last value of the integral is returned along with its relative error and an error message.

3.D.1.b. Panel Integration. Using panels, an integration scheme developed by Ganapol [priv. comm.] is similar to the iterative Gauss-Legendre scheme in that an initial quadrature order N_0, a maximum quadrature order N_{max}, and a quadrature interval N_{int} are provided. Also, the value of the integral is calculated at successive quadrature orders and the value is returned when three successive quadrature orders provide a value of the integral within the desired relative error. However, an additional input is the number of panels N_p. At each quadrature order, the integral is divided into N_p regions of equal length. Each of these regional integrals is then evaluated at the quadrature order and the sum of the

individual integrals provides the value of the original integral. The collection of quadrature weights and abscissas are considered to be a quadrature set for the original integral.

3.D.2. Tabular and Graphical Results for the Finite Line and Surface Sources.

Tables 3.1, 3.2, and 3.3 provide an error convergence analysis of the output from the finite line, finite disk, and finite rectangular sources, respectively. The scattering of the infinite medium is described by $c = 0.9$. Each source is centered at the origin and lies in the transverse plane. The line has a length of 2, the disk has a radius of 1, and the side-lengths of the rectangular source are 2×2 for the table and 3×2 for the graph in the x and y dimensions, respectively. Note in each case that the results from the lower desired relative errors is better than the desired error itself; that is, if the desired relative error is 10^{-2}, the answer may be good to 10^{-4} (assuming that the 10^{-4} answer is "correct"). This is due to requiring three successive values of the integrals to be within this error thus causing the algorithm to perform two additional sets of greater quadrature orders beyond the required one to obtain the desired error. Figures 3.4 through 3.6 display the scalar flux as a function of position 0.1 mean free paths above the sources. The source considered is clearly discernible from the shape of the scalar flux.

Each of the figures show the symmetry which is inherent in the respective sources. The scalar flux is radially symmetric and axially symmetric for the finite line source. As the scalar fluxes are displayed using Cartesian coordinates, and all sources lie in the x-y plane, it is readily apparent that the scalar flux will be symmetric with respect to the z-axis. In each case, if the source lies in the transverse plane then $\phi_i(x,y,z) = \phi_i(x,y,-z)$. For the line source, symmetry in x is described as $\phi_l(x,y,z) = \phi_l(-x,y,z)$, and likewise for the symmetry in y. The same symmetries are true of the disk and rectangular sources; however, if the transverse plane is described in polar coordinates, the disk source's scalar flux has an additional symmetry of being a function of radius only.

The final analysis concerns the scattering parameter c. Fig. 3.7 contains the scalar flux from the same finite isotropic line source used in previous studies for several values of c. Again the scalar flux is evaluated at $z = 0.1$ above the source. It is noted that the magnitude of the scalar flux does not change appreciably near the source; however, once the edit point moves away from the source the scattering properties become more evident. At large c the decrease in the scalar flux is rather slow, while for strongly absorbing media the decrease is quite rapid. Similar figures may be generated for the finite disk and rectangular sources but are not presented here.

These finite sources can be related to the sources in the last chapter by considering the behavior of the scalar fluxes when the sources become very large or small.

Table 3.1. Error Analysis for Finite Line Source.

x	$err = 10^{-2}$	$err = 10^{-3}$	$err = 10^{-4}$	$err = 10^{-5}$	$err = 10^{-6}$
0	2.613298	2.613244	2.613236	2.613232	2.613230
0.1	2.597215	2.597151	2.597142	2.597138	2.597137
0.2	2.542069	2.542018	2.542010	2.542006	2.542005
0.3	2.418634	2.418585	2.418578	2.418574	2.418573
0.4	2.128753	2.128709	2.128703	2.128700	2.128698
0.5	1.434917	1.434883	1.434878	1.434876	1.434875
0.6	0.738528	0.738504	0.738500	0.738499	0.738498
0.7	0.440736	0.440718	0.440715	0.440714	0.440714
0.8	0.303207	0.303193	0.303191	0.303190	0.303190
0.9	0.226140	0.226127	0.226126	0.226125	0.226125
1	0.177168	0.177158	0.177157	0.177156	0.177156
1.2	0.118824	0.118816	0.118816	0.118815	0.118815
1.4	0.085582	0.085576	0.085575	0.085575	0.085575
1.6	0.064380	0.064375	0.064375	0.064374	0.064374
1.8	0.049870	0.049866	0.049866	0.049866	0.049866
2	0.039454	0.039450	0.039450	0.039450	0.039450

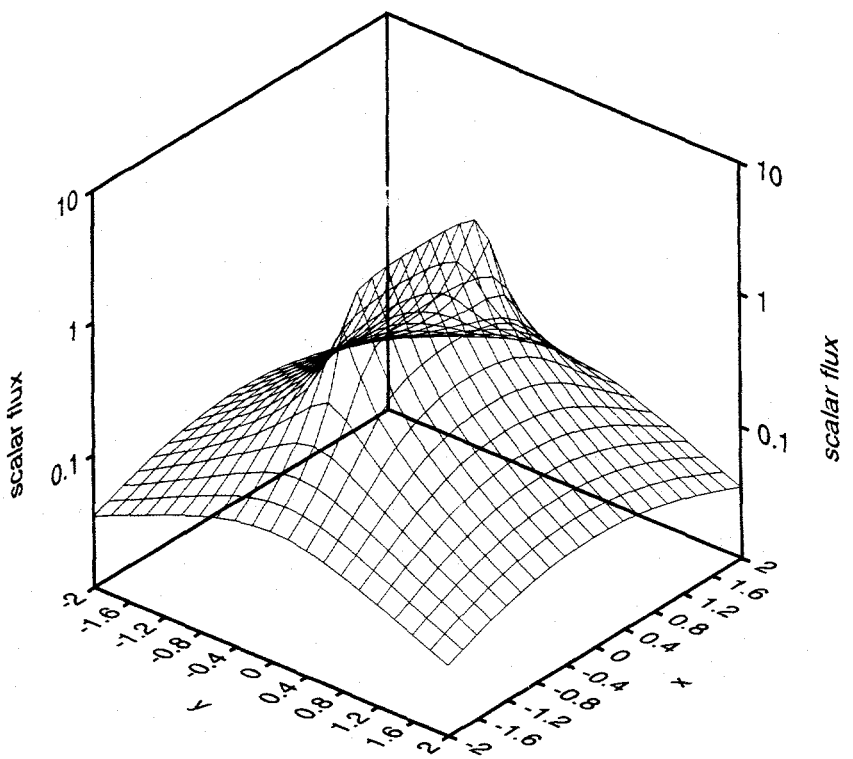

Fig. 3.4. Scalar flux at $z = 0.1$ resulting from a single isotropic line source.

Table 3.2. Error Analysis for Disk Source.

x	$err = 10^{-2}$	$err = 10^{-3}$	$err = 10^{-4}$	$err = 10^{-5}$	$err = 10^{-6}$
0	1.609829	1.609769	1.609764	1.609762	1.609762
0.1	1.605837	1.605778	1.605770	1.605769	1.605769
0.2	1.593678	1.593619	1.593611	1.593610	1.593610
0.3	1.572775	1.572719	1.572712	1.572710	1.572710
0.4	1.542054	1.541998	1.541991	1.541990	1.541989
0.5	1.499666	1.499620	1.499614	1.499613	1.499612
0.6	1.442529	1.442484	1.442478	1.442477	1.442477
0.7	1.365090	1.365067	1.365066	1.365065	1.365065
0.8	1.256601	1.256626	1.256636	1.256636	1.256636
0.9	1.094148	1.094239	1.094273	1.094276	1.094276
1	0.848130	0.848203	0.848234	0.848237	0.848238
1.2	0.465982	0.465956	0.465953	0.465953	0.465953
1.4	0.308673	0.308653	0.308651	0.308651	0.308651
1.6	0.223391	0.223375	0.223373	0.223373	0.223373
1.8	0.169387	0.169374	0.169373	0.169373	0.169373
2	0.132254	0.132243	0.132242	0.132242	0.132242

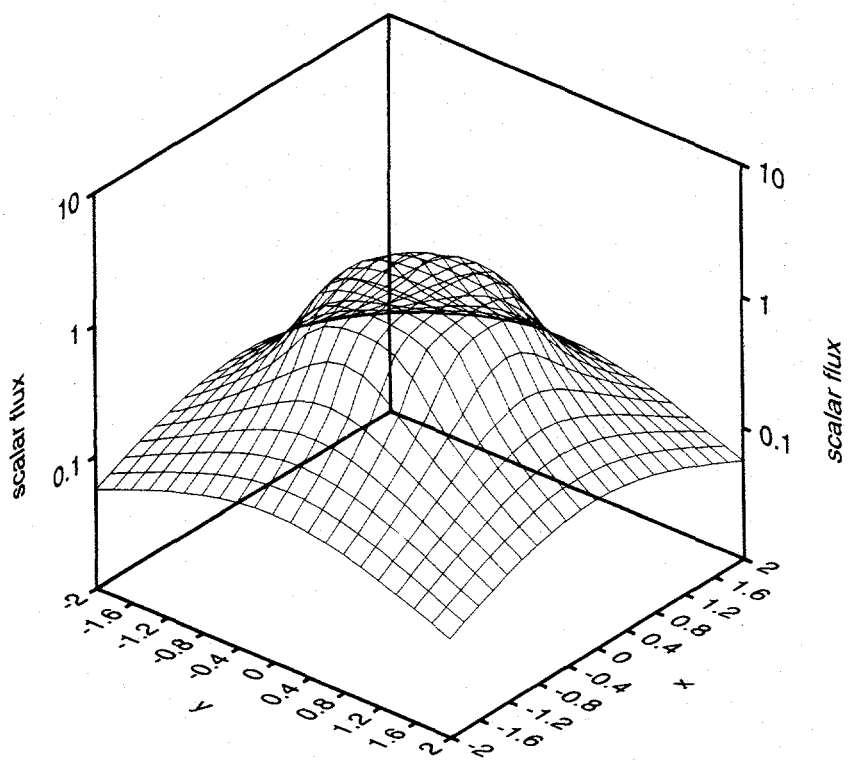

Fig. 3.5. Scalar flux at $z = 0.1$ resulting from a single isotropic disk source.

Table 3.3. Error Analysis for Finite Rectangular Source.

x	$err = 10^{-2}$	$err = 10^{-3}$	$err = 10^{-4}$	$err = 10^{-5}$	$err = 10^{-6}$
0	1.710737	1.709970	1.709856	1.709856	1.709855
0.1	1.706061	1.706309	1.706480	1.706470	1.706468
0.2	1.695915	1.696045	1.696110	1.696112	1.696110
0.3	1.675519	1.678027	1.678142	1.678150	1.678151
0.4	1.651532	1.651230	1.651415	1.651423	1.651416
0.5	1.614112	1.613969	1.613919	1.613922	1.613921
0.6	1.562586	1.562402	1.562350	1.562350	1.562349
0.7	1.490813	1.490865	1.490843	1.490854	1.490853
0.8	1.387889	1.388126	1.388133	1.388132	1.388131
0.9	1.230001	1.229974	1.229973	1.229970	1.229970
1	0.982521	0.982428	0.982421	0.982419	0.982419
1.2	0.573942	0.573905	0.573900	0.573899	0.573899
1.4	0.391059	0.391030	0.391027	0.391026	0.391026
1.6	0.286739	0.286716	0.286713	0.286713	0.286713
1.8	0.218785	0.218767	0.218765	0.218764	0.218764
2	0.171329	0.171313	0.171312	0.171312	0.171311

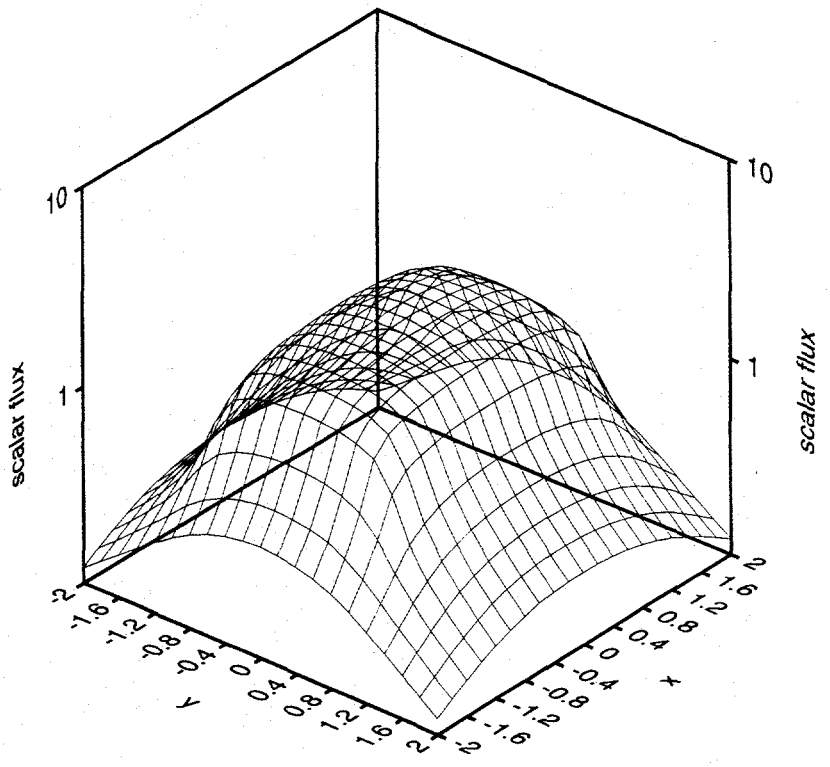

Fig. 3.6. Scalar flux at $z = 0.1$ resulting from a single isotropic rectangle source.

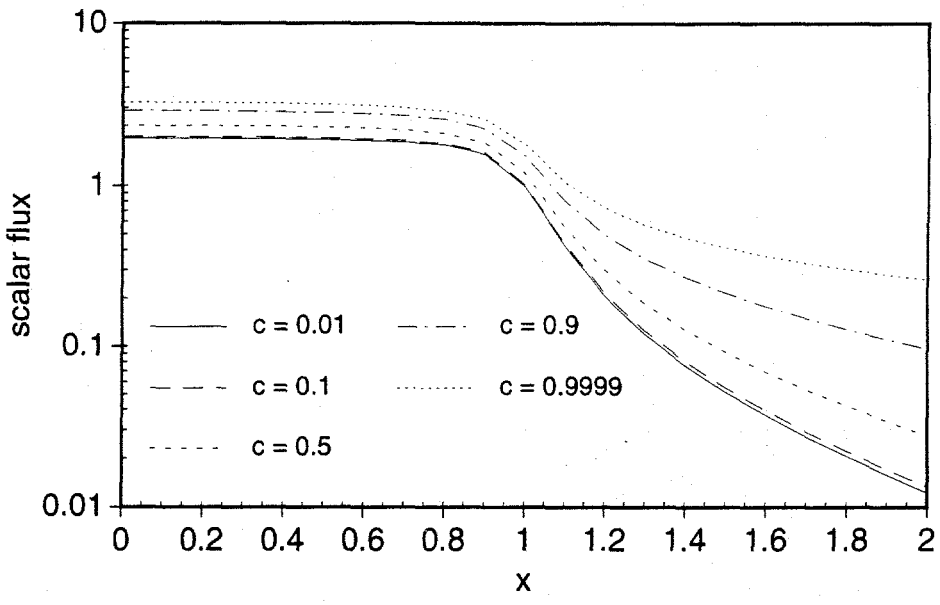

Fig. 3.7. Scalar flux at 0.1 mfp from the finite line source at several values of c.

3.D.3. Finite Sources in Large and Small Limits.

One of the numerical tests which help confirm the derived expressions for the scalar fluxes from the finite line, disk, and rectangular sources is the determination of the scalar flux in the limits of source extent. When the disk and rectangular sources (properly normalized) are large, the resultant flux should approach the flux from an infinite plane source, and when the finite line is long it should approximate an infinite line source. Conversely, when all these sources are small, the scalar flux should approach that from an isotropic point source (when the source strength is renormalized according to the physical size of the source).

Figs. 3.8, 3.9, and 3.10 contain the scalar fluxes for sources of increasingly larger extent for the finite line, disk, and rectangular sources, respectively. In each case $c = 0.9$ and the distances are measured from the center of the source in a direction normal to the source. As is evident, the fluxes quickly converge to the flux from the appropriate infinite sources.

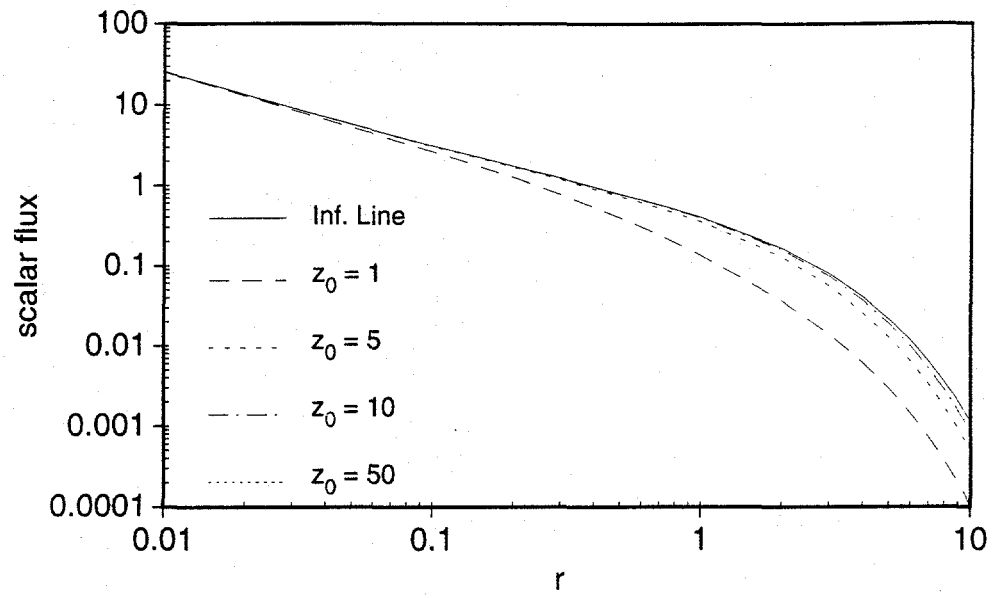

Fig. 3.8. Scalar fluxes from successively longer finite line sources.

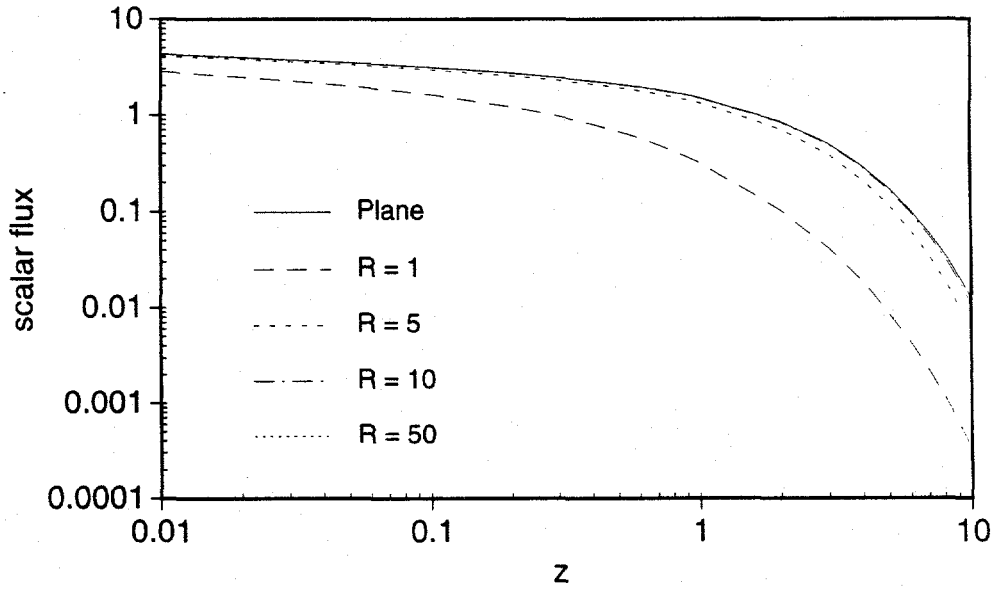

Fig. 3.9. Scalar fluxes from successively longer radii for finite disk sources.

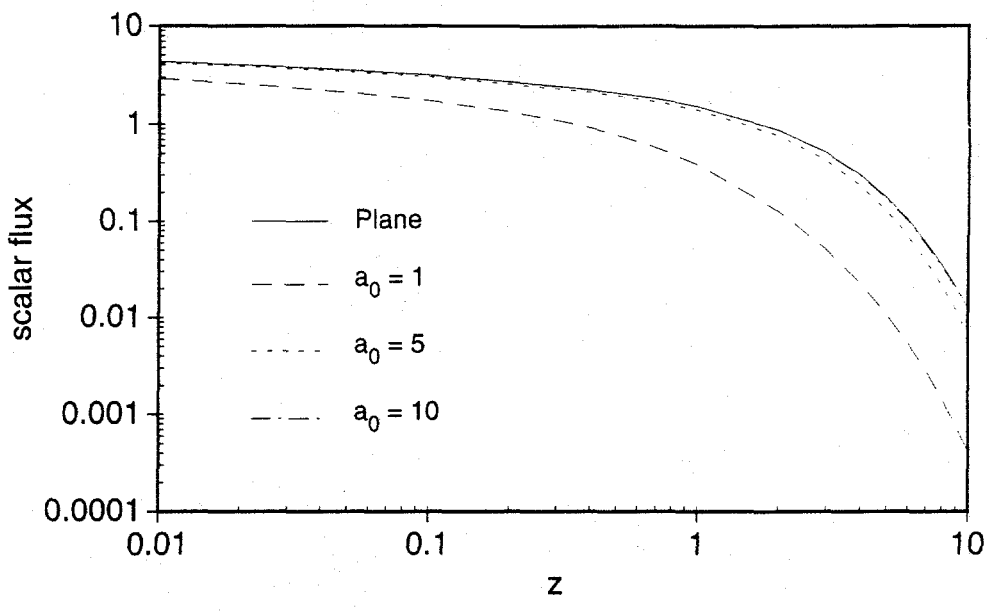

Fig. 3.10. Scalar fluxes from successively longer half-widths for finite rectangular sources.

When the finite sources are very small, the scalar flux resulting from these sources should approach the scalar flux from an isotropic point source. In the derivation of the scalar flux from the finite sources, the isotropic point source solution was integrated over a finite distance or area *without* the expression being normalized according to the size of the source. For example, the finite line source was obtained by integrating the point source solution over the finite range $[-z_0,z_0]$. To normalize the flux so that each source, regardless of size, has the same strength, the expression for the scalar flux from the finite line source would have to be divided by $2z_0$. Therefore, when the sources become exceedingly small, so do the unnormalized scalar fluxes - normalization provides a meaningful ratio with which to compare the scalar flux from the small source with that from the isotropic point source. Table 3.4 contains the scalar flux from an isotropic point source at 1 mean free path from the source. The sizes of the finite sources are characterized by a distance L_0 which corresponds to the half-length z_0, the radius R_0, and the half-width a_0 =

b_0 for the finite line, disk, and rectangular sources, respectively. The tabulated fluxes from the finite sources have been normalized (i.e. the actual scalar flux has been divided by the length or area of the source) so that the fluxes may be compared to the flux from the isotropic point source. Note that as the size of the source decreases, the normalized scalar flux does, in fact, approach the point source flux in each case.

Table 3.4. Scalar Flux Analysis for Small Finite Sources.

L_0	Point Source	Finite Line	Disk	Rectangle
1	0.143284	0.133802	0.102186	0.094609
0.1	0.143284	0.143177	0.142643	0.142431
0.01	0.143284	0.143283	0.143277	0.143275
0.001	0.143284	0.143284	0.143284	0.143284
0.0001	0.143284	0.143284	0.143284	0.143284

In the final limiting case we consider the rectangular and line sources. If one of the dimensions of the rectangular source becomes very small, the resulting scalar flux should approach that from the finite line source. In Fig. 3.11, $z_0 = a_0 = 1$ and b_0 becomes very small. Note how quickly the thin rectangular source flux approaches that from the finite line source, as expected. The mathematical limiting process in this case is easily seen by taking the limit as b_0 approaches zero in Eq. (3.13b).

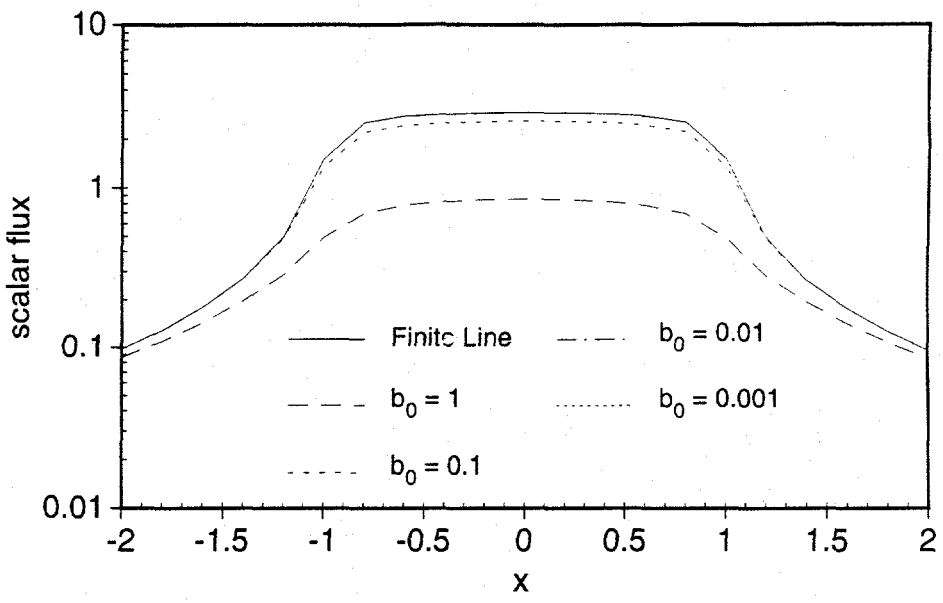

Fig. 3.11. Scalar fluxes from thin rectangular sources and a finite line source.

3.D.4. Small z, r Approximations.

In Appendix A the asymptotic scalar fluxes near isotropic point, infinite line, and infinite planar sources are derived. As the scalar fluxes from the isotropically emitting finite sources were constructed by integrating the point source solution, it is logical to assume that approximate scalar fluxes near the finite sources can be obtained by integrating the asymptotic scalar flux near an isotropic point source. This is also done in Appendix A. Figures 3.12 through 3.14 contain the scalar fluxes for the finite line, disk, and rectangular sources. In each case the characteristic length is 1 and $c = 0.9$. Note that the approximations are very accurate for each source near the center of the source. Also, for each source at the two distances nearest the source ($z = 0.01$ and $z = 0.1$), the approximate fluxes approach each other once the edit points no longer lie above the source as do the actual scalar fluxes. The approximate flux matches the trend that the scalar flux for these points near the source to be nearly the same; that is, the scalar fluxes at large r are nearly the

same for $z = 0.1$ and $z = 0.01$. However well the approximate fluxes match this trend, the values of the approximate fluxes with respect to the actual fluxes are errant.

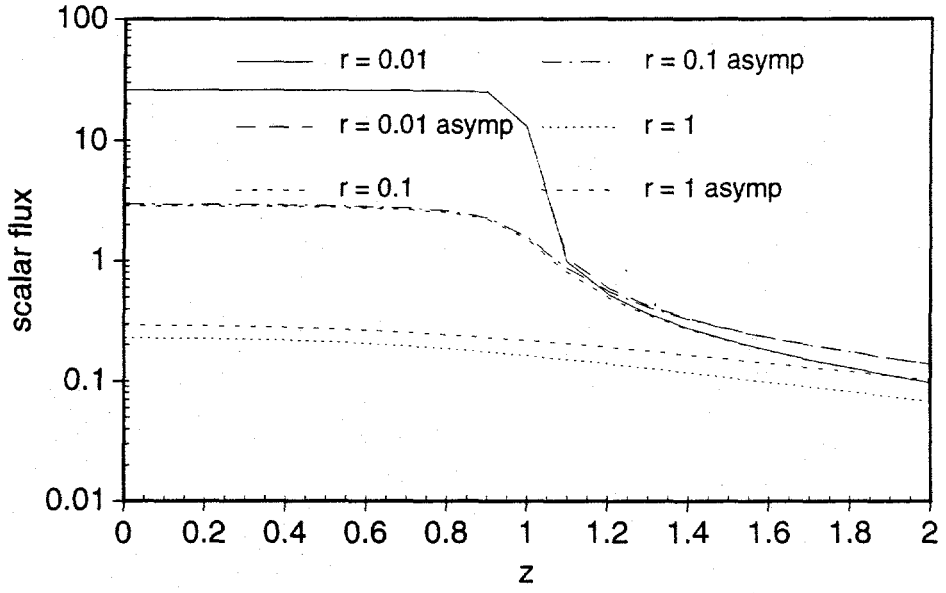

Fig. 3.12. Actual and approximate scalar fluxes from a finite line source.

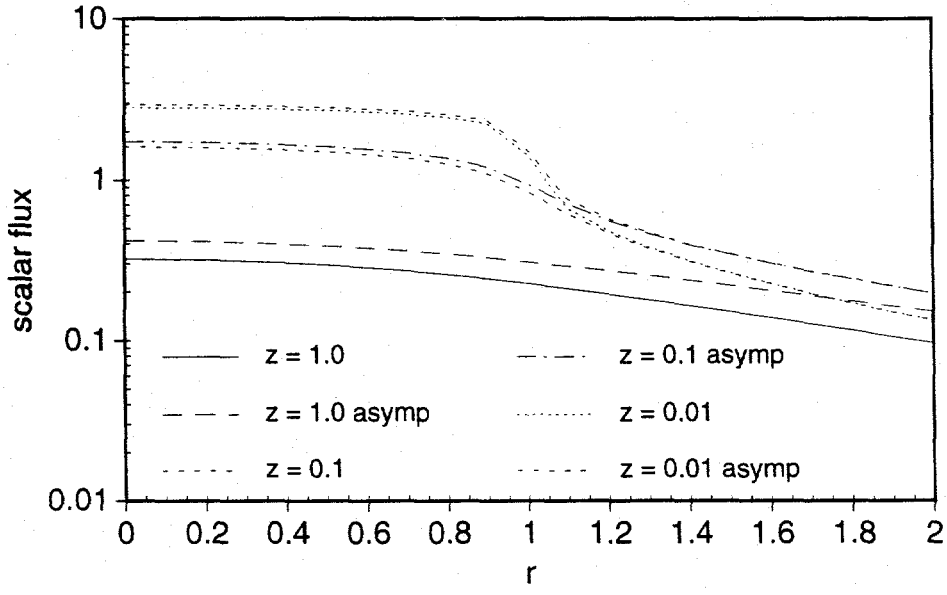

Fig. 3.13. Actual and approximate scalar fluxes from a disk source.

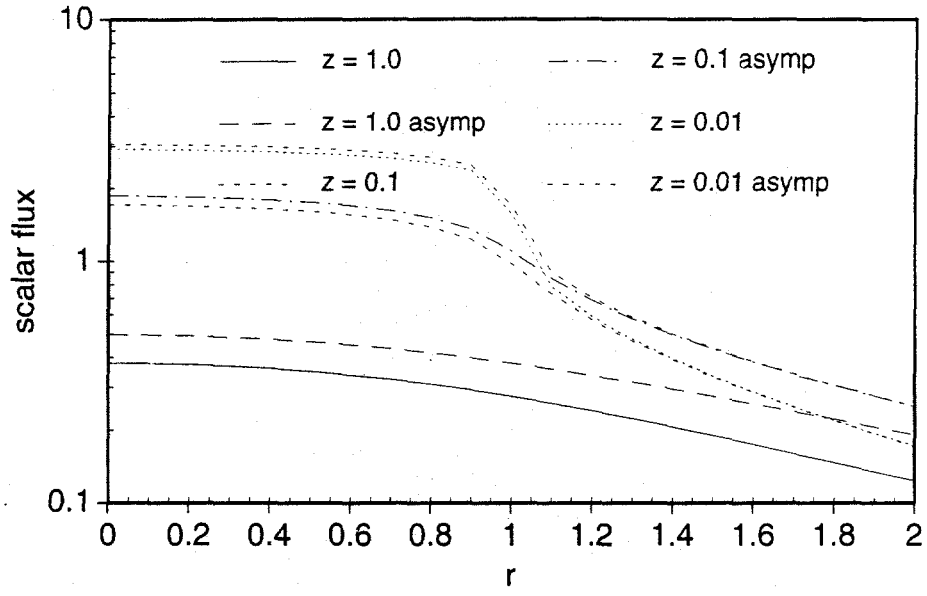

Fig. 3.14. Actual and approximate scalar fluxes from a rectangular source.

3.E. The Isotropic Slab Source in an Infinite Medium

In every case discussed thus far, the source is in some form or another spatially singular. This creates a singularity in the evaluation of the scalar flux at the point where the source resides. In order to avoid the numerical inconvenience of not being able to evaluate the scalar flux on the source, a more physically realistic source may be constructed by integrating the spatially singular source to create a spatially distributed source. One such source may be constructed by integrating the isotropic plane source solution over an interval to create a slab isotropic source. This is effectively the same as integrating the isotropic point source over a slab volume to create a simple volumetric source. Such a construction adds one more piece to the completion of Fig. 1.2 (see Fig. 1.2e below). Fig. 1.2e notes that the integration is over a finite volume, but the concept remains unaltered.

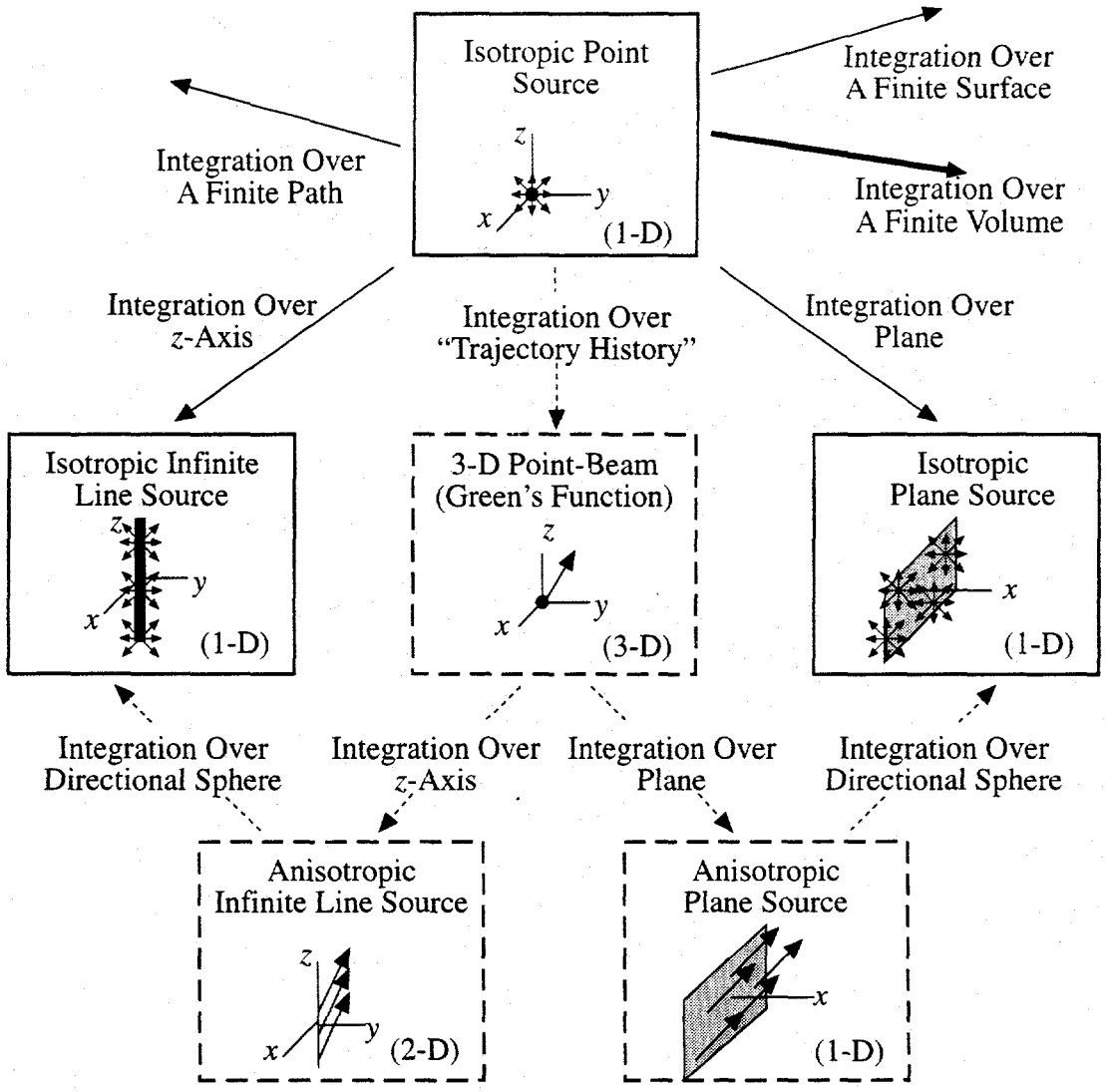

Fig. 1.2e. The sixth step in constructing the suite of infinite medium benchmarks - a volumetric source.

Physically, a source of neutral particles is now uniformly distributed in some region and is intimately mixed with the scattering material (i.e. the scattering properties within the source are identical to those of the medium). Mathematically, this source is constructed via the following equation:

$$\phi_{slab}(x) = \frac{1}{2x_0}\int_{-x_0}^{x_0} dx'\ \phi_{pl}(x - x') \quad , \tag{3.19}$$

where $\phi_{pl}(x)$ is given by Eq. (2.15). Inserting this expression and interchanging integrals yields

$$\phi_{slab}(x) = \frac{1}{2\pi x_0}\int_0^{\infty} dk\, f(k) \int_{-x_0}^{x_0} dx' \cos[k(x - x')] \ . \tag{3.20}$$

Evaluating the cosine integral and using the addition formula for the sine results in the scalar flux from an isotropic slab source at the center of an infinite medium:

$$\phi_{slab}(x) = \frac{1}{\pi x_0}\int_0^{\infty} dk \frac{f(k)}{k} \cos(kx)\ \sin(kx_0) \ . \tag{3.21}$$

The numerical evaluation of Eq. (3.21) is similar to that used for the other sources. The scalar flux resulting from an isotropically emitting slab source where $x_0 = 1$ is displayed in Fig. 3.15. The scalar flux is nearly constant inside the source region and then falls away outside the source region, as expected. As with the planar source, the scalar flux in a nearly conservative medium would be almost uniform and large. Also, examination of Eq. (3.21) shows that as x_0 approaches zero the equation for the scalar flux from an isotropic plane source is recovered. This limiting process is shown physically in Fig. 3.16 where the slab thicknesses are successively reduced and shown with the isotropic plane source solution. The scalar flux from the thin sources approaches that from the plane source, and the scalar flux from a 0.02 mfp thick source is indistinguishable from the plane source scalar flux.

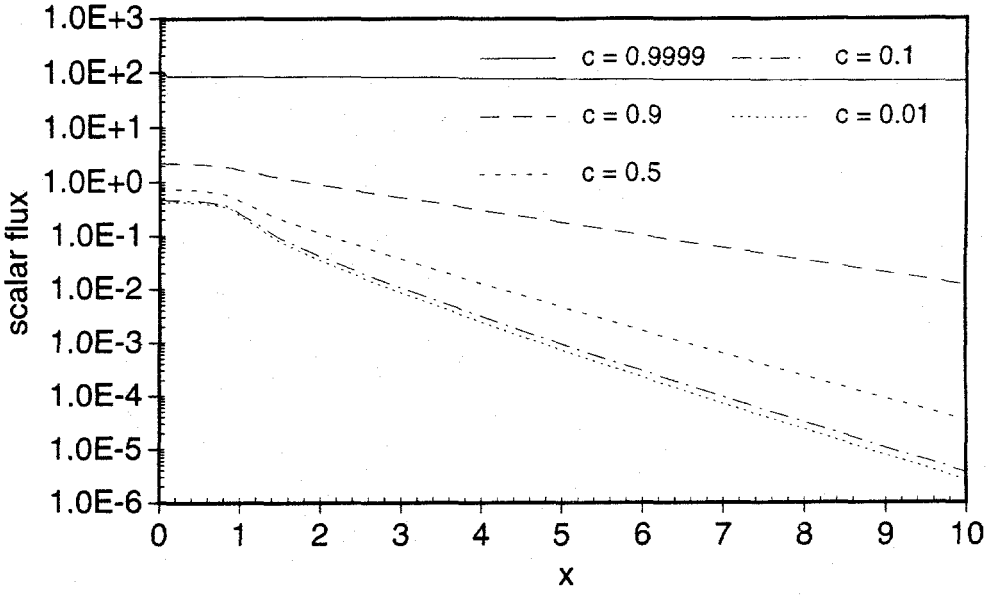

Fig. 3.15. The scalar flux from an isotropic slab source as a function of position for several values of *c*.

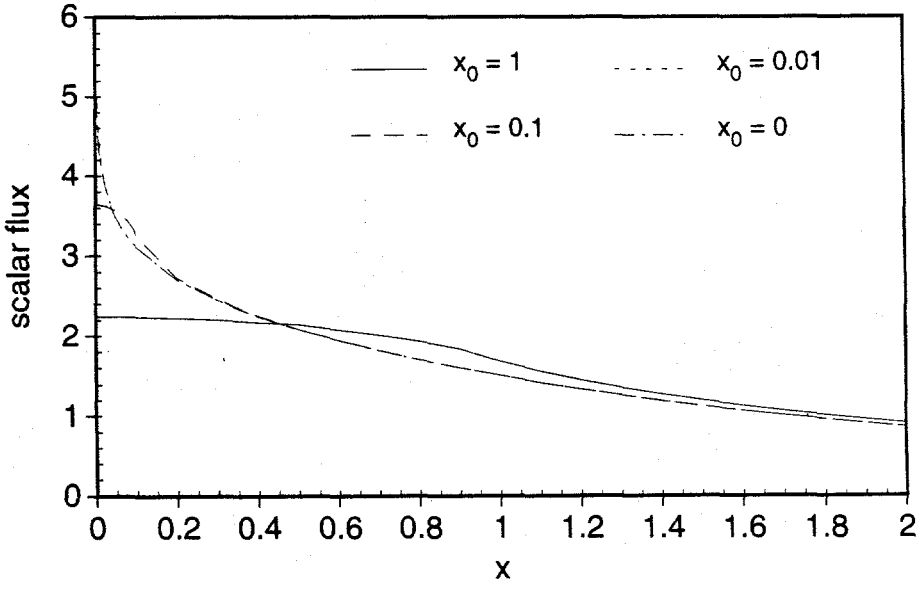

Fig. 3.16. The scalar flux from thin isotropic slab sources as a function of position for several thicknesses.

With the suite of benchmarks fairly complete with respect to sources which emit particles isotropically, the next level of complexity is to consider those sources which emit particles anisotropically. The most basic such source is the Green's function (or point-beam) source. Although this source may be thought of as the most basic source in infinite homogeneous transport theory (see Fig. 1.1), it will be found that the flux from this "most basic" source may be expressed in terms of the flux from the isotropic point source (see Fig. 1.2).

CHAPTER 4: THE INFINITE MEDIUM GREEN'S FUNCTION

One of the most fundamental problems in neutral particle transport theory is an anisotropically emitting point source located at the center of an infinite homogeneous medium which scatters particles isotropically. The source is thus described by spatial and angular delta functions. It will be shown in this chapter that the scalar flux from this Green's function source may be derived from that of the isotropic point source. This additional piece of Fig 1.2 is displayed below in Fig. 1.2f. Then the Green's function source will be used to construct the solution from the anisotropic plane source.

4.A. Simplification of the Transport Equation

Because the methods used to determine the scalar flux from the Green's function source are used for other sources, a more extensive explanation of the mathematics involved will be presented, including the standard simplifications of the transport equation that are usually done.

Beginning with a general form of the linear transport equation (time-dependent, continuous energy, arbitrary scattering, homogeneous medium, general source)

$$\left[\frac{1}{v}\frac{\partial}{\partial t} + \vec{\Omega}\cdot\nabla + \Sigma_t(E)\right]\phi(\vec{r},E,\vec{\Omega},t) =$$

$$= \int_{4\pi} d\vec{\Omega}' \int_0^\infty dE'\, \Sigma_s(\vec{\Omega}'\rightarrow\vec{\Omega},E'\rightarrow E)\, \phi(\vec{r},E',\vec{\Omega}',t) + S(\vec{r},E,\vec{\Omega},t) \quad , \tag{4.1}$$

where

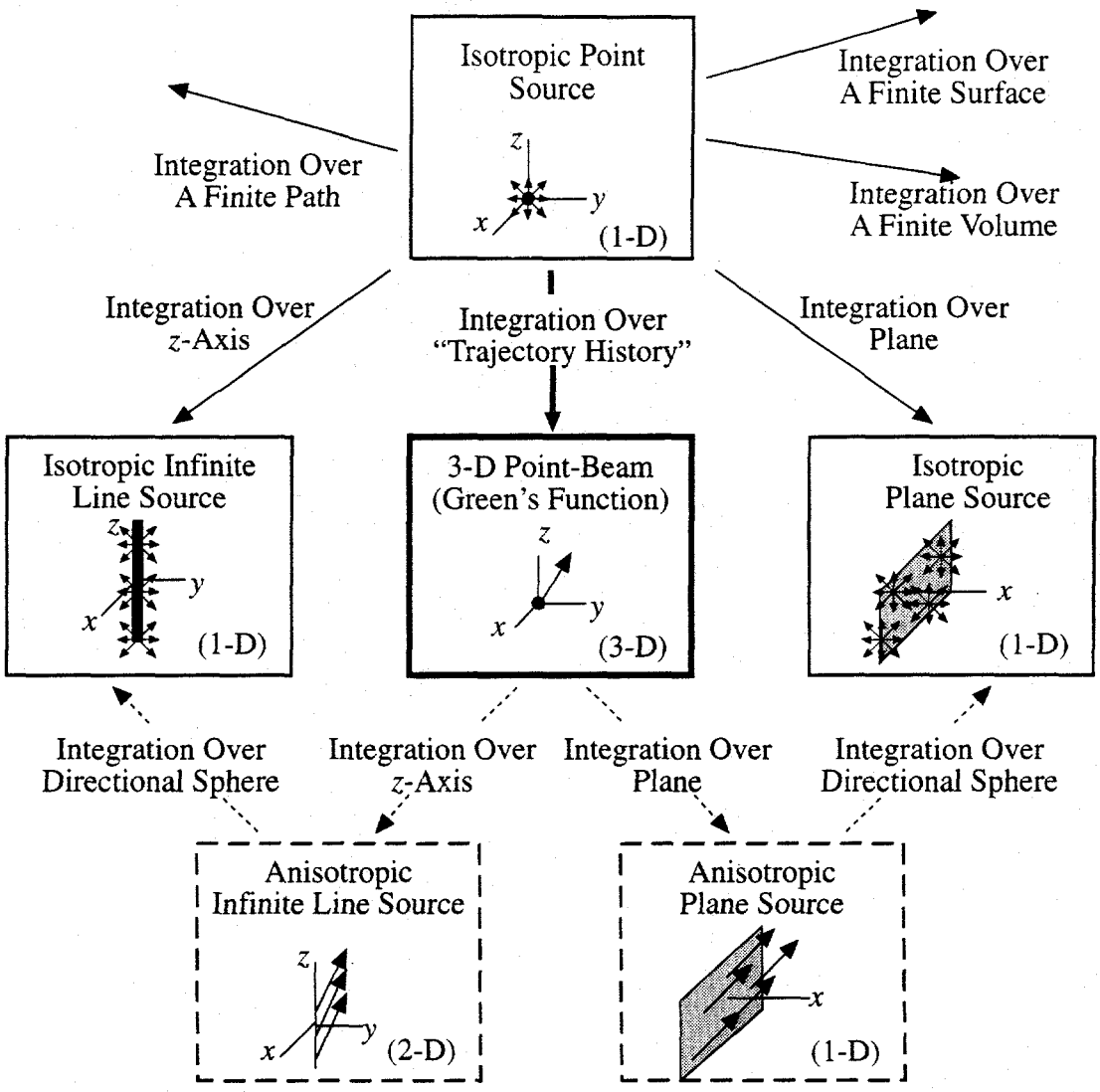

Fig. 1.2f. The seventh step in constructing the suite of infinite medium benchmarks - the Green's function source.

$\phi(\vec{r},E,\vec{\Omega},t)$ = neutron flux [neutrons/m^2-ster-MeV-sec],

$\Sigma_t(E)$ = total macroscopic cross section [1/m],

$\Sigma_s(\vec{\Omega}'\rightarrow\vec{\Omega},E'\rightarrow E)$ = differential scattering macroscopic cross section [1/m-ster-MeV],

$S(\vec{r},E,\vec{\Omega},t)$ = external neutron source strength [neutrons/m^3-ster-MeV-sec],

$\vec{\Omega}$ = solid angle direction [steradians],

v = neutron speed [m/sec],

and with boundary conditions that the flux remains finite everywhere, the first simplifications are to assume a stationary system and monoenergetic scattering. This produces

$$\left[\vec{\Omega}\cdot\nabla + \Sigma_t\right]\phi(\vec{r},\vec{\Omega}) = \int_{4\pi} d\vec{\Omega}'\,\Sigma_s(\vec{\Omega}'\rightarrow\vec{\Omega})\,\phi(\vec{r},\vec{\Omega}') + S(\vec{r},\vec{\Omega}) \quad , \tag{4.2a}$$

where

$$\phi(\vec{r},\vec{\Omega}) \equiv \int_0^\infty dE\,\phi(\vec{r},E,\vec{\Omega}) \quad , \tag{4.2b}$$

$$\Sigma_s(\vec{\Omega}'\rightarrow\vec{\Omega},E'\rightarrow E) \equiv \Sigma_s(\vec{\Omega}'\rightarrow\vec{\Omega})\,\delta(E'-E) \quad , \tag{4.2c}$$

$$S(\vec{r},\vec{\Omega}) \equiv \int_0^\infty dE\,S(\vec{r},E,\vec{\Omega}) \quad . \tag{4.2d}$$

The second simplification is to assume a medium which scatters neutral particles isotropically in the laboratory reference frame, i.e. $\Sigma_s(\vec{\Omega}'\rightarrow\vec{\Omega}) = \Sigma_s/4\pi$, which yields

$$\left[\vec{\Omega}\cdot\nabla + \Sigma_t\right]\phi(\vec{r},\vec{\Omega}) = \frac{\Sigma_s}{4\pi}\int_{4\pi} d\vec{\Omega}'\,\phi(\vec{r},\vec{\Omega}') + S(\vec{r},\vec{\Omega}) \quad . \tag{4.3}$$

With some foresight regarding the most convenient coordinate system in which to place the point-beam source, the spatial gradient is specified in cylindrical coordinates via a longitudinal dimension (z) and a transverse plane vector [$\vec{\rho} = \vec{\rho}(\rho,\alpha)$]. Therefore,

$$\nabla = \frac{\partial}{\partial z}\hat{z} + \frac{\partial}{\partial \vec{\rho}}\hat{\rho} \quad , \quad \vec{\Omega} = \cos\theta\,\hat{z} + \vec{\omega}$$

where (being careful to distinguish between the flux ϕ and the angle ϕ)

$$\vec{\omega} = \sin\theta\cos\phi\,\hat{x} + \sin\theta\sin\phi\,\hat{y} = (1-\mu^2)^{1/2}[\cos\phi\,\hat{x} + \sin\phi\,\hat{y}]$$

and the transport equation becomes

$$\left[\mu\frac{\partial}{\partial z} + \vec{\omega}\cdot\frac{\partial}{\partial \vec{\rho}} + \Sigma_t\right]\phi(z,\vec{\rho},\vec{\Omega}) = \frac{\Sigma_s}{4\pi}\int_{4\pi} d\vec{\Omega}'\,\phi(z,\vec{\rho},\vec{\Omega}') + S(z,\vec{\rho},\vec{\Omega}) \quad , \tag{4.4}$$

where $\mu = \cos\theta$. Specifying the source as one which exists at the center of this infinite medium ($\rho = 0$, $z = 0$) and emits neutral particles in the direction $\vec{\Omega}_0(\mu_0,\phi_0)$ produces the following simplified transport equation:

$$\left[\mu\frac{\partial}{\partial z} + \vec{\omega}\cdot\frac{\partial}{\partial \vec{\rho}} + \Sigma_t\right]\phi(z,\vec{\rho},\vec{\Omega}) = \frac{\Sigma_s}{4\pi}\int_{4\pi} d\vec{\Omega}'\,\phi(z,\vec{\rho},\vec{\Omega}') +$$

$$+ \frac{\delta(\rho)}{2\pi\rho}\delta(z)\delta(\mu-\mu_0)\delta(\phi-\phi_0) \quad . \tag{4.5}$$

The spatial variables are non-dimensionalized according to the total cross section so that all distances are in mean free paths ($z^* = \Sigma_t z$, $\rho^* = \Sigma_t \rho$). Dropping the asterisks and dividing by the total cross section produces the final form of the simplified transport equation for a point-beam source at the center of an infinite medium:

$$\left[\mu\frac{\partial}{\partial z} + \vec{\omega}\cdot\frac{\partial}{\partial \vec{\rho}} + 1\right]\phi(z,\vec{\rho},\vec{\Omega}) = \frac{c}{4\pi}\int_{4\pi} d\vec{\Omega}'\,\phi(z,\vec{\rho},\vec{\Omega}') +$$

$$+ \frac{\delta(\rho)}{2\pi\rho}\delta(\mu-\mu_0)\delta(\phi-\phi_0)\delta(z) \quad , \tag{4.6a}$$

where $c = \Sigma_s/\Sigma_t$ (interpreted as the mean number of secondary neutrons produced per collision) and the boundary conditions are specified as

$$\lim_{|z|\to\infty}\phi(z,\vec{\rho},\vec{\Omega}) < \infty \quad , \quad \lim_{|\vec{\rho}|\to\infty}\phi(z,\vec{\rho},\vec{\Omega}) < \infty \quad . \tag{4.6b}$$

4.B. The Transformed Equation

The solution method begins by taking a two-dimensional Fourier transform in the transverse plane. It then proceeds to integral transport theory to provide an integral equation for the transformed angular flux, which is then integrated to give the transformed scalar flux.

4.B.1. Fourier Transform in the Transverse Plane.

Multiplying Eq. (4.6a) by $e^{i\vec{k}\cdot\vec{\rho}}$, where the transformed variable is $\vec{k} = \vec{k}(k,\psi)$ (see Fig. 4.1), and integrating over the entire transverse plane yields

$$\left[\mu\frac{\partial}{\partial z} + u(\vec{\Omega},\vec{k})\right] \bar{\Psi}(z,\vec{\Omega};\vec{k}) = \frac{c}{4\pi}\int_{4\pi} d\vec{\Omega}\,' \; \bar{\Psi}(z,\vec{\Omega}';\vec{k}) +$$

$$+\delta(\mu-\mu_0)\delta(\phi-\phi_0)\delta(z) \quad , \tag{4.7a}$$

where the Fourier transform pair is defined as

$$\bar{\Psi}(z,\vec{\Omega};\vec{k}) \equiv \int d\vec{\rho}\; e^{i\vec{k}\cdot\vec{\rho}}\; \phi(z,\vec{\rho},\vec{\Omega}) \quad , \tag{4.7b}$$

$$\phi(z,\vec{\rho},\vec{\Omega}) \equiv \frac{1}{(2\pi)^2}\int d\vec{k}\; e^{-i\vec{k}\cdot\vec{\rho}}\; \bar{\Psi}(z,\vec{\Omega};\vec{k}) \quad , \tag{4.7c}$$

and

$$u(\vec{\Omega},\vec{k}) = 1 - ik\left(1-\mu^2\right)^{1/2}\cos(\phi-\psi) \quad . \tag{4.7d}$$

The application of the transform and the result are obvious except for the definition of $u(\vec{\Omega},\vec{k})$. As usual when using the Fourier transform, the transform of a derivative produces the transformed function times a factor $-i\vec{k}$ (the sign of the factor depends on the

sign chosen on the exponential's argument in the transform). Thus, $u(\vec{\Omega},\vec{k}) = 1 - i\vec{k} \cdot \vec{\omega}$, where

$$\vec{k} = k\cos\psi\,\hat{\imath} + k\sin\psi\,\hat{\jmath} \quad .$$

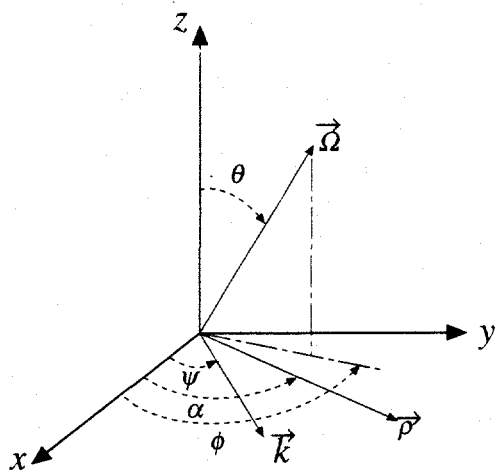

Fig. 4.1. Coordinate and vector systems definitions for transformed and real spaces.

4.B.2. Formation of Integral Equation.

The Fourier transformed equation (4.7a) is still in an integro-differential form. This equation may be transformed into an integral equation by integrating Eq. (4.7a) along the particle trajectory. For the case where $\mu > 0$, the trajectory extends from $-\infty$ to z. Using the integrating factor $e^{uz/\mu}$, we find

$$\frac{d}{dz}\left[e^{uz/\mu}\,\bar{\Psi}(z,\vec{\Omega};\vec{k})\right] = \frac{c}{4\pi\mu}e^{uz/\mu}\int_{4\pi} d\vec{\Omega}\,'\;\bar{\Psi}(z,\vec{\Omega}';\vec{k}) +$$

$$+ e^{uz/\mu}\frac{\delta(\mu-\mu_0)}{\mu}\delta(\phi-\phi_0)\delta(z) \quad , \tag{4.8}$$

which upon integrating over the range $(-\infty,z]$ yields

$$\bar{\Psi}(z,\vec{\Omega};\vec{k}) = \frac{c}{4\pi\mu}\int_{-\infty}^{z} dz'\, e^{u(z'-z)/\mu}\ \bar{\Psi}(z';\vec{k}) +$$

$$+\frac{1}{\mu_0}\delta(\mu-\mu_0)\delta(\phi-\phi_0)e^{-uz/\mu} \quad , \ \mu>0 \tag{4.9a}$$

where the transformed scalar flux is given by

$$\bar{\Psi}(z;\vec{k}) = \int_{4\pi} d\vec{\Omega}\,'\ \bar{\Psi}(z,\vec{\Omega}';\vec{k}) \ .$$

Since it is assumed that $\mu_0 > 0$, there is no source (other than the scattering term) for the case where $\mu < 0$. Thus, upon using a similar analysis as above,

$$\bar{\Psi}(z,\vec{\Omega};\vec{k}) = -\frac{c}{4\pi\mu}\int_{z}^{\infty} dz'\, e^{u(z'-z)/\mu}\ \bar{\Psi}(z';\vec{k}) \quad , \ \mu<0 \ . \tag{4.9b}$$

4.B.3. The Transformed Scalar Flux.

To obtain the transformed scalar flux, the transformed angular flux is integrated over the unit sphere as shown previously:

$$\bar{\Psi}(z;\vec{k}) = \int_{4\pi} d\vec{\Omega}\ \ \bar{\Psi}(z,\vec{\Omega};\vec{k}) = \int_0^{2\pi} d\phi \int_{-1}^{1} d\mu\ \bar{\Psi}(z,\mu,\phi;\vec{k}) \ . \tag{4.10a}$$

By separating the μ integration into two integrals over positive and negative ranges and making a simple change of variable in the integral over negative μ, there results

$$\bar{\Psi}(z;\vec{k}) = \int_0^1 d\mu \int_0^{2\pi} d\phi\ \bar{\Psi}(z,\mu,\phi;\vec{k}) + \int_0^1 d\mu \int_0^{2\pi} d\phi\ \bar{\Psi}(z,-\mu,\phi;\vec{k}) \ . \tag{4.10b}$$

Letting $\mu \to -\mu$ in Eq. (4.9b) and inserting Eqs. (4.9) into Eq. (4.10b) yields

$$\bar{\Psi}(z;\vec{k}) = \frac{e^{-u_0 z/\mu_0}}{\mu_0} + \int_0^1 d\mu \int_0^{2\pi} d\phi\ \frac{c}{4\pi\mu}\int_{-\infty}^{z} dz'\, e^{u(z'-z)/\mu}\ \bar{\Psi}(z';\vec{k}) +$$

$$+ \int_0^1 d\mu \int_0^{2\pi} d\phi \, \frac{c}{4\pi\mu} \int_z^{\infty} dz' \, e^{-u(z'-z)/\mu} \, \bar{\Psi}(z';\vec{k}) \quad . \tag{4.11}$$

Note that in the first integral $z > z'$ and in the second integral $z < z'$ so that Eq. (4.11) may be rewritten as (with some rearrangement of integrals and factors)

$$\bar{\Psi}(z;\vec{k}) = \frac{e^{-u_0 z/\mu_0}}{\mu_0} + \frac{c}{4\pi} \int_{-\infty}^{z} dz' \, \bar{\Psi}(z';\vec{k}) \int_0^1 \frac{d\mu}{\mu} \int_0^{2\pi} d\phi \; e^{-u|z-z'|/\mu} +$$

$$+ \frac{c}{4\pi} \int_z^{\infty} dz' \, \bar{\Psi}(z';\vec{k}) \int_0^1 \frac{d\mu}{\mu} \int_0^{2\pi} d\phi \; e^{-u|z-z'|/\mu} \quad . \tag{4.12}$$

The above two integrals may now be combined to produce

$$\bar{\Psi}(z;\vec{k}) = \frac{e^{-z/U_0}}{|\mu_0|} \theta\left(\frac{z}{\mu_0}\right) + \frac{c}{2} \int_{-\infty}^{\infty} dz' \, K(|z-z'|) \bar{\Psi}(z';\vec{k}) \quad , \tag{4.13a}$$

where the absolute value signs and step-function $\theta(u)$ have been added to allow for μ_0 positive or negative and the kernel $K(z;\vec{k})$ is stated as

$$K(z;\vec{k}) = \frac{1}{2\pi} \int_0^1 \frac{d\mu}{\mu} \int_0^{2\pi} d\phi \; e^{-z/U} \quad , \quad z > 0 \tag{4.13b}$$

with

$$U \equiv \frac{\mu}{u(\vec{\Omega},\vec{k})} \quad . \tag{4.13c}$$

4.B.4. Alternative Expression for $K(z;\vec{k})$.

The kernel $K(z;\vec{k})$ may be reformulated using a Bessel function transformation so that a more convenient alternative form may be obtained. Substituting the expression for $u(\vec{\Omega},\vec{k})$ into Eq. (4.13b) produces

$$K(z;\vec{k}) = \int_0^1 \frac{d\mu}{\mu} \frac{1}{2\pi} \int_0^{2\pi} d\phi \; e^{-z[1 - ik(1-\mu^2)^{1/2}\cos(\phi-\psi)]/\mu} \quad , \tag{4.14a}$$

or by extracting the portion of the exponential which does not depend on ϕ,

$$K(z;\vec{k}) = \int_0^1 \frac{d\mu}{\mu} e^{-z/\mu} \frac{1}{2\pi} \int_0^{2\pi} d\phi \; e^{-zik(1-\mu^2)^{1/2}\cos(\phi-\psi)/\mu} \quad . \tag{4.14b}$$

Because the ϕ integral covers the full period of the cosine, the definition of the zeroth-order Bessel function

$$J_0(x) = \frac{1}{2\pi} \int_0^{2\pi} d\phi \; e^{\pm ix\cos\phi}$$

may be used so that $K(z;\vec{k})$ is seen to be

$$K(z;\vec{k}) = \int_0^1 \frac{d\mu}{\mu} e^{-z/\mu} J_0\left[\frac{zk}{\mu}(1 - \mu^2)^{1/2}\right] \quad . \tag{4.15}$$

Given the following formula for the Laplace transform of the Bessel function [Abramowitz and Stegun]

$$\mathcal{L}_s\left\{ J_0\left[a(t^2 - k^2)^{1/2}\right] u(t-k) \right\} = \frac{e^{-k(s^2+a^2)^{1/2}}}{(s^2 + a^2)^{1/2}} \quad , \quad k \geq 0 \quad , \tag{4.16a}$$

it then follows that

$$\int_1^\infty dt \; e^{-st} J_0\left[\eta(t^2 - 1)^{1/2}\right] = \frac{e^{-(s^2+\eta^2)^{1/2}}}{(s^2 + \eta^2)^{1/2}} \quad , \tag{4.16b}$$

where $k = 1$ and a is replaced by η. Integrating this expression with respect to s over the range $[z,\infty)$ yields

$$\int_1^\infty \frac{dt}{t} e^{-zt} J_0\left[\eta(t^2 - 1)^{1/2}\right] = \int_z^\infty ds \; \frac{e^{-(s^2+\eta^2)^{1/2}}}{(s^2 + \eta^2)^{1/2}} \quad , \tag{4.16c}$$

and by letting $t = 1/\mu$, the integral on the left becomes

$$\int_1^\infty \frac{dt}{t} e^{-zt} J_0\left[\eta\left(t^2 - 1\right)^{1/2}\right] = \int_0^1 \frac{d\mu}{\mu} e^{-z/\mu} J_0\left[\frac{\eta}{\mu}\left(1 - \mu^2\right)^{1/2}\right] , \qquad (4.16d)$$

which is immediately seen to be $K(z;\vec{k})$ when $\eta = zk$. Therefore, an alternative expression for $K(z;\vec{k})$ is

$$K(z;\vec{k}) = \int_z^\infty ds \frac{e^{-z(k^2+s^2/z^2)^{1/2}}}{z\left(k^2 + s^2/z^2\right)^{1/2}} , \qquad (4.17a)$$

which, when $s = z/\mu$, yields the final expression for $K(z;\vec{k})$:

$$K(z;\vec{k}) = \int_0^1 \frac{d\mu}{\mu} \frac{e^{-z(1-k^2\mu^2)^{1/2}/\mu}}{\left(1 + k^2\mu^2\right)^{1/2}} . \qquad (4.17b)$$

This alternative expression for $K(z;\vec{k})$ will allow the establishment of a pseudo problem to facilitate the scalar flux solution.

4.C. The Pseudo Problem

The solution of Eq. (4.5a) is relatively complicated as the mathematics involve an integral equation which contain a kernel which is itself an integral. However, transport problems similar to this one have been found to be variants of a one-dimensional "pseudo problem" as proposed by Williams [1982]. He introduces a fictitious (pseudo) function $\tilde{\phi}(z,\mu)$ which satisfies the one-dimensional transport equation with a generalized form of the direction and total cross section. When this fictitious function is integrated over μ (thus obtaining a pseudo scalar flux) and the generalized direction and cross section have a specific form an equivalence of the pseudo and direct problems is obtained.

4.C.1. Integral Equation for the Pseudo Scalar Flux.

The pseudo transport equation is written as

$$\left[\mu a(\mu)\frac{\partial}{\partial z} + b(\mu)\right] \tilde{\phi}(z,\mu;\mu^*) = \frac{c}{2}\int_{-1}^{1} d\mu' \, \tilde{\phi}(z,\mu';\mu^*) + \delta(\mu - \mu^*)\delta(z) \quad , \tag{4.18}$$

where the pseudo flux satisfies infinite medium boundary conditions and $a(\mu)$ and $b(\mu)$ are yet to be specified. Proceeding as before, the integral form of Eq. (4.18) is derived, and then the scalar flux is obtained by integrating over μ. The integrating factor is easily seen from Eq. (4.18) to be $e^{zb(\mu)/\mu a(\mu)}$, and upon integrating along the particle trajectory for both $\mu > 0$ and $\mu < 0$ there results

$$\tilde{\phi}(z,\mu;\mu^*) = \frac{\delta(\mu - \mu^*)}{\mu^* a(\mu^*)} e^{-zb(\mu)/\mu a(\mu)} +$$

$$+ \frac{c}{2\mu a(\mu)}\int_{-\infty}^{z} dz' \, e^{(z'-z)b(\mu)/\mu a(\mu)} \, \tilde{\phi}(z';\mu^*) \quad , \quad \mu > 0 \quad ; \tag{4.19a}$$

$$\tilde{\phi}(z,\mu;\mu^*) = \frac{c}{2\mu a(\mu)}\int_{\infty}^{z} dz' \, e^{(z'-z)b(\mu)/\mu a(\mu)} \, \tilde{\phi}(z';\mu^*) \quad , \quad \mu < 0 \quad , \tag{4.19b}$$

where the pseudo scalar flux is defined as

$$\tilde{\phi}(z;\mu^*) \equiv \int_{-1}^{1} d\mu \, \tilde{\phi}(z,\mu;\mu^*) = \int_{0}^{1} d\mu \, \tilde{\phi}(z,\mu;\mu^*) + \int_{0}^{1} d\mu \, \tilde{\phi}(z,-\mu;\mu^*) \quad . \tag{4.20}$$

As with the previous procedures, upon substituting Eqs. (4.19) into Eq. (4.20), with the change of variable that $\mu \to -\mu$ in Eq. (4.19b), there results

$$\tilde{\phi}(z;\mu^*) = \frac{e^{-z/\xi^*}}{\mu^* a(\mu^*)} + \frac{c}{2}\int_{0}^{1} \frac{d\mu}{\mu a(\mu)} \int_{-\infty}^{z} dz' \, e^{(z'-z)/\xi} \, \tilde{\phi}(z';\mu^*) +$$

$$+ \frac{c}{2}\int_{0}^{1} \frac{d\mu}{\mu a(\mu)} \int_{z}^{\infty} dz' \, e^{-(z'-z)/\xi} \, \tilde{\phi}(z';\mu^*) \quad ,$$

or

$$\tilde{\phi}(z;\mu^*) = \frac{e^{-z/\xi^*}}{\mu^* a(\mu^*)} + \frac{c}{2}\int_0^1 \frac{d\mu}{\mu a(\mu)} \int_{-\infty}^{\infty} dz'\, e^{|z-z'|/\xi}\, \tilde{\phi}(z';\mu^*) \quad , \tag{4.21a}$$

where

$$\xi(\mu) \equiv \frac{\mu a(\mu)}{b(\mu)} \quad , \quad \xi^* = \xi(\mu^*) \quad . \tag{4.21b}$$

Multiplying Eq. (4.21a) by $a(\mu^*)$, defining $\phi(z;\mu^*) \equiv a(\mu^*)\tilde{\phi}(z;\mu^*)$, rearranging the integral, and allowing for all values of μ^*(via the absolute value signs and the step function) produces the final form for the pseudo scalar flux:

$$\phi(z;\mu^*) = \frac{e^{-z/\xi^*}}{|\mu^*|}\theta\left(\frac{z}{\mu^*}\right) + \frac{c}{2}\int_{-\infty}^{\infty} dz'\, \tilde{K}(|z - z'|)\phi(z';\mu^*) \quad , \tag{4.21c}$$

where

$$\tilde{K}(z) = \int_0^1 \frac{d\mu}{\mu} \frac{e^{-zb(\mu)/\mu a(\mu)}}{a(\mu)} \quad . \tag{4.21d}$$

Comparing the equations for the kernels [Eq. (4.17b) and (4.21d)] leads to the conclusion that if

$$a(\mu) = \left(1 + k^2\mu^2\right)^{1/2} \quad , \quad b(\mu) = 1 + k^2\mu^2 \tag{4.21e}$$

then $\tilde{K}(z) = K(z;\vec{k})$.

With $a(\mu)$ and $b(\mu)$ thus defined, by comparison of Eq. (4.21c) with Eq. (4.13a), it is evident that these two equations are identical in form. Therefore, a formal expression for the relationship between the actual and pseudo scalar fluxes is given as

$$\bar{\Psi}(z;\vec{k}) = \int d\mu^* \frac{d\xi^*}{d\mu^*} \delta(\xi^* - U_0)\phi(z;\mu^*) \quad . \tag{4.22}$$

Thus, the determination of the desired scalar flux is easily obtained given the solution for the pseudo scalar flux - a standard transport problem in an infinite medium with a generalized direction $\mu a(\mu)$ and a generalized relative total cross section $b(\mu)$.

4.C.2. Solution to the Pseudo Problem.

The solution to the pseudo problem is readily obtained via Fourier transform methods. A Fourier transform is applied to Eq. (4.18) (formally restated here)

$$\left[\mu a(\mu,k)\frac{\partial}{\partial z} + b(\mu,k)\right] \tilde{\phi}(z,\mu;\mu^*,k) = \frac{c}{2}\int_{-1}^{1} d\mu' \; \tilde{\phi}(z,\mu';\mu^*,k) + \delta(\mu - \mu^*)\delta(z) \quad ,$$

to give

$$[b(\mu,k) + ip\mu a(\mu,k)] \; \bar{\tilde{\phi}}(p,\mu;\mu^*,k) = \frac{c}{2}\int_{-1}^{1} d\mu' \; \bar{\tilde{\phi}}(p,\mu';\mu^*,k) +$$

$$+ a(\mu,k)\delta(\mu - \mu^*) \quad , \tag{4.23a}$$

where the Fourier transform pair is given by

$$\bar{\tilde{\phi}}(p,\mu;\mu^*,k) \equiv \int_{-\infty}^{\infty} dz \; e^{-ipz} \; \phi(z,\mu;\mu^*,k) \tag{4.23b}$$

$$\phi(z,\mu;\mu^*,k) \equiv \frac{1}{2\pi}\int_{-\infty}^{\infty} dp \; e^{ipz} \; \bar{\tilde{\phi}}(p,\mu;\mu^*,k) \quad , \tag{4.23c}$$

and the modified definition that $\phi(z,\mu;\mu^*) \equiv a(\mu^*)\tilde{\phi}(z,\mu;\mu^*)$ has been used. Defining the transformed pseudo scalar flux as

$$\bar{\tilde{\phi}}(p;\mu^*,k) \equiv \int_{-1}^{1} d\mu' \; \bar{\tilde{\phi}}(p,\mu;\mu^*,k^*)$$

and solving for the transformed angular pseudo flux yields

$$\bar{\phi}(p,\mu;\mu^*,k) = \frac{c}{2}\frac{\bar{\phi}(p;\mu^*,k)}{b(\mu,k) + ip\mu a(\mu,k)} + \frac{a(\mu,k)\delta(\mu - \mu^*)}{b(\mu,k) + ip\mu a(\mu,k)} \quad . \tag{4.24a}$$

Eq. (4.24a) can now be integrated over μ to give

$$\bar{\phi}(p;\mu^*,k) = \frac{c}{2}\bar{\phi}(p;\mu^*,k)\int_{-1}^{1}\frac{d\mu}{b(\mu,k) + ip\mu a(\mu,k)} + \frac{a(\mu^*,k)}{b(\mu^*,k) + ip\mu^* a(\mu^*,k)} \quad , \tag{4.24b}$$

or upon solving for $\bar{\phi}(p;\mu^*,k)$,

$$\bar{\phi}(p;\mu^*,k) = \frac{a(\mu^*,k)}{b(\mu^*,k) + ip\mu^* a(\mu^*,k)}\frac{1}{1 - cL(p,k)} \quad , \tag{4.25a}$$

where

$$L(p,k) = \frac{1}{2}\int_{-1}^{1}\frac{d\mu}{b(\mu,k) + ip\mu a(\mu,k)} \quad . \tag{4.25b}$$

The next task is to evaluate $L(p,k)$. By letting $s = ip$ and recalling the definition of $\xi(\mu,k)$, $L(p,k)$ can be rewritten as

$$L(p,k) = \frac{1}{2}\int_{-1}^{1}\frac{d\mu}{b(\mu,k)}\frac{1}{1 + s\xi(\mu,k)} \quad , \tag{4.26a}$$

or

$$L(p,k) = \frac{1}{2}\int_{-1}^{1}\frac{d\mu}{1 + \mu^2 k^2}\frac{1}{1 + s\xi(\mu,k)} \quad . \tag{4.26b}$$

Given the definitions of $a(\mu,k)$, $b(\mu,k)$, and $\xi(\mu,k)$, it is readily seen that

$$\mu = \frac{\xi}{\left(1 - k^2\xi^2\right)^{1/2}} \quad , \tag{4.27a}$$

and

$$1 + \mu^2 k^2 = \frac{1}{1 - k^2\xi^2} \quad . \tag{4.27b}$$

Taking the derivative of the equation for μ with respect to ξ yields

$$\frac{d\mu}{d\xi} = \frac{1}{\left(1 - k^2\xi^2\right)^{3/2}} \ , \tag{4.27c}$$

which upon substituting Eqs. (4.27b) and (4.27c) into Eq. (4.6b) gives

$$L(p,k) = \frac{1}{2}\int_{-(1+k^2)^{-1/2}}^{(1+k^2)^{-1/2}} \frac{d\xi}{\left(1 - k^2\xi^2\right)^{1/2}} \frac{1}{1 + s\xi} \ . \tag{4.28}$$

Eq. (4.28) is evaluated via the trigonometric substitution $\cos\theta = \left(1 - k^2\xi^2\right)^{1/2}$, giving (upon extracting the even form of the integrand)

$$L(p,k) = \frac{1}{k}\int_0^a \frac{d\theta}{1 - \frac{s^2}{k^2}\sin^2\theta} \ , \tag{4.29a}$$

where $a = \sin^{-1}\left[\frac{k}{\left(1 + k^2\right)^{1/2}}\right]$. Finally, making the substitution $x = (k^2 + p^2)\tan\theta$ yields

$$L(p,k) = k\int_0^{(k^2+p^2)k} \frac{dx}{x^2 + (k^2 + p^2)k^2} \ , \tag{4.29b}$$

which is readily evaluated to be the familiar expression

$$L(p,k) = \frac{\tan^{-1}u}{u} \ , \quad u = \left(k^2 + p^2\right)^{1/2} \ . \tag{4.30}$$

Given this closed form for $L(p,k)$, the next task is to solve for the pseudo scalar flux. Again recalling the definition of $\xi(\mu;k)$, the pseudo scalar flux is obtained by simply taking the inverse Fourier transform of Eq. (4.25a):

$$\phi(z,k) = \frac{1}{\mu^*}\,\mathcal{F}_z^{-1}\left\{\frac{\xi(\mu^*)}{1 + ip\xi(\mu^*)}\,\frac{1}{1 - cL(p,k)}\right\} \ . \tag{4.31}$$

Then using the equivalence relation between the pseudo scalar flux and the transverse transformed scalar flux [Eq. (4.22)] provides the desired result

$$\bar{\Psi}(z;\vec{k}) = \frac{1}{\mu_0}\,\mathcal{F}_z^{-1}\left\{\frac{U_0}{1+ipU_0}\,\frac{1}{1-cL(p,k)}\right\}\,. \tag{4.32}$$

It is usually convenient to extract the uncollided portion of the flux, done by setting $c = 0$ in the above equation. Thus, the transformed uncollided scalar flux is given by

$$\bar{\Psi}_0(z;\vec{k}) = \frac{1}{\mu_0}\,\mathcal{F}_z^{-1}\left\{\frac{U_0}{1+ipU_0}\right\}\,, \tag{4.33a}$$

which upon inversion yields

$$\bar{\Psi}_0(z;\vec{k}) = \frac{e^{-z/U_0}}{|\mu_0|}\theta\left(\frac{z}{\mu_0}\right)\,. \tag{4.33b}$$

Note that this also agrees with the equation for the transformed scalar flux [Eq. (4.13a)] with $c = 0$. Having extracted the uncollided transformed flux, this leaves

$$\bar{\Psi}(z;\vec{k}) = \bar{\Psi}_0(z;\vec{k}) + \frac{c}{\mu_0}\,\mathcal{F}_z^{-1}\left\{\frac{U_0}{1+ipU_0}\,\frac{L(p,k)}{1-cL(p,k)}\right\} \tag{4.34}$$

as the form for the transformed scalar flux.

4.D. Two-Dimensional Fourier Transform Inversion

Once the transform of an equation has been taken and all subsequent algebraic manipulations made, the desired solution is obtained via inversion. Thus, the desired scalar flux is given by

$$\Psi(z,\vec{\rho}) = \mathcal{F}_{\vec{\rho}}^{-1}\left\{\bar{\Psi}_0(z;\vec{k})\right\} + \mathcal{F}_{\vec{\rho}}^{-1}\left\{\bar{\Psi}_c(z;\vec{k})\right\}\,, \tag{4.35}$$

where the subscripts 0 and c denote uncollided and collided fluxes, respectively. It is possible to obtain a closed form solution for the inversion of the uncollided flux.

4.D.1. Inversion of the Uncollided Flux.

The uncollided scalar flux is again given by the inversion of Eq. (4.33b)

$$\Psi_0(z,\vec{\rho}) = \mathcal{F}_{\vec{\rho}}^{-1}\left\{\bar{\Psi}_0(z;\vec{k})\right\} \quad , \tag{4.36a}$$

or explicitly

$$\Psi_0(z,\vec{\rho}) = \frac{1}{\mu_0}\frac{1}{(2\pi)^2}\int_0^\infty dk\ k\int_0^{2\pi} d\psi\ e^{-ik\rho\cos(\alpha-\psi)}\ e^{-z/U_0} \quad . \tag{4.36b}$$

Inserting the expression for U_0 yields

$$\Psi_0(z,\vec{\rho}) = \frac{e^{-z/\mu_0}}{\mu_0}\frac{1}{(2\pi)^2}\int_0^\infty dk\ k\int_0^{2\pi} d\psi\ e^{-ik[\rho\cos(\alpha-\psi)-(z/\mu_0)(1-\mu_0^2)^{1/2}\cos(\phi_0-\psi)]} \quad . \tag{4.36c}$$

To perform the inversion we first assume there exists a function of the form

$$f(\vec{\rho}) = \frac{1}{\rho}\,\delta[\rho - x(\alpha)]\delta[\alpha - y(\rho)] \tag{4.37a}$$

where $x(\alpha)$ and $y(\rho)$ are arbitrary functions. The double Fourier transform of this function is given by

$$\bar{f}(z;\vec{k}) = \int_0^\infty d\rho\ \rho\int_0^{2\pi} d\alpha\ e^{ik\rho\cos(\alpha-\psi)}\ \frac{\delta(\rho - x(\alpha))}{\rho}\ \delta(\alpha - y(\rho)) \quad , \tag{4.37b}$$

or

$$\bar{f}(z;\vec{k}) = e^{ikx(y)\cos(y-\psi)} \quad . \tag{4.37c}$$

Thus, upon inversion, the original function is given by

$$f(\vec{\rho}) = \frac{1}{(2\pi)^2}\int_0^\infty dk\ k\int_0^{2\pi} d\psi\ e^{-ik[\rho\cos(\alpha-\psi)-x(y)\cos(y-\psi)]} \quad , \tag{4.37d}$$

which is similar in form to the uncollided scalar flux. Comparing Eq. (4.37d) to Eq. (4.36c) leads to the conclusion that for the equivalence of the two equations the following must be true:

$$x(y) = \frac{z}{\mu_0}\left(1 - \mu_0^2\right)^{1/2} \quad , \quad y = \phi_0 \ . \tag{4.38a}$$

Thus, the uncollided scalar flux is given by

$$\Psi_0(z,\vec{\rho}) = \frac{e^{-z/\mu_0}}{\mu_0 \rho}\ \delta(\alpha - \phi_0)\delta\left[\rho - \frac{z}{\mu_0}\left(1 - \mu_0^2\right)^{1/2}\right] , \tag{4.38b}$$

and upon inserting the collided flux and the step function in consideration of the sign of μ_0, the scalar flux becomes

$$\Psi(z,\vec{\rho}) = \frac{e^{-z/\mu_0}}{\mu_0 \rho}\ \delta(\alpha - \phi_0)\delta\left[\rho - \frac{z}{\mu_0}\left(1 - \mu_0^2\right)^{1/2}\right] \theta\left(\frac{z}{\mu_0}\right) +$$

$$+ c\ \mathcal{F}_{\vec{\rho}}^{-1}\ \mathcal{F}_{z}^{-1}\left\{\frac{U_0/\mu_0}{1 + ipU_0}\ \frac{L(p,k)}{1 - cL(p,k)}\right\} \ . \tag{4.39}$$

4.D.2. Inversion of the Collided Flux.

The advantage of transform methods is that they allow a differential equation to be solved by algebra in the transformed space; the danger of using transform methods is that one may not be able to evaluate the inverse. Usually, taking a transform is relatively easy; however, difficulty often arises in attempting the inverse transform. In Eq. (4.39), there are two inversions required - a one-dimensional Fourier inversion in the z-variable, and a two-dimensional Fourier inversion in the $\vec{\rho}$-variable. This equates to performing a triple integral. However, by considering some of the apparent symmetries, we may efficiently evaluate Eq. (4.39) by first assuming that the beam is normal to the transverse plane (emits along the z-axis). Thus upon setting $\mu_0 = 1$ and $\phi_0 = 0$ (although since $\mu_0 = 1$, ϕ_0 is

effectively arbitrary), $U_0 = 1$ and the transformed scalar flux is now a function of k only and not $\vec{k}$. This simplification may be done for a beam at a general position and emitting in a general direction by translation and rotation of coordinate axes. This procedure will be discussed later. By inserting the integrals associated with the inversions we have

$$\Psi_c(z,\vec{\rho}) = \frac{c}{(2\pi)^2}\int_0^{\infty} dk\ k \int_0^{2\pi} d\psi\ e^{-ik\rho\cos(\alpha-\psi)}\ \mathcal{F}_z^{-1}\left\{\frac{1}{1+ip}\ \frac{L(p,k)}{1-cL(p,k)}\right\},$$

which upon recognition of the integral form for the zeroth order Bessel function becomes

$$\Psi_c(z,\rho) = \frac{c}{2\pi}\int_0^{\infty} dk\ k\ J_0(\rho k)\ \mathcal{F}_z^{-1}\left\{\frac{1}{1+ip}\ \frac{L(p,k)}{1-cL(p,k)}\right\}. \qquad (4.40)$$

Clearly, there will be no closed form solution for the inverted scalar flux; therefore, a numerical evaluation of an expression like Eq. (4.40) must be performed. Such an evaluation would be relatively difficult owing to the double inversion both of which involve infinite limits of integration. Instead of doing this, it is more convenient to reformulate the problem in terms of the solution for an isotropic point source at the center of an infinite homogeneous medium. As shown in Fig. 1.1 (the intuitive big picture), the isotropic point source solution may be obtained by integrating the point-beam solution [Eq. (4.39)] over all source directions.

4.D.2.a. Generation of the Isotropic Point Source Solution. As previously mentioned, in principle, the scalar flux given by Eq. (4.39) serves as a Green's function for all infinite homogeneous medium transport problems (that seek the scalar flux) which are generally of interest to transport theorists. For an isotropic point source at the center of an infinite medium, the Green's function is integrated over all source angles to provide the solution in spherical geometry where $r = \left(\rho^2 + z^2\right)^{1/2}$ as

$$\phi_i(z,\rho) = \frac{1}{4\pi}\int_0^{2\pi} d\phi_0 \int_{-1}^{1} d\mu_0 \; \Psi(z,\vec{\rho})$$

or

$$\phi_i(z,\rho) = \frac{1}{4\pi}\int_0^{2\pi} d\phi_0 \int_{-1}^{1} d\mu_0 \, \frac{e^{-z/\mu_0}}{\mu_0\rho}\,\delta(\alpha-\phi_0)\,\delta\left[\rho - \frac{z}{\mu_0}\left(1-\mu_0^2\right)^{1/2}\right]\theta\left(\frac{z}{\mu_0}\right) +$$

$$+ \frac{c}{4\pi}\int_0^{2\pi} d\phi_0 \int_{-1}^{1} d\mu_0 \; \mathcal{F}_{\vec{\rho}}^{-1}\;\mathcal{F}_z^{-1}\left\{\frac{U_0/\mu_0}{1+ipU_0}\;\frac{L(p,k)}{1-cL(p,k)}\right\} . \qquad (4.41)$$

Bringing the angular integrals inside the transform inversions, it is evident that the primary integral to be evaluated in the above equation is

$$I = \frac{1}{4\pi}\int_0^{2\pi} d\phi \int_{-1}^{1} \frac{d\mu}{\mu}\;\frac{U}{1+ipU} . \qquad (4.42a)$$

By letting $s = ip$ and switching the integrals, Eq. (4.42a) can be restated as

$$I = \frac{1}{4\pi}\int_{-1}^{1} \frac{d\mu}{\mu}\int_0^{2\pi} d\phi\;\frac{1}{s+1/U} . \qquad (4.42b)$$

Noting that both s and U are complex numbers and recalling the residue theorem yields

$$I = \frac{1}{4\pi}\int_{-1}^{1} \frac{d\mu}{\mu}\int_0^{2\pi} d\phi\left\{\frac{1}{2\pi i}\int_C dz\;\frac{1}{z+1/U}\;\frac{1}{s-z}\right\} . \qquad (4.42c)$$

An integral for the $(z + 1/U)^{-1}$ factor is substituted and upon rearrangement of integrals there results

$$I = \frac{1}{4\pi i}\int_C \frac{dz}{s-z}\int_{-1}^{1}\frac{d\mu}{\mu}\int_0^{\infty} dt\; e^{-tz}\,\frac{1}{2\pi}\int_0^{2\pi} d\phi\; e^{-t/\mu U} \quad , \qquad (4.42d)$$

which after recalling the definition of $K(z;\vec{k})$ in Sec. 4.B.3 produces

$$I = \frac{1}{4\pi i}\int_C \frac{dz}{s - z}\int_0^\infty dt\, e^{-tz}\int_{-1}^{1}\frac{d\mu}{\mu}\,\frac{e^{-t(1+k^2\mu^2)^{1/2}/\mu}}{(1 + k^2\mu^2)^{1/2}} \quad . \tag{4.42e}$$

By separating the μ integration over positive and negative regions and evaluating the integral over t, I becomes

$$I = \frac{1}{4\pi i}\int_C \frac{dz}{s - z}\int_0^1\frac{d\mu}{\mu}\,\frac{1}{(1 + k^2\mu^2)^{1/2}}\left[\frac{1}{z + \frac{(1+k^2\mu^2)^{1/2}}{\mu}} - \frac{1}{z - \frac{(1+k^2\mu^2)^{1/2}}{\mu}}\right] \quad . \tag{4.43a}$$

Recalling the definition of ξ Eq. (4.43a) is simplified as

$$I = \frac{1}{2}\int_0^1\frac{d\mu}{\mu}\,\frac{1}{(1 + k^2\mu^2)^{1/2}}\,\frac{1}{2\pi i}\int_C \frac{dz}{s - z}\left[\frac{\xi}{1 + \xi z} + \frac{\xi}{1 - \xi z}\right] \quad . \tag{4.43b}$$

Again using the residue theorem gives

$$I = \frac{1}{2}\int_0^1\frac{d\mu}{\mu}\,\frac{1}{(1 + k^2\mu^2)^{1/2}}\left[\frac{\xi}{1 + \xi s} + \frac{\xi}{1 - \xi s}\right] \quad , \tag{4.43c}$$

or

$$I = \frac{1}{2}\int_{-1}^1\frac{d\mu}{\mu}\,\frac{1}{(1 + k^2\mu^2)^{1/2}}\,\frac{\xi}{1 + \xi s} \quad , \tag{4.43d}$$

which finally reduces to

$$I = \frac{1}{2}\int_{-1}^1 \frac{d\mu}{b(\mu,k) + \mu a(\mu,k)s} = L(p,k) \quad . \tag{4.43e}$$

Thus, by integration of Eq. (4.39) over the entire range of the source angle

$$\phi_i(z,\rho) = \phi_{i0}(z,\rho) + \frac{c}{2\pi}\int_0^\infty dk\, k\, J_0(\rho k)\, \mathcal{F}_z^{-1}\left\{\frac{L^2(p,k)}{1 - cL(p,k)}\right\} \quad . \tag{4.44}$$

The uncollided portion must now be determined. The uncollided flux from an isotropic point source is given by

$$\phi_{i0}(z,\rho) = \frac{1}{4\pi}\int_0^{2\pi} d\phi_0 \int_{-1}^{1} d\mu_0 \frac{e^{-z/\mu_0}}{\mu_0\rho}\,\delta(\alpha-\phi_0)\,\delta\left[\rho - \frac{z}{\mu_0}\left(1-\mu_0^2\right)^{1/2}\right]\theta\left(\frac{z}{\mu_0}\right) . \qquad (4.45a)$$

The ϕ_0 integral is trivial, and the μ_0 integral simply requires use of some delta-function identities. Upon evaluation of the ϕ_0 integral

$$\phi_{i0}(z,\rho) = \frac{1}{4\pi}\int_{-1}^{1} d\mu_0 \frac{e^{-z/\mu_0}}{\mu_0\rho}\,\delta\left[\rho - \frac{z}{\mu_0}\left(1-\mu_0^2\right)^{1/2}\right]\theta\left(\frac{z}{\mu_0}\right) . \qquad (4.45b)$$

Using the following relationship regarding the arguments of delta-functions

$$\delta(x-y)|dx| = \delta(y-x)|dy|$$

it is seen that

$$\delta\left[\rho - \frac{z}{\mu_0}\left(1-\mu_0^2\right)^{1/2}\right] = \delta\left[\mu_0 - \frac{z}{\left(z^2+\rho^2\right)^{1/2}}\right]\left[\frac{\rho z}{\left(z^2+\rho^2\right)^{3/2}}\right] . \qquad (4.46)$$

Inserting this into Eq. (4.45b) yields upon evaluation of the now trivial μ_0 integral

$$\phi_{i0}(z,\rho) = \frac{1}{4\pi}\frac{e^{-(z^2+\rho^2)^{1/2}}}{z^2+\rho^2} , \qquad (4.47a)$$

which with $r^2 = z^2 + \rho^2$ produces the well-known result for the uncollided flux from an isotropic point source in an infinite homogeneous medium

$$\phi_{i0}(z,\rho) = \frac{e^{-r}}{4\pi r^2} . \qquad (4.47b)$$

Thus, the scalar flux from an isotropic point source is given by

$$\phi_i(z,\rho) = \frac{e^{-r}}{4\pi r^2} + c\ \mathcal{F}_{\vec{\rho}}^{-1}\ \mathcal{F}_z^{-1}\left\{\frac{L^2(p,k)}{1 - cL(p,k)}\right\}\ , \tag{4.48a}$$

or without separating out the uncollided flux

$$\phi_i(z,\rho) = \frac{1}{2\pi}\int_0^\infty dk\ k\ J_0(\rho k)\ \mathcal{F}_z^{-1}\left\{\frac{L(p,k)}{1 - cL(p,k)}\right\}\ . \tag{4.48b}$$

If the function f is defined by

$$f\left[\left(p^2 + k^2\right)^{1/2}\right] = \frac{L(p,k)}{1 - cL(p,k)}\ , \tag{4.49a}$$

and the change of variable $u = \left(p^2 + k^2\right)^{1/2}$ is made, the longitudinal inverse Fourier transform,

$$\mathcal{F}_z^{-1}\ \{f(u)\} = \frac{1}{2\pi}\int_{-\infty}^{\infty} dp\ e^{ipz} f\left[\left(p^2 + k^2\right)^{1/2}\right]\ ,$$

becomes (upon using even/odd arguments)

$$\mathcal{F}_z^{-1}\{f(u)\} = \frac{1}{\pi}\int_k^\infty \frac{du\ u}{\left(u^2 - k^2\right)^{1/2}} \cos\left[z\left(u^2 - k^2\right)^{1/2}\right] f(u)\ . \tag{4.49b}$$

Inserting this into the expression for the scalar flux [Eq. (4.48b)] and extending the lower limit of Eq. (4.49b) to zero by using a step function yields

$$\phi_i(z,\rho) = \frac{1}{2\pi^2}\int_0^\infty dk\ k\ J_0(\rho k)\ \int_0^\infty \frac{du\ u\ f(u)}{\left(u^2 - k^2\right)^{1/2}} \cos\left[z\left(u^2 - k^2\right)^{1/2}\right]\ \theta(u - k)\ , \tag{4.50a}$$

which upon exchange of integrations and use of the step function in the k integral leads to

$$\phi_i(z,\rho) = \frac{1}{2\pi^2}\int_0^\infty du\ uf(u) \int_0^u dk\ k \frac{J_0(\rho k)}{\left(u^2 - k^2\right)^{1/2}} \cos\left[z\left(u^2 - k^2\right)^{1/2}\right]\ . \tag{4.50b}$$

The integral over k can be evaluated analytically as [Gradshteyn and Ryzhik]

$$\int_0^u dk\ k\frac{J_0(\rho k)}{\left(u^2-k^2\right)^{1/2}}\cos\left[z\left(u^2-k^2\right)^{1/2}\right]=\frac{\sin\left[u\left(\rho^2+z^2\right)^{1/2}\right]}{\left(\rho^2+z^2\right)^{1/2}}\ , \tag{4.50c}$$

which leads to the final result, the well-known expression for the scalar flux from an isotropic point source in an infinite homogeneous medium [see Eqs. 2.25)]:

$$\rho(r)\equiv\phi_i(z,\rho)=\frac{1}{2\pi^2 r}\int_0^\infty du\ uf(u)\sin(ur)\ . \tag{4.51}$$

4.D.2.b. Inversion in Terms of the Scalar Flux from an Isotropic Point Source. In the last section, it was shown that the scalar flux from an isotropic point source may be expressed as

$$\phi_i(z,\rho)=\frac{1}{2\pi}\int_0^\infty dk\ k\ J_0(\rho k)\ \mathcal{F}_z^{-1}\left\{\frac{L(p,k)}{1-cL(p,k)}\right\}\ . \tag{4.52a}$$

Again, defining the function f as

$$f\left[\left(p^2+k^2\right)^{1/2}\right]=\frac{L(p,k)}{1-cL(p,k)}\ , \tag{4.52b}$$

and multiplying Eq. (4.52a) by e^z produces

$$e^z\phi_i(z,\rho)=\frac{1}{(2\pi)^2}\int_0^\infty dk\ k\ J_0(\rho k)\int_{-\infty}^\infty dp\ e^{z(1+ip)}f\left[\left(p^2+k^2\right)^{1/2}\right]\ . \tag{4.52c}$$

This is now integrated over $(-\infty,z]$ so that

$$\int_{-\infty}^z dz'\ e^{z'}\phi_i(z',\rho)=\frac{e^z}{(2\pi)^2}\int_0^\infty dk\ kJ_0(\rho k)\int_{-\infty}^\infty dp\frac{e^{ipz}}{1+ip}f\left[\left(p^2+k^2\right)^{1/2}\right]\ , \tag{4.52d}$$

or

$$\int_{-\infty}^{z} dz'\, e^{z'} \phi_i(z',\rho) = \frac{e^z}{2\pi} \int_0^{\infty} dk\, kJ_0(\rho k)\ \mathcal{F}_z^{-1} \left\{ \frac{1}{1+ip} \frac{L(p,k)}{1-cL(p,k)} \right\} , \qquad (4.52e)$$

the right hand side of which, except for some factors, is the desired scalar flux from the point-beam source. Thus,

$$\Psi(z,\rho) = ce^{-z} \int_{-\infty}^{z} dz'\, e^{z'}\, \phi_i(z',\rho) = c \int_{-\infty}^{z} dz'\, e^{-(z-z')}\, \phi_i(z',\rho) \quad . \qquad (4.53)$$

Note that the solution for what seems to be the more basic point-beam/Green's function source problem is obtainable from the isotropic point source solution. The phrase "more basic" is used because the isotropic point source may be constructed by integrating the Green's function over all directions. The physical relevance of Eq. (4.53) is most easily seen using a simple change of variable and rearrangement so that

$$\Psi(z,\rho) = \int_0^{\infty} dz'\, e^{-z'}\, c\, \phi_i(z - z',\rho) \quad .$$

Now it is easily seen that the scalar flux from the Green's function source is the result of neutral particles being emitted along the positive z-axis, attenuating exponentially, colliding with the material at some z' with the probability c of surviving, and then appearing as if they came from an isotropic source due to the isotropic scattering of the medium. This phenomenon of deriving the flux from an anisotropic source from that of an isotropic source has been seen in previous work. When analyzing the infinite medium anisotropic plane source, Bell and Glasstone conclude after showing that the scalar flux from the anisotropic source may be written in terms of the flux from an isotropic source "[t]hus it is seen that the solution to a problem with an anisotropic source in a medium with isotropic scattering can be obtained from the solution for an isotropic source" (p. 85).

Eq. (4.51), with a change of variable and contour, and extracting the pole contribution, can be shown to be [Case, DeHoffmann, and Placzek]

$$\phi_i(z,\rho) = \frac{1}{4\pi r}\left[\frac{\partial k_0^2}{\partial c}\, e^{-k_0 r} + \int_0^1 \frac{d\mu}{\mu^2}\, e^{-r/\mu}\, g(c,\mu)\right] , \tag{4.54a}$$

where

$$g(c,\mu) \equiv \left[\left(1 - c\mu \tanh^{-1}\mu\right)^2 + \left(\frac{\pi}{2}c\mu\right)^2\right]^{-1} , \tag{4.54b}$$

$$\frac{\partial k_0^2}{\partial c} = \frac{2k_0^2(k_0^2 - 1)}{c(1 - c - k_0^2)} , \tag{4.54c}$$

and k_0 satisfies the familiar dispersion relation

$$1 - \frac{c}{k_0}\tanh^{-1}(k_0) = 0 . \tag{4.54d}$$

Inserting Eqs. (4.54) into the equation for the scalar flux in terms of an integral over the isotropic scalar flux [Eq. (4.53)] gives the general scalar flux for a normally incident beam as

$$\Psi(z,\rho) = \frac{c}{4\pi}\left[\frac{\partial k_0^2}{\partial c}\, \chi_p\left(z,\rho;k_0\right) + \int_0^1 \frac{d\mu}{\mu^2}\, \chi_p\left(z,\rho;\frac{1}{\mu}\right) g(c,\mu)\right] , \tag{4.55a}$$

where

$$\chi_p(z,\rho;a) \equiv \int_{-z}^{\infty} dz' \, \frac{e^{-(z'+z)}}{\left(\rho^2 + z'^2\right)^{1/2}}\, e^{-a(\rho^2+z'^2)^{1/2}} . \tag{4.55b}$$

Thus, the Green's function may be expressed as an integral of the point source solution. It is interesting to note that the isotropic point source solution may be obtained by integrating the point-beam solution (over source angle) yet the point-beam solution may be obtained by integrating the isotropic point source solution. With the form of the Green's function solution as given by Eqs. (4.55), the next step is to obtain numerical results for this basic

transport problem. However, due to the singular nature of the source, possible singularities are expected in the evaluation of Eq. (4.55b).

4.E. Reformulations of the Scalar Flux to Address Singularities

The infinite medium Green's function when emitting from the origin along the longitudinal (z) axis exhibits variation in the radial and axial dimensions. By examining Eqs. (4.55) it is clear that a double integration must be evaluated. The nature of the source indicates that there will be a different treatment of the solutions for positive and negative z. The uncollided flux is zero behind the source indicating that a simpler treatment is possible for $z < 0$. For $z > 0$, the key to the special treatment lies with the term $\chi_p(z,\rho;a)$.

4.E.1. The Scalar Flux for $z < 0$.

Examination of Eq. (4.55b) reveals that if $z > 0$ and ρ is equal to 0, then a singularity will occur as the integration variable (z'), whose limits are $[-z,\infty)$, passes through zero. It is also evident that if $z < 0$ there is no singularity in the integrand. Thus for $z < 0$ and with the change of variable $\omega = e^{-(z+z')}$, $\chi_p(z,\rho;a)$ may be written as

$$\chi_p(z,\rho;a) = \int_0^1 d\omega \; \frac{e^{-a\left[\rho^2+(\ln\omega+z)^2\right]^{1/2}}}{\left[\rho^2 + (\ln\omega + z)^2\right]^{1/2}} \; . \tag{4.56}$$

The integral over μ in Eq. (4.55a) is convergent because the term $\chi_p\left(z,\rho;\frac{1}{\mu}\right)$ tends to zero exponentially as μ approaches zero. This overcomes the infinity of the $1/\mu^2$ term. However, it is numerically expedient to reformulate the μ integral by "creating" another zero in the numerator (besides the $e^{-z/\mu}$ term) to counter the zero in the denominator. Noting that $g(c,\mu)$ tends to 1 as μ approaches zero, it is logical to rewrite Eq. (4.55a) for $z < 0$ as

$$\Psi(z,\rho) = \frac{c}{4\pi}\left\{\frac{\partial k_0^2}{\partial c}\,\chi_p\left(z,\rho;k_0\right) + \int_0^1 \frac{d\mu}{\mu^2}\,\chi_p\left(z,\rho;\frac{1}{\mu}\right)\,[g(c,\mu) - 1] + Q_g\right\}\ , \qquad (4.57a)$$

where

$$Q_g = \int_0^1 \frac{d\mu}{\mu^2}\int_0^1 d\omega\ \frac{e^{-(1/\mu)\left[\rho^2+(\ln\omega+z)^2\right]^{1/2}}}{\left[\rho^2 + (\ln\omega + z)^2\right]^{1/2}}\ . \qquad (4.57b)$$

Interchanging the integrals in Eq. (4.58b) and evaluating the μ integral yields for Q_g

$$Q_g = \int_0^1 d\omega\ \frac{e^{-\left[\rho^2+(\ln\omega+z)^2\right]^{1/2}}}{\rho^2 + (\ln\omega + z)^2}\ . \qquad (4.57c)$$

4.E.2. The Scalar Flux for $z \geq 0$.

Recalling that for $z > 0$ there is a singularity in $\chi_p(z,\rho;a)$, the treatment of $\chi_p(z,\rho;a)$ becomes critical. By dropping the term e^{-z} from $\chi_p(z,\rho;a)$ and separating the integral there results

$$\chi_p(z,\rho;a) = \int_{-z}^{z} \frac{dz' e^{-z'}}{\left(\rho^2 + z'^2\right)^{1/2}} e^{-a(\rho^2+z'^2)^{1/2}} + \int_{z}^{\infty} \frac{dz' e^{-z'}}{\left(\rho^2 + z'^2\right)^{1/2}} e^{-a(\rho^2+z'^2)^{1/2}}\ . \qquad (4.58a)$$

If the substitution $z = -z$ is made then the following results

$$\chi_p(-z,\rho;a) = -\int_{-z}^{z} \frac{dz' e^{-z'}}{\left(\rho^2 + z'^2\right)^{1/2}} e^{-a(\rho^2+z'^2)^{1/2}} + \int_{-z}^{\infty} \frac{dz' e^{-z'}}{\left(\rho^2 + z'^2\right)^{1/2}} e^{-a(\rho^2+z'^2)^{1/2}}, \qquad (4.58b)$$

and it is immediately seen that

$$\chi_p(-z,\rho;a) = \chi_p(z,\rho;a) - f_0(z,\rho;a)\ , \qquad (4.59a)$$

where

$$f_0(z,\rho;a) = \int_{-z}^{z} \frac{dz\, e^{-z'}}{\left(\rho^2 + z'^2\right)^{1/2}} e^{-a(\rho^2+z'^2)^{1/2}} \quad . \tag{4.59b}$$

Thus, the key to the evaluation of $\chi_p(z,\rho;a)$ now rests on the evaluation of $f_0(z,\rho;a)$. Substituting Eq. (4.59a) into Eq. (4.55a) yields

$$\Psi(z,\rho) = \frac{ce^{-z}}{4\pi}\frac{\partial k_0^2}{\partial c}\left[e^{-z}\chi_p\left(-z,\rho;k_0\right) + f_0(z,\rho;k_0)\right] +$$

$$+ \frac{ce^{-z}}{4\pi}\int_0^1 \frac{d\mu}{\mu^2}\left[e^{-z}\chi_p\left(-z,\rho;\frac{1}{\mu}\right) + f_0\left(z,\rho;\frac{1}{\mu}\right)\right] g(c,\mu) \quad , \tag{4.60a}$$

or upon noting that the corresponding scalar flux for negative z is contained in this equation, it is evident that

$$\Psi(z,\rho) = e^{-2z}\Psi(-z,\rho) + \frac{ce^{-z}}{4\pi}\left[\frac{\partial k_0^2}{\partial c} f_0(z,\rho;k_0) + \int_0^1 \frac{d\mu}{\mu^2} f_0\left(z,\rho;\frac{1}{\mu}\right) g(c,\mu)\right] . \tag{4.60b}$$

There are no concerns regarding singularities in the evaluation of the term $\Psi(-z,\rho)$ in Eq. (4.60b). Given the functional form of $f_0(z,\rho;k_0)$ from Eq. (4.59b) it may be seen that the singularity at $\rho = 0$ in $\chi_p(z,\rho;a)$ previously discussed is now present in this function. If ρ is zero then the integrand will eventually pass through $z' = 0$ creating a zero in the denominator which is not countered by a zero in the numerator. This singularity will now be extracted. The change of variable $\omega = z'/z$ is made to give

$$f_0(z,\rho;a) = z\int_{-1}^{1} d\omega\, \frac{e^{-\omega z}}{\left(\rho^2 + \omega^2 z^2\right)^{1/2}} e^{-a(\rho^2+\omega^2 z^2)^{1/2}} \quad , \tag{4.61a}$$

or upon separating the integral over negative and positive ranges, making a simple change of variable in the [–1,0] integral, and combining the result yields

$$f_0(z,\rho;a) = z\int_0^1 d\omega\,\frac{e^{\omega z}+e^{-\omega z}}{\left(\rho^2+\omega^2 z^2\right)^{1/2}}\,e^{-a(\rho^2+\omega^2 z^2)^{1/2}} \quad . \tag{4.61b}$$

A singularity occurs in the integrand only when both ρ and ω equal 0; therefore the evaluation of this integral as is will be difficult due to the singularity at the lower limit. When this singularity occurs, the numerator has the value 2, which is now extracted to give

$$f_0(z,\rho;a) = z\int_0^1 \frac{d\omega}{\left(\rho^2+\omega^2 z^2\right)^{1/2}}\left[\left(e^{\omega z}+e^{-\omega z}\right)e^{-a(\rho^2+\omega^2 z^2)^{1/2}}-2\right]+Q_0 \quad , \tag{4.62a}$$

where

$$Q_0 = 2z\int_0^1 \frac{d\omega}{\left(\rho^2+\omega^2 z^2\right)^{1/2}}$$

which explicitly contains the singularity and can be shown to be

$$Q_0 = 2\ln\left[\left(1+\frac{z^2}{\rho^2}\right)^{1/2}+\frac{z}{\rho}\right] \quad . \tag{4.62b}$$

As with the case for $z < 0$, it is desirable to make the μ integral more convenient for numerical evaluation by countering the zero in the denominator at $\mu = 0$. As before, this gives

$$\Psi(z,\rho) = \Psi(-z,\rho) +$$

$$+\frac{ce^{-z}}{4\pi}\left\{\frac{\partial k_0^2}{\partial c}f_0(z,\rho;k_0)+\int_0^1 \frac{d\mu}{\mu^2}f_0\left(z,\rho;\frac{1}{\mu}\right)\left[g(c,\mu)-1\right]+Q_g\right\} \quad , \tag{4.63a}$$

where

$$Q_g = \int_0^1 \frac{d\mu}{\mu^2} \int_0^1 d\omega \, \frac{z\left(e^{\omega z} + e^{-\omega z}\right)}{\left(\rho^2 + \omega^2 z^2\right)^{1/2}} e^{-(1/\mu)(\rho^2+\omega^2 z^2)^{1/2}} \quad . \tag{4.63b}$$

Again, interchanging the integrals and evaluating the μ integral yields for Q_g

$$Q_g = \int_0^1 d\omega \, \frac{z\left(e^{\omega z} + e^{-\omega z}\right)}{\rho^2 + \omega^2 z^2} e^{-(\rho^2+\omega^2 z^2)^{1/2}} \quad . \tag{4.63c}$$

Thus, for $z > 0$, in order to evaluate the scalar flux, the scalar flux for the corresponding point at $-z$ must be evaluated, and then the single and double integrals specific to the formulation for positive z must also be evaluated.

As seen in Sec. 4.D, the solution for the Green's function source may be expressed as an integral of the isotropic point source solution. It has also been seen that the solution for any source which emits particles isotropically may be constructed by integrating the point source solution over the source region. Thus, assuming all anisotropic sources may be constructed from this Green's function source, it is therefore noted that the isotropic point source in an infinite medium is the source from which all others may be constructed.

4.F. Results for the Scalar Flux from the Green's Function Source

Obtaining numerical results requires the accurate evaluation of integrals. The methods which accomplish this task have been discussed in the previous chapter. The other important task for the computer algorithm is to evaluate the scalar flux at spatial edit points so that the results are visually and conceptually useful, be they in tabular or graphical form. In order to use the equations derived for the Green's function source (and the finite sources as well), a general source must be placed in a convenient reference frame so that the source is at the center of the reference frame and is oriented appropriately. For the Green's function source, this means that the beam emits along the z-axis of the reference frame.

This is accomplished by translation and rotation of coordinate axes into a convenient reference frame for each type of source.

4.F.1. Rotations of Axes.

The solutions and solution methods discussed in the last two chapters are at least two-dimensional. However, since a source can be arbitrarily translated and rotated to any position and orientation in an infinite medium, the actual variation of the scalar flux in the infinite medium will be three-dimensional. Given the principle of superposition, a variety of sources can be placed in an infinite medium. The flux at any point can be evaluated by determining how that point relates to a convenient reference frame for the source. That is, by translating and rotating the general (transport frame) axes into a reference frame which is suitable for evaluation of the scalar flux (source frame), a problem with three-dimensional variation (using an "inconvenient" coordinate system) of the scalar flux may be numerically evaluated using two-dimensional techniques.

Fig. 4.2 displays the necessary rotations to transform the general frame of reference into a convenient frame for solution methods. Note that translations are not shown; any necessary translations are assumed to have been completed so that the origin for the transport frame is at the same location as the origin for the source frame. The figure assumes that the source is the Green's function source; however, any source may be substituted given that the placement in the source frame is appropriate for the kind of source. The beam source is placed in an arbitrary direction by assigning to it longitudinal and azimuthal angles. As is standard in transport theory, the longitudinal angle, θ_0, is measured from the z-axis, and the azimuthal angle, ϕ_0, is measured from the x-axis. The first step is to rotate the axes in the transport frame an angle ϕ_0 about the z-axis so that the source in the intermediate frame lies in the z'-x' plane. The second step is to rotate the intermediate frame an angle θ_0 about the y'-axis so that the source lies along the z''-axis.

The first axes rotation is displayed in Fig. 4.3a. The coordinate transformations for this first step going from the transport frame (unprimed) to the intermediate frame (primed) are

$$x' = x\cos\phi_0 + y\sin\phi_0$$

$$y' = -x\sin\phi_0 + y\cos\phi_0$$

$$z' = z \ .$$

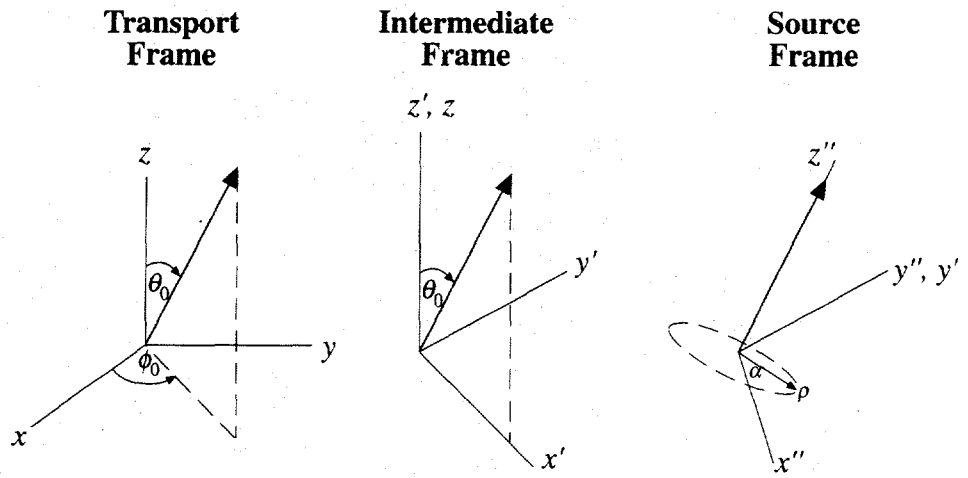

Fig. 4.2. Rotation of arbitrary transport frame into source frame convenient for numerical evaluation.

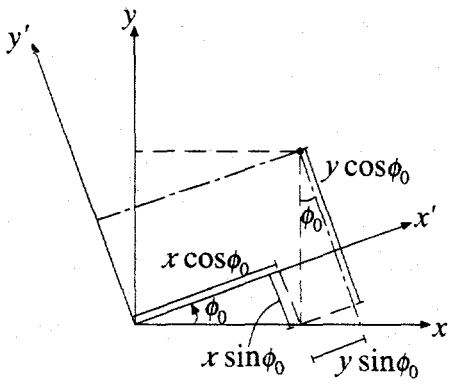

Fig. 4.3a

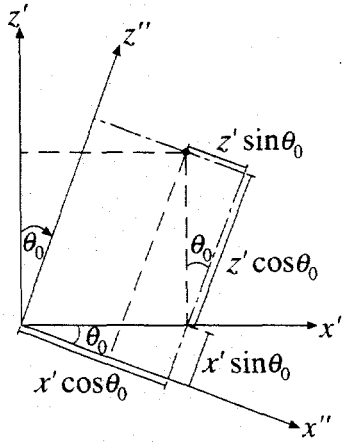

Fig. 4.3b

Fig. 4.3. Explicit rotations of axes for determination of coordinate transformations.

The second axes rotation is displayed in Fig. 4.3b. The coordinate transformations for the intermediate frame (primed) to the source frame (double primed) are

$$x'' = x'\cos\theta_0 - z'\sin\theta_0$$

$$y'' = y'$$

$$z'' = x'\sin\theta_0 + z'\cos\theta_0 \ ,$$

which gives for the net result of the two rotations

$$x'' = x\cos\phi_0\cos\theta_0 + y\sin\phi_0\cos\theta_0 - z\sin\theta_0 \tag{4.64a}$$

$$y'' = -x\sin\phi_0 + y\cos\phi_0 \tag{4.64b}$$

$$z'' = x\cos\phi_0\sin\theta_0 + y\sin\phi_0\sin\theta_0 + z\cos\theta_0 \ . \tag{4.64c}$$

Thus, with the above coordinate transformation, a spatial point in general space (x,y,z) can be expressed relative to the source frame (x'',y'',z'') and is then expressed in a format convenient to the source rather than the original geometry. Note also when $\theta_0 = \phi_0 = 0$ (when the source happens to already be in a convenient coordinate system) the source frame and transport frame are equivalent.

4.F.2. Spatial Edit Point Grids.

In the last section, the means by which an arbitrary point in space may be expressed relative to a coordinate system convenient to a source was derived. This section examines a couple of ways by which the arbitrary spatial points may be placed in convenient grids for use by a computer algorithm.

4.F.2.a. Planar Grid. The most prevalent and convenient grid is a rectangular planar grid. In order to make the edit grid as general as possible, the finite grid is specified so that it may be rotated in the transverse plane and vertically. Given that the initial edit

point is specified as (x_0,y_0,z_0) and the distance between points in the grid is specified as Δx and Δy, the grid may be rotated in the x-y plane an angle α_0 so that (see Fig. 4.4)

$$x_{ij} = x_0 + i\Delta x\cos\alpha_0 - j\Delta y\sin\alpha_0$$

$$y_{ij} = y_0 + i\Delta x\sin\alpha_0 + j\Delta y\cos\alpha_0$$

$$z_{ij} = z_0 \ ,$$

where i and j are the edit point index for x and y, respectively.

Next, to make the location of the grid plane completely arbitrary, the grid is rotated about the axis labeled "Second Rotation Axis" in Fig. 4.4 an angle β_0. Now, the projection of the grid in the x-y plane is such that Δy is unaffected and $\Delta x \rightarrow \Delta x\cos\beta_0$. Thus,

$$x'_{ij} = x_0 + i\Delta x\cos\beta_0\cos\alpha_0 - j\Delta y\sin\alpha_0 \qquad (4.65a)$$

$$y'_{ij} = y_0 + i\Delta x\cos\beta_0\sin\alpha_0 + j\Delta y\cos\alpha_0 \ . \qquad (4.65b)$$

Because the axis of rotation is along the rotated y-axis (y'), the hypotenuse of the triangle with base angle β_0 is $i\Delta x$, and therefore the height of the edit point is given as

$$z'_{ij} = z_0 + i\Delta x\sin\beta_0 \ . \qquad (4.65c)$$

This planar grid is most useful as a standard means of viewing the scalar flux as a function of position. Another means of selecting edit points is to have them on the surface of a sphere.

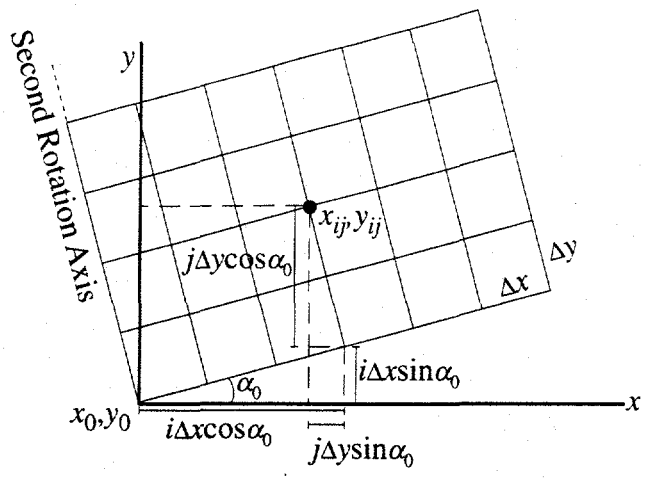

Fig. 4.4. Rotation of edit grid in x-y plane.

4.F.2.b. Spherical Surface Grid (Global View). Because the Green's function source is a directed source, it is desirable to obtain some means of examining the directional variation (or gradient) of the scalar flux. When direction is mentioned, one naturally thinks of the unit sphere with which to express the direction. To this end, an input option is provided to allow the set of edit points to lie on the surface of a sphere, denoted as a "global view" of the edit points. Such a set is specified when the center of the sphere (x_0,y_0,z_0), the number of points in the ϕ and θ dimensions, and the radius of the sphere (R_0) are provided. Assuming the usual ranges for the angular variables, $0 \le \theta \le \pi$, $0 \le \phi \le 2\pi$, then $\theta_i = i\pi/N_\theta$, and $\phi_j = j2\pi/N_\phi$. Therefore, the spatial edit points are given by

$$x_{ij} = x_0 + R_0\sin\theta_i\cos\phi_j \tag{4.66a}$$

$$y_{ij} = y_0 + R_0\sin\theta_i\sin\phi_j \tag{4.66b}$$

$$z_{ij} = z_0 + R_0\cos\theta_i \ . \tag{4.66c}$$

A pictorial view of the edit grid for the global view is given in Fig. 4.5. Again, this grid allows in some sense examination of directional variations in the scalar flux.

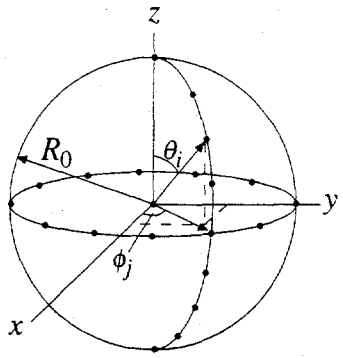

Fig. 4.5. Global view edit grid.

4.F.3. Results for Individual Sources.

Most results were generated used the panels method described in Ch. 3. The outer integral is performed as described in this method and the inner integral is evaluated only at the quadrature order of the outer integral. Thus, convergence on the inner integral is not performed based on quadrature order. For those sources which require evaluation of three integrals, the innermost integral is evaluated at one set quadrature order. The supposition in this scheme is that the accuracy of the inner integrals is not as important as the outer ones. Thus, less care is taken in the second integral's evaluation than for the first integral, and less care is taken in evaluating the third integral than the second integral.

When the iterative Gauss-Legendre scheme is used, it is used on all integrals. This generally requires more computer time, but by comparing the results from these two integration schemes confidence that both are performing the integrals accurately may be built.

The first set of results is an analysis of the two types of integration methods for all four sources discussed in the last two chapters. The mean number of secondaries per collision is set to $c = 0.9$. The Green's function source is located at the origin and emits along the positive x-axis. The other sources have the same characteristics as those used for

the error analysis in the last chapter. Table 4.1 shows a comparison of the two integration schemes as discussed above. For the iterative Gauss-Legendre quadrature schemes the initial and incremental quadrature orders were both set to 10. For the panels method the initial and incremental quadrature orders were set to 5, the number of panels was 4, and the quadrature order of the third integral was 20. Excellent agreement between the two schemes is obtained as shown in Table 4.1. There is some minor discrepancy in the last digits of the results from the rectangular source; this is due to the asymmetric nature of the source resulting in the need for slightly greater accuracy in the inner integrals. Increasing the quadrature order (to 50) in the third integral improves the agreement to within the given error of 10^{-6}. Also, in the treatment of numerical singularities, the non-singular μ integral was treated by subtracting 1 from $g(c,\mu)$ to counter a $1/\mu^2$ term. Again, this term is non-singular, but adding this zero in the numerator for $\mu = 0$ makes it numerically easier to evaluate such integrals. The evaluation times for the case where these integrals are treated are typically three times faster than when the integrals are left as is.

An error analysis and typical plot of the scalar flux as a function of position are provided in Table 4.2 and Fig. 4.6. In both cases the source is at the origin emitting particles along the positive x-axis.

Table 4.1. Integration Scheme Analysis.

x	Iterative G-L	Panels	x	Iterative G-L	Panels
	Green's Function			Disk	
-2	1.69154E-02	1.69154E-02	0	1.60976E+00	1.60976E+00
-1	5.29437E-02	5.29437E-02	0.5	1.49961E+00	1.49961E+00
0	1.11956E+00	1.11956E+00	1	8.48238E-01	8.48238E-01
1	9.93167E-01	9.93167E-01	1.5	2.60607E-01	2.60607E-01
2	4.03002E-01	4.03002E-01	2	1.32242E-01	1.32242E-01
	Finite Line			Rectangle	
0	2.86975E+00	2.86975E+00	0	1.70986E+00	1.70985E+00
0.5	2.79039E+00	2.79039E+00	0.5	1.61392E+00	1.61392E+00
1	1.50877E+00	1.50877E+00	1	9.82419E-01	9.82413E-01
1.5	2.16606E-01	2.16606E-01	1.5	3.32724E-01	3.32726E-01
2	9.72665E-02	9.72666E-02	2	1.71311E-01	1.71312E-01

Table 4.2. Error Analysis for Green's Function Source.

x	$err = 10^{-2}$	$err = 10^{-3}$	$err = 10^{-4}$	$err = 10^{-5}$	$err = 10^{-6}$
0	1.119593	1.119563	1.119558	1.119557	1.119556
0.1	1.617215	1.617177	1.617171	1.617169	1.617168
0.2	1.725982	1.725941	1.725934	1.725932	1.725931
0.3	1.686987	1.686945	1.686938	1.686936	1.686935
0.4	1.599191	1.599149	1.599143	1.599141	1.599140
0.5	1.494921	1.494882	1.494875	1.494873	1.494873
0.6	1.386851	1.386813	1.386807	1.386806	1.386805
0.7	1.280623	1.280587	1.280581	1.280580	1.280579
0.8	1.178900	1.178867	1.178861	1.178860	1.178859
0.9	1.082925	1.082894	1.082889	1.082887	1.082887
1	0.993203	0.993173	0.993169	0.993167	0.993167
1.2	0.832707	0.832681	0.832677	0.832676	0.832676
1.4	0.696105	0.696083	0.696079	0.696078	0.696078
1.6	0.580818	0.580800	0.580797	0.580796	0.580796
1.8	0.484020	0.484005	0.484002	0.484002	0.484001
2	0.403018	0.403004	0.403002	0.403002	0.403002

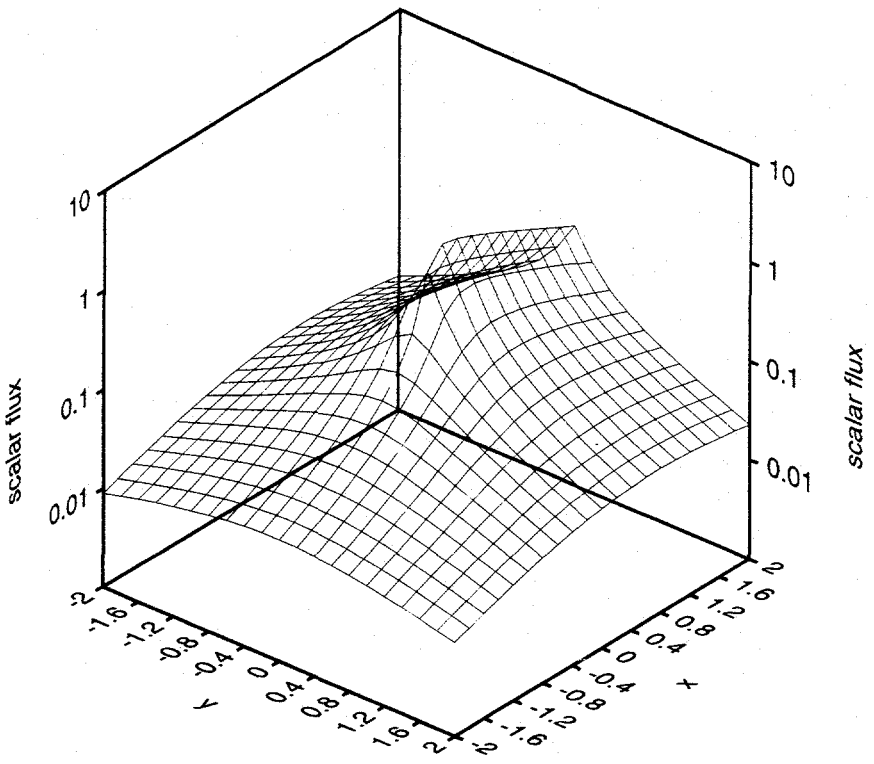

Fig. 4.6. Scalar flux at $z = 0.1$ resulting from a single Green's function source.

In the derivation of the Green's function, the scalar flux was expressed as an integral of the isotropic point source solution. The numerical solution uses the form of the isotropic point source solution expressed after a change of variable and contour in the complex plane (Case, DeHoffmann, and Placzek). The double inversion as given by Eq. (4.40) could have been done numerically as well; however, the numerical evaluation of Eq. (4.40) takes much longer than integrating the analytically continued point source solution as found in Eqs. (4.53) and (4.54). Table 4.3 provides a comparison of the scalar fluxes as obtained using these two formulations. The source is at the center of the infinite medium emitting particles along the z-axis. The number of secondaries is 0.9 and the desired error is 10^{-4}. Note that both sets of scalar fluxes agree within the desired error; however, the

evaluation time per point was about 0.14 seconds for the scalar flux after the analytic continuation and about 9 seconds for the scalar flux obtained via direct double inversion.

Table 4.3. Scalar Flux Analysis for Different Inversion Methods.

Scalar Flux After Analytic Continuation				
$z\backslash\rho$	0.5	1.0	1.5	2.0
0.5	0.255236	0.096383	0.049295	0.028570
1	0.215929	0.091662	0.048670	0.028590
1.5	0.160149	0.076275	0.043207	0.026325
2	0.113094	0.059072	0.035685	0.022719
Scalar Flux As Direct Inversion				
$z\backslash\rho$	0.5	1.0	1.5	2.0
0.5	0.255236	0.096384	0.049295	0.028570
1	0.215929	0.091662	0.048670	0.028590
1.5	0.160148	0.076275	0.043208	0.026325
2	0.113093	0.059072	0.035685	0.022719

With an algorithm to provide the scalar fluxes from these four sources which are derived from the isotropic point source, it is possible to combine the sources in a configuration that utilizes superposition to provide the scalar flux from an arbitrary distribution of sources. These specialized results will be presented in the next chapter. The Green's function source will now be used to construct the anisotropic plane source solution, thereby adding one more piece to Fig. 1.2.

4.G. The Anisotropic Plane Source

In this section, the anisotropic plane source solution will first be derived from the general Green's function, and will then be derived independently from an appropriately formed transport equation. The scalar flux from this source will, like the isotropic point, plane, and line sources, be one-dimensional; however, unlike these isotropic sources, the solution for the anisotropic plane source contains a parameter μ_0 describing the direction in which the particles are emitted.

4.G.1. Derivation of the Scalar Flux from an Anisotropic Plane Source.

The scalar flux from the anisotropic planar source can be derived by integrating the Green's function over the transverse plane as

$$\psi_{ani}(z) = \int d\ \vec{\rho}\ \ \Psi(\vec{\rho},z)\ . \tag{4.67a}$$

This step in the completion of the suite of infinite medium benchmarks discussed in this work is displayed in Fig. 1.2g. Expressing Eq. (4.67a) as a double Fourier transform leads to a very simple means of obtaining the desired scalar flux once it is noted that when $\vec{k} = \vec{0}$ in the longitudinally transformed scalar flux, the following results

$$\bar{\Psi}_{ani}(p) = \int d\vec{\rho}\ e^{i\vec{k}\cdot\vec{\rho}}\ \Psi(p,\vec{\rho})\Big|_{\vec{k}=\vec{0}} = \bar{\Psi}(p,\vec{0})\ . \tag{4.67b}$$

From the transform of the scalar flux from the Green's function source, we have

$$\bar{\Psi}(p;\vec{k}) = \frac{1}{\mu_0}\frac{U_0}{1 + ipU_0}\frac{1}{1 - cL(p,k)}\ . \tag{4.68}$$

So by setting $\vec{k} = \vec{0}$ in the above equation, $U_0 \rightarrow \mu_0$, and the longitudinally transformed scalar flux for the anisotropic planar source is therefore

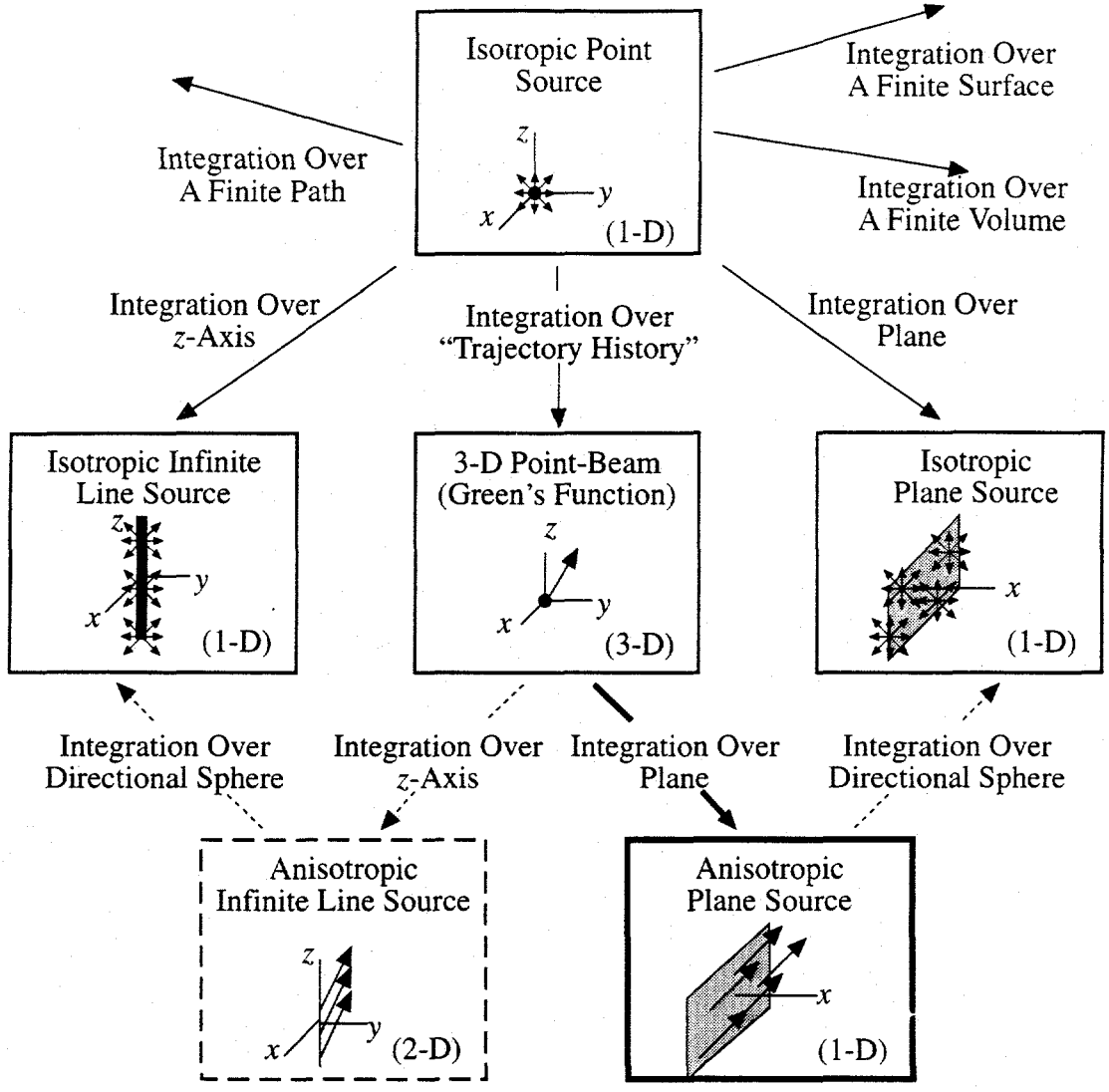

Fig. 1.2g. The eighth step in constructing the suite of infinite medium benchmarks - deriving the anisotropic plane source from the Green's function source.

$$\bar{\Psi}_{ani}(p) = \frac{1}{1 + ip\mu_0} \frac{1}{1 - cL(p)} , \tag{4.69}$$

which upon inversion yields the scalar flux from the anisotropic plane source as

$$\Psi_{ani}(x;\mu_0) = \frac{1}{2\pi}\int_{-\infty}^{\infty} dp\ \frac{e^{ipx}}{1 + ip\mu_0}\ \frac{1}{1 - cL(p)}\ . \tag{4.70}$$

The scalar flux from the anisotropic plane source can also be derived by using a transport equation which is written for this source in an infinite medium.

4.G.2. Derivation of the Scalar Flux Directly from the Transport Equation.

Beginning with a simplified form of the one-dimensional linear transport equation (time-independent, one-group, constant cross sections) with a spatial delta-function source at the origin emitting neutral particles in the single direction μ_0,

$$\left[\mu\frac{\partial}{\partial x} + \Sigma_t\right]\ \psi(x,\vec{\Omega}) = \frac{\Sigma_s}{4\pi}\int_{4\pi} d\vec{\Omega}'\ \psi(x,\vec{\Omega}') + \delta(x)\delta(\mu - \mu_0)\ , \tag{4.71}$$

we then assume azimuthal symmetry and scale the spatial variable by the total cross section (i.e. use mean free paths instead of distances) to obtain

$$\left[\mu\frac{\partial}{\partial x} + 1\right]\ \psi(x,\mu;\mu_0) = \frac{c}{2}\int_{-1}^{1} d\mu'\ \psi(x,\mu';\mu_0) + \delta(x)\delta(\mu - \mu_0)\ , \tag{4.72a}$$

where c is the single scatter albedo given by $c = \Sigma_s/\Sigma_t$. The flux is subject to the boundary condition

$$\lim_{|x|\to\infty}\ \psi(x,\mu;\mu_0) < \infty\ . \tag{4.72b}$$

As usual for infinite medium problems, the solution method utilizes Fourier transform methods. The Fourier transform pair is defined as

$$\bar{\psi}(k,\mu;\mu_0) \equiv \int_{-\infty}^{\infty} dx\ e^{-ikx}\ \psi(x,\mu;\mu_0) \tag{4.73a}$$

$$\psi(x,\mu;\mu_0) \equiv \frac{1}{2\pi}\int_{-\infty}^{\infty} dk\ e^{ikx}\ \bar{\psi}(k,\mu;\mu_0)\ . \tag{4.73b}$$

Taking the Fourier transform of Eq. (4.72a) results in the following transformed equation

$$[1 + ik\mu]\,\bar{\psi}(k,\mu;\mu_0) = \frac{c}{2}\,\bar{\psi}(k,;\mu_0) + \delta(\mu - \mu_0) \quad , \tag{4.74a}$$

where the transformed scalar flux is given by

$$\bar{\psi}(k;\mu_0) = \int_{-1}^{1} d\mu'\, \bar{\psi}(k,\mu';\mu_0) \quad . \tag{4.74b}$$

Solving Eq. (4.74a) for the transformed angular flux in terms of the transformed scalar flux yields

$$\bar{\psi}(k,\mu;\mu_0) = \frac{c}{2}\frac{\bar{\psi}(k;\mu_0)}{1 + ik\mu} + \frac{\delta(\mu - \mu_0)}{1 + ik\mu_0} \quad ; \tag{4.75}$$

thus, if the transformed scalar flux is known, then so is the transformed angular flux.

The transformed scalar flux is obtained by integrating Eq. (4.75) over μ [i.e. using the definition given in Eq. (4.74b)]. This integration gives

$$\bar{\psi}(k;\mu_0) = \frac{1}{1 + ik\mu_0} + \frac{c}{2}\,\bar{\psi}(k;\mu_0)\int_{-1}^{1}\frac{d\mu}{1 + ik\mu} \quad , \tag{4.76}$$

or upon solving for the desired quantity

$$\bar{\psi}(k;\mu_0) = \frac{1}{1 + ik\mu_0}\,\frac{1}{1 - cL(k)} \quad , \tag{4.77a}$$

where $L(k)$ is defined by

$$L(k) \equiv \frac{i}{2k}\ln\frac{i + k}{i - k} = \frac{\tan^{-1}k}{k} \quad . \tag{4.78b}$$

With this expression for the transformed scalar flux the desired scalar and angular fluxes can be found as

$$\psi(x;\mu_0) = \frac{1}{2\pi}\int_{-\infty}^{\infty} dk\ \frac{e^{ikx}}{1 + ik\mu_0}\ \frac{1}{1 - cL(k)} \tag{4.79a}$$

$$\psi(x,\mu;\mu_0) = \frac{c}{4\pi}\int_{-\infty}^{\infty} dk\ \frac{e^{ikx}}{(1+ik\mu_0)(1+ik\mu)}\ \frac{1}{1 - cL(k)} + \frac{\delta(\mu-\mu_0)}{|\mu_0|}\, e^{-x/\mu_0}\theta(x/\mu_0)\ . \tag{4.79b}$$

Recalling the expression for the scalar flux as derived from the Green's function source, it is seen that the two results [Eqs. (4.70) and (4.79a)] are identical, as expected.

The numerical evaluation of Eqs. (4.79) requires that the real and imaginary parts of the solution be explicitly expressed. As expected, when this is performed, the integrand of the imaginary part is odd with respect to k, and the integral therefore vanishes as it is over a symmetric range. Likewise, the integrand of the real portion is even with respect to k. This leaves for the scalar and angular fluxes

$$\psi(x;\mu_0) = \frac{1}{\pi}\int_{0}^{\infty} dk\ \frac{\cos(kx) + k\mu_0\sin(kx)}{(1 + k^2\mu_0^2)}\ \frac{1}{1 - cL(k)} \tag{4.80a}$$

$$\psi(x,\mu;\mu_0) = \frac{c}{2\pi}\int_{0}^{\infty} dk\ \frac{(1 - k^2\mu_0\mu)\cos(kx) + k(\mu + \mu_0)\sin(kx)}{(1 + k^2\mu_0^2)(1 + k^2\mu^2)}\ \frac{1}{1 - cL(k)} +$$

$$+ \frac{\delta(\mu - \mu_0)}{|\mu_0|}\, e^{-x/\mu_0}\ \theta(x/\mu_0)\ . \tag{4.80b}$$

The simplest method for evaluating these integrals is separation into two integrals, each of which contains the portion of the integrand multiplying the sine and cosine functions, and reformulate the integrals over a semi-infinite range as two infinite series of integrals over a finite interval. The finite intervals are defined as the zeroes of the sine and cosine functions so that the value of the integrands will be zero at the endpoints. The individual integrals are evaluated and the convergence of the series is accelerated by an Euler-Knopp transformation [Press, *et al.*].

Fig. 4.7 displays the collided scalar flux in an infinite medium resulting from an infinite plane source at the center emitting neutral particles in the direction $\mu_0 = 1$ [Eq. (4.80a)]. Note the discontinuity in the scalar flux at the origin resulting from the source emitting particles into the right half plane. When c is close to 1 the medium is approaching a conservative state where no particles are lost due to absorption. As with the isotropic plane source in Ch. 2, the scalar flux becomes uniform throughout the medium and increases without bound due to no loss of particles. Fig. 4.8 displays the collided angular flux for four positions relative to the source which again emits in the direction $\mu_0 = 1$ and for $c = 0.9$ [Eq. (4.80b)]. Note there is an increase in the angular flux for $\mu < 0$ and $z < 0$, indicating that the particles in this region come from backscatter. Likewise, for positive z the angular flux is mostly the result of particles scattering in positive directions due to the emission angle of the source.

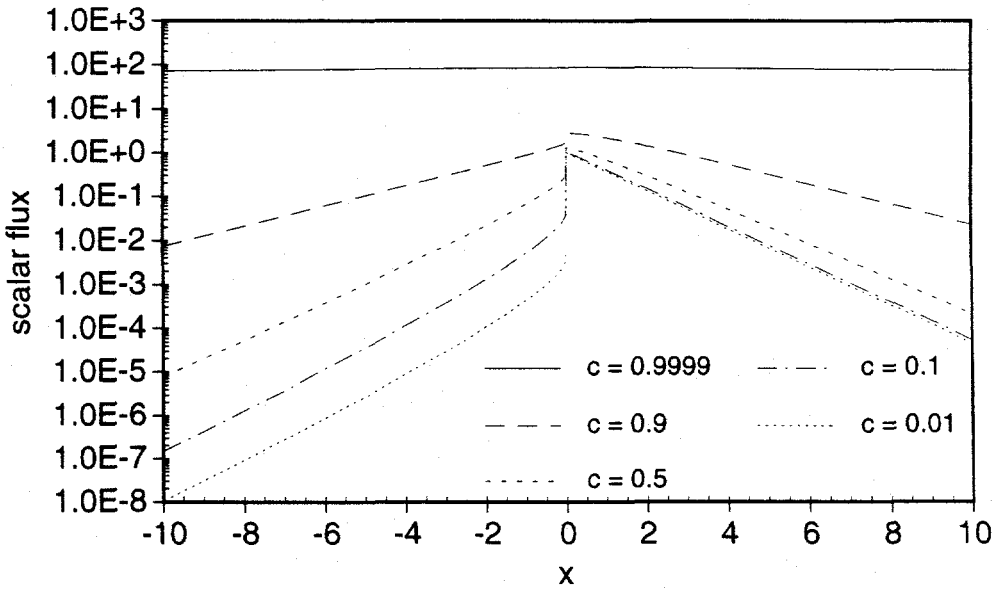

Fig. 4.7. Scalar flux as a function of position for a plane source emitting in the direction $\mu_0 = 1$ for several values of c.

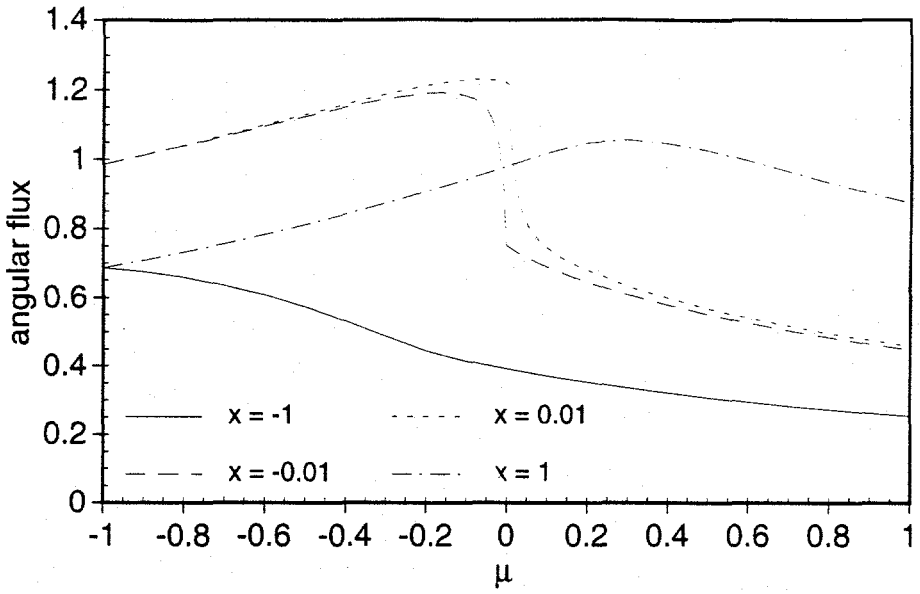

Fig. 4.8. Angular flux as a function of μ for a plane source emitting at $\mu_0 = 1$ for several values of z.

4.G.3. Derivation of the Flux from an Isotropic Plane Source.

Given the scalar and angular fluxes from the anisotropically emitting plane source, one should be able to obtain the solution for the scalar and angular fluxes from an isotropic planar source by integrating over the source emission angle. That is,

$$\psi_{iso}(x) = \frac{1}{2}\int_{-1}^{1} d\mu_0 \; \psi(x;\mu_0) \tag{4.81a}$$

$$\psi_{iso}(x,\mu) = \frac{1}{2}\int_{-1}^{1} d\mu_0 \; \psi(x,\mu;\mu_0) \quad . \tag{4.81b}$$

This completes one more connection in Fig. 1.2 as we show the self-consistency of these solutions - since the scalar flux from the isotropic plane source can be obtained by integrating the isotropic point source solution, the solution from that analysis should be

identical to the solution as obtained by using the method of integrating the anisotropic plane source over the emission direction. This process is pictorially shown in Fig. 1.2h. Performing these integrations over source emission angle [using Eqs. (6.79)] yields

$$\psi_{iso}(x) = \frac{1}{2\pi}\int_{-\infty}^{\infty} dk\, \frac{e^{ikx}}{1 - cL(k)}\, \frac{1}{2}\int_{-1}^{1} \frac{d\mu_0}{1 + ik\mu_0} \tag{4.82a}$$

$$\psi_{iso}(x,\mu) = \frac{c}{4\pi}\int_{-\infty}^{\infty} dk\, \frac{e^{ikx}}{1 + ik\mu}\, \frac{1}{1 - cL(k)}\, \frac{1}{2}\int_{-1}^{1} \frac{d\mu_0}{1 + ik\mu_0} +$$

$$+ \frac{1}{2}\int_{-1}^{1} d\mu_0\, \frac{\delta(\mu - \mu_0)}{\mu_0}\, e^{-x/\mu_0}\, \theta(x/\mu_0) \quad , \tag{4.82b}$$

or upon evaluating all the integrals over μ_0

$$\psi_{iso}(x) = \frac{1}{2\pi}\int_{-\infty}^{\infty} dk\, e^{ikx}\, \frac{L(k)}{1 - cL(k)} \tag{4.83a}$$

$$\psi_{iso}(x,\mu) = \frac{e^{-x/\mu}}{2\mu}\, \theta(x/\mu) + \frac{c}{4\pi}\int_{-\infty}^{\infty} dk\, \frac{e^{ikx}}{1 + ik\mu}\, \frac{L(k)}{1 - cL(k)} \quad . \tag{4.83b}$$

Converting the complex exponential in Eq. (4.83a) into sines and cosines leads to the realization that the imaginary integral vanishes due to the oddness of the integrand, and the remaining term for the scalar flux from an isotropic plane source is

$$\psi_{iso}(x) = \frac{1}{\pi}\int_{0}^{\infty} dk\, \cos(kx)\, \frac{L(k)}{1 - cL(k)} \quad , \tag{4.84}$$

which is equivalent to the equation for the scalar flux as derived in Ch. 2.

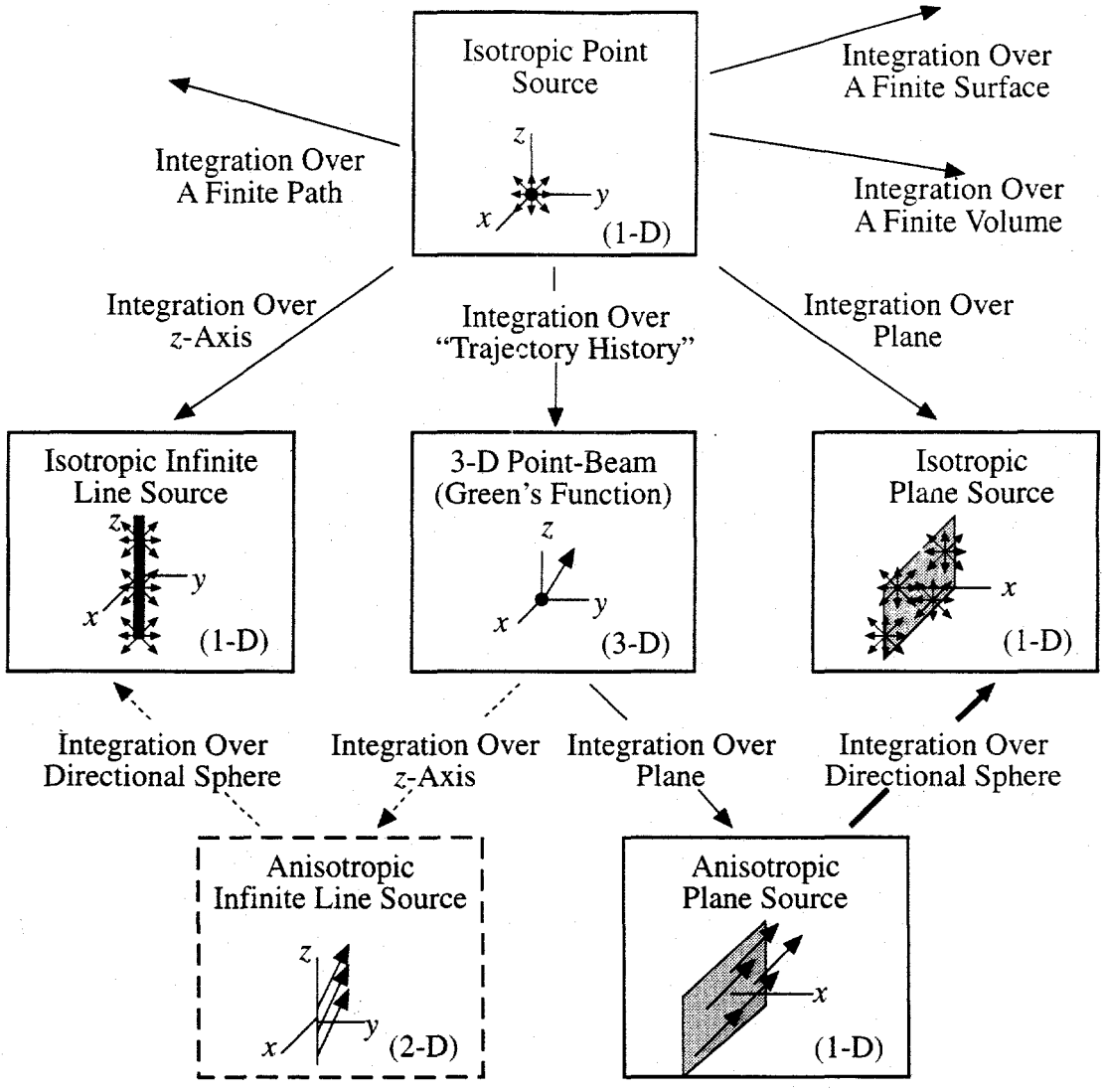

Fig. 1.2h. The ninth step in constructing the suite of infinite medium benchmarks - deriving the isotropic plane source from the anisotropic plane source.

CHAPTER 5: GENERAL RESULTS FOR THE GREEN'S FUNCTION AND FINITE SOURCES

In the last chapter two means of viewing general results were derived - the global view where the scalar flux is evaluated on the surface of a sphere, and the planar grid, where the scalar flux is evaluated on a grid of points which lie in a plane. The utility of both means of viewing results will be explored in this chapter. It was also noted that using the principle of superposition, one can evaluate the scalar flux at a point which is the result of an arbitrary array of sources. Such source configurations will also be examined.

5.A. Results which Utilize the Global View

As discussed in Ch. 4, one of the means of visualizing the data is on the surface of a sphere. The utility of this global view will now be demonstrated. Fig. 5.1 contains several global views of a Green's function source located at the origin emitting in the direction $\phi_0 = 90°$, $\theta_0 = 45°$; the beam is emitting particles in the y-z plane. The number of secondaries is 0.9 and the source strength is 0.25. Note that the scalar flux on the surfaces of the global view spheres contain sharp peaks where the beam passes through the spherical surfaces. The evaluation sphere is slightly offset (by 0.01 mfp) so that the beam does not hit any of the evaluation points directly. As the sphere is placed farther from the source, the peaks remain yet become smaller in magnitude, and the size of the peak near where the source enters the sphere (at $\phi_0 = 270°$, $\theta_0 = 135°$) is larger than the size of the peak where it exits ($\phi_0 = 90°$, $\theta_0 = 45°$).

The second example of viewing the scalar flux with the global view as shown in Fig. 5.2 contains a finite line source centered at (0,–1,0) of length 3 parallel to the x-axis and of unit strength. The detector spheres are all centered near the origin (0,0,0.01) and have different radii (0.5, 1.0, 1.5, and 3.0). When the edit sphere does not contact the line there is no sharp peak in the resulting scalar flux but only a rounded peak where the surface of the sphere is closest to the source. At $R_0 = 1.0$ the sphere barely touches the line source and therefore only one sharp peak is seen. At $R_0 = 1.5$ the sphere intersects the line at two points resulting in two sharp peaks in the scalar flux, and when the edit sphere is beyond the line, two smooth peaks are seen where the sphere's surface is closest to the source.

Fig. 5.3 displays the scalar flux as viewed by several detector spheres of an isotropic disk source. The disk has radius 2 and the detector spheres are centered at (0,0,0.51), (1,0,0.51), and (2,0,0.51) and have radius 1. When the sphere is directly above the center of the disk there is symmetry in the azimuthal angle ϕ. As the sphere moves off the center this symmetry is lost, and as the sphere extends beyond the edge of the disk, the depression in the scalar flux is evident.

The final example of the utility of the global view contains two finite line sources of length 1 centered at the origin lying on the x- and y-axes (see Fig 5.4). The spheres are very small (radius 0.01) so that in some sense the directional variation of the scalar flux may be examined. Note that the graphs for the points (0,1) and (1,0) have the same shape and magnitude with the peak being shifted in angle according to where the closest source points are. Also the graphs for the points (0.5,0.5) and (1,1) have the same shape with different magnitudes based on their distances from the sources. It is interesting to see where the peaks lie at the various points surrounding the sources. As expected, the peaks occur at 180°, 225°, and 270° for the points (1,0), (0.5,0.5), and (0,1), respectively. These angles are the directions from the detector spheres to the areas of high scalar flux.

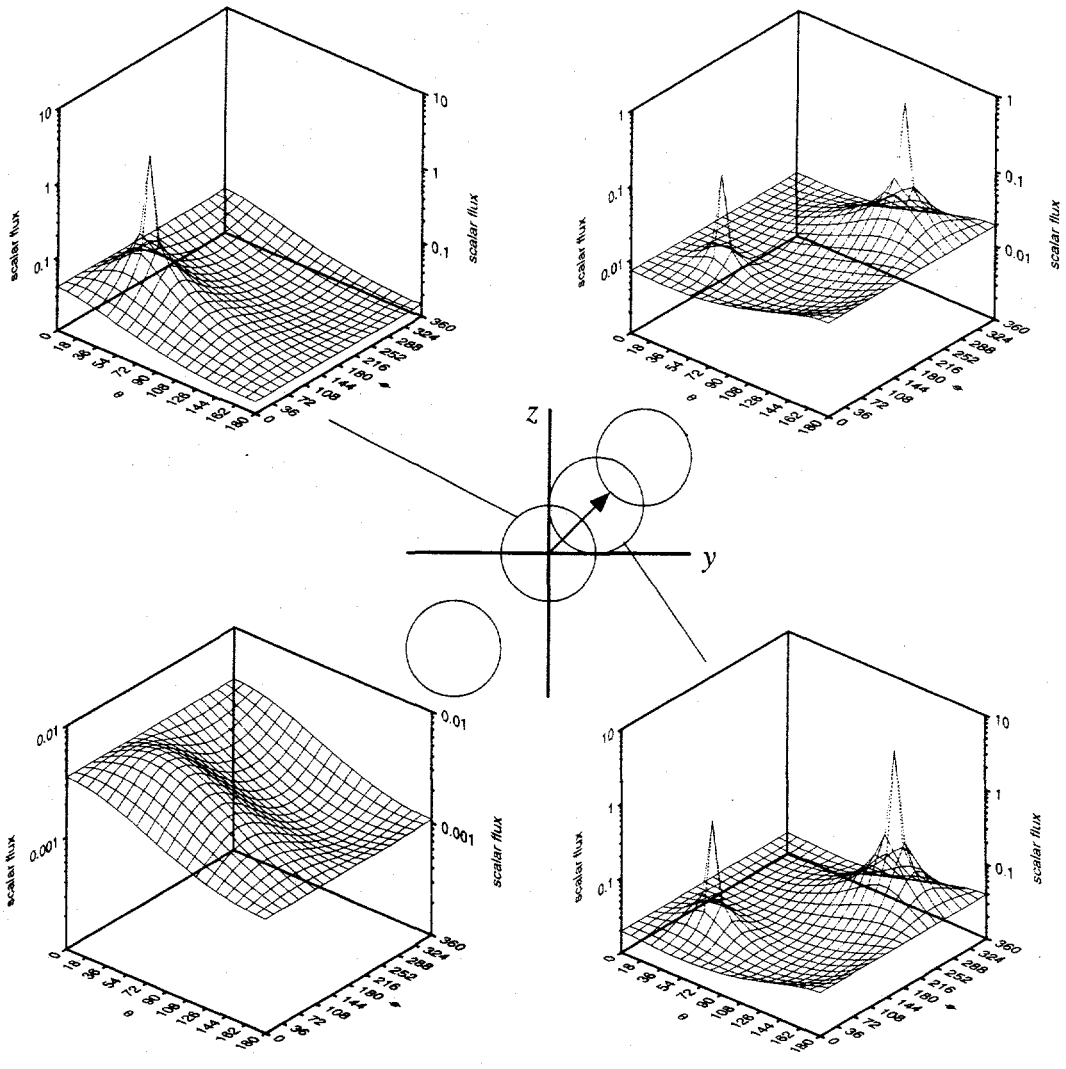

Fig. 5.1. Global views of Green's function source.

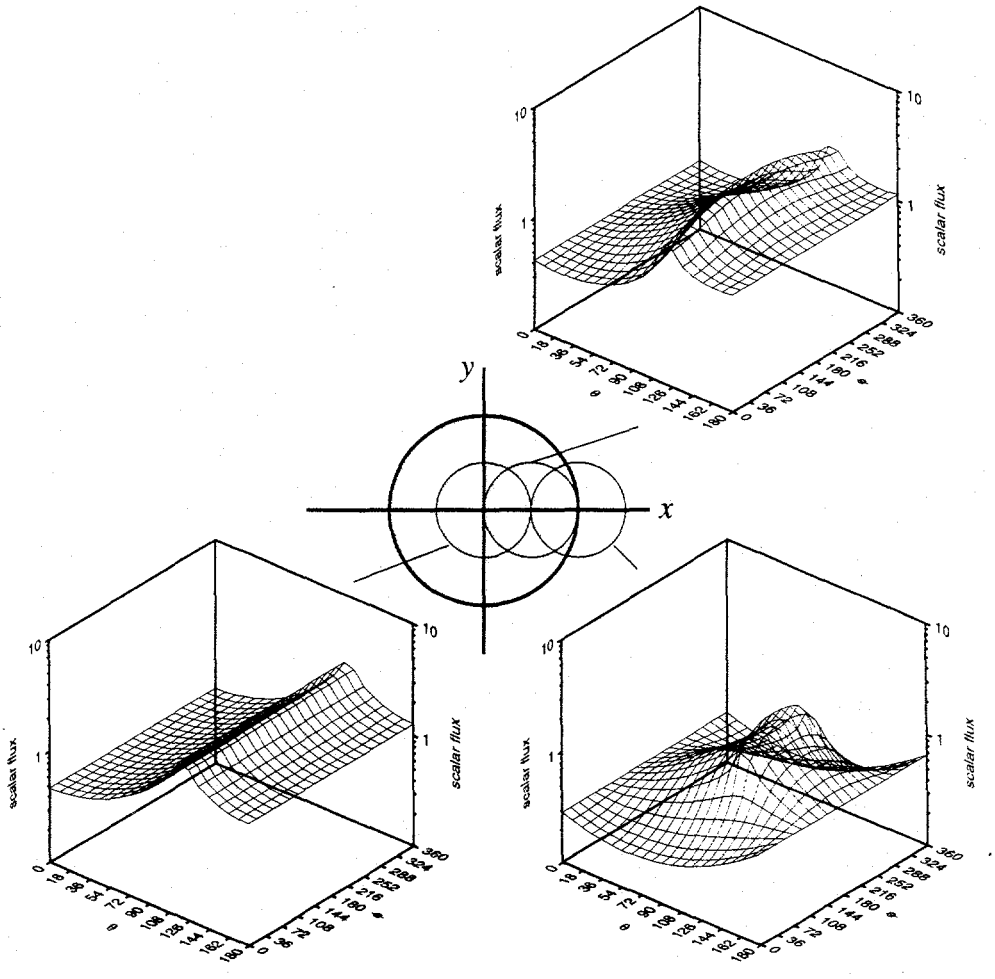

Fig. 5.3. Global views of disk source.

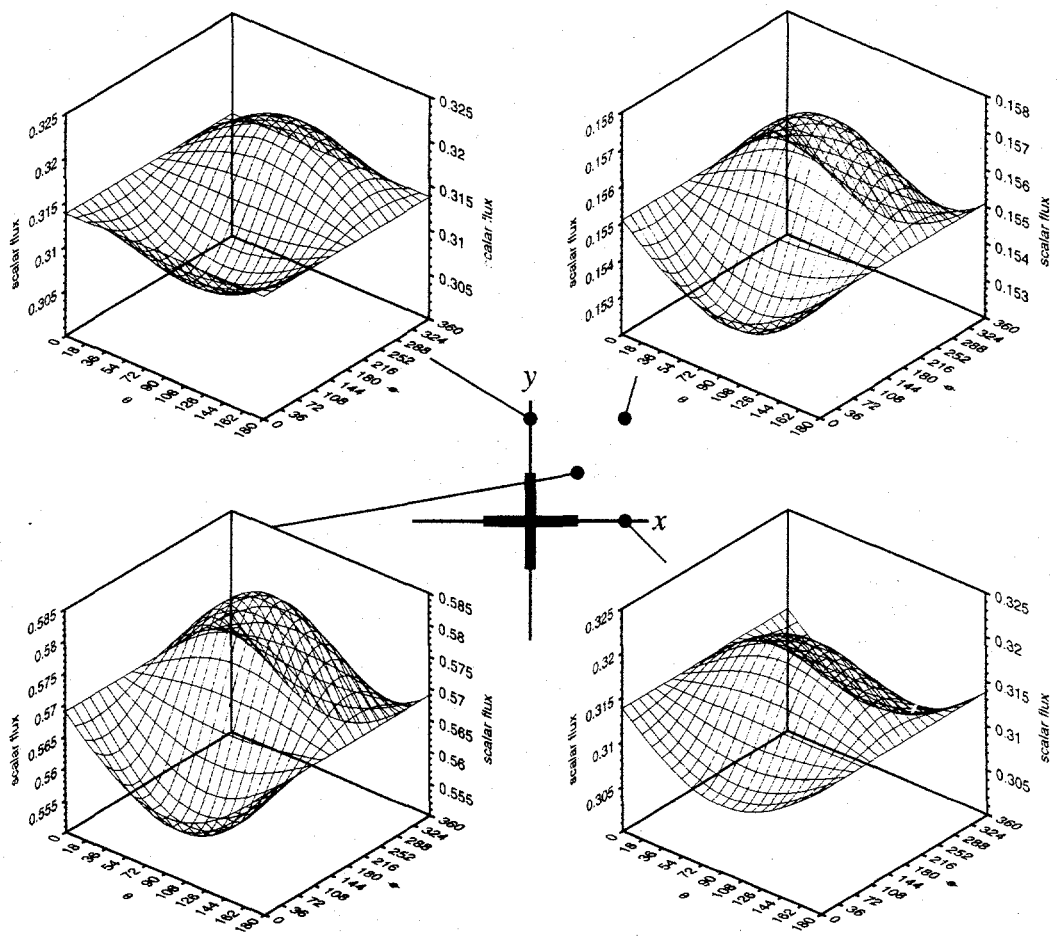

Fig. 5.4. Global views of two line sources in a "plus sign."

5.B. Multiple Source Results

There is an infinite set of possible source configurations, edit grids or formats, and case studies which may be constructed in an infinite medium. Following are two possible multiple source configurations, one composed of four Green's functions and two finite line sources and one composed of four square and two disk sources. In both cases c = 0.9.

The data regarding the first set of sources may be found in Table 5.1 and a pictorial representation of the source configuration is provided in Fig. 5.5.

Table 5.1. Source Specifications for Green's Functions/Finite Lines Example.

Point Sources	Coordinates (x,y,z,S_0)	Direction (θ_0,ϕ_0)
1	(–4,4,0,0.25)	(90°,–45°)
2	(3,4,0,0.25)	(90°,–90°)
3	(0,0,0,0.25)	(45°,90°)
4	(0,–3,0.5,0.25)	(135°,0°)
Point Sources	Coordinates $(x,y,z,2z_0,S_0)$	Direction (θ_0,ϕ_0)
5	(3,–1,0,4,1)	(90°,45°)
6	(–2,–2,0,2,1)	(90°,0°)

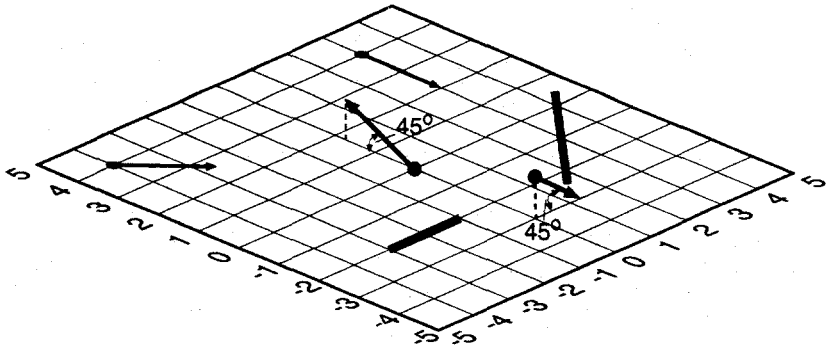

Fig. 5.5. Four Green's function and two finite line sources configuration.

Fig. 5.6 contains the contour mapping of the scalar flux and an enlargement at $z = 0$. The enlargement has a dual purpose. Because this is an analytic benchmark formulation, any desired magnification may be obtained by considering a smaller region with the same number of edit points in the grid. Also, the edit grid has been rotated an angle $\alpha_0 = -30°$ displaying the possibility of using the arbitrary windowing feature previously discussed. Fig. 5.7 displays the contour mapping at $z = 0.25$. Note that the sources in the x-y plane are less well defined because the edit grid is farther from the sources. The Green's function source at (0,–3,0.5) is barely visible. This is a result of the edit grid missing the source which is not in the plane of the edit grid; that is, none of the edit points are close enough to the source to provide a clear source definition. Therefore, an enlargement is provided to show that the solution methods will properly display the source given adequate resolution. The final contour in Fig. 5.8 is the scalar flux evaluated at $z = 0.5$. Again the sources in the $z = 0$ plane are poorly defined and the Green's function source which was located at the origin and emitted toward greater z at an angle of 45° is now shifted slightly toward higher y due to the emission angle. Also, the other Green's function source which emitted at an angle not in the x-y plane is clearly visible again because the edit grid passes close to the beam.

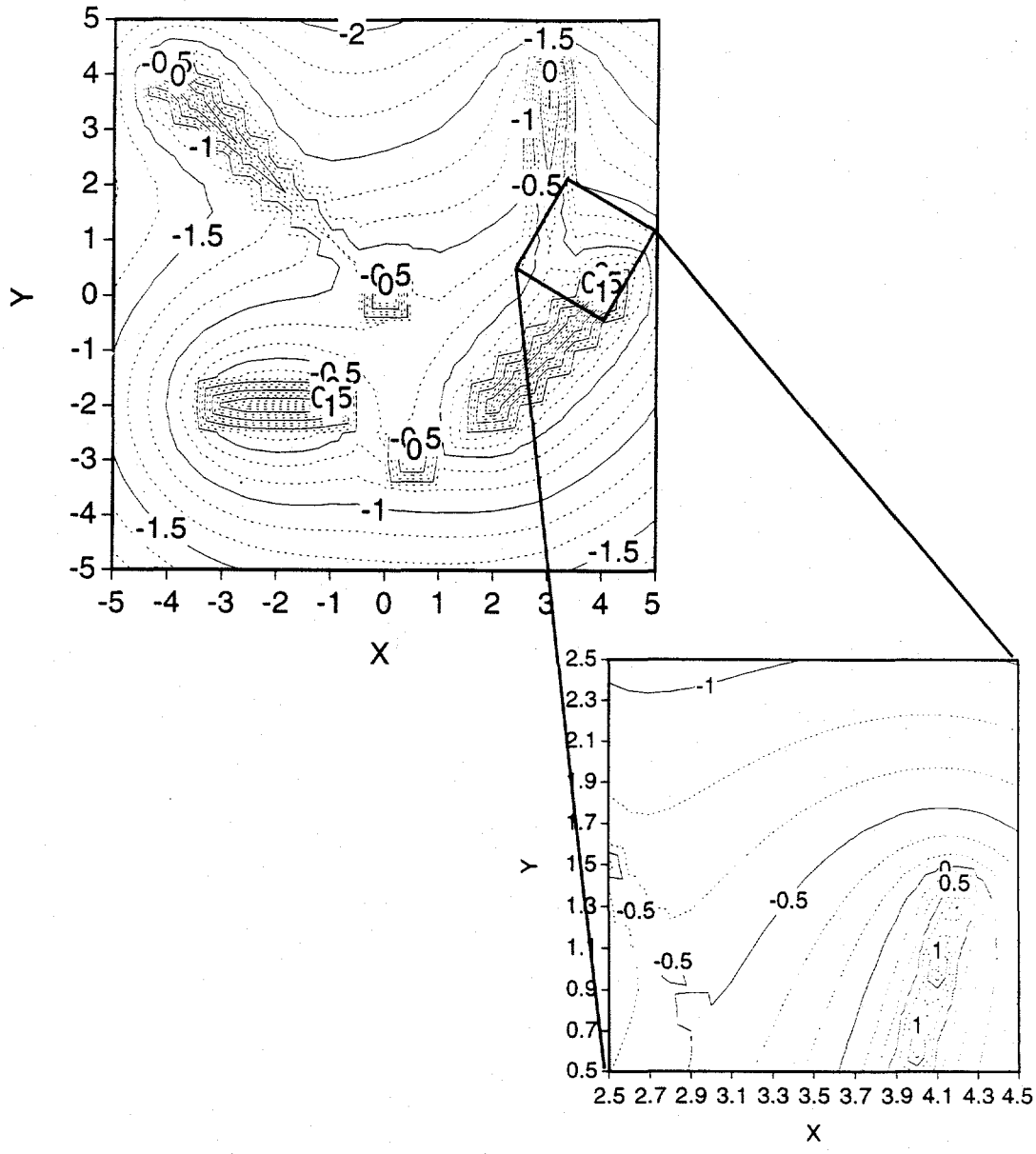

Fig. 5.6. Contour mapping at $z = 0$ for six source configuration plus enlargement.

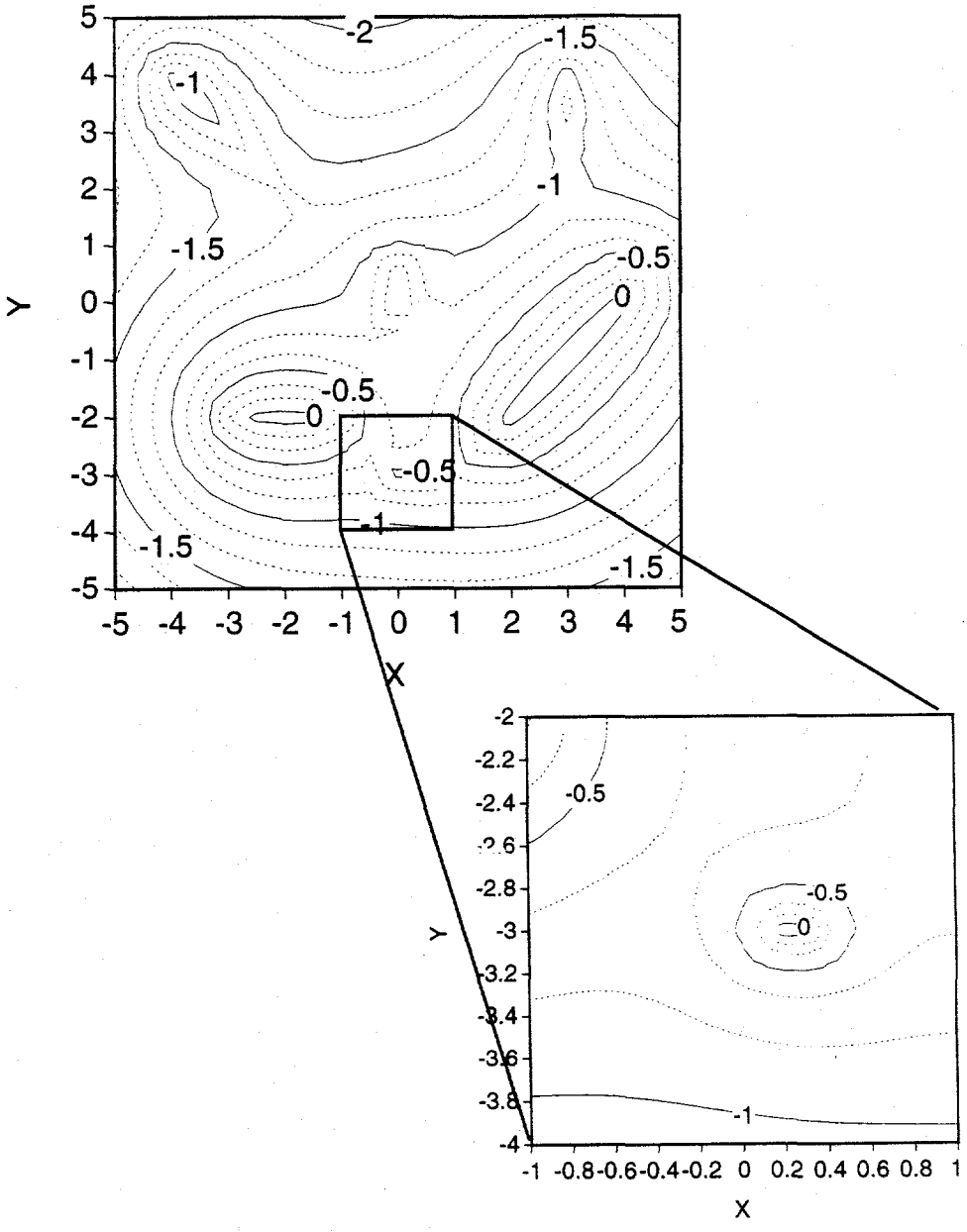

Fig. 5.7. Contour mapping at $z = 0.25$ for six source configuration plus enlargement.

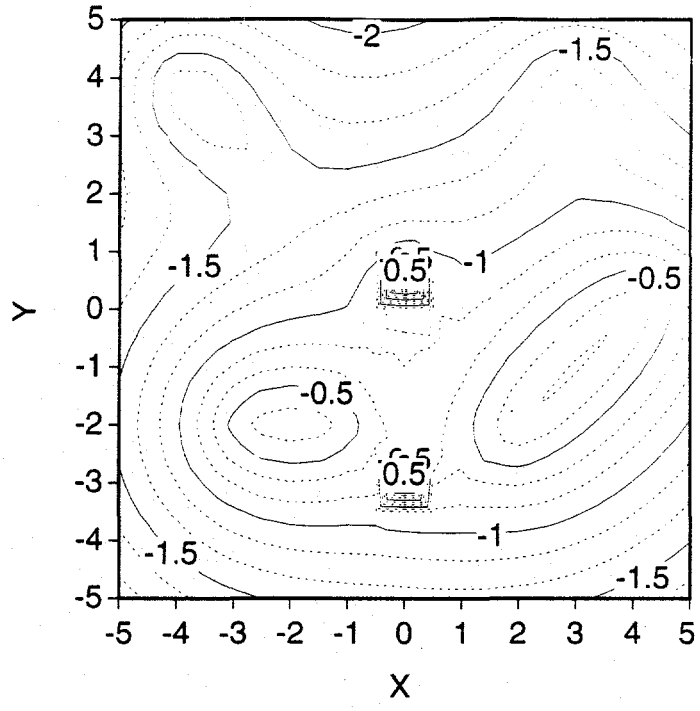

Fig. 5.8. Contour mapping at $z = 0.5$ for six source configuration.

The final example of a complicated source geometry consists of four rectangular and two disk sources surrounding the origin. The source specifications are given in Table 5.2. Figs. 5.9 and 5.10 provide a contour mapping of the scalar flux at $z = 0$ and $z = 0.9$, respectively. In Fig. 5.9 there is a depression in the scalar flux (as indicated by the depression marks) as the sources which contribute most to the scalar flux are the square sources. However, as the edit grid approaches the upper disk source in Fig. 5.10 the influence of the disk source is seen as a peak in the flux at the center which correspondingly produces depressions between the peak from the disk and the peaks from the square sources. It is postulated that source configurations similar to this one may be used to provide a radiation dose to cancerous tissue where the sources may be activated foils which emit gamma rays.

Table 5.2. Source Specifications for Disks/Rectangles Example.

Rectangular Sources	Coordinates (x,y,z,S_0)	Dimensions a_0,b_0	Direction (θ_0,ϕ_0)
1	(1.1,0,0,1)	1,1	(90°,0°)
2	(0,1.1,0,1)	1,1	(90°,90°)
3	(−1.1,0,0,1)	1,1	(90°,0°)
4	(0,−1.1,0,1)	1,1	(90°,90°)
Disk Sources	**Coordinates (x,y,z,S_0)**	**Dimensions R_0**	**Direction (θ_0,ϕ_0)**
5	(0,0,−1,1)	0.75	(0°,0°)
6	(0,0,1,1)	0.75	(0°,0°)

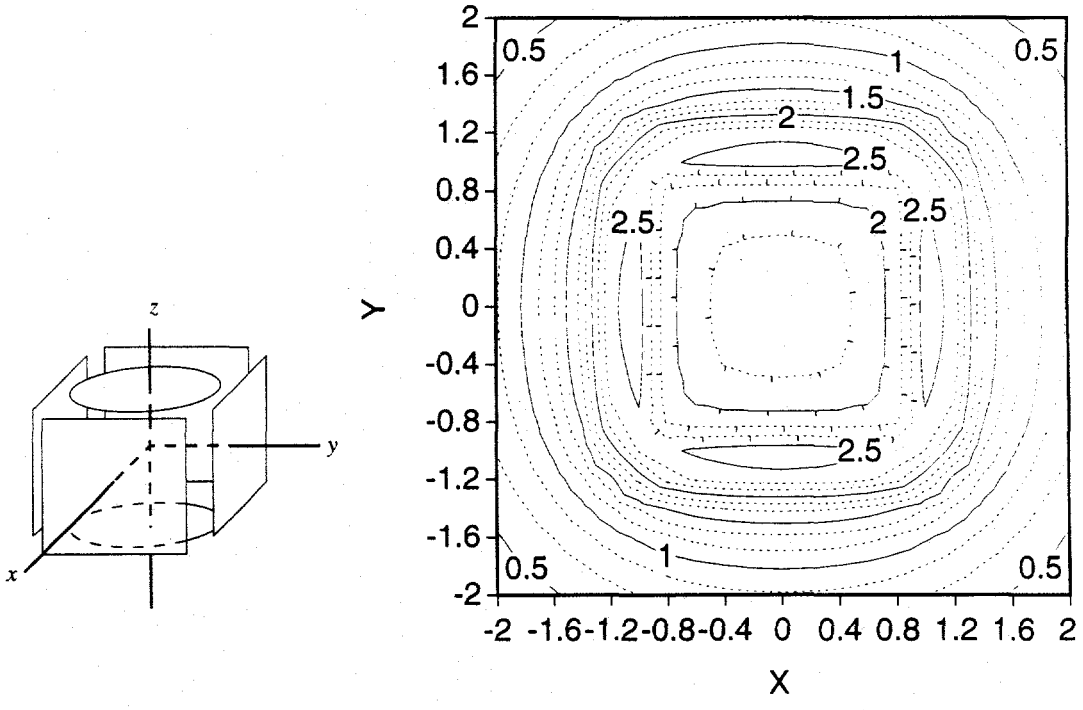

Fig. 5.9. Contour mapping of four square and two disk sources at $z = 0$.

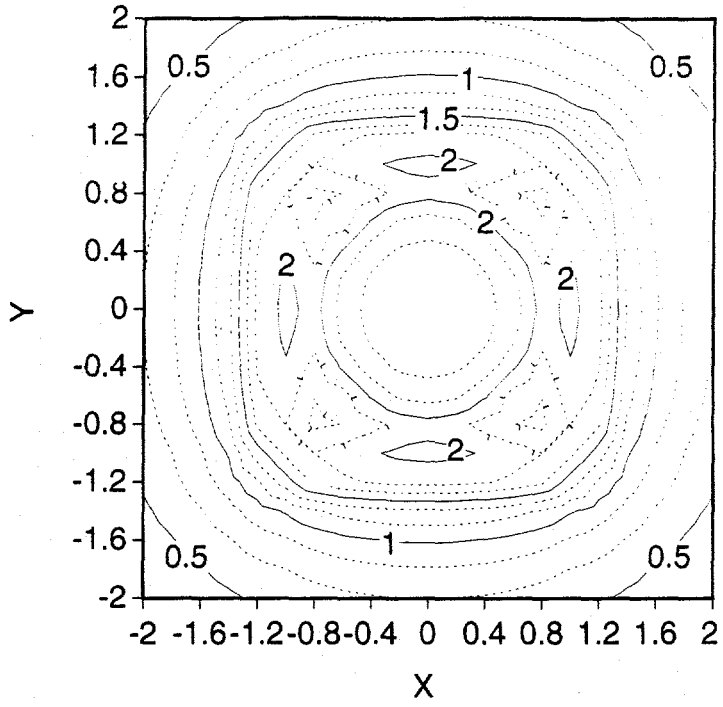

Fig. 5.10. Contour mapping of four square and two disk sources at $z = 0.9$.

5.C. Computational Environment

All calculations and results were obtained using a DEC 3000/400 Alpha workstation with 64 MB of memory. Table 5.3 provides some characteristic computational times for the various sources discussed here. The timing data are for the sources described in Tables 3.1, 3.2, 3.3, and 4.2 and displayed in Figs. 3.4, 3.5, 3.6, and 4.6 (all scalar fluxes are evaluated at $z = 0.1$). The calculation times for the Green's function and finite line sources are very short due to the evaluation of fewer integrals (the scalar flux expressions both contain double integrals), and the disk and rectangular sources require longer times for evaluation of the scalar flux due to the required evaluation of triple integrals. Evaluation times increase with stricter error requirements, as expected.

Table 5.3. Characteristic CPU Time for
Evaluation of Scalar Flux from Various Sources.

x	$err = 10^{-3}$	$err = 10^{-4}$	$err = 10^{-5}$	x	$err = 10^{-3}$	$err = 10^{-4}$	$err = 10^{-5}$
Green's Function				Disk			
0	0.03	0.07	0.16	0	0.96	1.62	3.86
0.5	0.02	0.05	0.14	0.5	2.28	4.45	7.99
1	0.02	0.06	0.16	1	1.42	3.30	9.46
1.5	0.03	0.07	0.17	1.5	1.16	3.66	9.47
2	0.03	0.06	0.22	2	1.80	3.37	8.47
Finite Line				Rectangle			
0	0.05	0.08	0.19	0	1.54	7.50	34.45
0.5	0.02	0.04	0.09	0.5	1.13	5.95	22.06
1	0.02	0.04	0.10	1	0.71	3.09	8.47
1.5	0.03	0.04	0.07	1.5	0.44	0.96	4.34
2	0.03	0.04	0.07	2	0.43	0.86	2.37

The final source analysis required to complete Fig. 1.2 is the infinite anisotropic line source in an infinite homogeneous medium. The analysis of this source will use many of the mathematical and numerical techniques seen thus far.

CHAPTER 6: THE ANISOTROPICALLY EMITTING INFINITE LINE SOURCE

The next step in the progression of analytical benchmarks in infinite homogeneous media involves a source which is analyzed more for its mathematical curiosity than for its physical relevance. Benchmarks have been provided for those geometries which have one-dimensional (isotropic point source; isotropic infinite line; isotropic and anisotropic infinite plane), two-dimensional (isotropic finite line, isotropic disk, Green's function), and three-dimensional (isotropic rectangular source) variations in the scalar flux. However, in all cases of finite-sized sources, the variation in the scalar flux is seen to be three-dimensional by intelligently rotating axes and coordinate translations to place the source(s) at arbitrary locations in the medium; therefore, a three-dimensional scalar flux variation may be numerically evaluated using two-dimensional techniques. In general, the dimensionality of the solution method is associated to the number of implicit integrals which must be evaluated to obtain a numerical solution.

The ultimate goal of this work is to obtain numerical results for a problem which is truly three-dimensional in nature - the classical searchlight problem with a canted incident beam. In order to expand the benchmarks which are available, to provide for a complete picture of benchmarks in infinite homogeneous media, and to study the mathematics and numerics required for the searchlight problem, a two-dimensional benchmark is considered in this chapter where an anisotropically emitting infinite line source is placed in an infinite medium, and the scalar flux is determined. Where most two-dimensional benchmarks for the scalar flux provide results in Cartesian (x,y) or cylindrical (ρ,z) coordinates, this analysis presents a two-dimensional benchmark in polar (ρ,α) geometry.

6.A. Anisotropic Infinite Line Problem Definition

The setting for this problem is an infinite homogeneous medium which scatters particles isotropically. The properties of this medium are described by the factor c, which is the mean number of secondary particles produced per collision. A cylindrical coordinate system (ρ,α,z) best fits the geometry. The source is an infinitely long line located at $\rho = 0$ along the z-axis which emits particles in a single direction $\vec{\Omega}_0(\phi_0,\theta_0)$. A pictorial view of the source geometry is given in Fig. 6.1, and the step in the progression toward completion of Fig. 1.2 is shown in Fig. 1.2i.

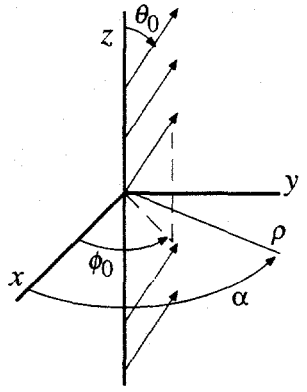

Fig. 6.1. Source geometry for an infinite line source emitting particles in the direction $\vec{\Omega}_0(\phi_0,\theta_0)$.

The flux from the anisotropically emitting line source is mathematically constructed by integrating the solution for a monodirectional point source (Green's function) emitting in a specific direction over the full range of the z-axis. Using cylindrical geometry, the one energy group transport equation for this point source located at the origin and emitting particles in the direction $\vec{\Omega}_0(\phi_0,\theta_0)$ is

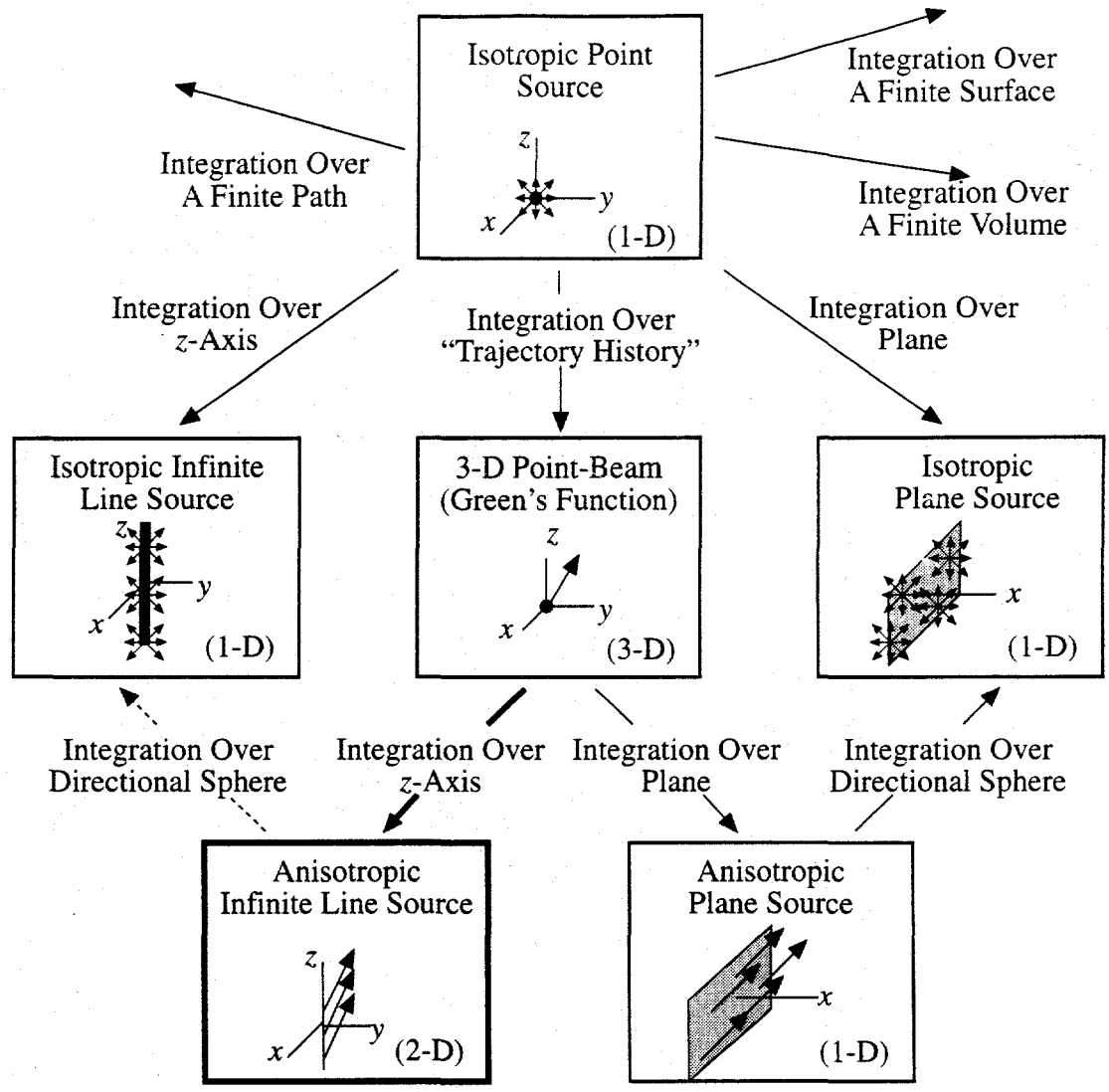

Fig. 1.2i. The tenth step in constructing the suite of infinite medium benchmarks - the anisotropic infinite line source.

$$\left[\mu\frac{\partial}{\partial z} + \vec{\omega}\cdot\frac{\partial}{\partial \vec{\rho}} + 1\right]\phi(z,\vec{\rho},\vec{\Omega}) = \frac{c}{4\pi}\int_{4\pi} d\vec{\Omega}'\,\phi(z,\vec{\rho},\vec{\Omega}') +$$

$$+\frac{\delta(\rho)}{2\pi\rho}\delta(\mu-\mu_0)\delta(\phi-\phi_0)\delta(z)\ , \qquad (6.1a)$$

with the boundary conditions

$$\lim_{z\to\infty} \phi(z,\vec{\rho},\vec{\Omega}) < \infty \quad , \quad \lim_{|\vec{\rho}|\to\infty} \phi(z,\vec{\rho},\vec{\Omega}) < \infty \quad . \tag{6.1b}$$

By taking a 2-D Fourier transform in the transverse $\vec{\rho}(\rho,\alpha)$ plane [with $\vec{k}(k,\psi)$ as the corresponding transform variable], constructing a 1-D pseudo problem, and taking a 1-D Fourier transform in the transverse (z) direction, it was shown in Chapter 4 that the transformed scalar flux from this Green's function source is given by

$$\bar{\bar{\psi}}(z;\vec{k}) = \frac{1}{\mu_0}\mathcal{F}_z^{-1}\left\{\frac{U_0}{1 + ipU_0}\,\frac{1}{1 - cL(p,k)}\right\} \quad , \tag{6.2a}$$

where $\mathcal{F}_z^{-1}$ is the inverse Fourier transform in the longitudinal direction with transform variable p, and U_0 is defined by

$$U_0 \equiv \frac{\mu_0}{1 - ik\left(1 - \mu_0^2\right)^{1/2}\cos(\phi_0 - \psi)} \quad . \tag{6.2b}$$

$L(p,k)$ is the generalization of the one-dimensional transformed single scatter kernel

$$L(p,k) = \frac{\tan^{-1}\left(k^2 + p^2\right)^{1/2}}{\left(k^2 + p^2\right)^{1/2}} \quad . \tag{6.2c}$$

As previously noted, the scalar flux for the anisotropically emitting infinite line source is obtained by integrating the Green's function source over the entire z-axis as

$$\phi_l(\rho,\alpha) = \int_{-\infty}^{\infty} dz\ \phi_{pt}(\vec{\rho},z) \quad . \tag{6.3a}$$

By cleverly using the definition of the Fourier transform, it is readily seen that the transversely transformed scalar flux resulting from the line source can be obtained by setting $p = 0$ in the following equation:

$$\phi_l(\rho,\alpha) = \int_{-\infty}^{\infty} dz\ e^{-ipz}\ \phi_{pt}(\vec{\rho},z)\Big|_{p=0} \quad , \tag{6.3b}$$

$$\phi_0(\rho,\alpha) = \int_{-\infty}^{\infty} dz \, \frac{e^{-z/\mu_0}}{\mu_0 \rho} \, \delta(\alpha - \phi_0) \delta\left[\rho - \frac{z}{\mu_0}\left(1 - \mu_0^2\right)^{1/2}\right] \theta(z/\mu_0) \ . \tag{6.5b}$$

Assuming $\mu_0 > 0$ leaves

$$\phi_0(\rho,\alpha) = \delta(\alpha - \phi_0) \int_0^{\infty} dz \, \frac{e^{-z/\mu_0}}{\mu_0 \rho} \, \delta\left[\rho - \frac{z}{\mu_0}\left(1 - \mu_0^2\right)^{1/2}\right] \ , \tag{6.5c}$$

and with the following means of changing the argument of the delta function

$$\delta[\rho - f(z)]|d\rho| = \delta[z - f(\rho)]|dz|$$

it is seen that

$$\delta\left[\rho - \frac{z}{\mu_0}\left(1 - \mu_0^2\right)^{1/2}\right] = \delta\left[z - \frac{\mu_0}{\left(1 - \mu_0^2\right)^{1/2}} \rho\right] \frac{\mu_0}{\left(1 - \mu_0^2\right)^{1/2}} \ ,$$

which leaves for the uncollided scalar flux from the infinite anisotropically emitting line source

$$\phi_0(\rho,\alpha) = \frac{e^{-\rho/\gamma_0}}{\rho \gamma_0} \, \delta(\alpha - \phi_0) \ . \tag{6.5d}$$

Because of the symmetries inherent in the problem, ϕ_0 is arbitrarily set to zero as the solution for a specific emission angle may be obtained by a simple rotation of coordinates axes.

6.B. One-Dimensional Cases Derived from the Anisotropic Infinite Line Source

In order to provide simple generalizations of the two-dimensional source, cases which reduce to one dimension are considered. The two cases under consideration have

the beam emitting particles along the z-axis (thus losing any angular dependence) and an integration over the unit circle so that particles are emitting along the surface of a cone.

6.B.1 One-Dimensional Cases: $\mu_0 = 1$.

A special case arises when $\mu_0 = 1$ ($\gamma_0 = 0$). The source is now directed along the z-axis; thus, there is no α dependence in the solution. Setting $\gamma_0 = 0$ in Eqs. (6.4) and recalling the definition of the zeroth order Bessel function, the solution to this one-dimensional case is obtained as

$$\phi(\rho;\gamma_0=0) = \frac{c}{2\pi}\int_0^\infty dk\ k\, f(k)\ J_0(k\rho)\ . \tag{6.6a}$$

As shown previously, the scalar flux in an infinite medium containing an isotropically emitting line source at $\rho = 0$ is given by

$$\phi_{iso}(\rho) = \frac{1}{2\pi}\int_0^\infty dk\ k\, f(k)\ J_0(k\rho)\ . \tag{6.6b}$$

Thus, the one-dimensional case considered here may be written in terms of the isotropic source solution as

$$\phi(\rho;\gamma_0=0) = c\,\phi_{iso}(\rho)\ . \tag{6.6c}$$

This result may be interpreted in the following manner: because the source is emitting strictly along the z-axis ($\rho = 0$), the only means by which particles may appear at a position $\rho > 0$ is for the particles to have scattered somewhere along the z-axis. When the particles have collisions on the z-axis, there is a probability, $1 - c$, that they will be absorbed, and if they scatter, they scatter isotropically as this is a property of the medium. Thus, the particles appear to have come from an isotropic source at $\rho = 0$, and the scalar

flux is adjusted by the fraction of surviving particles which were not absorbed in their first collision on the z-axis.

6.B.2 One-Dimensional Cases: Emission Into All Transverse Angles.

Another one-dimensional problem may be constructed by integrating Eqs. (6.4) over the full range of α. This is actually an integration over the emission angle ϕ_0; however, since ϕ_0 was arbitrarily set to zero, the equivalent result is obtained by an integral over α. Thus, this problem contains a source which emits particles in directions along the surface of a cone the angle of which is given by the parameter γ_0 as shown in Fig. 6.2. Note in the figure that only the emission from the point $z = 0$ is shown explicitly; however, such emission occurs at each point along the z-axis.

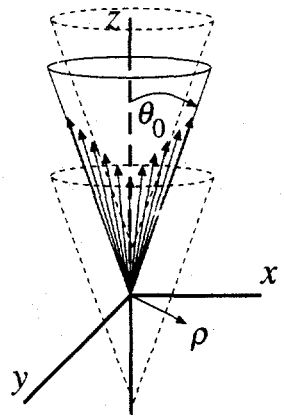

Fig. 6.2. Source emission into all transverse angles (onto surface of a cone).

The scalar flux is therefore given by

$$\phi_{cone}(\rho) = \frac{1}{2\pi}\int_0^{2\pi} d\alpha\ \phi(\rho,\alpha) \quad . \tag{6.7}$$

The primary integral to be evaluated in this case is

$$I(\rho) = \int_0^{2\pi} d\alpha\, I(\rho,\alpha;k) =$$

$$= I(k,\rho) = \frac{1}{2\pi}\int_0^{2\pi} \frac{d\psi}{1 - ik\gamma_0\cos\psi}\int_0^{2\pi} d\alpha\, e^{-ik\rho\cos(\psi - \alpha)} \quad . \tag{6.8a}$$

Recognizing the integral for $J_0(x)$ yields

$$I(k,\rho) = J_0(\rho k)\int_0^{2\pi} \frac{d\psi}{1 - ik\gamma_0\cos\psi} \quad , \tag{6.8b}$$

and by letting $x = k\gamma_0$ $(x > 0)$, the integral in Eq. (6.8a) is rewritten as

$$u(x) = \int_0^{2\pi} \frac{d\psi}{1 - ix\cos\psi} \quad . \tag{6.8c}$$

A standard change of variable for an integration using complex variables containing a cosine function is to let $z = e^{i\psi}$ which gives (after some simplification)

$$u(x) = \frac{2}{x}\int_{|z|=1} \frac{dz}{z^2 + \frac{2i}{x}z + 1} \quad , \tag{6.8d}$$

or

$$u(x) = \frac{2}{x}\int_{|z|=1} \frac{dz}{(z - p)(z - q)} \quad , \tag{6.8e}$$

where the poles lie on the imaginary axis and have the values $p = \frac{i}{x}\left[-1 + \left(x^2 + 1\right)^{1/2}\right]$, $q = \frac{i}{x}\left[-1 - \left(x^2 + 1\right)^{1/2}\right]$. The following limits

$$\lim_{x\to 0} p(x) = 0 \quad , \quad \lim_{x\to\infty} p(x) = i \quad ,$$

$$\lim_{x\to 0} q(x) = -i\infty \quad , \quad \lim_{x\to\infty} q(x) = -i \quad ,$$

show that the value of q ranges along the negative imaginary axis outside the unit circle and the value of p is on the positive imaginary axis inside the unit circle. Therefore, when the residue theorem is applied to Eq. (6.8e) the only pole which contributes is p. Applying the residue theorem gives

$$u(x) = \frac{4\pi i}{x} \frac{1}{(p - q)} \ , \tag{6.9a}$$

or upon introduction of the values for p and q:

$$u(x) = \frac{2\pi}{\left(x^2 + 1\right)} \ . \tag{6.9b}$$

By reverting to the original variables it is seen that

$$I(\rho;k) = \frac{2\pi J_0(\rho k)}{\left(1 + k^2\gamma_0^2\right)^{1/2}} \ . \tag{6.9c}$$

Thus, for an infinitely long source which emits particles with equal probabilities into each transverse angular direction along the surface of a cone, the scalar flux is

$$\phi_{cone}(\rho) = \frac{e^{-\rho/\gamma_0}}{2\pi\rho\gamma_0} + \frac{c}{2\pi} \int_0^\infty dk \ k \ f(k) \ \frac{J_0(k\rho)}{\left(1 + k^2\gamma_0^2\right)^{1/2}} \ . \tag{6.10}$$

Note that if $\gamma_0 = 0$, the uncollided takes the following form

$$\lim_{\gamma_0 \to 0} \frac{e^{-\rho/\gamma_0}}{2\pi\rho\gamma_0} = \frac{\delta(\rho)}{2\pi\rho} \ ,$$

and the form for the isotropic line source scaled by the factor c is obtained [Eq. (6.6c)] as expected. Again, if the beam emits along the z-axis, the above limit indicates that there are no particles found at $\rho > 0$ that are uncollided. Also, if $\gamma_0 = 1$, the source emits perpendicularly to the z-axis in the $\vec{\rho}$-plane.

6.C. Alternative Formulation for Scalar Flux Solution: Infinite Series

The scalar flux from the anisotropically emitting line source is given by Eqs. (6.4). In order to better facilitate the numerical evaluation of the scalar flux, it may be desirable to obtain an alternative formulation which is more amenable to numerical evaluation. This alternative formulation is obtained by representing the complex exponential in terms of an infinite series over Bessel functions [Crosbie and Lee]:

$$e^{-i\eta\cos\theta} = \sum_{m=0}^{\infty}(2 - \delta_{m0})(-i)^m J_m(\eta)\cos(m\theta) \quad . \tag{6.11a}$$

Recalling the expression for the collided portion of the scalar flux,

$$\phi_c(\rho,\alpha) = \frac{c}{2\pi}\int_0^{\infty} dk\ k\ f(k)\ \frac{1}{2\pi}\int_0^{2\pi} d\psi\ \frac{e^{-ik\rho\cos(\psi - \alpha)}}{1 - ik\gamma_0\cos(\psi - \phi_0)} \quad , \tag{6.11b}$$

we then define for convenience

$$u(k;\rho,\alpha) \equiv \frac{1}{2\pi}\int_0^{2\pi} d\psi\ \frac{e^{-ik\rho\cos(\psi - \alpha)}}{1 - ik\gamma_0\cos\psi} \quad . \tag{6.11c}$$

The series formula for the complex exponential is substituted into Eq. (6.11c) and the remaining term is rewritten as an integral by noting that

$$\frac{1}{1 - ik\gamma_0\cos\psi} = \int_0^{\infty} dz\ e^{-z(1 - ik\gamma_0\cos\psi)} \tag{6.12}$$

so that (with rearrangement of integrals and the summation)

$$u(k;\rho,\alpha) = \frac{1}{2\pi}\sum_{m=0}^{\infty}(2 - \delta_{m0})(-i)^m J_m(k\rho)\ u_m(k\alpha) \quad , \tag{6.13a}$$

where

$$u_m(k\alpha) = \int_0^\infty dz\ e^{-z} \int_0^{2\pi} d\psi \cos[m(\psi - \alpha)] e^{izk\gamma_0 \cos\psi} \ . \tag{6.13b}$$

By expanding the cosine via its addition formula it may be seen that

$$u_m(k\alpha) = \int_0^\infty dz\ e^{-z} \cos(m\alpha) \int_0^{2\pi} d\psi\ e^{i\eta\cos\psi} \cos(m\psi) +$$

$$+ \int_0^\infty dz\ e^{-z} \sin(m\alpha) \int_0^{2\pi} d\psi\ e^{i\eta\cos\psi} \sin(m\psi) \ , \tag{6.13c}$$

where $\eta = zk\gamma_0$. Using the following relations [Crosbie and Lee]

$$\int_0^{2\pi} e^{-i\eta\cos(\psi - \alpha)} \left\{ \begin{matrix} \sin(m\psi) \\ \cos(m\psi) \end{matrix} \right\} d\psi = 2\pi\,(-i)^m J_m(\eta) \left\{ \begin{matrix} \sin(m\alpha) \\ \cos(m\alpha) \end{matrix} \right\} \ , \tag{6.14}$$

with $\alpha = 0$, Eq. (6.13c) becomes

$$u_m(k\alpha) = \int_0^\infty dz\ e^{-z} \cos(m\alpha)\ 2\pi\,(-i)^m J_m(-zk\gamma_0) \ ; \tag{6.15a}$$

noting that $J_m(-x) = (-1)^m J_m(x)$ and rearranging leaves

$$u_m(k\alpha) = \cos(m\alpha)\ 2\pi\,(i)^m \int_0^\infty dz\ e^{-z} J_m(zk\gamma_0) \ . \tag{6.15b}$$

The integral in Eq. (6.15b) is of the form of a Laplace transform and the formula for the Laplace transform of a Bessel function or order m is [Abramowitz and Stegun]

$$\int_0^\infty dz\ e^{-st} J_m(at) = \frac{1}{a^m} \frac{\left[\left(s^2 + a^2\right)^{1/2} - s\right]^m}{\left(s^2 + a^2\right)^{1/2}} \ . \tag{6.16}$$

It is then seen that

$$u_m(k\alpha) = \frac{2\pi}{\left(1 + k^2\gamma_0^2\right)^{1/2}} \cos(m\alpha)\ (i)^m \left[\frac{\left(1 + k^2\gamma_0^2\right)^{1/2} - 1}{k\gamma_0}\right]^m \ . \tag{6.17}$$

Inserting this into Eq. (6.13a), it is found that the inner integral may be written as the infinite sum (after some simplification):

$$u(k;\rho,\alpha) = \sum_{m=0}^{\infty}(2 - \delta_{m0}) \frac{J_m(k\rho)}{\left(1 + k^2\gamma_0^2\right)^{1/2}} \cos(m\alpha)\left[\frac{\left(1 + k^2\gamma_0^2\right)^{1/2} - 1}{k\gamma_0}\right]^m . \qquad (6.18)$$

This gives for the collided portion of the scalar flux

$$\phi_c(\rho,\alpha) = \frac{c}{2\pi}\int_0^{\infty} \frac{dk\ k\ f(k)}{\left(1 + k^2\gamma_0^2\right)^{1/2}} \sum_{m=0}^{\infty}(2 - \delta_{m0})\ J_m(k\rho) \times$$

$$\times \cos(m\alpha)\left[\frac{\left(1 + k^2\gamma_0^2\right)^{1/2} - 1}{k\gamma_0}\right]^m , \qquad (6.19a)$$

or with the integration and summation operations interchanged

$$\phi_c(\rho,\alpha) = \frac{c}{2\pi}\sum_{m=0}^{\infty}(2 - \delta_{m0})\cos(m\alpha) \times$$

$$\times \int_0^{\infty} dk\ \frac{k\ f(k)}{\left(1 + k^2\gamma_0^2\right)^{1/2}} J_m(\rho k)\left[\frac{\left(1 + k^2\gamma_0^2\right)^{1/2} - 1}{k\gamma_0}\right]^m . \qquad (6.19b)$$

A cursory examination of Eqs. (6.19) results in the realization that this alternative series formulation of the scalar flux from the anisotropically emitting infinite line source is a Fourier cosine series.

6.D. The One-Dimensional Cases Using the Alternative Series Formulation

A quick check that the results of the alternative series formulation is consistent with the integral formulation, from which it was derived, is to derive the one-dimensional cases from the alternative formulation. Again, the two cases under consideration are if the beam

emits particles along the z-axis (thus losing angular dependence) and an integration over the unit circle so that particles are emitted along the surface of a cone.

6.D.1 One-Dimensional Cases: $\mu_0 = 1$.

The alternative formulation has the same uncollided flux as the integral formulation; therefore, only the collided portion is examined. The only terms in Eqs. (6.19) which are affected by setting $\gamma_0 = 0$ ($\mu_0 = 1$) lie inside the integrals. Therefore the limit L_0 is defined as

$$L_0 = \lim_{\gamma_0 \to 0} \frac{1}{\left(1 + k^2\gamma_0^2\right)^{1/2}} \left[\frac{\left(1 + k^2\gamma_0^2\right)^{1/2} - 1}{k\gamma_0}\right]^m = \lim_{\gamma_0 \to 0} \left[\frac{\left(1 + k^2\gamma_0^2\right)^{1/2} - 1}{k\gamma_0}\right]^m ,$$

which is seen to be 0 except when $m = 0$, where it is 1. Therefore, $L_0 = \delta_{m0}$ and

$$\phi_c(\rho;\gamma_0{=}0) = \frac{c}{2\pi} \sum_{m=0}^{\infty} (2 - \delta_{m0}) \cos(m\alpha) \int_0^{\infty} dk\, k\, f(k)\, J_m(\rho k)\, \delta_{m0} \quad . \tag{6.20a}$$

or

$$\phi_c(\rho;\gamma_0{=}0) = \frac{c}{2\pi} \int_0^{\infty} dk\, k\, f(k)\, J_0(\rho k) \quad . \tag{6.20b}$$

which agrees with Eqs. (6.6) as expected.

6.D.2 One-Dimensional Cases: Emission Into All Transverse Angles.

The second one-dimensional problem integrates Eqs. (6.19) over the full range of α, indicating emission on the surface of a cone. The only place where there is dependence on α is in the term $\cos(\alpha m)$. Noting that the appropriate integration is expressed as

$$\phi_{cone}(\rho) = \frac{1}{2\pi} \int_0^{2\pi} d\alpha\, \phi(\rho,\alpha) \quad , \tag{6.21a}$$

and noting the integration over α yields

$$\frac{1}{2\pi}\int_0^{2\pi} d\alpha \cos(\alpha m) = \delta_{m0} \ , \tag{6.21b}$$

it is immediately seen that the expected form for $\phi_{cone}(\rho)$ is obtained as

$$\phi_{cone}(\rho) = \frac{e^{-\rho/\gamma_0}}{2\pi\rho\gamma_0} + \frac{c}{2\pi}\int_0^{\infty} dk\ k\ f(k)\ \frac{J_0(k\rho)}{\left(1 + k^2\gamma_0^2\right)^{1/2}} \ . \tag{6.21c}$$

6.E. Reformulation of Inversion in Cartesian Coordinates

The cylindrical coordinate system is the most natural for this problem; however, the singularity along $\alpha = 0$ creates problems for the numerical evaluation of the double integration for small α. Certain restrictions may be placed on α (examined in a later section) which will be seen to allow the inversion in cylindrical coordinates at smaller α than otherwise obtainable, but those restrictions violate the general philosophies of analytical benchmarking in that they restrict the values of the spatial angular variable at which the evaluation may be performed. Therefore, it is desirable to restate the inversion so that the singularity in angle is not so apparent. This is accomplished by reformulating the inversion integrals in terms of the variables obtained from an analysis using a Cartesian coordinate system. Again, the desired quantity is the scalar flux resulting from a source which is an infinitely long line on the z-axis located at $x = 0$, $y = 0$. The source emits particles anisotropically in a single direction $\vec{\Omega}_0(\phi_0,\theta_0)$. As in Eqs. (6.4), the uncollided and collided portions of the scalar flux may be separated resulting in the following equation

$$\phi(\rho,\alpha) = \phi_0(\rho,\alpha) + \phi_c(\rho,\alpha) \ , \tag{6.22a}$$

where

$$\phi_0(\rho,\alpha) = \frac{e^{-\rho/\gamma_0}}{\rho\gamma_0}\delta(\alpha) \quad , \tag{6.22b}$$

and

$$\phi_c(\rho,\alpha) = \frac{c}{4\pi^2}\int_0^\infty dk\ k\ \frac{L(k)}{1 - cL(k)}\int_0^{2\pi} d\psi\ \frac{e^{-ik\rho\cos(\psi - \alpha)}}{1 - ik\gamma_0\cos(\psi)} \quad . \tag{6.22c}$$

6.E.1. Direct and Transform Coordinate Transformations.

Transforming the scalar flux in direct space and in transformed space requires two simple trigonometric changes of variables as seen in Fig. 6.3.

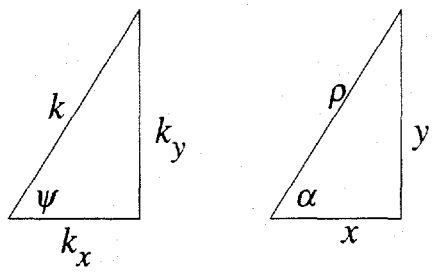

Fig. 6.3. Trigonometric changes of variables for direct and transformed space relating cylindrical and Cartesian coordinates.

With the figure as a guide, it is easy to see that the following transformations hold

$$k^2 = k_x^2 + k_y^2 \quad , \tag{6.23a}$$

$$\psi = \tan^{-1}\left(\frac{k_y}{k_x}\right) \quad , \tag{6.23b}$$

$$\rho^2 = x^2 + y^2 \quad , \tag{6.23c}$$

$$\alpha = \tan^{-1}\left(\frac{y}{x}\right) , \tag{6.23d}$$

$$k_x = k\cos\psi \ . \tag{6.23e}$$

Using the addition formula for the cosine, it is seen that

$$\cos(\psi - \alpha) = \cos\psi\cos\alpha + \sin\psi\sin\alpha \tag{6.23f}$$

which becomes (upon substituting the appropriate quantities as determined from Fig. 6.3)

$$\cos(\psi - \alpha) = \frac{k_x}{k}\frac{x}{\rho} + \frac{k_y}{k}\frac{y}{\rho}$$

or

$$k\rho\cos(\psi - \alpha) = xk_x + yk_y \ . \tag{6.23g}$$

The integration range is over the entire transverse transformed plane; therefore, upon utilizing the Jacobian of the double integral operator [Zwillinger] given as

$$J = \begin{vmatrix} \frac{\partial k}{\partial k_x} & \frac{\partial \psi}{\partial k_x} \\ \frac{\partial k}{\partial k_y} & \frac{\partial \psi}{\partial k_y} \end{vmatrix} , \tag{6.24}$$

the transformation of the integrals

$$\int_0^\infty dk\ k \int_0^{2\pi} d\psi \Rightarrow \int_{-\infty}^{\infty} dk_x \int_{-\infty}^{\infty} dk_y$$

results.

6.E.2. The Scalar Flux in Cartesian Coordinates.

Substituting Eqs. (6.23e) and (6.23g) into Eq. (6.22c) yields the inversion using Cartesian coordinates:

$$\phi_c(x,y) = \frac{c}{4\pi^2} \int_{-\infty}^{\infty} dk_x \int_{-\infty}^{\infty} dk_y \frac{e^{-ixk_x} e^{-iyk_y}}{1 - i\gamma_0 k_x} \frac{L(k_x,k_y)}{1 - cL(k_x,k_y)} \quad , \tag{6.25a}$$

where

$$L(k_x,k_y) = \frac{\tan^{-1}\left(k_x^2 + k_y^2\right)^{1/2}}{\left(k_x^2 + k_y^2\right)^{1/2}} \quad . \tag{6.25b}$$

6.E.3. The Uncollided Scalar Flux in Cartesian Coordinates.

As usual, it is possible to obtain analytically the uncollided scalar flux in a closed form. The uncollided scalar flux in cylindrical direct and transformed variables is

$$\phi_0(\rho,\alpha) = \frac{1}{4\pi^2} \int_0^{\infty} dk\ k \int_0^{2\pi} d\psi \frac{e^{-ik\rho\cos(\psi - \alpha)}}{1 - ik\gamma_0\cos(\psi)} \quad . \tag{6.26}$$

Making the same substitutions as in the last section yields the corresponding equation in Cartesian direct and transformed variables,

$$\phi_0(x,y) = \frac{1}{4\pi^2} \int_{-\infty}^{\infty} dk_x \int_{-\infty}^{\infty} dk_y \frac{e^{-ixk_x} e^{-iyk_y}}{1 - i\gamma_0 k_x} \quad , \tag{6.27a}$$

which upon rearrangement becomes

$$\phi_0(x,y) = \frac{1}{4\pi^2} \int_{-\infty}^{\infty} dk_y\ e^{-iyk_y} \int_{-\infty}^{\infty} dk_x \frac{e^{-ixk_x}}{1 - i\gamma_0 k_x} \quad . \tag{6.27b}$$

The two integrals which can now be evaluated independently of one another are given as

$$I_0(y) = \int_{-\infty}^{\infty} dk_y\ e^{-iyk_y} \quad , \tag{6.28a}$$

$$I_1(x) = \int_{-\infty}^{\infty} dk_x \, \frac{e^{-ixk_x}}{1 - i\gamma_0 k_x} \quad . \tag{6.28b}$$

$I_0(y)$ is immediately seen to be the formula for the Fourier transform inversion of the function $\bar{f}(k_y) = 2\pi$, which is the transform of $f(y) = 2\pi\delta(y)$. $I_1(x)$ is determined by using the residue theorem and the standard contour for Fourier transform inversions. It's value may be seen to be $(2\pi/\gamma_0)e^{-x/\gamma_0}\theta(x)$. Thus, the uncollided flux in Cartesian coordinates is

$$\phi_0(x,y) = \frac{e^{-x/\gamma_0}}{\gamma_0} \, \theta(x)\delta(y) \quad . \tag{6.29}$$

Comparing Eq. (6.29) to Eq. (6.5d) shows complete agreement between the uncollided scalar flux found using cylindrical coordinate systems and the same using Cartesian coordinate systems, as expected. The delta-function in y indicates the singularity at $\alpha = 0$ and the step function indicates that the beam emits only along the positive x-axis.

6.F. Generation of the Isotropic Line Source Solution

The source under consideration is an infinite line which emits neutral particles in a general direction, thus making it an anisotropic line source. However, as a mathematical check, it is desirable to derive the solution for an isotropic line source in an infinite medium from this anisotropic source, thus completing Fig. 1.2 (see Fig. 1.2j following). This is accomplished by integrating the solution for the anisotropic line source over all possible emission angles as

$$\phi_{iso}(\rho) = \frac{1}{4\pi} \int_0^{2\pi} d\phi_0 \int_{-1}^{1} d\mu_0 \; \phi(\rho,\alpha;\mu_0,\phi_0) \quad . \tag{6.30}$$

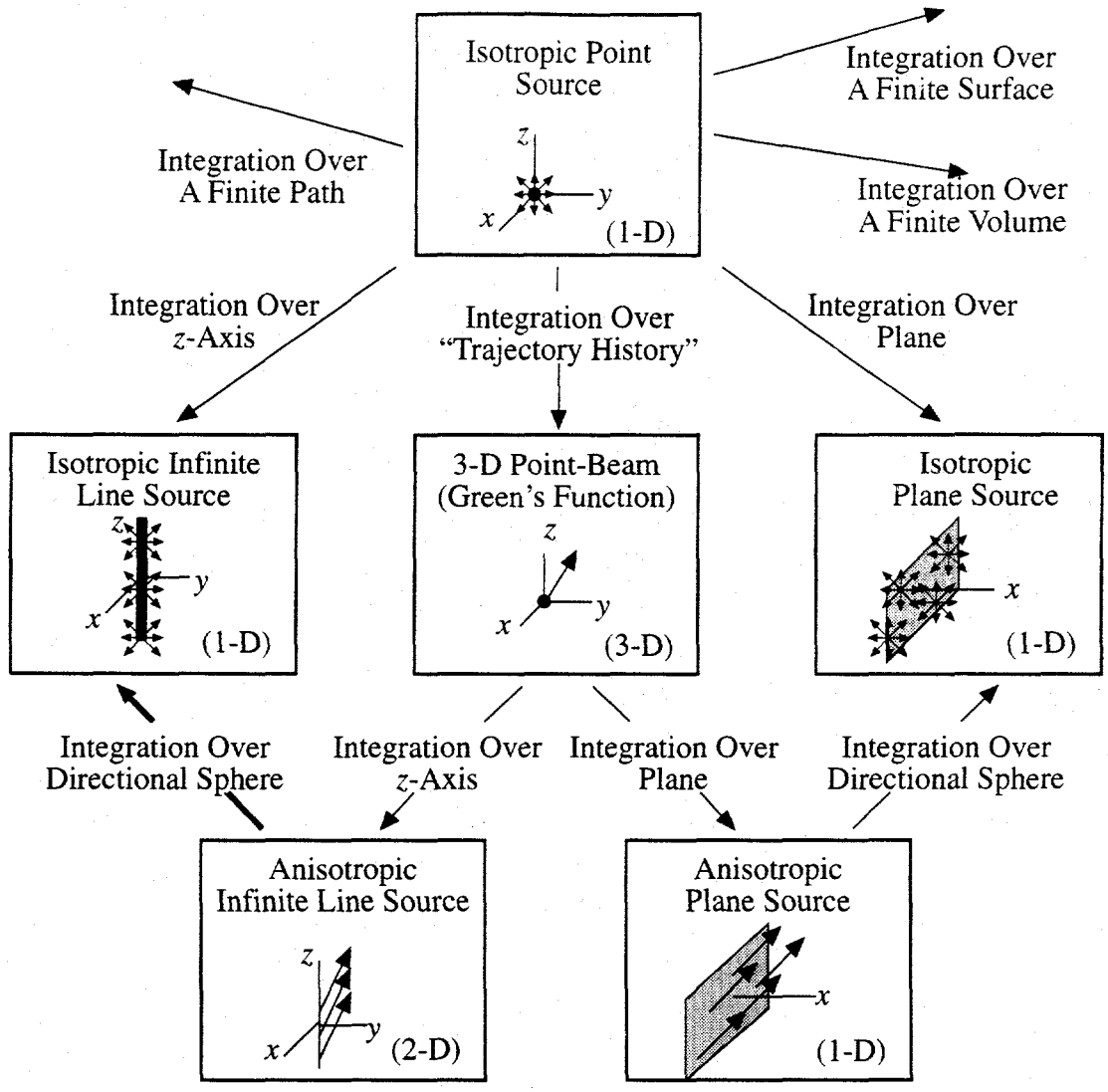

Fig. 1.2j. The eleventh step in constructing the suite of infinite medium benchmarks - deriving the isotropic infinite line source from the anisotropic infinite line source.

6.F.1. Integration of Integral Formulation Equation.

The integral formulation of the scalar flux is given by

$$\phi(\rho,\alpha) = \frac{e^{-\rho/\gamma_0}}{\rho\gamma_0}\delta(\alpha) + \frac{c}{2\pi}\int_0^{\infty} dk\ k\ f(k)\ \frac{1}{2\pi}\int_0^{2\pi} d\psi\ \frac{e^{-ik\rho\cos(\psi-\alpha)}}{1 - ik\gamma_0\cos\psi}\ , \qquad (6.33)$$

where ϕ_0 was arbitrarily set to 0 due to symmetry arguments. ϕ_0 is measured relative to the spatial variable α; therefore, in the above equation the integral over ϕ_0 may be replaced by one over α. Thus, upon using the appropriate integrals there results for the scalar flux from the integrated anisotropic line source

$$\phi_{iso}(\rho) = I_0 + \frac{c}{8\pi^2}\int_0^\infty dk\ k\ f(k) \int_0^{2\pi} d\psi \int_{-1}^{1} \frac{d\mu_0}{1 - ik\gamma_0 \cos\psi} \times$$

$$\times \frac{1}{2\pi}\int_0^{2\pi} d\alpha\ e^{-ik\rho\cos(\psi - \alpha)} \quad , \tag{6.32a}$$

where

$$I_0 = \frac{1}{4\pi}\int_0^{2\pi} d\alpha \int_{-1}^{1} d\phi_0 \frac{e^{-\rho/\gamma_0}}{\rho\gamma_0}\delta(\alpha) = \frac{1}{2\pi\rho}\int_0^1 \frac{d\mu_0}{(1 - \mu_0^2)^{1/2}} e^{-\rho/(1-\mu_0^2)^{1/2}} \quad . \tag{6.32b}$$

Recognizing the integral for the zeroth order Bessel function in Eq. (6.32a) we have

$$\phi_{iso}(\rho) = I_0 + \frac{c}{8\pi^2}\int_0^\infty dk\ k\ f(k)\ J_0(k\rho)\ I_1(k) \quad , \tag{6.33a}$$

where

$$I_1(k) = \int_0^{2\pi} d\psi \int_{-1}^{1} \frac{d\mu_0}{1 - ik\gamma_0 \cos\psi} \quad . \tag{6.33b}$$

The two tasks which must now be performed are the evaluations of the integrals I_0 and I_1. Noting that the integral in Eq. (6.33a) has the zeroth order Bessel function integrated over a semi-infinite range, it is reasonable to evaluate I_0 by using Fourier-Bessel transforms. The Fourier-Bessel transform pair is defined as

$$F_B(k) \equiv \int_0^\infty d\rho\ \rho\ J_0(k\rho)\ f(\rho) \tag{6.34a}$$

$$f(\rho) \equiv \int_0^\infty dk\ k\ J_0(k\rho)\ F_B(k)\ . \tag{6.34b}$$

If it is assumed that $f(\rho)$ is given by

$$f(\rho) = \frac{1}{\rho} \int_0^1 \frac{dx}{\left(1 - x^2\right)^{1/2}} e^{-\rho/(1-x^2)^{1/2}}\ , \tag{6.35a}$$

then upon using the formula for the inverse Fourier-Bessel transform we have

$$I_0 = \frac{1}{2\pi} \int_0^\infty dk\ k\ J_0(k\rho)\ F_B(k)\ , \tag{6.35b}$$

where $F_B(k)$ is the Fourier-Bessel transform of Eq. (6.34a). Thus the evaluation of I_0 is reduced to finding the Fourier-Bessel transform of $f(\rho)$:

$$F_B(k) = \int_0^\infty d\rho\ J_0(k\rho) \int_0^1 \frac{dx}{\left(1 - x^2\right)^{1/2}} e^{-\rho/(1-x^2)^{1/2}}\ . \tag{6.35c}$$

Reversing the integrals yields

$$F_B(k) = \int_0^1 \frac{dx}{\left(1 - x^2\right)^{1/2}} \int_0^\infty d\rho\ J_0(k\rho)\ e^{-\rho/(1-x^2)^{1/2}}\ , \tag{6.36a}$$

for which the second is immediately seen to be of the form of a Laplace transform of J_0. Thus, after evaluating the inner integral,

$$F_B(k) = \int_0^1 \frac{dx}{\left(1 - x^2\right)^{1/2}} \frac{1}{\left[k^2 + (1-x^2)^{-1}\right]^{1/2}}\ , \tag{6.36b}$$

which upon simplification becomes

$$F_B(k) = \frac{1}{k} \int_0^1 \frac{dx}{\left(a^2 - x^2\right)^{1/2}}\ , \tag{6.36c}$$

where $a^2 = \frac{1+k^2}{k^2}$. This is immediately evaluated as

$$F_B(k) = \frac{\tan^{-1}k}{k} = L(k) \ , \tag{6.36d}$$

which leaves for I_0

$$I_0 = \frac{1}{2\pi}\int_0^\infty dk\ k\ J_0(k\rho)\ L(k) \ . \tag{6.36e}$$

The second task is to evaluate I_1, given again as

$$I_1(k) = 2\int_0^{2\pi} d\psi \int_0^1 \frac{d\mu}{1 - ik\left(1-\mu^2\right)^{1/2}\cos\psi} \ . \tag{6.37a}$$

By restating the inner integrand as an integral over an exponential and rearranging the integrals we have

$$I_1(k) = 2\int_0^1 d\mu \int_0^\infty dt\ e^{-t} \int_0^{2\pi} d\psi\ e^{ikt(1-\mu^2)^{1/2}\cos\psi} \ , \tag{6.37b}$$

which upon recognition of the Bessel function becomes

$$I_1(k) = 4\pi\int_0^1 d\mu \int_0^\infty dt\ e^{-t}\ J_0\left[kt\left(1-\mu^2\right)^{1/2}\right] \ . \tag{6.37c}$$

Again recognizing the Laplace transform of the Bessel function yields

$$I_1(k) = 4\pi\int_0^1 \frac{d\mu}{\left(1+k^2-k^2\mu^2\right)^{1/2}} \ , \tag{6.37d}$$

which, as in the last section, is (after some simplification) seen to be

$$I_1(k) = 4\pi\frac{\tan^{-1}k}{k} = 4\pi\, L(k) \ . \tag{6.37e}$$

Now that the integrals I_0 and I_1 have been evaluated, the integration of the anisotropically emitting line source over all emission directions is (with the functional form of $f(k)$ inserted)

$$\phi_{iso}(\rho) = \frac{1}{2\pi}\int_0^\infty dk\ k\ J_0(k\rho)\ L(k) + \frac{c}{2\pi}\int_0^\infty dk\ k\ \frac{L(k)}{1 - cL(k)}\ J_0(k\rho)\ L(k)\ , \qquad (6.38a)$$

which upon combining the integrals yields

$$\phi_{iso}(\rho) = \frac{1}{2\pi}\int_0^\infty dk\ k\ J_0(k\rho)\left[L(k) + \frac{cL^2(k)}{1 - cL(k)}\right]\ , \qquad (6.38b)$$

or

$$\phi_{iso}(\rho) = \frac{1}{2\pi}\int_0^\infty dk\ k\ J_0(k\rho)\left[\frac{L(k)}{1 - cL(k)}\right] = \frac{1}{2\pi}\int_0^\infty dk\ k\ J_0(k\rho)\ f(k)\ . \qquad (6.38c)$$

This is again seen to be the scalar flux from an infinite isotropic line source at the center of an infinite medium, as anticipated.

6.F.2 Integration of Series Formulation.

The series formulation of the scalar flux was seen to be

$$\phi(\rho,\alpha) = \frac{e^{-\rho/\gamma_0}}{\rho\gamma_0}\delta(\alpha) +$$

$$+\frac{c}{2\pi}\sum_{m=0}^{\infty}(2 - \delta_{m0})\cos(m\alpha)\int_0^\infty dk\ \frac{k\,f(k)\,J_m(\rho k)}{\left(1 + k^2\gamma_0^2\right)^{1/2}}\left[\frac{\left(1 + k^2\gamma_0^2\right)^{1/2} - 1}{k\gamma_0}\right]^m\ . \qquad (6.39)$$

As mentioned in the last section, ϕ_0 has been set to zero and it is appropriate to replace the ϕ_0 integral with one over α. When the angular integrals are applied to the above equation, there results

$$\phi_{iso}(\rho) = I_0 + \frac{c}{8\pi^2} \sum_{m=0}^{\infty} (2 - \delta_{m0}) I_{\alpha m} \int_0^{\infty} dk\, k\, f(k)\, J_m(\rho k)\, I_{\mu_0 m}(k) \quad , \tag{6.40a}$$

where I_0 was evaluated in the previous section,

$$I_{\alpha m} = \int_0^{2\pi} d\alpha \cos(m\alpha) = 2\pi\delta_{m0} \quad , \tag{6.40b}$$

and

$$I_{\mu_0 m}(k) = \int_{-1}^{1} \frac{d\mu_0}{\left(1 + k^2\gamma_0^2\right)^{1/2}} \left[\frac{\left(1 + k^2\gamma_0^2\right)^{1/2} - 1}{k\gamma_0}\right]^m \quad . \tag{6.40c}$$

Because of the Kroneker delta in Eq. (6.40b), only the $m = 0$ term survives in the infinite series, which leaves for $I_{\mu_0 0}(k)$

$$I_{\mu_0 0}(k) = \int_{-1}^{1} \frac{d\mu_0}{\left(1 + k^2\gamma_0^2\right)^{1/2}} \quad , \tag{6.41a}$$

which after using the same techniques as in the last section is

$$I_{\mu_0 0}(k) = 2\frac{\tan^{-1}k}{k} = 2\,L(k) \quad . \tag{6.41b}$$

Inserting the functional forms of the integrals into Eq. (6.40a) yields

$$\phi_{iso}(\rho) = \frac{1}{2\pi} \int_0^{\infty} dk\, k\, J_0(k\rho)\, L(k) + \frac{c}{8\pi^2}\, 2\pi \int_0^{\infty} dk\, k\, f(k)\, J_0(\rho k)\, 2\, L(k) \quad , \tag{6.42a}$$

which after simplification again yields the scalar flux from an isotropic line source in an infinite homogeneous medium:

$$\phi_{iso}(\rho) = \frac{1}{2\pi} \int_0^{\infty} dk\, k\, f(k)\, J_0(\rho k) \quad . \tag{6.42b}$$

With the theory discussed above, the next task is to consider some of the numerical methods and techniques which will be used to evaluate the scalar flux. Again, one of the purposes of considering this problem is to gain insight into the numerics required for the three-dimensional searchlight problem.

6.G. Numerical Methods

The numerical evaluation of the expressions found in the last chapter requires that the values of improper integrals and infinite series be determined. Standard, yet advanced, numerical techniques are employed to achieve this.

6.G.1. Direct Double Fourier Inversion.

The scalar flux resulting from the anisotropic infinite line source is given by Eqs. (6.4). To numerically evaluate these expressions, which involve a double integral, standard integration techniques are used. The outer integral has the form

$$I_o = \int_0^\infty dk\ k\, f(k)\, I(\rho,\alpha;k) \quad , \tag{6.43a}$$

where $f(k)$ is strictly positive and $I(\rho,\alpha;k)$ is oscillatory. Given that

$$I(\rho,\alpha;k) = \int_0^{2\pi} d\psi\, \frac{e^{-ik\rho\cos(\psi-\alpha)}}{1 - ik\gamma_0\cos(\psi)} \quad , \tag{6.43b}$$

it may be noted that for $\gamma_0 = 0$ the inner integral reduces to the zeroth order Bessel function. Because it is easy to obtain the zeroes of this function and because the general form of the inner integral closely resembles the Bessel function, the outer integral is converted into an infinite series of integrals over the zeroes of the Bessel function. Thus, Eq. (6.43a) takes the form

$$I_o = \sum_{m=0}^{\infty} \int_{\nu_m}^{\nu_{m+1}} dk\ k\, f(k)\, I(\rho,\alpha;k) \quad , \tag{6.44}$$

where $J_0(\nu_m) = 0$ and the series is almost purely oscillatory, that is occasionally two consecutive terms may have the same sign. The individual integrals in Eq. (6.44) may be evaluated by the iterative Gauss-Legendre quadrature scheme discussed previously or by Romberg integration [Press, *et al.*, Zwillinger]. Once each integral has been evaluated it is simply another term in an infinite series. Because the integrand of the original integral decreases with increasing k and oscillates, the terms of the series will also generally have alternating signs, the series is an excellent candidate for acceleration via the Euler-Knopp transformation [Press, *et al.*]. Again, this transformation was designed to accelerate the convergence of an oscillating series. The series is considered to be converged when three consecutive values of the accelerated series are within a given error.

The basic kernel in Eq. (6.43a) contains the function $f(k)$, the kernel for the scalar flux. It is shown in Appendix B that the individual scalar collided fluxes (e.g. first collided, second collided, etc.) may be obtained by manipulating this kernel. Thus, an option is made included in the computer code for the user to choose the desired collided flux to be determined.

The final task in the inversion scheme is to determine the value of the inner ψ integral given in Eq. (6.43b). Expanding the complex exponential into sines and cosines, rationalizing the denominator, and separating the integral into real and imaginary parts yields

$$I(\rho,\alpha;k) = \int_0^{2\pi} d\psi\, \frac{\cos[k\rho\cos(\alpha-\psi)] + k\gamma_0\cos(\psi)\sin[k\rho\cos(\alpha-\psi)]}{1 + k^2\gamma_0^2\cos^2(\psi)} +$$

$$+\ i \int_0^{2\pi} d\psi\, \frac{k\gamma_0\cos(\psi)\cos[k\rho\cos(\alpha-\psi)] - \sin[k\rho\cos(\alpha-\psi)]}{1 + k^2\gamma_0^2\cos^2(\psi)} \quad . \tag{6.45a}$$

Separating the integrals over the ranges $[0,\pi]$ and $[\pi,2\pi]$, using the cosine addition formulas, and simplifying eliminates the imaginary integral and leaves for the inner integral

$$I(\rho,\alpha;k) = 2\int_0^{\pi} d\psi \, \frac{\cos[k\rho\cos(\alpha-\psi)] + k\gamma_0\cos(\psi)\sin[k\rho\cos(\alpha-\psi)]}{1 + k^2\gamma_0^2\cos^2(\psi)} \quad . \tag{6.45b}$$

The nature of this integral indicates that Chebyshev integration may be useful for evaluation of this integral. The following quadrature rule is given as [Abramowitz and Stegun]

$$\int_{-1}^{1} dx \, \frac{f(x)}{(1-x^2)^{1/2}} \approx \frac{\pi}{N}\sum_{i=1}^{N} f\left[\cos\frac{\pi}{N}(i - {}^1/_2)\right] \quad . \tag{6.46a}$$

Making the change of variable $x = \cos u$ converts the rule to

$$\int_0^{\pi} du \, f(\cos u) \approx \frac{\pi}{N}\sum_{i=1}^{N} f\left[\frac{\pi}{N}(i - {}^1/_2)\right] \quad , \tag{6.46b}$$

which may now be used for evaluating Eq. (6.45b). As with the iterative Gauss-Legendre quadrature, the quadrature order N in Eq. (6.46b) is successively increased until three consecutive values of the integral are within a given relative error or if the maximum N is reached an error message is returned.

6.G.2. Fourier Inversion and Series Formulation.

Eq. (6.19a) gives the scalar flux after the inner integral has been converted into an infinite series; the form of the outer integral is the same as Eq. (6.43a) with the function $I(\rho,\alpha;k)$ given by

$$I(\rho,\alpha;k) = \sum_{m=0}^{\infty}(2-\delta_{m0}) \, \frac{\cos(m\alpha)\, J_m(k\rho)}{\left(1 + k^2\gamma_0^2\right)^{1/2}} \left[\frac{\left(1 + k^2\gamma_0^2\right)^{1/2} - 1}{k\gamma_0}\right]^m \quad . \tag{6.47}$$

This series is evaluated without acceleration and is considered converged when five consecutive partial sums agree within a given relative error. This series converges rather quickly as the exponentiated fraction (the term in square brackets) is strictly less than one. That is, after only a few terms the term in brackets upon exponentiation to the mth power becomes exceedingly small. Generally, evaluating the scalar flux by performing this sum inside the k integral is the most convenient means of producing numerical results. However, this formulation is not efficient for small values of the angular variable α.

6.G.3. Restrictions on α to Obtain Purely Oscillating Series.

Generally the numerical evaluation of the scalar flux converges quickest when the series is evaluated inside the integral [Eq. (6.19a)], except for small values of α ($\alpha < 15°$). The outer semi-infinite integral is accelerated by converting it into an infinite series of integrals and then using the Euler-Knopp accelerator, which works best when the series is purely oscillating. The pure oscillatory behavior does not necessarily occur in either Eq. (6.19a) or Eq. (6.19b) due to the $\cos(m\alpha)$ term; this is especially true for small α; therefore, it is desirable to obtain a formulation which is purely oscillating even in this range. As the problem is stated, the only way to do this is to numerically search for the zeroes of the outermost integrand and evaluate between these zeroes. This would be a very time consuming process. To avoid this undesirable task, it is possible to "intelligently" choose the value of α so that it is numerically convenient. Therefore, at small α, α is restricted to be π/N, where N is an integer. In this case, the series

$$S = \sum_{j=0}^{\infty} a_j \cos(\alpha j) \tag{6.48a}$$

becomes

$$S = \sum_{j=0}^{\infty} a_j \cos\left(\frac{\pi j}{N}\right) = \sum_{j=1}^{\infty} \sum_{m=(j-1)N}^{jN-1} a_m \cos\left(\frac{\pi m}{N}\right) . \qquad (6.48b)$$

Letting $m' = m - (j-1)N$ and $j' = j-1$ results in

$$S = \sum_{j=0}^{\infty} \sum_{m=0}^{N-1} (-1)^j a_{m+jN} \cos\left(\frac{m}{N}\pi\right) , \qquad (6.48c)$$

where the primes have been dropped and the cosine expanded in its addition formula which resulted in the $(-1)^j$ term. Now, the range on the inner summation may be conveniently separated so that in the first half of the series the cosine is positive and in the second half the cosine is negative. Therefore, the inner series is separated into two summations whose ranges on m are $[0,N/2]$ and $[N/2+1,N-1]$. If N is odd then the $N/2$ term is truncated; this ensured that the terms where the value of the cosine switches from positive to negative remain with the proper summations. Upon such a separation there results for the series S

$$S = \sum_{j=0}^{\infty} (-1)^j \sum_{m=0}^{N/2} a_{m+jN} \cos\left(\frac{\pi m}{N}\right) + \sum_{j=0}^{\infty} (-1)^j \sum_{m=N/2+1}^{N-1} a_{m+jN} \cos\left(\frac{\pi m}{N}\right) , \qquad (6.49)$$

where the a_m are found from Eq. (719b) to be

$$a_m = \frac{c}{2\pi}(2 - \delta_{m0}) \int_0^{\infty} dk \, \frac{k\, f(k)}{\left(1 + k^2\gamma_0^2\right)^{1/2}} J_m(\rho k) \left[\frac{\left(1 + k^2\gamma_0^2\right)^{1/2} - 1}{k\gamma_0}\right]^m . \qquad (6.50)$$

This restriction on α produces a strictly alternating series, which allows effective use of the Euler-Knopp accelerator. However, it is generally undesirable to place such a restriction on a basic parameter such as the spatial angle α. Therefore, the initial purpose of the above

exercise may be expanded beyond being able to evaluate the scalar flux for small α to include a form of check on the other calculational methods.

6.G.4. Numerical Considerations for the Inversion in Cartesian Coordinates.

The expressions which are to be numerically evaluated are

$$\phi_c(x,y) = \frac{c}{4\pi^2} \int_{-\infty}^{\infty} dk_x \int_{-\infty}^{\infty} dk_y \frac{e^{-ixk_x} e^{-iyk_y}}{1 - i\gamma_0 k_x} \frac{L(k_x,k_y)}{1 - cL(k_x,k_y)} , \tag{6.51a}$$

where

$$L(k_x,k_y) = \frac{\tan^{-1}\left(k_x^2 + k_y^2\right)^{1/2}}{\left(k_x^2 + k_y^2\right)^{1/2}} . \tag{6.51b}$$

6.G.4.a. Simplification of Integral Expressions. As some programming languages, such as FORTRAN, allow the user to create programs which are able to perform algebra using complex numbers the above equations could be programmed essentially as is; however, in order to avoid unnecessary computations such algebra will be done here. The first important point is to note that $L(k_x,k_y)$ is even in both k_x and k_y. Eq. (6.51a) may be rewritten as

$$\phi_c(x,y) = \frac{c}{4\pi^2} \int_{-\infty}^{\infty} dk_x \frac{e^{-ixk_x}}{1 - i\gamma_0 k_x} \int_{-\infty}^{\infty} dk_y \, e^{-iyk_y} \frac{L(k_x,k_y)}{1 - cL(k_x,k_y)} . \tag{6.52}$$

The k_y integral is over a symmetric range and the kernel is even in k_y. Separating the complex exponential into cosine and sine functions immediately results in the elimination of the imaginary integral as it contains an even function multiplied by the odd sine function. Thus the inner integral may be rewritten as,

$$\int_{-\infty}^{\infty} dk_y \, e^{-iyk_y} \frac{L(k_x,k_y)}{1 - cL(k_x,k_y)} = 2\int_0^{\infty} dk_y \cos(yk_y) \frac{L(k_x,k_y)}{1 - cL(k_x,k_y)} \ ,$$

and the collided scalar flux is then given by

$$\phi_c(x,y) = \frac{c}{2\pi^2} \int_{-\infty}^{\infty} dk_x \frac{e^{-ixk_x}}{1 - i\gamma_0 k_x} I(k_x;y) \ , \tag{6.53a}$$

where

$$I(k_x;y) = \int_0^{\infty} dk_y \cos(k_y y) \frac{L(k_x,k_y)}{1 - cL(k_x,k_y)} \ . \tag{6.53b}$$

Next, the exponential and denominator in Eq. (6.53a) are expanded and rationalized, respectively. This yields

$$\phi_c(x,y) = \frac{c}{2\pi^2} \int_{-\infty}^{\infty} dk_x \frac{\cos(k_x x) + \gamma_0 k_x \sin(k_x x)}{1 + \gamma_0^2 k_x^2} I(k_x;y) +$$

$$+ i \frac{c}{2\pi^2} \int_{-\infty}^{\infty} dk_x \frac{\gamma_0 k_x \cos(k_x x) - \sin(k_x x)}{1 + \gamma_0^2 k_x^2} I(k_x;y) \ . \tag{6.54a}$$

Again noting that $I(k_x;y)$ is even in k_x, the integral associated with the imaginary term is seen to vanish as its integrand is odd with respect to k_x. The scalar flux is now written as

$$\phi_c(x,y) = \frac{c}{\pi^2} \int_0^{\infty} dk_x \frac{\cos(k_x x) + \gamma_0 k_x \sin(k_x x)}{1 + \gamma_0^2 k_x^2} I(k_x;y) \ . \tag{6.54b}$$

Because the infinite integrals will be broken into a series of finite integrals that range over the zeros of the integrand, and the zeros nominally occur at the zeros of the sine and cosine functions, it is desirable to make the two changes of variable $v = k_x x$ and $u = k_y y$. After making the changes of variable and separating the cosine and sine integrals there results

$$\phi_c(x,y) = \frac{c}{\pi^2} \left[I_c(x,y) + I_s(x,y) \right] \ , \tag{6.55a}$$

where

$$I_c(x,y) = \int_0^\infty dv \, \frac{x\cos(v)}{x^2 + \gamma_0^2 v^2} I\left(\frac{v}{x};y\right) , \tag{6.55b}$$

$$I_s(x,y) = \int_0^\infty dv \, \frac{\gamma_0 v\sin(v)}{x^2 + \gamma_0^2 v^2} I\left(\frac{v}{x};y\right) , \tag{6.55c}$$

$$I\left(\frac{v}{x};y\right) = \frac{1}{y}\int_0^\infty du \, \cos(u) \, \frac{L\left(\frac{v}{x},\frac{u}{y}\right)}{1 - cL\left(\frac{v}{x},\frac{u}{y}\right)} . \tag{6.55d}$$

6.G.4.b. Transformation of Integral Expressions into Series. Given that a computer is not able to evaluate an integral which has an infinite range, such expressions are most often converted into an infinite series of finite integrals and the series is ultimately truncated. This will be done for the integral expressions $I_c(x,y)$, $I_s(x,y)$, and I. Noting that the integrand of I_c contains the $\cos(v)$ term, it is reasonable to break the cosine integral into a series of integrals which range along the zeroes of the cosine. Thus, I_c may be written as

$$I_c(x,y) = \int_0^{\pi/2} dv \, \frac{x\cos(v)}{x^2+\gamma_0^2 v^2} I\left(\frac{v}{x};y\right) + \sum_{j=1}^{\infty} \int_{(2j-1)\pi/2}^{(2j+1)\pi/2} dv \, \frac{x\cos(v)}{x^2+\gamma_0^2 v^2} I\left(\frac{v}{x};y\right) . \tag{6.56a}$$

The limits on all the integrals may be transformed so that all integrals have the same limits of integration. As Gauss-Legendre quadrature is often used for integrating functions, it is natural to make the limit on the integrals [0,1]. This is done by making the change of variable $v' = 2v/\pi$ in the first integral and $v' = v/\pi - j + 1/2$ in the integrals under the summation. Completing this process (and dropping the primes) yields

$$I_c(x,y) = \frac{\pi}{2}\int_0^1 dv\ \frac{x\cos(\pi v/2)}{x^2 + \gamma_0^2\ (\pi v/2)^2}\, I\left(\frac{\pi v}{2x};y\right) +$$

$$+ \pi\sum_{j=1}^{\infty}\int_0^1 dv\ \frac{x\cos[\pi(v+j-1/2)]}{x^2 + \gamma_0^2\,\pi^2(v+j-1/2)^2}\, I\left[\frac{\pi}{x}\left(v+j-\tfrac{1}{2}\right);y\right] \ . \qquad (6.56b)$$

The same procedure is necessary for the sine integral. However, in this case, there is no need for a special first term as all the zeroes are at multiple of π. Thus,

$$I_s(x,y) = \sum_{j=0}^{\infty}\int_{\pi j}^{\pi(j+1)} dv\ \frac{\gamma_0 v\sin(v)}{x^2 + \gamma_0^2\ v^2}\, I\left(\frac{v}{x};y\right) \ , \qquad (6.57a)$$

and by making the change of variable $v' = v/\pi - j$ there results

$$I_s(x,y) = \pi\sum_{j=0}^{\infty}\int_0^1 dv\ \frac{\gamma_0\pi(v+j)\sin[\pi(v+j)]}{x^2 + \gamma_0^2\pi^2(v+j)^2}\, I\left[\frac{\pi}{x}(v+j);y\right] \ . \qquad (6.57b)$$

One further simplification is found in the sine and cosine arguments under the new integrals. Using the addition formulas for the sine and cosine functions, it may be seen that

$$\sin[\pi(v+j)] = (-1)^j\sin(\pi v) \ ;$$

$$\cos[\pi(v+j-1/2)] = (-1)^j\sin(\pi v) \ .$$

Thus Eqs. (6.56b) and (6.57b) become

$$I_c(x,y) = \frac{\pi}{2}\int_0^1 dv\ \frac{x\cos(\pi v/2)}{x^2 + \gamma_0^2\ (\pi v/2)^2}\, I\left(\frac{\pi v}{2x};y\right) +$$

$$+ \pi\sum_{j=1}^{\infty}(-1)^j\int_0^1 dv\ \frac{x\sin(\pi v)}{x^2 + \gamma_0^2\,\pi^2(v+j-1/2)^2}\, I\left[\frac{\pi}{x}\left(v+j-\tfrac{1}{2}\right);y\right] \ ; \qquad (6.58a)$$

$$I_s(x,y) = \pi\sum_{j=0}^{\infty}(-1)^j\int_0^1 dv\ \frac{\gamma_0\pi(v+j)\sin(\pi v)}{x^2 + \gamma_0^2\pi^2(v+j)^2}\, I\left[\frac{\pi}{x}(v+j);y\right] \ . \qquad (6.58b)$$

The inner integral [Eq. (6.55d)] is also a cosine integral and will therefore have the same form as Eq. (6.58a) after breaking up the infinite integral and making changes of variable so that all integrals have the limits [0,1]. The result of these operations is

$$I\left(\frac{v}{x};y\right) = \frac{\pi}{2y}\int_0^1 du\, \cos\left(\frac{\pi u}{2}\right) f\left(\frac{v}{x},\frac{\pi u}{2y}\right) +$$

$$+ \frac{\pi}{y}\sum_{j=1}^{\infty}(-1)^j \int_0^1 du\, \sin(\pi u)\, f\left[\frac{v}{x},\frac{\pi}{y}\left(u+j-\tfrac{1}{2}\right)\right] , \qquad (6.59a)$$

where

$$f(p,q) = \frac{L(p,q)}{1 - cL(p,q)} . \qquad (6.59b)$$

6.G.4.c. Treatment for Small x and Small y. As with the other numerical methods associated with this problem, difficulties occur when the spatial variables x and y become small. A procedure has been developed for such instances [Ganapol, priv. comm.]. When the spatial variables are small, the series in Eqs. (6.58) are dominated by the first term; however, these are also the terms which are most difficult to evaluate. Therefore, the first terms may be treated specially to assist the numerical method. The change of variable $v' = v/x$ in the first term of the outer integral series gives the following result (after dropping the primes):

$$I_{c0}(x,y) = \frac{\pi}{2}\int_0^{1/x} dv\, \frac{x\cos(\pi v x/2)}{1 + \gamma_0^2\ (\pi v/2)^2}\, I\left(\frac{\pi v}{2};y\right) ; \qquad (6.60a)$$

$$I_{s0}(x,y) = \pi\int_0^{1/x} dv\, \frac{\gamma_0 \pi v \sin(\pi v x)}{1 + \gamma_0^2\pi^2 v^2}\, I(\pi v;y) . \qquad (6.60b)$$

Now as x decreases, the range on the integral increases, allowing the numerical methods to better determine the value of these first terms. A similar expression may be derived for the first term in the sum of the inner integrals as

$$I_{i0}(x,y) = \frac{\pi}{2}\int_0^{1/y} du\, \cos\left(\frac{\pi u y}{2}\right) f\left(\frac{v}{x}, \frac{\pi u}{2}\right) , \tag{6.61}$$

where f is given in Eq. (6.59b).

These integrals in Eqs. (6.60) and (6.61), which are the first terms in a series of integrals, are now separated into a series as well. The first term of this sub-series is always over the range $[0,x]$ or $[0,y]$. Assuming that x is small (the treatments for small x and small y are formally the same) the integration range for the first sub-integral $[0,x]$ necessitates that the entirety of the remaining sub-integrals is over the range $[x,1/x]$ so that the total sum of all sub-integrals is over the range $[0,1/x]$ as shown in Eqs. (6.60). For the sub-integrals, the number of integration intervals N_m is specified. The logarithms of the integration endpoints are taken; because the endpoints of the quadrature scheme are $\ln x$ and $\ln(1/x) = -\ln x$, the range is symmetric. The endpoints of the individual sub-integrals are then set arbitrarily to the abscissas of the Gauss-Legendre quadrature scheme for a quadrature order N_m. The abscissas a_i are determined and the $[x,1/x]$ integral is divided according to

$$\int_0^{1/x} dv\, f(v) = \sum_{i=0}^{N_m} \int_{b_i}^{b_{i+1}} dv\, f(v) \quad , \tag{6.62}$$

where $b_0 = x$, $b_{N_m+1} = 1/x$, and $b_i = e^{a_i}$. Obtaining the abscissas via the logarithms of the endpoints and then exponentiating these abscissas has the effect of concentrating the integration on the regions near x, where the integration is most difficult. For example, assuming $x = 0.01$ and $N_m = 4$ produces the abscissas and interval endpoints shown in Table 6.1. Note that the Gauss-Legendre abscissas are symmetric and that the integration intervals will lead to concentrated integration effort toward the small end of the interval $[0.01,100]$.

Table 6.1. Example of Small x Integration Intervals.

a_i	$b_i = \exp(a_i)$
-3.96568	0.01896
-1.56567	0.20895
1.56567	4.78588
3.96568	52.7561

With these numerical methods the scalar flux from the anisotropically emitting infinite line source may be evaluated. This is done in the following sections.

6.H. Results for the Anisotropically Emitting Infinite Line Source

The nature of the anisotropically emitting infinite line source limits the means by which results may be displayed. Because the scalar flux is not axially (z) dependent, the general means of viewing results will require three-dimensional plots of the scalar flux versus position in the transverse plane. However, before using this benchmark to generate the scalar flux in the transverse plane, several studies will be performed.

6.H.1. Numerical Studies: Error Analysis.

One of the primary premises of analytical benchmarks is that the numerical results are accurate to a specified error. Table 6.2 provides the scalar flux as a function of radius and the relative error. The scalar flux was evaluated at $\alpha = 30°$ (an angle for which numerical evaluation is relatively easy), $\mu_0 = 0$ (emitting perpendicular to the z-axis), and $c = 0.9$. In all cases, the relative errors when compared to the data for $error = 10^{-6}$ agree to the number of digits required; for example, at $r = 1$ the relative difference between the scalar fluxes for $error = 10^{-4}$ and $error = 10^{-6}$ is 5.73×10^{-5}, which is within the specified error. Fig. 6.4 displays the CPU times required to obtain the data in Table 6.2. Note that

CPU times become greater with stricter error requirements, and that times decrease as the edit points become farther from the source.

Table 6.2. Scalar flux as a Function of Radius and Solution Relative Error.

radius	*error* 10^{-2}	10^{-3}	10^{-4}	10^{-5}	10^{-6}
1	4.73518E-1	4.71409E-1	4.71268E-1	4.71245E-1	4.71242E-1
2	2.32571E-1	2.31634E-1	2.31566E-1	2.31585E-1	2.31583E-1
3	1.20027E-1	1.20656E-1	1.20572E-1	1.20563E-1	1.20564E-1
4	6.41931E-2	6.44720E-2	6.44351E-2	6.44320E-2	6.44317E-2
5	3.48666E-2	3.50104E-2	3.49902E-2	3.49883E-2	3.49884E-2
6	1.91669E-2	1.92029E-2	1.92148E-2	1.92143E-2	1.92141E-2
7	1.06210E-2	1.06369E-2	1.06409E-2	1.06415E-2	1.06416E-2
8	5.92155E-3	5.93171E-3	5.93340E-3	5.93374E-3	5.93370E-3
9	3.32761E-3	3.32868E-3	3.32672E-3	3.32695E-3	3.32693E-3
10	1.87282E-3	1.87487E-3	1.87390E-3	1.87398E-3	1.87399E-3

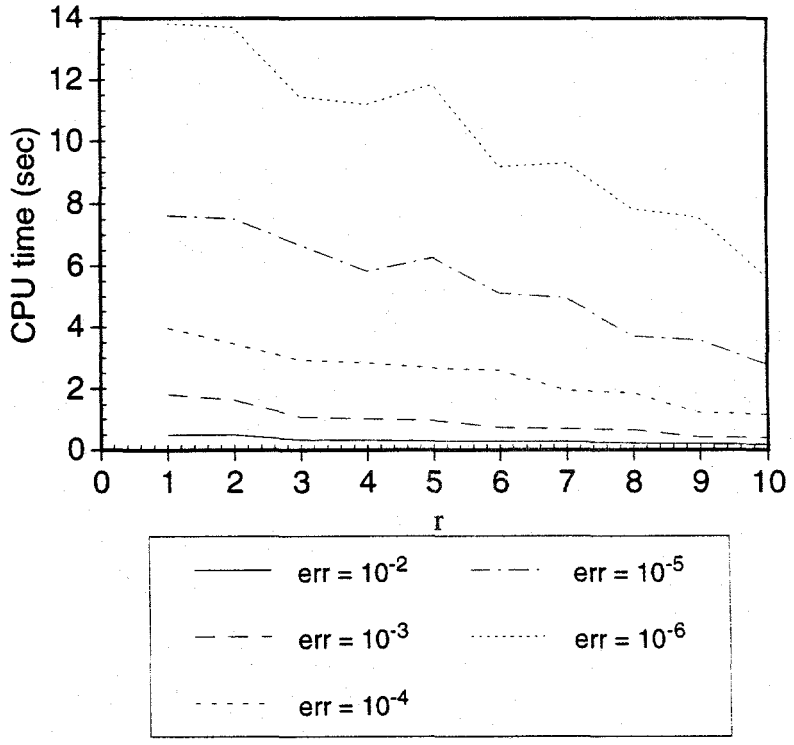

Fig. 6.4. CPU time study for anisotropic infinite line source.

6.H.2. Numerical Studies: Individual and Total Collided Flux Analysis.

Recalling that the individual and collective collided fluxes may be obtained by making simple changes to the kernel $f(k)$ allows an analysis of the collided fluxes to test the numerics of the individual evaluations. Fig. 6.5 displays the first, second, third, and remaining collided fluxes along with the total collided flux. The curves in Fig. 6.5 are for $r = 1$, $c = 0.9$, $\mu_0 = 0$ and $error = 10^{-5}$. Summing the individual components of the collided flux yields a number equal to the total collided flux, as expected. The relative magnitudes of the individual fluxes are interesting.

Near the source (small α) there is an increase in the individual fluxes, and the first collided flux is greater than the second and the second collided is greater than the third. However, as seen in the figure near $\alpha = 40°$ the first collided flux falls below the second collided flux. Although not visible, the magnitude of the second collided flux falls below the third collided flux around $\alpha = 130°$. This phenomena indicates that near the source the first collided flux is largest and the individual fluxes decrease monotonically. This results from particles having their first collision near the regions in which they appear. However, after the particles have some collisions, they are distributed into other regions and the individual fluxes of successively greater collision numbers increase; that is, far from the source there are many particles which have had many collisions and few particles which have had few collisions. This agrees with physical intuition and theory. The remaining flux (4th+ Collided) is large because it is the accumulation of all individual fluxes with four or more collisions.

6.H.3. Numerical Studies: Numerical Inversion Comparisons.

Based on the theory and numerical methods discussed in the previous sections, there are several means by which numerical results may be obtained. The most restrictive

requires the angular variable α to be an integer multiple of π ($\alpha = \pi/N$). However, this converts the series formulation into a series where the terms are purely oscillatory.

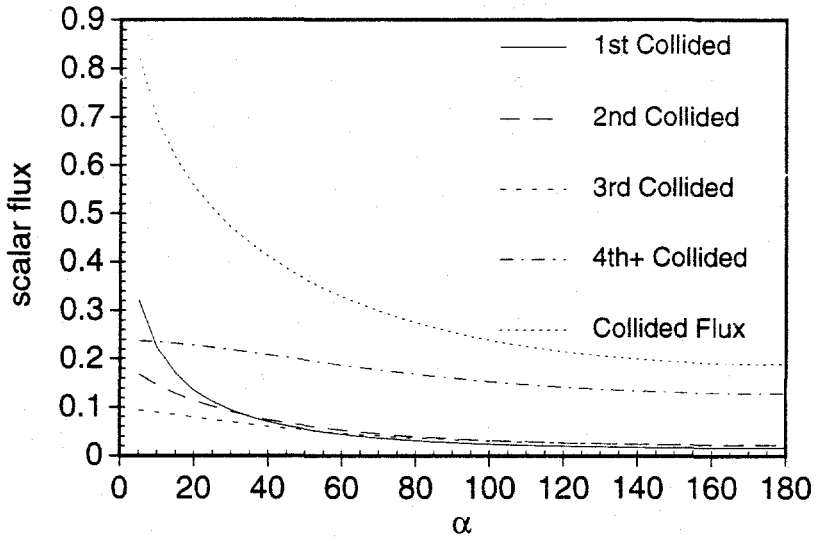

Fig. 6.5. Individual collided fluxes at $r = 1$ for anisotropic line source.

The other methods which may be employed to achieve a numerical result are the (k,ψ) inversion technique. However, the inner integral may be evaluated by iterative Chebyshev quadrature as given by Eq. (6.45b) or by its reformulation as an infinite series as given by Eq. (6.47a). The former method is listed in Table 6.3 as "(k,ψ) Integral" and the latter as "(k,ψ) Series." The other means of evaluation is in terms of the transformed Cartesian coordinate system (k_x,k_y). The data in Table 6.3 have been converged to a 10^{-6} relative error tolerance and have all been evaluated at $r = 1$ and $\mu_0 = 0$. Note that for all cases where convergence was achieved, the different inversion methods agree to the given tolerance. However, by examining the CPU time data, it is clear that when a numerical scheme has difficulty evaluating the series or integrals that computer usage increases dramatically. In general, it may be seen that the (k_x,k_y) inversion scheme works best for small α and the (k,ψ) series inversion scheme works best when the edit point is not very

close to the source. When large production computer runs are performed, it is suggested to use the (k_x,k_y) inversion scheme if $\alpha < 30°$ and the (k,ψ) series scheme otherwise.

Table 6.3. Comparison of Inversion Methods for Anisotropic Infinite Line Source.

	Scalar Flux			
α	$(\alpha = \pi/N)$	(k,ψ) Integral	(k,ψ) Series	(k_x,k_y) Inversion
5	8.21449E-01	8.22856E-01*	8.22887E-01*	8.21449E-01
10	6.92765E-01	6.92804E-01*	6.92805E-01*	6.92765E-01
15	6.13547E-01	6.13547E-01	6.13547E-01	6.13547E-01
20	5.55406E-01	5.55406E-01	5.55406E-01	5.55406E-01
30	4.71242E-01	4.71242E-01	4.71242E-01	4.71242E-01
45	3.86502E-01	3.86502E-01	3.86502E-01	3.86502E-01
60	3.28470E-01	3.28470E-01	3.28470E-01	3.28470E-01
90	2.55429E-01	2.55429E-01	2.55429E-01	2.55429E-01
180	1.88063E-01	1.88063E-01	1.88063E-01	--**
	CPU time			
α	$(\alpha = \pi/N)$	(k,ψ) Integral	(k,ψ) Series	(k_x,k_y) Inversion
5	467.78	656.15*	335.4*	6.16
10	105.9	656.51*	335.65*	13.99
15	54.82	463.69	193.68	13.2
20	36.53	253.37	58.88	9.18
30	21.83	111.86	13.91	8.14
45	13.51	68.19	2.75	10.49
60	10.55	21.6	1.26	9.23
90	6.2	19.39	1.14	0.74
180	3.09	17.4	0.92	--**

*Did not converge after 200 terms in the series.
**Unable to compute along x-axis.

6.H.4. One-Dimensional Results.

There are two one-dimensional forms of the anisotropically emitting infinite line source: emitting along the z-axis; and emitting along the surface of a cone. Because the numerical results come from single instead of double inversions, the computer times are greatly reduced.

6.H.4.a. Emission Along the z-axis. When the anisotropic line source emits along the z-axis, the variation in the spatial angle α disappears. It has been shown that this specific case is related to the solution for the scalar flux from an isotropic infinite line source. Table 6.4 lists the scalar fluxes as a function of distance from an isotropic infinite line source and from an anisotropic infinite line source emitting along the z-axis. The mean number of secondaries is conveniently set to 0.1 so that it is immediately apparent from the data that $\phi(\rho;\gamma_0=0) = c\phi_{iso}(\rho)$.

Table 6.4. Comparison of the Scalar Fluxes from Isotropic Line and Anisotropic Line Sources

r	Anisotropic Line ($\mu_0 = 1$)	Isotropic Line
1	6.0054E-03	6.0054E-02
2	9.3991E-04	9.3991E-03
3	2.0685E-04	2.0685E-03
4	5.2562E-05	5.2562E-04
5	1.4471E-05	1.4471E-04
6	4.1944E-06	4.1944E-05
7	1.2600E-06	1.2600E-05
8	3.8864E-07	3.8864E-06
9	1.2233E-07	1.2233E-06
10	3.9128E-08	3.9130E-07

6.H.4.b. Emission Along the Surface of a Cone. When the particles are emitted uniformly in transverse angle at the same longitudinal angle, they are emitted along the surface of a cone. This produces a one-dimensional spatial variation in the scalar flux. However, the emission angle is a parameter which may be manipulated. A typical three-dimensional plot of the scalar flux from this source is provided in Fig. 6.6. Note that it is displayed as a function of position and as a function of the emission angle. The data were obtained with a relative error of 10^{-5} and $c = 0.9$.

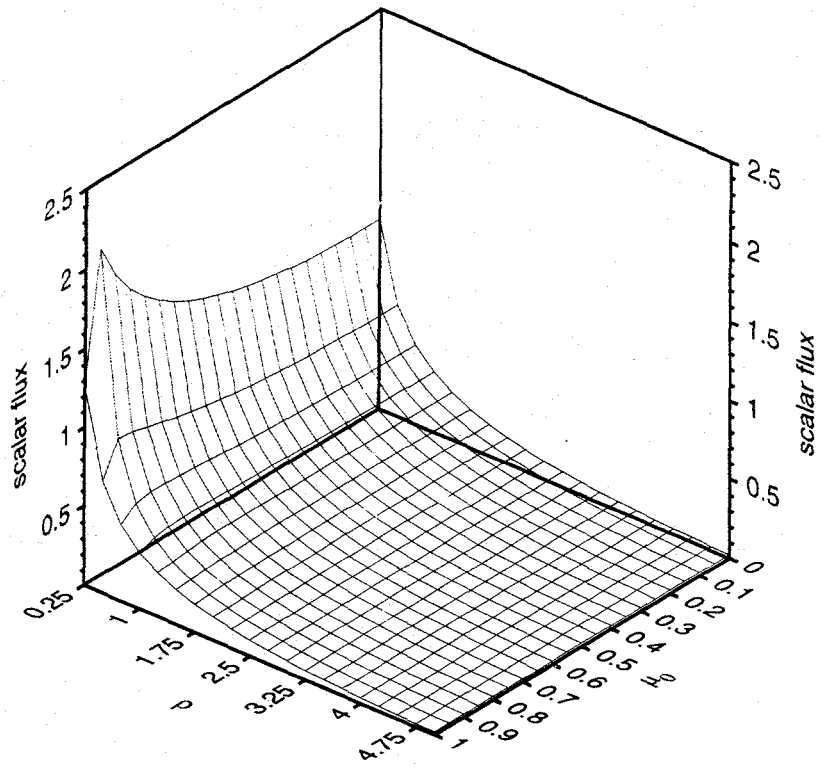

Fig. 6.6. The scalar flux as a function of distance and emission angle when the particles are emitted along the surface of a cone.

A typical decrease in the scalar flux as the distance from the source increases is evident, but an interesting feature may be noted by examining the μ_0 dependence. At small ρ, there is a peak and then a sudden decrease in the scalar flux at $\mu_0 = 1$ (emission along the z-axis). As μ_0 approaches 1, particles are emitted on the surface of a very narrow cone. Hence, there are many particles near $\rho = 0$, which contribute to an increase in the scalar flux. At $\mu_0 = 1$, the uncollided flux is lost for $\rho > 0$, and the total scalar flux therefore decreases. The primary source of the peak is that the uncollided particles are included in the total flux. Because the uncollided flux is not singular after integration in angle, it can be analytically determined. Magnified views which display this peak in the scalar flux arising from the uncollided flux are included in Figs. 6.7a and 6.7b. By noting the scales of μ_0 in these two figures one can see how sharply peaked the scalar flux becomes when the cone

becomes exceedingly narrow and when the edit point is near the source. However, as should be true with all benchmark quality calculations, greater resolution of such peaks should be obtainable via magnification in a certain region of geometric or parametric space.

6.H.5. General Results at Constant ρ.

In order to present the general results from an anisotropically emitting infinite line source in an infinite homogeneous medium, the parameters of importance must be identified. Clearly the dependent variable will be the scalar flux resulting from this source. The independent variables are the two variables which describe the position in a plane - either (ρ,α) or (x,y). However, the cosine of the emission angle μ_0 is such a crucial parameter that it may also be considered as an independent variable. Therefore, three-dimensional plots will generally be the scalar flux as a function of two of the three variables ρ, α, or μ_0; in this section the primary independent variables will be α and μ_0.

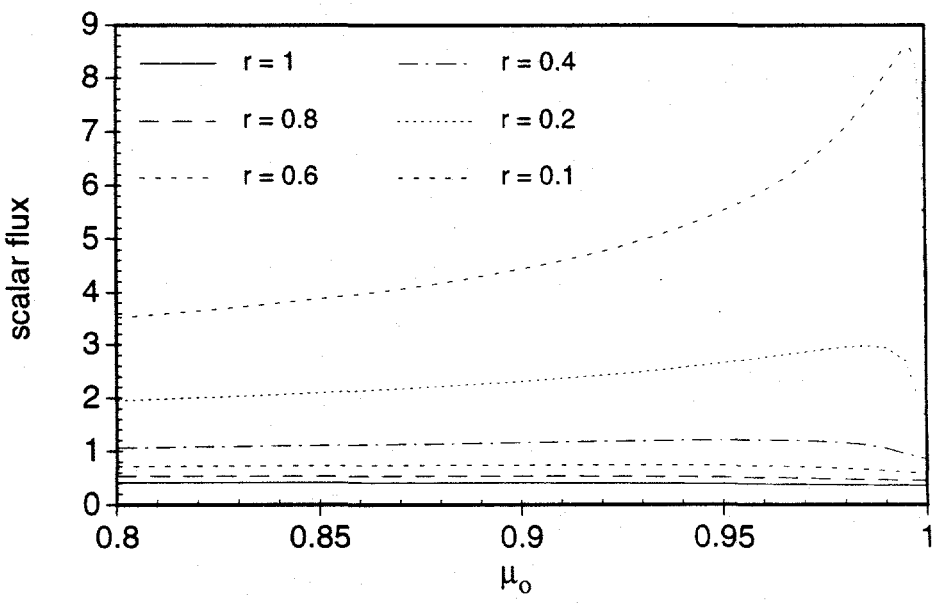

Fig. 6.7a. The scalar flux as a function of distance and emission angle when the particles are emitted along the surface of a cone (magnified).

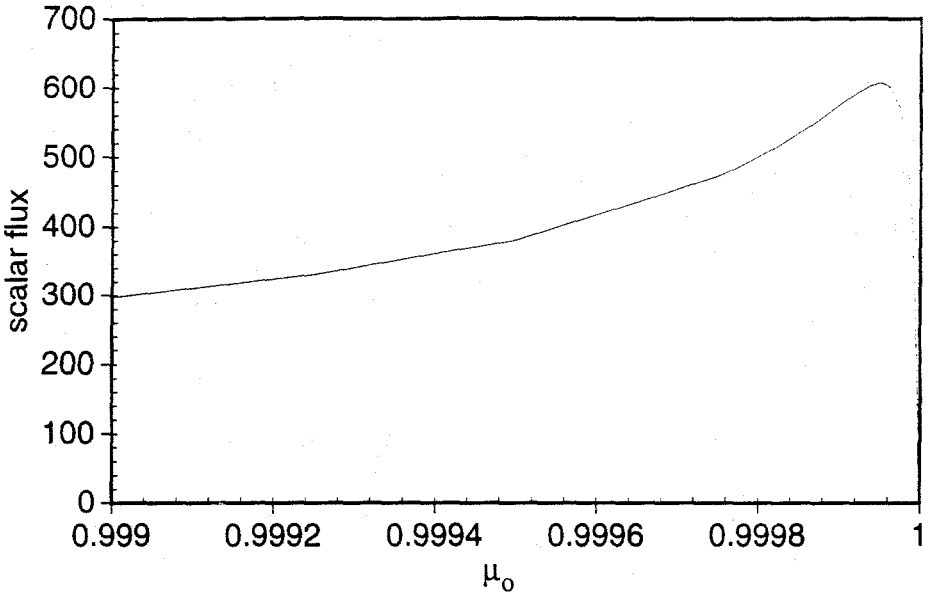

Fig. 6.7b. The scalar flux as a function of emission angle for $\rho = 0.01$ when the particles are emitted along the surface of a cone (magnified).

Fig. 6.8a, displays the scalar flux as a function of α and μ_0 at the radial position $\rho = 1$ and $c = 0.9$. Included in the figure is a magnification of the region $0.9 \leq \mu_0 \leq 1$. The magnified region clearly demonstrates one of the abilities of a benchmark-quality calculation. Note that for $\mu_0 = 1$ (emitting along the z-axis) the flux is independent of angle, as required. The effect of the directional source is seen as the flux increases dramatically at low angles. As μ_0 approaches 1, the flux approaches that of the one-dimensional case, i.e. the difference in the flux values between the one- and two-dimensional cases diminishes. With the use of the numerical inversion in (k_x,k_y) space, it is possible to evaluate the scalar flux at very small values of the angular variable α. Fig. 6.8b provides a magnification of the region at small α for $\rho = 1$ and $c = 0.9$. Note again the qualitative consistency in Figs. 6.8.

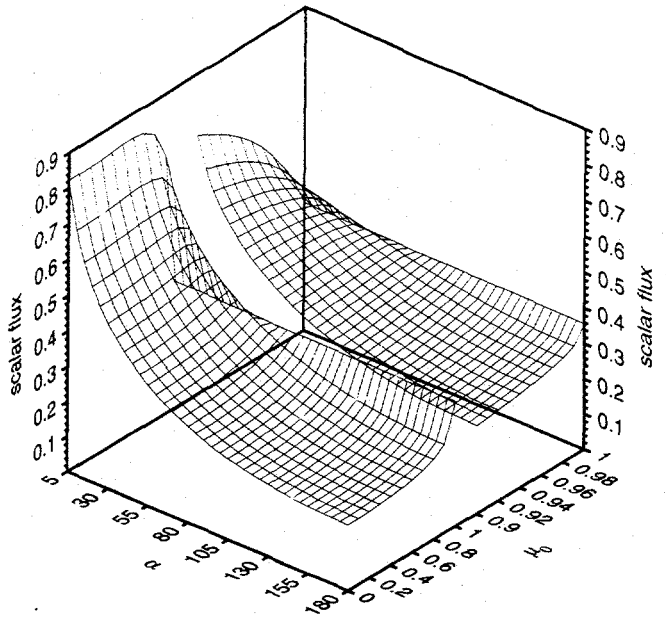

Fig. 6.8a. The scalar flux as a function of angle and emission angle for the anisotropic infinite line source with $c = 0.9$ and $\rho = 1$ (Note standard and magnified μ_0 scales).

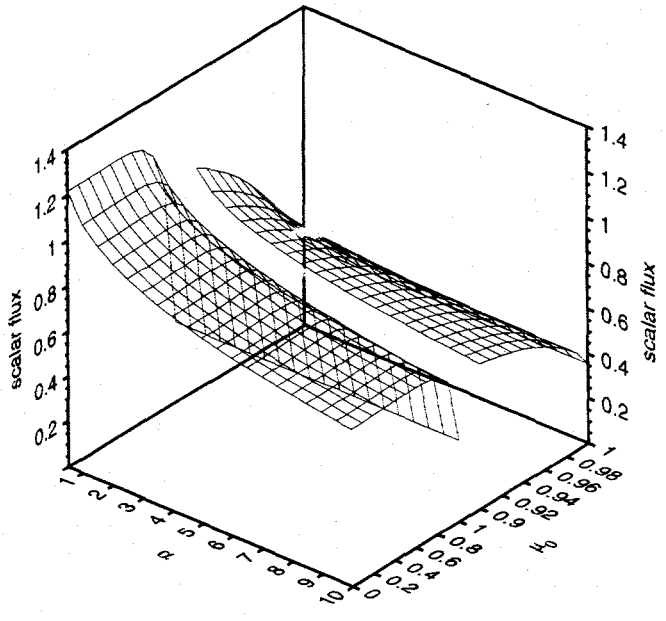

Fig. 6.8b. The scalar flux as a function of angle and emission angle for the anisotropic infinite line source with $c = 0.9$ and $\rho = 1$ at small α (Note standard and magnified μ_0 scales).

As the angle from the source increases, the flux decreases, eventually falling below the one-dimensional values. In order for particles to appear in regions behind the source (α near π) they must be scattered from the region where $0 \leq \alpha \leq \pi/2$. However, when the source emits along the z-axis, the particles scatter on the z-axis and then move away from the z-axis isotropically, making the z-axis appear as an isotropic source. Thus particles are emitted directly into regions of large angle. Therefore, the scattering source of particles into regions behind the directional source is not as great as when the one-dimensional source emits some particles directly into these regions. This phenomenon is analyzed in Fig. 6.9. As μ_0 approaches 1, the "cross-over" angle approaches 90° (this "cross-over" angle is determined by calculating the scalar flux as a position of angle, and then interpolating between the scalar fluxes which are on both sides of the scalar flux from the one-dimensional case). This is expected since as μ_0 approaches 1 many particles are having their first collisions near $\rho = 0$. When this happens, the scattering source for regions behind the source increases and the point at which the two-dimensional and one-dimensional scalar fluxes are equal approaches the symmetric 90°. At large radii the "cross-over" angle is closer to 90° for all values of μ_0 as the farther the edit point is from the source, the more the source looks isotropic. In general, as the source emits closer to the z-axis, more particles are scattered behind the source and the more the source looks isotropic from regions behind the source.

Figs. 6.10, and 6.11 display the scalar flux as a function of α and μ_0 with $c = 0.9$ at the positions, $\rho = 0.1$, and $\rho = 10$, respectively. Note that for $\rho = 0.1$ two sets of magnifications are required in order to see the smooth region at large μ_0; the closer, the edit point is to the source, the more anisotropic it appears. For $\rho = 10$, not only is the magnitude of the scalar flux smaller than for $\rho = 0.1$ and $\rho = 1$, but the variation of the scalar flux relative to the one-dimensional case is also less. That is, the scalar flux at large distances from the source gradually approaches the scalar flux from an isotropic source.

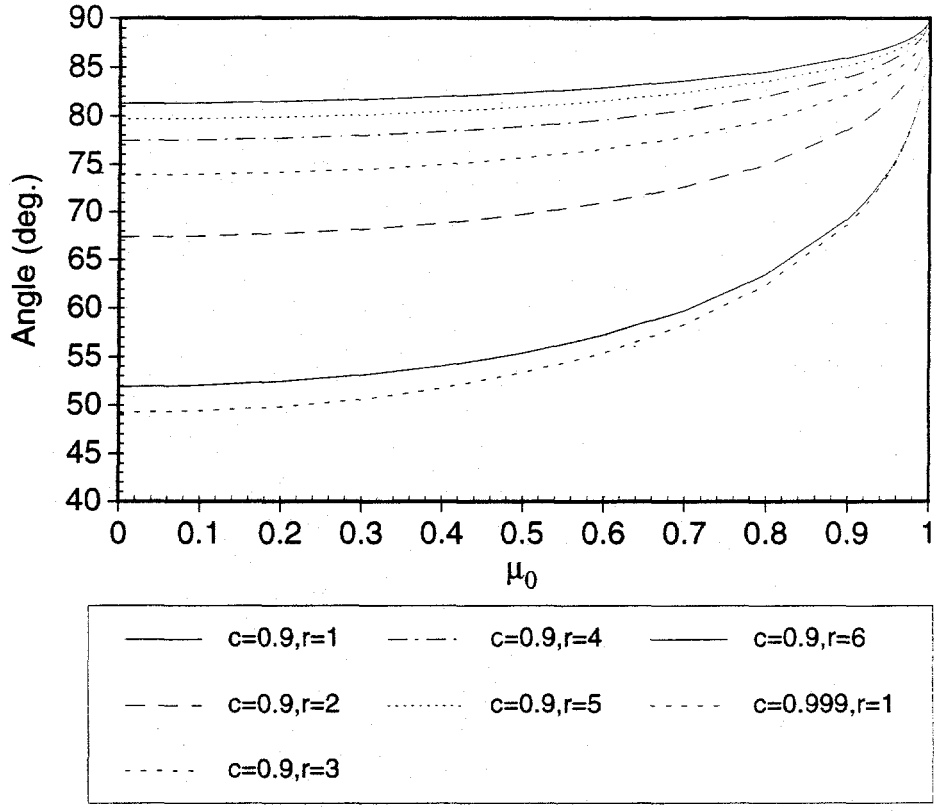

Fig. 6.9. Angle at which the value of the scalar flux from the anisotropic source is equal to the one-dimensional case with $\mu_0 = 1$ as a function of μ_0.

In a final examination ρ is considered to be a parameter with c very small. In this case, (Fig. 6.12) the medium is very strongly absorbing which makes it difficult for particles to scatter behind the source. Therefore, the anisotropic nature of the source is exaggerated with respect to cases with larger values of c. That is, the increase in the scalar flux near $\alpha = 0$ is very large as compared to the scalar flux away from the source; for the case where $c = 0.9$, the ratio of the maximum to the one-dimensional scalar fluxes is approximately 2.3, where the same ratio is 6.8 for $c = 0.01$. This is expected as once the particles move away from the source, they are quickly absorbed, effectively creating the relatively large scalar flux at angles near the source.

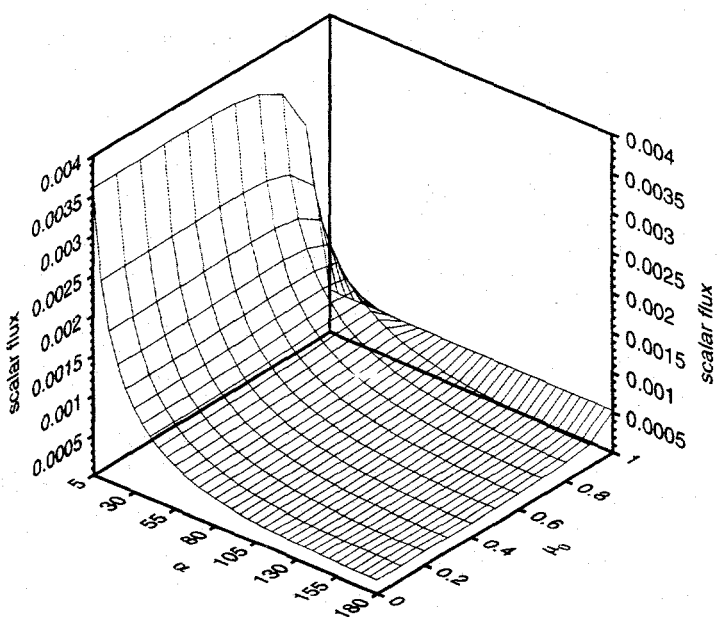

Fig. 6.12. The scalar flux as a function of angle and emission angle for the anisotropic infinite line source with $c = 0.01$ and $\rho = 1$.

6.H.6. General Results in the Transverse Plane.

To this point the primary means of displaying the scalar flux from the anisotropically emitting infinite line was as a function of the spatial angle and (the cosine of) the emission angle. However, in order to display the scalar flux as a function of position the independent variables are those which describe position in the transverse plane. Such a display is provided in Fig. 6.13. The mean number of secondaries (c) for these cases is 0.9 and μ_0 is considered a parameter which is different for each of the four plots found in the figure. As μ_0 changes from 0 to 1, the directed peak becomes more symmetric about the x-axis (it is always symmetric about the y-axis) until it becomes truly symmetric at $\mu_0 = 1$. This provides a qualitative assessment of the effect of changing emission angle on the scalar flux in the transverse plane.

With the analysis of this source complete, the suite of infinite medium benchmarks, as presented in Fig. 1.2 is complete. While constructing this suite the simplest problems in the form of those with isotropic sources, were presented first, and then the level of complexity was increased to consider anisotropic sources, culminating with the anisotropic line source. With the mathematics and numerical techniques established for this source, the next step is to utilize them to obtain results for the three-dimensional searchlight problem in a semi-infinite medium.

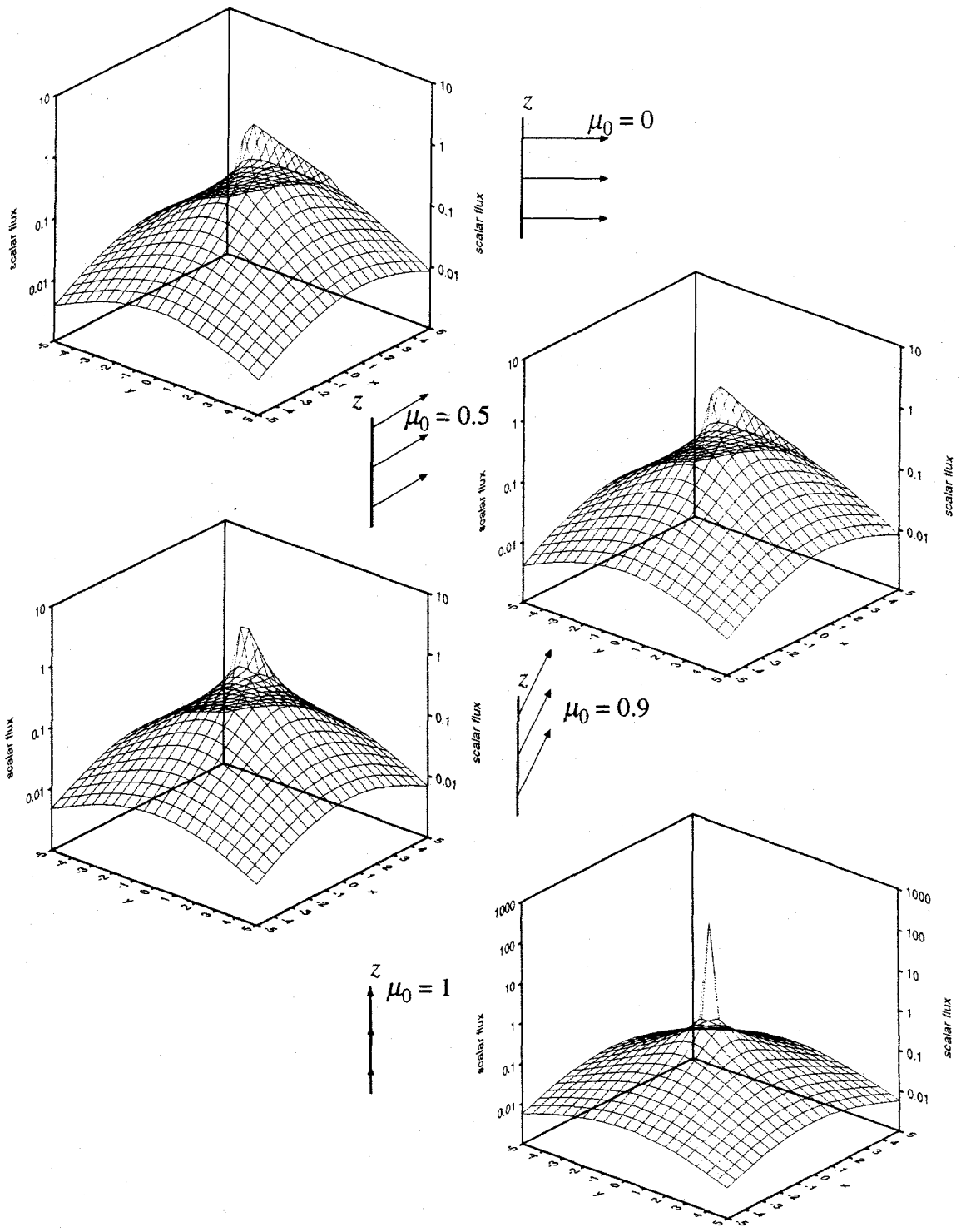

Fig. 6.13. The scalar flux in the transverse plane for four different values of μ_0 and c = 0.9.

CHAPTER 7: THE SEARCHLIGHT PROBLEM

7.A. Searchlight Problem Background

The searchlight problem was originally proposed by Chandrasekhar in the radiative transfer context [1958]. The problem is defined by the illumination of a semi-infinite medium's free surface by a radiation source, with the resultant surface and interior fluxes desired. In this analysis, the medium is assumed to be an isotropically scattering medium and the source is assumed to be monodirectional impinging at the center of the free surface.

7.B. Searchlight Problem Solution Formulation

The simplified form of the transport equation in cylindrical coordinates is similar to the one from the Green's function formulation [Eq. (4.6a)] except that the source is now described as a boundary condition:

$$\left[\mu\frac{\partial}{\partial z} + \vec{\omega}\cdot\frac{\partial}{\partial \vec{\rho}} + 1\right]\phi(z,\vec{\rho},\vec{\Omega}) = \frac{c}{4\pi}\int_{4\pi} d\vec{\Omega}'\,\phi(z,\vec{\rho},\vec{\Omega}') \quad , \tag{7.1a}$$

where

$$\phi(0,\vec{\rho},\vec{\Omega}) = S(\vec{\rho})\delta(\mu-\mu_0)\delta(\phi-\phi_0) \quad , \tag{7.1b}$$

for $\mu_0 > 0$ and the other boundary conditions

$$\lim_{z\to\infty}\phi(z,\vec{\rho},\vec{\Omega}) < \infty \quad , \tag{7.1c}$$

$$\lim_{|\vec{\rho}|\to\infty}\phi(z,\vec{\rho},\vec{\Omega}) < \infty \quad . \tag{7.1d}$$

The current is defined in its usual form as

$$J(z;\vec{\rho}) = \int_{4\pi} d\vec{\Omega}\ \mu\ \phi(z,\vec{\rho},\vec{\Omega}) \quad . \tag{7.1e}$$

The geometry of the beam boundary source (illuminating flux) is described by the function $S(\vec{\rho})$. The source is normalized such that $\int d\vec{\rho}\ S(\vec{\rho}) = 1$. The solution method begins by taking a two-dimensional Fourier transform of the transport equation in the transverse plane.

7.B.1. Fourier Transform in the Transverse Plane.

Taking a Fourier transform in the transverse plane as in Ch. 4 yields

$$\left[\mu\frac{\partial}{\partial z} + u(\vec{\Omega},\vec{k})\right] \bar{\Psi}(z,\vec{\Omega};\vec{k}) = \frac{c}{4\pi}\int_{4\pi} d\vec{\Omega}\,'\ \bar{\Psi}(z,\vec{\Omega}';\vec{k}) \quad , \tag{7.2a}$$

where the Fourier transform pair is defined as usual as

$$\bar{\Psi}(z,\vec{\Omega};\vec{k}) \equiv \int d\vec{\rho}\ e^{i\vec{k}\cdot\vec{\rho}}\ \phi(z,\vec{\rho},\vec{\Omega}) \quad , \tag{7.2b}$$

$$\phi(z,\vec{\rho},\vec{\Omega}) \equiv \frac{1}{(2\pi)^2}\int d\vec{k}\ e^{-i\vec{k}\cdot\vec{\rho}}\ \bar{\Psi}(z,\vec{\Omega};\vec{k}) \quad , \tag{7.2c}$$

and

$$u(\vec{\Omega},\vec{k}) = 1 - ik\left(1 - \mu^2\right)^{1/2}\cos(\phi - \psi) \quad . \tag{7.2d}$$

7.B.2. Formation of an Integral Equation.

As before, the procedure established in Ch. 4 for the infinite medium Green's function source is utilized for the derivation of the transformed and direct scalar fluxes for the searchlight problem. By using the integrating factor $e^{uz/\mu}$ and integrating along the characteristics of motion the transformed angular fluxes are placed in integral form as

$$\bar{\Psi}(z,\vec{\Omega};\vec{k}) = \frac{c}{4\pi\mu}\int_0^z dz'\, e^{u(z'-z)/\mu}\ \bar{\Psi}(z';\vec{k}) + \bar{S}(\vec{k})\delta(\mu-\mu_0)\delta(\phi-\phi_0)e^{-uz/\mu}\ ,\ \mu>0 \qquad (7.3a)$$

$$\bar{\Psi}(z,\vec{\Omega};\vec{k}) = -\frac{c}{4\pi\mu}\int_z^\infty dz'\, e^{u(z'-z)/\mu}\ \bar{\Psi}(z';\vec{k}) \quad ,\quad \mu<0\ , \qquad (7.3b)$$

where

$$\bar{\Psi}(z;\vec{k}) = \int_{4\pi} d\vec{\Omega}'\ \bar{\Psi}(z,\vec{\Omega}';\vec{k})\ .$$

To obtain the transformed scalar flux, the transformed angular flux is integrated over the unit sphere; this procedure yields (after considering positive and negative μ)

$$\bar{\Psi}(z;\vec{k}) = \bar{S}(\vec{k})\, e^{-z/U_0} + \frac{c}{2}\int_0^\infty dz'\, K(|z-z'|)\bar{\Psi}(z';\vec{k})\ , \qquad (7.4a)$$

where the kernel $K(z;\vec{k})$ is given as

$$K(z;\vec{k}) = \frac{1}{2\pi}\int_0^1 \frac{d\mu}{\mu}\int_0^{2\pi} d\phi\ \ e^{-z/U} \quad ,\quad z>0 \qquad (7.4b)$$

with

$$U \equiv \frac{\mu}{u(\vec{\Omega},\vec{k})}\ . \qquad (7.4c)$$

As shown in Sec. 4.B.4 it can be shown that the kernel $K(z;\vec{k})$ may be reformulated using Bessel function transformations as

$$K(z;\vec{k}) = \int_0^1 \frac{d\mu}{\mu}\ \frac{e^{-z(1-k^2\mu^2)^{1/2}/\mu}}{\left(1+k^2\mu^2\right)^{1/2}}\ . \qquad (7.5)$$

This alternative expression for $K(z;\vec{k})$ will allow the establishment of a pseudo problem to facilitate the scalar flux solution.

7.B.3. The Pseudo Problem.

The solution to the transformed transport equation is accomplished by considering a corresponding one-dimensional pseudo transport equation [Rybicki, Williams]. The pseudo transport equation for a half-space is written as

$$\left[\mu a(\mu)\frac{\partial}{\partial z} + b(\mu)\right] \tilde{\phi}(z,\mu;\mu^*) = \frac{c}{2}\int_{-1}^{1} d\mu' \, \tilde{\phi}(z,\mu';\mu^*) \quad , \tag{7.6a}$$

where the pseudo flux satisfies the source condition

$$\tilde{\phi}(0,\mu;\mu^*) = Q_0 \, \delta(\mu - \mu^*) \quad , \tag{7.6b}$$

for $\mu,\mu^* > 0$ and the boundary condition

$$\lim_{z\to\infty} \tilde{\phi}(z,\mu;\mu^*) < \infty \quad . \tag{7.6c}$$

As usual, the integral form of Eq. (7.6a) is derived, and then the scalar flux is obtained by integrating over μ. The integral form is obtained by integrating along the particle trajectory for both $\mu > 0$ and $\mu < 0$ giving

$$\tilde{\phi}(z,\mu;\mu^*) = \delta(\mu - \mu^*)\, e^{-z/\xi} + \frac{c}{2\mu a(\mu)}\int_0^z dz' \, e^{(z'-z)/\xi} \, \tilde{\phi}(z';\mu^*) \quad , \quad \mu > 0 \quad , \tag{7.7a}$$

$$\tilde{\phi}(z,\mu;\mu^*) = \frac{c}{2\mu a(\mu)}\int_\infty^z dz' \, e^{(z'-z)/\xi} \, \tilde{\phi}(z';\mu^*) \quad , \quad \mu < 0 \quad , \tag{7.7b}$$

where the scalar pseudo flux is defined as usual and

$$\xi(\mu) \equiv \frac{\mu a(\mu)}{b(\mu)} \quad . \tag{7.7c}$$

The pseudo scalar flux is now obtained by integrating the angular flux over the full range of μ to give, after combining and arranging terms

$$\tilde{\phi}(z;\mu^*) = e^{-z/\xi^*} + \frac{c}{2}\int_0^\infty dz'\, \tilde{K}(|z - z'|)\,\tilde{\phi}(z';\mu^*) \quad , \tag{7.8a}$$

where

$$\tilde{K}(z) = \int_0^1 \frac{d\mu}{\mu}\,\frac{e^{-z/\xi}}{a(\mu)} \quad . \tag{7.8b}$$

As with the Green's function formulation, comparing the equations for the actual and pseudo kernels leads to the conclusion that if

$$a(\mu) = \left(1 + k^2\mu^2\right)^{1/2} \quad , \quad b(\mu) = 1 + k^2\mu^2 \tag{7.8c}$$

then $\tilde{K}(z) = K(z;\vec{k})$. With the equivalence of the actual and pseudo kernels, the formal expression for the relationship between the actual and pseudo scalar fluxes is given as

$$\bar{\Psi}(z;\vec{k}) = \bar{S}(\vec{k})\int d\mu^*\,\frac{d\xi^*}{d\mu^*}\,\delta(\xi^* - U_0)\,\tilde{\phi}(z;\mu^*) \quad . \tag{7.9}$$

Thus, the determination of the desired scalar flux is easily obtained given the solution for the pseudo scalar flux in a semi-infinite medium.

7.B.4. Solution to the Pseudo Problem in a Half-Space.

The solution to the half-space pseudo problem is obtained by following the methods established by Busbridge. The integral operator

$$L_z(\bullet) \equiv \frac{c}{2}\int_0^\infty dz'\, K(|z - z'|)(\bullet) \tag{7.10}$$

is defined, giving for the scalar pseudo flux

$$(1 - L_z)\tilde{\phi}(z';\mu^*) = e^{-z/\xi^*} \quad . \tag{7.11}$$

Next, Eq. (7.8a) is differentiated with respect to z as

$$\frac{\partial}{\partial z}\tilde{\phi}(z;\mu^*) + \frac{1}{\xi^*}\,e^{-z/\xi^*} = \frac{c}{2}\int_0^\infty dz'\;\tilde{\phi}(z';\mu^*)\,\frac{\partial}{\partial z}K(|z-z'|)\quad , \tag{7.12a}$$

which by substituting Eq. (7.11), adding and subtracting the term $L_z\frac{\partial}{\partial z'}\tilde{\phi}(z';\mu^*)$ on the left hand side, and rearranging terms yields

$$(1-L_z)\left[\frac{\partial}{\partial z} + \frac{1}{\xi^*}\right]\tilde{\phi}(z;\mu^*) =$$

$$= -L_z\frac{\partial}{\partial z'}\tilde{\phi}(z';\mu^*) + \frac{c}{2}\int_0^\infty dz'\;\tilde{\phi}(z';\mu^*)\,\frac{\partial}{\partial z}K(|z-z'|)\quad . \tag{7.12b}$$

The right hand side of Eq. (7.12b) is explicitly expressed as

$$\text{RHS} = -\frac{c}{2}\int_0^\infty dz'\left[K(|z-z'|)\frac{\partial}{\partial z'}\tilde{\phi}(z';\mu^*) - \tilde{\phi}(z';\mu^*)\,\frac{\partial}{\partial z}K(|z-z'|)\right]\quad . \tag{7.13a}$$

and may be restated by noting that

$$\frac{d}{dx}f(|x-y|) = -\frac{d}{dy}f(|x-y|)\quad ,$$

or in terms of the kernel under consideration

$$\frac{d}{dz}K(|z-z'|) = -\frac{d}{dz'}K(|z-z'|)\quad .$$

Inserting this into Eq. (7.13a) gives

$$\text{RHS} = -\frac{c}{2}\int_0^\infty dz'\left[K(|z-z'|)\frac{\partial}{\partial z'}\tilde{\phi}(z';\mu^*) + \tilde{\phi}(z';\mu^*)\,\frac{\partial}{\partial z'}K(|z-z'|)\right]\quad , \tag{7.13b}$$

which is immediately seen to be a perfect differential:

$$\text{RHS} = -\frac{c}{2}\int_0^\infty dz'\,\frac{\partial}{\partial z'}\left[K(|z-z'|)\tilde{\phi}(z';\mu^*)\right]\quad . \tag{7.13c}$$

Application of the fundamental theorem of calculus then gives

$$\text{RHS} = -\frac{c}{2} K(|z - z'|) \tilde{\phi}(z';\mu^*) \Big|_0^\infty \quad . \tag{7.13c}$$

or upon substitution of the limits

$$\text{RHS} = \frac{c}{2} K(z) \tilde{\phi}(0;\mu^*) \quad . \tag{7.13d}$$

Thus, the final result is obtained as

$$(1 - L_z)\left[\frac{\partial}{\partial z} + \frac{1}{\xi^*}\right] \tilde{\phi}(z;\mu^*) = \frac{c}{2} K(z) \tilde{\phi}(0;\mu^*) \quad . \tag{7.14}$$

The next step involves the kernel $K(z)$. By noting the structure of $K(z)$ and that it contains the exponential term which can be written in terms of the integral operator L_z, it is easily seen from Eqs. (7.11) and (7.8b) that

$$K(z) = \int_0^1 \frac{d\mu}{\mu} \frac{e^{-z/\xi}}{a(\mu)} = (1 - L_z) \int_0^1 \frac{d\mu}{\mu a(\mu)} \tilde{\phi}(z;\mu) \quad . \tag{7.15}$$

Inserting this expression for $K(z)$ into Eq. (7.14) and collecting terms yields

$$(1 - L_z)\left\{ \left[\frac{\partial}{\partial z} + \frac{1}{\xi^*}\right] \tilde{\phi}(z;\mu^*) - \frac{c}{2} \tilde{\phi}(0;\mu^*) \int_0^1 \frac{d\mu}{\mu a(\mu)} \tilde{\phi}(z;\mu) \right\} = 0 \quad . \tag{7.16}$$

As Busbridge shows for the albedo problem, the expression inside the operator $1 - L_z$ can be shown to be in the null space of the operator; therefore,

$$\left[\frac{\partial}{\partial z} + \frac{1}{\xi^*}\right] \tilde{\phi}(z;\mu^*) = \frac{c}{2} \tilde{\phi}(0;\mu^*) \int_0^1 \frac{d\mu}{\mu a(\mu)} \tilde{\phi}(z;\mu) \quad . \tag{7.17}$$

A reciprocity relation between μ and μ^* is obtained by a standard technique of multiplication and subtraction of the following equations:

$$(1 - L_z)\tilde{\phi}(z;\mu) = e^{-z/\xi} \tag{7.18a}$$

$$(1 - L_z)\tilde{\phi}(z;\mu^*) = e^{-z/\xi^*} \quad . \tag{7.18b}$$

If Eq. (7.18a) is multiplied by $\tilde{\phi}(z';\mu^*)$ and Eq. (7.18b) is multiplied by $\tilde{\phi}(z';\mu)$, and both equations are integrated with respect to z' over $[0,\infty)$, there results

$$\int_0^\infty dz'\ \tilde{\phi}(z';\mu^*)(1 - L_{z'})\tilde{\phi}(z;\mu) = \int_0^\infty dz'\ e^{-z'/\xi}\ \tilde{\phi}(z';\mu^*) \tag{7.19a}$$

$$\int_0^\infty dz'\ \tilde{\phi}(z';\mu)(1 - L_{z'})\tilde{\phi}(z;\mu^*) = \int_0^\infty dz'\ e^{-z'/\xi^*}\ \tilde{\phi}(z';\mu) \quad . \tag{7.19b}$$

Subtracting Eq. (7.19b) from Eq. (7.19a) gives

$$-\int_0^\infty dz'\ \tilde{\phi}(z';\mu^*)L_{z'}\ \tilde{\phi}(z;\mu) + \int_0^\infty dz'\ \tilde{\phi}(z';\mu)L_{z'}\ \tilde{\phi}(z;\mu^*) =$$

$$= \int_0^\infty dz'\ e^{-z'/\xi}\ \tilde{\phi}(z';\mu^*) - \int_0^\infty dz'\ e^{-z'/\xi^*}\ \tilde{\phi}(z';\mu) \quad . \tag{7.20}$$

Expressing the integral operator L_z explicitly immediately shows that the left hand side of Eq. (7.20) is equal to zero. Thus,

$$\frac{c}{2}\int_0^\infty dz'\ e^{-z'/\xi}\ \tilde{\phi}(z';\mu^*) = \frac{c}{2}\int_0^\infty dz'\ e^{-z'/\xi^*}\ \tilde{\phi}(z';\mu) \quad . \tag{7.21}$$

From Eq. (7.7b) evaluated at $z = 0$ for $\mu > 0$

$$\tilde{\phi}(0,-\mu;\mu^*) = \frac{c}{2\mu a(\mu)}\int_0^\infty dz'\ e^{-z'/\xi}\ \tilde{\phi}(z';\mu^*) \tag{7.22a}$$

$$\tilde{\phi}(0,-\mu^*;\mu) = \frac{c}{2\mu^* a(\mu^*)}\int_0^\infty dz'\ e^{-z'/\xi^*}\ \tilde{\phi}(z';\mu) \quad , \tag{7.22b}$$

the desired reciprocity relation is obtained as

$$\mu a(\mu)\tilde{\phi}(0,-\mu;\mu^*) = \mu^* a(\mu^*)\ \tilde{\phi}(0,-\mu^*;\mu) \quad . \tag{7.23}$$

The final step in the solution involves manipulation of Eq. (7.17). Multiplying by the term $e^{-z/\xi}$ and integrating over z on the range $[0,\infty)$ gives

$$\int_0^\infty dz\ e^{-z/\xi}\ \frac{\partial}{\partial z}\ \tilde{\phi}(z';\mu^*) + \frac{1}{\xi^*}\int_0^\infty dz\ e^{-z/\xi}\ \tilde{\phi}(z;\mu^*) =$$

$$= \frac{c}{2}\,\tilde{\phi}(0;\mu^*)\int_0^1 \frac{d\mu'}{\mu' a(\mu')}\int_0^\infty dz\ e^{-z/\xi}\ \tilde{\phi}(z;\mu')\ . \qquad (7.24a)$$

The first term on the left hand side can be integrated by parts and yields upon collection of terms and some minor simplification

$$\tilde{\phi}(0;\mu^*)\left[1 + \frac{c}{2}\int_0^1 \frac{d\mu'}{\mu' a(\mu')}\int_0^\infty dz\ e^{-z/\xi}\ \tilde{\phi}(z;\mu')\right] = \frac{\xi + \xi^*}{\xi^*\xi}\int_0^\infty dz\ e^{-z/\xi}\ \tilde{\phi}(z;\mu^*)\ . \qquad (7.24b)$$

Noting again that

$$\frac{2}{c}\,\mu a(\mu)\,\tilde{\phi}(0,-\mu;\mu^*) = \int_0^\infty dz'\ e^{-z/\xi}\ \tilde{\phi}(z;\mu^*)\ ,$$

it is quickly seen upon substitution into Eq. (7.24b) that

$$\tilde{\phi}(0;\mu^*)\left[1 + \frac{c}{2}\int_0^1 \frac{d\mu'}{\mu' a(\mu')}\,\mu a(\mu)\,\tilde{\phi}(0,-\mu;\mu')\right]\frac{\xi^*\xi}{\xi + \xi^*} = \frac{2}{c}\,\mu a(\mu)\,\tilde{\phi}(0,-\mu;\mu^*)\ . \qquad (7.25a)$$

The reciprocity relation [Eq. (7.23)] is now used in the integral on the left hand side to give

$$\tilde{\phi}(0;\mu^*)\left[1 + \int_0^1 d\mu'\ \tilde{\phi}(0,-\mu';\mu)\right]\frac{\xi^*\xi}{\xi + \xi^*} = \frac{2}{c}\,\mu a(\mu)\,\tilde{\phi}(0,-\mu;\mu^*)\ . \qquad (7.25b)$$

By setting $z = 0$ in Eq. (7.8a), substituting the form of $K(z)$ from Eq. (7.8b), and noting the definition of $\tilde{\phi}(0,-\mu;\mu^*)$ from Eq. (7.22a), it is seen that

$$\tilde{\phi}(0;\mu^*) = 1 + \int_0^1 d\mu\ \tilde{\phi}(0,-\mu;\mu^*)\ , \qquad (7.26)$$

from which it follows that

$$\tilde{\phi}(0;\mu^*)\,\tilde{\phi}(0;\mu)\,\frac{\xi^*\xi}{\xi+\xi^*} = \frac{2}{c}\,\mu a(\mu)\,\tilde{\phi}(0,-\mu;\mu^*)\ , \tag{7.27a}$$

or

$$\tilde{\phi}(0,-\mu;\mu^*) = \frac{c}{2}\,\frac{1}{\mu a(\mu)}\,\frac{\xi^*\xi}{\xi+\xi^*}\,\tilde{\phi}(0;\mu^*)\,\tilde{\phi}(0;\mu)\ . \tag{7.27b}$$

Now, an integral equation for $\tilde{\phi}(0;\mu^*)$ is established by substituting Eq. (7.27b) into Eq. (7.26) as

$$\tilde{\phi}(0;\mu^*) = 1 + \tilde{\phi}(0;\mu^*)\xi^*\,\frac{c}{2}\int_0^1 d\mu\,\frac{1}{\mu a(\mu)}\,\frac{\xi}{\xi+\xi^*}\,\tilde{\phi}(0;\mu)\ , \tag{7.28}$$

or upon renaming $\tilde{\phi}(0;\mu^*)$ as $H(\xi^*;k)$ and letting $\xi^* \to \xi$ there results the following non-linear integral equation for the H-function:

$$H(\xi;k) = 1 + \xi H(\xi;k)\,\frac{c}{2}\int_0^1 \frac{d\mu'}{b(\mu')}\,\frac{H(\xi';k)}{\xi'+\xi}\ . \tag{7.29}$$

7.B.5. The Transformed Scalar Flux and Surface Current.

The surface scalar flux and current along with the interior transformed scalar flux may now be obtained. Recollection of the equivalence relation between the pseudo scalar flux and the transformed scalar flux [Eq. (7.9)]

$$\bar{\Psi}(z;\vec{k}) = \bar{S}(\vec{k})\int d\mu^*\,\frac{d\xi^*}{d\mu^*}\,\delta(\xi^* - U_0)\,\tilde{\phi}(z;\mu^*)\ ,$$

and noting that $\tilde{\phi}(0;\mu^*) = H(\xi^*;k)$ leads immediately to the conclusion that the transformed scalar flux at the surface of the semi-infinite medium is given by

$$\bar{\Psi}(0;\vec{k}) = \bar{S}(\vec{k})H(U_0;k)\ . \tag{7.30}$$

The interior transformed scalar flux is obtained from Eq. (7.22a). It is easily seen that the Laplace transform of the interior pseudo flux is the integral term if $\xi = 1/s$; thus,

$$\frac{2}{c}\,\mu a(\mu)\,\tilde{\phi}(0,-\mu;\mu^*) = \mathcal{L}_s\left\{\tilde{\phi}(z;\mu^*)\right\} \quad , \tag{7.31a}$$

where $\mathcal{L}_s$ is the Laplace transform. Inserting this expression into Eq. (7.27b) then leaves for the Laplace transform of the interior pseudo flux

$$\mathcal{L}_s\left\{\tilde{\phi}(z;\mu^*)\right\} = \frac{\xi^*(1/s)}{(1/s)+\xi^*}\,H(\xi^*;k)\,H[(1/s);k] \quad . \tag{7.31b}$$

Considering again the equation relating the pseudo flux to the transformed scalar flux yields

$$\bar{\Psi}(z;\vec{k}) = \bar{S}(\vec{k})\;\mathcal{L}_z^{-1}\left\{\frac{U_0}{1+sU_0}\,H(U_0;k)\,H\left[\frac{1}{s};k\right]\right\} \quad ,$$

or

$$\bar{\Psi}(z;\vec{k}) = \bar{S}(\vec{k})\;U_0\,H(U_0;k)\;\mathcal{L}_z^{-1}\left\{\frac{1}{1+sU_0}\,H\left[\frac{1}{s};k\right]\right\} \quad . \tag{7.32}$$

Using similar methods the transformed current at the surface is obtained as

$$\bar{J}(0;\vec{k}) = \bar{S}(\vec{k})\left\{\mu_0 \;-\; \frac{c}{2}\,U_0 H(U_0;k)\int_0^1 d\mu\;\frac{\xi}{\xi+U_0}\,H(\xi;k)\right\} \quad . \tag{7.33}$$

A detailed derivation of the transformed current at the surface is provided in Appendix C.

7.C. The Scalar Fluxes and Current via Fourier Transform Inversion

7.C.1. The General Incident Beam.

The direct scalar flux is obtained by inverting the double Fourier transform as given in the inversion [Eq. (7.2c)]:

$$\phi(z,\vec{\rho}) = \frac{1}{(2\pi)^2}\int d\vec{k}\;e^{-i\vec{k}\cdot\vec{\rho}}\;\bar{\Psi}(z;\vec{k}) \quad ,$$

which is more explicitly written as

$$\phi(z,\vec{\rho}) = \frac{1}{(2\pi)^2}\int_0^\infty dk\ k \int_0^{2\pi} d\psi\ e^{-ik\rho\cos(\psi-\alpha)}\ \bar{\Psi}(z,;\vec{k})\ . \tag{7.34}$$

Upon substitution of the transformed surface and interior scalar fluxes [Eqs. (7.30) and (7.32)] the scalar fluxes are

$$\phi(0,\vec{\rho}) = \frac{1}{(2\pi)^2}\int_0^\infty dk\ k \int_0^{2\pi} d\psi\ e^{-ik\rho\cos(\psi-\alpha)}\ \bar{S}(\vec{k})H(U_0;k)\ ; \tag{7.35a}$$

$$\phi(z,\vec{\rho}) = \frac{1}{(2\pi)^2}\int_0^\infty dk\ k\int_0^{2\pi} d\psi\ e^{-ik\rho\cos(\psi-\alpha)}\bar{S}(\vec{k})U_0H(U_0;k)\ \mathcal{L}_z^{-1}\left\{\frac{H\left[\frac{1}{s};k\right]}{1+sU_0}\right\}\ . \tag{7.35b}$$

The current at the surface is similarly given by

$$J(0,\vec{\rho}) = \frac{1}{(2\pi)^2}\int d\vec{k}\ e^{-i\vec{k}\cdot\vec{\rho}}\ \bar{J}(0;\vec{k})\ , \tag{7.36a}$$

Substitution of the transformed current [Eq. (7.33)] into the above equation yields

$$J(0,\vec{\rho}) = \frac{1}{(2\pi)^2}\int_0^\infty dk\ k \int_0^{2\pi} d\psi\ e^{-ik\rho\cos(\psi-\alpha)}\ \bar{S}(\vec{k})\times$$

$$\times\left\{\mu_0\ -\frac{c}{2}U_0H(U_0;k)\int_0^1 d\mu\ \frac{\xi}{\xi+U_0}H(\xi;k)\right\}\ , \tag{7.36b}$$

or upon evaluating the source portion

$$J(0,\vec{\rho}) = \mu_0 S(\vec{\rho}) - \frac{1}{(2\pi)^2}\int_0^\infty dk\ k \int_0^{2\pi} d\psi\ e^{-ik\rho\cos(\psi-\alpha)}\ \bar{S}(\vec{k})\times$$

$$\times\left\{\frac{c}{2}U_0H(U_0;k)\int_0^1 d\mu\ \frac{\xi}{\xi+U_0}H(\xi;k)\right\}\ . \tag{7.37}$$

With this expression for the current two important items are evident. First, the current is composed of a term $\mu_0 S(\vec{\rho})$ which is the incoming current from the source. Second, the

other term is negative in sign indicating the current coming out of the medium. Thus the current is composed of an incoming source component and an outgoing component resulting from the scattering inside the medium.

7.C.2. The Normal Incident Beam.

A significant simplification occurs if the anisotropic source impinges normal to the surface. In this case $\mu_0 = 1$, which implies that $U_0 = 1$, and $\bar{S}(\vec{k})$ is only a function of the magnitude of $\vec{k}$. The entire dependence on ψ in the kernels in Eqs. (7.35) is lost except for the complex exponential; the ψ integral then becomes the zeroth order Bessel function. This leaves for the scalar fluxes and surface current:

$$\phi(0,\rho) = \frac{1}{2\pi}\int_0^\infty dk\ k\ \bar{S}(k)\ H(1;k)\ J_0(\rho k)\ ; \tag{7.38a}$$

$$\phi(z,\rho) = \frac{1}{2\pi}\int_0^\infty dk\ k\ J_0(\rho k)\ \bar{S}(k)\ H(1;k)\ \mathcal{L}_z^{-1}\left\{\frac{H\left[\frac{1}{s};k\right]}{1+s}\right\}\ . \tag{7.38b}$$

$$J(0,\vec{\rho}) = S(\rho) - \frac{1}{2\pi}\int_0^\infty dk\ k\ J_0(k\rho)\ \bar{S}(k)\left\{\frac{c}{2}\,H(1;k)\int_0^1 d\mu\ \frac{\xi}{\xi+1}\,H(\xi;k)\right\}\ . \tag{7.38c}$$

Clearly if $\mu_0 = 1$ the scalar flux is two-dimensional and the surface current is one-dimensional. This case has been treated numerically [Ganapol, *et al.* 1994]. In general, however, if $\mu_0 \neq 1$ the scalar flux is three-dimensional.

7.D. Numerical Considerations

As evident in Eqs. (7.35) the numerical solution for the scalar flux involves many procedures including a double Fourier transform inversion, Laplace transform inversion, and the determination of the H-function. Each will be discussed separately.

7.D.1. Numerical Evaluation of the H-Function.

The numerical evaluation of the H-function is essential for the determination of the scalar fluxes. The non-linear integral equation to be solved is [with $b(\mu)$ specified]

$$H(\xi;k) = 1 + \xi H(\xi;k) \frac{c}{2} \int_0^1 \frac{d\mu'}{1 + k^2\mu'^2} \frac{H(\xi';k)}{\xi' + \xi} \quad , \tag{7.39a}$$

which may be rearranged so that

$$H(\xi;k) = \left[1 - \xi \frac{c}{2} \int_0^1 \frac{d\mu'}{1 + k^2\mu^2} \frac{H(\xi';k)}{\xi' + \xi} \right]^{-1} \quad . \tag{7.39b}$$

By using the relationship between μ and ξ, the integral in Eq. (7.39b) may be rewritten as

$$H(\xi;k) = \left[1 - \xi \frac{c}{2} \int_0^{1/(1+k^2)^{1/2}} \frac{d\xi'}{(1 - k^2\xi'^2)^{1/2}} \frac{H(\xi';k)}{\xi' + \xi} \right]^{-1} \quad . \tag{7.40}$$

When $k = 0$ then $\xi = \mu$ and Eq. (7.40) reduces to the integral equation for Chandrasekhar's H-function (1960). A moment relation for the general H-function

$$\alpha_0 = \int_0^1 d\mu \frac{H(\xi;k)}{b(\mu)} \quad , \tag{7.41}$$

may be derived which then reduces to the zeroth moment from Chandrasekhar when $k = 0$. α_0 may be evaluated by dividing Eq. (7.39a) by $b(\mu)$ and integrating with respect to μ over [0,1] to give

$$\alpha_0 = \int_0^1 \frac{d\mu}{b(\mu)} + \frac{c}{2}\int_0^1 d\mu\, \frac{\xi H(\xi;k)}{b(\mu)} \int_0^1 \frac{d\mu'}{1 + k^2\mu'^2} \frac{H(\xi';k)}{\xi' + \xi} \quad . \tag{7.42a}$$

The first integral may be evaluated as $\gamma = (\tan^{-1}k)/k$ so that

$$0 = \gamma - \alpha_0 + \frac{c}{2}\int_0^1 d\mu\, \frac{\xi H(\xi;k)}{b(\mu)} \int_0^1 \frac{d\mu'}{b(\mu')} \frac{H(\xi';k)}{\xi' + \xi} \quad . \tag{7.42b}$$

Rearranging the second integral's kernel in Eq. (7.42b) as

$$0 = \gamma - \alpha_0 + \frac{c}{2}\int_0^1 d\mu\, \frac{H(\xi;k)}{b(\mu)} \int_0^1 d\mu'\, \frac{H(\xi';k)}{b(\mu')} \left(1 - \frac{\xi'}{\xi' + \xi}\right) \tag{7.43a}$$

results in

$$0 = \gamma - \alpha_0 + \frac{c}{2}\alpha_0^2 - \frac{c}{2}\int_0^1 d\mu\, \frac{H(\xi;k)}{b(\mu)} \int_0^1 d\mu'\, \frac{H(\xi';k)}{b(\mu')} \frac{\xi'}{\xi' + \xi} \quad . \tag{7.43b}$$

Adding Eqs. (7.42b) and (7.43b) yields (after recognizing that the integral terms cancel) the following quadratic equation in α_0

$$0 = 2\gamma - 2\alpha_0 + \frac{c}{2}\alpha_0^2 \quad . \tag{7.44}$$

Solving for α_0 shows that

$$\alpha_0 = \frac{2}{c}\left[1 \pm (1 - c\gamma)^{1/2}\right] \quad . \tag{7.45}$$

It is desirable that α_0 remain finite if $c = 0$; therefore the "–" sign is chosen and α_0 is seen to be

$$\alpha_0 = \frac{2}{c}\left[1 - \left(1 - c\frac{\tan^{-1}k}{k}\right)^{1/2}\right] \quad . \tag{7.46}$$

A potential numerical difficulty is present in the evaluation of $H(\xi;k)$ [Eq. (7.40)]. Near the upper limit ξ' will be equal to $1/k$, creating a weak singularity in the integrand. This problem is mitigated by making the change of variable

$$\xi' = \frac{\sin(a\theta)}{k}$$

where $a = \sin^{-1}[k/(1+k^2)^{1/2}] = \tan^{-1}k$. With this change of variable Eq. (7.40) becomes

$$H(\xi;k) = \left\{ 1 - \xi \frac{c}{2} \frac{a}{k} \int_0^1 d\theta \frac{H\left[\frac{\sin(a\theta)}{k}\right]}{\xi + \frac{\sin(a\theta)}{k}} \right\}^{-1} , \tag{7.47}$$

and the moment relation is

$$\alpha_0 = \frac{a}{k} \int_0^1 d\mu \, H\left[\frac{\sin(a\theta)}{k}\right] . \tag{7.48}$$

An important point which makes the evaluation of the H-function simpler is that the range of integration and the argument of the H-function inside the integrals in Eqs. (7.47) and (7.48) are real. Thus, an iteration scheme may be used to determine the H-function in the range of integration, and then this "converged" H-function is used to generate the value of the general H-function for any ξ, which may be complex [Ganapol, *et al.* 1994]. The iteration scheme uses Gauss-Legendre quadrature of order L_m to evaluate the integrals; thus, an iteration is performed for each $H(\xi_m;k)$ where $\xi_m = \sin(a\theta_m)/k$. The iteration begins by setting the m values of $H(\xi_m;k)$ to the analytic value for α_0 as

$$H_m^0 = \alpha_0 . \tag{7.49a}$$

The next step is to use these values inside the integral equation for the H-function to determine a new value for the H_m's (with j being the iteration index):

$$H_m^{j+1/2} = \left\{ 1 - \frac{\sin(a\theta_m)}{k} \frac{c}{2} \frac{a}{k} \sum_{m'=1}^{L_m} \omega_{m'} \frac{H_{m'}^j}{\frac{\sin(a\theta_m)}{k} + \frac{\sin(a\theta_{m'})}{k}} \right\}^{-1} . \qquad (7.49b)$$

Now the moments may be calculated as

$$\alpha_0^{j+1/2} = \frac{a}{k} \sum_{m'=1}^{L_m} \omega_{m'} H_{m'}^{j+1/2} , \qquad (7.49c)$$

and the values of H_m can be adjusted according to these approximate values of the moment and the exact values of the moment:

$$H_m^{j+1} = \frac{\alpha_0}{\alpha_0^{j+1/2}} H_m^{j+1/2} . \qquad (7.49d)$$

The last two steps are repeated until the approximate value of the moment is equal (within a desired relative error) to the exact value of the moment for each H_m. At this point, the process has converged and the converged values are denoted as H_m^c. Thus, for a general ξ the H-function is given by

$$H(\xi;k) = \left\{ 1 - \xi \frac{c}{2} \frac{a}{k} \sum_{m'=1}^{L_m} \omega_{m'} \frac{H_{m'}^c}{\xi + \frac{\sin(a\theta_{m'})}{k}} \right\}^{-1} . \qquad (7.50)$$

Because the evaluation of both the surface scalar flux and interior scalar flux involve the term $H(U_0;k)$ and the interior scalar flux involves evaluation of $H(1/s;k)$ in the Laplace transform inversion, proper treatment of the H-function for complex arguments is required. A dispersion relation for the H-function and a factorization may be obtained for a complex argument and are derived in Appendix D. These may be used as a measure to determine how well an algorithm is calculating the H-function for a general complex argument.

7.D.2. The Laplace Transform Inversion.

The Laplace transform pair in its general form and like the Fourier transform pair contain integrals in the complex plane. The Laplace transform pair is defined as

$$F(s) = \mathcal{L}_s\{f(t)\} \equiv \int_0^\infty dt\, e^{-st} f(t) \quad ; \tag{7.51a}$$

$$f(t) = \mathcal{L}_t^{-1}\{F(s)\} \equiv \frac{1}{2\pi i} \int_{\gamma-i\infty}^{\gamma+i\infty} ds\, e^{st} F(s) \quad . \tag{7.51b}$$

By making the change of variable $s = \gamma + i\omega$, the inversion becomes

$$f(t) = \frac{e^{\gamma t}}{2\pi} \int_{-\infty}^{\infty} d\omega\, e^{i\omega t} F(\gamma + i\omega) \quad . \tag{7.52}$$

If it is known that $f(t)$ is real, it can be shown [Ganapol, 1989] that the inversion may be expressed as

$$f(t) = \frac{2e^{\gamma t}}{\pi} \int_0^\infty d\omega \cos(\omega t)\, \mathrm{Re} F(\gamma + i\omega) \quad . \tag{7.53}$$

When dealing with quantities such as a scalar flux, it is evident that the final result must be mathematically real in order to be of physical significance. However, this does not imply that the kernels of integrals which produce real quantities must also be real. In order for an integral over a real variable to be real either the integrand itself must be real or the imaginary part of the integrand must integrate to zero. The latter case often occurs when an odd function is integrated over a symmetric range. The integrand for the interior scalar flux [Eq. (7.35b) contains a Laplace transform inversion; however, this inversion is multiplied by a complex exponential and other complex quantities such as U_0 and $H(U_0;k)$. Therefore, if the scalar flux is determined as shown in Eq. (7.35b), the result of the

Laplace transform inversion will be complex and therefore Eq. (7.53) may not be used as is. Only if the integral over ψ is taken inside the Laplace transform inversion giving

$$\phi(z,\vec{\rho}) = \frac{1}{(2\pi)^2}\int_0^\infty dk\ k\ \mathcal{L}_z^{-1}\left\{H\left[\frac{1}{s};k\right]\int_0^{2\pi} d\psi\ e^{-ik\rho\cos(\psi-\alpha)}\overline{S}(\vec{k})\ \frac{U_0 H(U_0;k)}{1+sU_0}\right\}\ , \quad (7.54)$$

can Eq. (7.53) be used. The only means by which the interior scalar flux is real for all z and $\vec{\rho}$ is if the integrand (i.e. the Laplace transform inversion) is itself real. However, it will be desirable to determine the interior scalar flux by both means. By separating the integral in Eq. (7.52) over the ranges $(-\infty,0]$ and $[0,\infty)$, making a simple change of variable in the first integral, and combining terms yields

$$f(t) = \frac{e^{\gamma t}}{2\pi}\int_0^\infty d\omega\ \left[e^{i\omega t}\ F(\gamma+i\omega) + e^{-i\omega t}\ F(\gamma-i\omega)\right]\ . \quad (7.55a)$$

Assuming that $f(t)$ is complex and that there are no interesting symmetries in the integrands over this range of integration it can be shown (Appendix E) that Eq. (7.55a) may be written as

$$f(t) = \frac{e^{\gamma t}}{\pi}\int_0^\infty d\omega\ \cos(\omega t)\ [F(\gamma+i\omega) + F(\gamma-i\omega)]\ . \quad (7.55b)$$

The complex function $f(t)$ is separated into real and imaginary parts by separating the complex function in the integrand into real and imaginary parts:

$$f(t) = \frac{e^{\gamma t}}{\pi}\int_0^\infty d\omega\ \cos(\omega t)\ \mathrm{Re}[F(\gamma+i\omega) + F(\gamma-i\omega)] +$$

$$+ i\frac{e^{\gamma t}}{\pi}\int_0^\infty d\omega\ \cos(\omega t)\ \mathrm{Im}[F(\gamma+i\omega) + F(\gamma-i\omega)]\ . \quad (7.55c)$$

Now two integrals must be evaluated; however, the same numerical techniques which are used to evaluate the Laplace transform inversion for real functions can also be employed

here. A few examples of some "simple" complex functions and their inverses are shown in Table 7.1. In these cases the desired relative error was 10^{-8} and $U_0 = 0.5 + 0.5i$.

7.D.3. The Double Fourier Transform Inversion.

The double Fourier transform inversion is common to the surface and interior scalar fluxes and the surface current. It is of the form

$$F(\vec{\rho}) = \frac{1}{(2\pi)^2} \int_0^\infty dk\ k \int_0^{2\pi} d\psi\ e^{-ik\rho\cos(\psi-\alpha)}\, \overline{F}(k,\psi) \quad . \tag{7.56}$$

One fortunate occurrence in the integrands of the Fourier inversions is that all H-functions are parameterized in k only. For example, consider the function $H(U_0;k)$. A converged H-function can be determined as in Sec. 7.D.1 for a given k. U_0 is a function of ψ, but the same set of converged H-functions can be used for each ψ in the evaluation of $H(U_0;k)$ as given by Eq. (7.50). The iteration to determine the converged H-function may then be performed outside the ψ integral, and all that need be done inside the integral is the interpolation of this H-function to give $H(U_0;k)$. The ability to do the iteration in the outermost integral saves much computational effort.

Table 7.1. The Complex Laplace Transform Inversion for Some Complex Functions.

$F(s)$	Analytical $f(t)$	t	Numerical $f(t)$	Error
$\frac{1}{s + U_0}$	$e^{-U_0 t}$			
		0.01	(7.95000E-01,-4.97504E-03)	7.06E-10
		0.1	(7.50041E-01,-4.75417E-02)	8.48E-10
		1	(5.32281E-01,-2.90786E-01)	4.64E-10
		10	(1.91130E-03,6.46118E-03)	1.86E-10
$\frac{1}{(s + U_0)^2}$	$te^{-U_0 t}$			
		0.01	(7.95000E-03,-4.97504E-05)	7.04E-10
		0.1	(7.50041E-02,-4.75417E-03)	8.47E-10
		1	(5.32281E-01,-2.90786E-01)	4.83E-10
		10	(1.91130E-02,6.46118E-02)	4.29E-10
$\frac{1}{s^2 + U_0^2}$	$\frac{\sin(U_0 t)}{U_0}$			
		0.01	(1.00000E-02,-8.33333E-08)	5.62E-09
		0.1	(1.00000E-01,-8.33333E-05)	7.94E-10
		1	(7.97917E-01,-8.33085E-02)	2.81E-10
		10	(-5.01131E+01,9.22104E+01)	7.47E-10
$\frac{s}{s^2 + U_0^2}$	$\cos(U_0 t)$			
		0.01	(1.00000E+00,-2.50000E-05)	1.67E-08
		0.1	(7.99999E-01,-2.50000E-03)	6.87E-10
		1	(7.89585E-01,-2.49826E-01)	1.07E-10
		10	(2.10506E+01,7.11553E+01)	9.19E-10
$\frac{1}{s^{1/2}}$	$\frac{1}{(\pi t)^{1/2}}$			
		0.01	(5.64190E+00,0.00000E+00)	3.79E-10
		0.1	(1.78412E+00,0.00000E+00)	3.04E-10
		1	(5.64190E-01,0.00000E+00)	2.03E-10
		10	(1.78412E-01,0.00000E+00)	4.56E-10
$\ln\left[\frac{s^2 + U_0^2}{s^2}\right]$	$\frac{2}{t}\left[1 - \cos(U_0 t)\right]$			
		0.01	--	--
		0.1	(2.08333E-05,5.00000E-02)	7.93E-10
		1	(2.08302E-02,4.99653E-01)	2.82E-10
		10	(-4.01011E+00,-1.42311E+01)	6.35E-10

The k integral in Eq. (7.56) is evaluated by converting the infinite-ranged integral into an infinite series of finite-ranged integrals. That is,

$$F(\vec{\rho}) = \frac{1}{(2\pi)^2} \sum_{j=0}^{\infty} \int_{a_j}^{a_{j+1}} dk\ k\ \bar{F}(k) \quad . \tag{7.57}$$

where the a_j are points at which the k integral is partitioned. Because the function $\bar{F}(k)$ contains a zeroth order Bessel function the a_j points may be set to the zeros of $J_0(k)$; however, in general a zero finding scheme (such as the bisection method) may be used to determine the zeroes of $\bar{F}(k)$ itself and these zeroes may be used as the points a_j. The ψ integrals are generally performed by Chebyshev integration as discussed in Sec. 7.G.

7.D.3.a. The Scalar Flux at the Surface. The only source considered for the searchlight problem is a point source which impinges the surface of the half-space at the origin. Thus, $\bar{S}(\vec{\rho}) = \delta(\rho)/(2\pi\rho)$ and $\bar{S}(\vec{k}) = 1$. It is numerically convenient to extract the particles which come directly from the source by subtracting 1 from $H(U_0;k)$ giving for a general source variation on the surface

$$\phi(0,\vec{\rho}) = \bar{S}(\vec{\rho}) + \frac{1}{(2\pi)^2} \int_0^{\infty} dk\ k \int_0^{2\pi} d\psi\ e^{-ik\rho\cos(\psi-\alpha)} [H(U_0;k) - 1] \quad , \tag{7.58a}$$

and for the point source

$$\phi_c(0,\vec{\rho}) = \frac{1}{(2\pi)^2} \int_0^{\infty} dk\ k \int_0^{2\pi} d\psi\ e^{-ik\rho\cos(\psi-\alpha)} [H(U_0;k) - 1] \quad . \tag{7.58b}$$

Because the H-function of a complex argument is also complex, it is desirable to determine some of the characteristics of this function. This is done by turning our attention to Eq. (7.40). First, note that $k, \xi' \in \Re$, k is a parameter which ranges along $[0,\infty)$, and ξ' ranges in value along $[0,1]$. Letting $\xi = a + ib$ where a and b are real and rationalizing the denominator inside the integral yields

$$H(\xi;k) = \left[1 - \frac{c}{2} \int_0^{1/(1+k^2)^{1/2}} \frac{d\xi' \, H(\xi';k)}{(1 - k^2\xi'^2)^{1/2}} \frac{a^2 + b^2 + a\xi' + ib\xi'}{(a + \xi')^2 + b^2} \right]^{-1} , \qquad (7.59a)$$

or after separating into real and imaginary parts

$$H(\xi;k) = \left[1 - \frac{c}{2} \int_0^{1/(1+k^2)^{1/2}} \frac{d\xi' \, H(\xi';k)}{(1 - k^2\xi'^2)^{1/2}} \frac{a^2 + b^2 + a\xi'}{(a + \xi')^2 + b^2} - \right.$$

$$\left. - i \frac{c}{2} \int_0^{1/(1+k^2)^{1/2}} \frac{d\xi' \, H(\xi';k)}{(1 - k^2\xi'^2)^{1/2}} \frac{b\xi'}{(a + \xi')^2 + b^2} \right]^{-1} . \qquad (7.59b)$$

This may be written in simpler notation as

$$H(\xi;k) = \frac{1}{x - iy} = \frac{x}{x^2 + y^2} + i \frac{y}{x^2 + y^2} = H_R(\xi;k) + i \, H_I(\xi;k) , \qquad (7.60a)$$

where $H_R(\xi;k)$, $H_I(\xi;k) \in \Re$ and

$$x = 1 - \frac{c}{2} \int_0^{1/(1+k^2)^{1/2}} \frac{d\xi' \, H(\xi';k)}{(1 - k^2\xi'^2)^{1/2}} \frac{a^2 + b^2 + a\xi'}{(a + \xi')^2 + b^2} , \qquad (7.60b)$$

$$y = \frac{c}{2} \int_0^{1/(1+k^2)^{1/2}} \frac{d\xi' \, H(\xi';k)}{(1 - k^2\xi'^2)^{1/2}} \frac{b\xi'}{(a + \xi')^2 + b^2} . \qquad (7.60c)$$

It is easily seen now that if ξ is real ($b = 0$) then $H(\xi;k)$ will also be real. It is also obvious that $H_I(\xi;k)$ is odd with respect to the imaginary part of ξ [i.e. $H_I(a + ib;k) = - H_I(a - ib;k)$]. Thus, the H-functions of a complex conjugate pair are also complex conjugates [i.e. $H(\xi^*;k) = H^*(\xi;k)$ where "*" denotes conjugation].

With the H-function separated into real and imaginary parts, the complex algebra may be done for the integrand in Eq. (7.58b). Expanding the complex exponential into sines and cosines, and writing the H-function as above there results

$$\phi_c(0,\vec{\rho}) = \frac{1}{(2\pi)^2}\int_0^\infty dk\ k\int_0^{2\pi} d\psi[\cos(q)-i\sin(q)]\left[H_R(U_0;k)-1+iH_I(U_0;k)\right] , \quad (7.61a)$$

where $q = k\rho\cos(\psi-\alpha)$. Separating real and imaginary parts yields

$$\phi_c(0,\vec{\rho}) = \frac{1}{(2\pi)^2}\int_0^\infty dk\ k\int_0^{2\pi} d\psi\cos(q)[H_R(U_0;k)-1] + \sin(q)H_I(U_0;k) +$$

$$+\frac{i}{(2\pi)^2}\int_0^\infty dk\ k\int_0^{2\pi} d\psi\cos(q)H_I(U_0;k) - i\sin(q)[H_R(U_0;k)-1] \ . \quad (7.61b)$$

Rationalization of U_0 [Eq. (7.4c)] shows that (with $\gamma_0^2 = 1-\mu_0^2$)

$$U_0 = \frac{\mu_0}{1+k^2\gamma_0^2\cos^2(\psi)} + i\frac{k\mu_0\gamma_0\cos(\psi)}{1+k^2\gamma_0^2\cos^2(\psi)} , \quad (7.62)$$

from which it may be noted that U_0 on the range $[\pi,2\pi]$ is the complex conjugate of U_0 on the range $[0,\pi]$. Noting that the integral over ψ covers the full range of the cosine and sine it is immediately seen that the imaginary integral is zero as this integral over $[0,\pi]$ is equal and opposite in sign to this integral over $[\pi,2\pi]$. Thus, the scalar flux on the surface of the half-space is given by

$$\phi_c(0,\vec{\rho}) = \frac{1}{2\pi^2}\int_0^\infty dk\ k\int_0^{\pi} d\psi\left\{\cos(q)[H_R(U_0;k)-1] + \sin(q)H_I(U_0;k)\right\} . \quad (7.63)$$

When the beam is normal, $U_0 = 1$, $H_I = 0$ [as $b = 0$ in Eqs. (7.60)], and the cosine term integrates to a zeroth order Bessel function to give the expected two-dimensional result.

As in Ch. 6 with the anisotropic infinite line source, it is possible to perform the double Fourier inversion in (k_x,k_y) space instead of (k,ψ). This will provide a check for some of the numerical results from the evaluation of Eq. (7.63) and will be briefly summarized in Appendix F. Unfortunately the H-functions in the derivation are still parameterized by $k = (k_x^2 + k_y^2)^{1/2}$. Thus, the iteration which produces the H-function must

be done inside both integrals where in Eq. (7.63) it is done outside the ψ integral. The computational cost is enormous.

7.D.3.b. The Interior Scalar Flux. Evaluation of the interior scalar flux is extremely difficult as there are effectively three inversions to be performed. However, some simplifications can be made by noting that the final result must be real. When the ψ integral is performed inside the Laplace transform inversion [see Eq. (7.54)], the result of the inversion must be real for the scalar flux to be real. Stating the Laplace transform inversion explicitly as

$$\phi(z,\vec{\rho}) = \frac{1}{(2\pi)^2}\int_0^\infty dk\, k\, \frac{e^{\gamma z}}{\pi z}\int_0^\infty d\omega\, \cos(\omega)[F(\gamma + i\omega/z) + F(\gamma - i\omega/z)] \ , \qquad (7.64a)$$

where $F(s)$ is the image function given by

$$F(s) = H\left(\frac{1}{s};k\right)T_1(s,k) \ , \qquad (7.64b)$$

and

$$T_1(s,k) = \int_0^{2\pi} d\psi\, e^{-ik\rho\cos\psi}\, \frac{H(U_0;k)}{s + 1/U_0} \ . \qquad (7.64c)$$

Note that the spatial parameter α has been moved from the argument of the complex exponential into the $\cos\psi$ terms in U_0. Defining the integrand of the ω integral as

$$\bar{g}(\omega) \equiv F(\gamma + i\omega/z) + F(\gamma - i\omega/z) = F(s) + F(s^*)$$

and inserting the form of $F(s)$ yields

$$\bar{g}(\omega) = H\left(\frac{1}{s};k\right)T_1(s,k) + H\left(\frac{1}{s^*};k\right)T_1(s^*,k) \ . \qquad (7.65a)$$

Expressing the H-function in real and imaginary parts and collecting terms gives for $\bar{g}(\omega)$

$$\overline{g}(\omega) = H_R\left(\frac{1}{s};k\right)\left[T_1(s,k) + T_1(s^*,k)\right] + i\,H_I\left(\frac{1}{s};k\right)\left[T_1(s,k) - T_1(s^*,k)\right] \quad . \qquad (7.65b)$$

It can be shown that the terms above in square brackets, when expressed as integrals "simplify" to

$$\begin{Bmatrix} T_1(s,k) + T_1(s^*,k) \\ T_1(s,k) - T_1(s^*,k) \end{Bmatrix} = 2\int_0^{2\pi} d\psi\, e^{-ik\rho\cos\psi}\, \frac{H(U_0;k)}{ss^* + \dfrac{2\mathrm{Re}(s)}{U_0} + \dfrac{1}{U_0^2}} \begin{Bmatrix} \mathrm{Re}(s)+\dfrac{1}{U_0} \\ -i\,\mathrm{Im}(s) \end{Bmatrix} . \qquad (7.66)$$

For an integral of a function of angle (ψ) over the full period of the cosine it is also easily shown that separating the ψ integral into two integrals over the ranges $[0,\pi]$ and $[\pi,2\pi]$ and making a simple change of variable in the second integral yields

$$\int_0^{2\pi} d\psi\, e^{-i\sigma} f(\psi) = \int_0^{\pi} d\psi \left[e^{-i\sigma} f(\psi) + e^{i\sigma} f(\psi+\pi)\right] \quad . \qquad (7.67)$$

Now by inserting Eqs. (7.66) and (7.67) into the equation for $\overline{g}(\omega)$, there results

$$\overline{g}(\omega) = 2H_R\left(\frac{1}{s};k\right)\int_0^{\pi} d\psi\, S_1(\psi) + 2H_I\left(\frac{1}{s};k\right)\int_0^{\pi} d\psi\, S_2(\psi) \quad , \qquad (7.68a)$$

where

$$S_1(\psi) = e^{-i\sigma}\frac{H(U_0;k)\left[\mathrm{Re}(s) + \dfrac{1}{U_0}\right]}{ss^* + \dfrac{2\mathrm{Re}(s)}{U_0} + \dfrac{1}{U_0^2}} + e^{i\sigma}\frac{H(U_0^*;k)\left[\mathrm{Re}(s) + \dfrac{1}{U_0^*}\right]}{ss^* + \dfrac{2\mathrm{Re}(s)}{U_0^*} + \dfrac{1}{U_0^{*2}}} \qquad (7.68b)$$

$$S_2(\psi) = e^{-i\sigma}\frac{H(U_0;k)\,\mathrm{Im}(s)}{ss^* + \dfrac{2\mathrm{Re}(s)}{U_0} + \dfrac{1}{U_0^2}} + e^{i\sigma}\frac{H(U_0^*;k)\,\mathrm{Im}s}{ss^* + \dfrac{2\mathrm{Re}(s)}{U_0^*} + \dfrac{1}{U_0^{*2}}} \quad . \qquad (7.68c)$$

With $S_1(\psi)$ and $S_2(\psi)$ expressed as above, it is easily seen that the first and second terms of the two sums are complex conjugate pairs. Therefore, $S_1(\psi)$, $S_2(\psi) \in \Re$ and

$$S_1(\psi) = 2\mathrm{Re}\left\{ e^{-i\sigma} \frac{H(U_0;k)\left[\mathrm{Re}(s) + \frac{1}{U_0}\right]}{ss^* + \frac{2\mathrm{Re}(s)}{U_0} + \frac{1}{U_0^2}} \right\} \tag{7.69a}$$

$$S_2(\psi) = 2\mathrm{Re}\left\{ e^{-i\sigma} \frac{H(U_0;k)\,\mathrm{Im}(s)}{ss^* + \frac{2\mathrm{Re}(s)}{U_0} + \frac{1}{U_0^2}} \right\} . \tag{7.69b}$$

Since $S_1(\psi)$ and $S_2(\psi)$ are real, then $\bar{g}(\omega)$ must also be real, and so is the interior scalar flux.

If the scalar flux is determined by performing the Laplace transform inversion inside the double Fourier inversion, then the Laplace transform inversion will be a complex function and must be determined by using Eq. (7.55c). However, as usual the final result must be real to be of physical significance. Manipulating the form of the scalar flux [Eq. (7.35b)] and using Eq. (7.67) to change the ψ integral over $[0,2\pi]$ to one over the range $[0,\pi]$ provides the following equation for the scalar flux:

$$\phi(z,\vec{\rho}) = \frac{1}{(2\pi)^2} \int_0^\infty dk\, k \int_0^\pi d\psi \left[e^{-ik\rho\cos(\psi-\alpha)} T_2(\psi) + e^{ik\rho\cos(\psi-\alpha)} T_2(\psi+\pi) \right] , \tag{7.70a}$$

where

$$T_2(\psi) = H(U_0;k)\, \mathcal{L}_z^{-1}\left\{ \frac{H\left[\frac{1}{s};k\right]}{1/U_0 + s} \right\} . \tag{7.70b}$$

Again, adding π to the argument of the function $T_2(\psi)$ has the effect of conjugating the terms U_0. The integrand of the modified inverse Laplace transform is an addition of two functions with complex conjugates as their arguments. Therefore, it follows that $T_2(\psi)$ and $T_2(\psi+\pi)$ are complex functions which are also complex conjugates. Eq. (7.70a) is then

seen to have an integrand which is the sum of complex conjugates, is therefore real, and may be expressed as

$$\phi(z,\vec{\rho}) = \frac{1}{2\pi^2}\int_0^\infty dk\, k \int_0^\pi d\psi\, \mathrm{Re}\left[e^{-ik\rho\cos(\psi-\alpha)} T_2(\psi)\right] \quad . \tag{7.71}$$

Again, if the beam is normal to the surface, $T_2(\psi)$ is no longer a function of ψ (but is still a function of the parameter k) as it was such only through the term U_0, which is 1 for a normal beam. The complex exponential in Eq. (7.71) becomes $J_0(k\rho)$, and the two-dimensional form for the interior flux is recovered.

7.D.3.c. The Current at the Surface. The current at the surface is given by the inversion of Eq. (7.33). This is explicitly given as

$$J(0,\vec{\rho}) = \frac{1}{(2\pi)^2}\int_0^\infty dk\, k \int_0^{2\pi} d\psi\, e^{-k\rho\cos(\psi-\alpha)}\, \mu_0 \overline{S}(\vec{k}) - J_c(0,\vec{\rho}) \quad , \tag{7.72a}$$

where

$$J_c(0,\vec{\rho}) = \frac{c}{8\pi^2}\int_0^\infty dk k \int_0^{2\pi} d\psi\, e^{-k\rho\cos(\psi-\alpha)} \overline{S}(\vec{k}) H(U_0;k) \int_0^1 d\mu\, \frac{U_0\xi}{\xi+U_0} H(\xi;k) \quad . \tag{7.72b}$$

The inversion of the transformed source is simply the source itself and for a beam source $\overline{S}(\vec{k}) = 2\pi$. Thus

$$J(0,\vec{\rho}) = \mu_0 S(\vec{\rho}) - J_c(0,\vec{\rho}) \quad . \tag{7.73}$$

Using the relationship between μ and ξ so that the innermost integral in Eq. (7.72b) is integrated over ξ', and making the change of variable $\xi' = \sin(a\theta)/k$, $a = \tan^{-1}k$, as in Sec. 7.D.1 yields for the emerging current

$$J_c(0,\vec{\rho}) = \frac{c}{4\pi}\int_0^{\infty} dk\, \tan^{-1}k \int_0^{2\pi} d\psi\, e^{-k\rho\cos(\psi-\alpha)}\, H(U_0;k) \times$$

$$\times \int_0^{1} \frac{d\theta}{\cos^2(a\theta)} \frac{H\left[\dfrac{\sin(a\theta)}{k}\right]}{\dfrac{k}{\sin(a\theta)} + \dfrac{1}{U_0}} . \qquad (7.74a)$$

or upon interchanging the ψ and θ integrals

$$J_c(0,\vec{\rho}) = \frac{c}{4\pi}\int_0^{\infty} dk\, \tan^{-1}k \int_0^{1} \frac{d\theta}{\cos^2(a\theta)} H\left[\frac{\sin(a\theta)}{k}\right] I_\psi(k,\theta) \quad , \qquad (7.74b)$$

where

$$I_\psi(k,\theta) = \int_0^{2\pi} d\psi\, e^{-k\rho\cos(\psi-\alpha)} \frac{H(U_0;k)}{\dfrac{k}{\sin(a\theta)} + \dfrac{1}{U_0}} . \qquad (7.74c)$$

Separating I_ψ into two integrals, one with the range of integration $[0,\pi]$ and the other over $[\pi,2\pi]$, making a change of variable in the second integral so that both are over $[0,\pi]$, and combining the integrals shows that the two integrated terms are a sum of complex conjugates. Therefore,

$$I_\psi(k,\theta) = 2\int_0^{\pi} d\psi\, \mathrm{Re}\left[e^{-k\rho\cos(\psi-\alpha)} \frac{H(U_0;k)}{\dfrac{k}{\sin(a\theta)} + \dfrac{1}{U_0}}\right] , \qquad (7.75)$$

and

$$J_c(0,\vec{\rho}) = \frac{c}{2\pi}\int_0^{\infty} dk\, \tan^{-1}k \int_0^{1} \frac{d\theta}{\cos^2(a\theta)} H\left[\frac{\sin(a\theta)}{k}\right] \times$$

$$\times \int_0^{\pi} d\psi\, \mathrm{Re}\left[e^{-k\rho\cos(\psi-\alpha)} \frac{H(U_0;k)}{\dfrac{k}{\sin(a\theta)} + \dfrac{1}{U_0}}\right] . \qquad (7.76)$$

The results for the current at the surface of the half-space is clearly a real number, as required, and the evaluation of the integral expression contains three embedded integrals. If the beam is normal to the surface of the half-space, $\mu_0 = U_0 = 1$ and Eq. (7.76) reduces to

$$J_c(0,\vec{\rho}) = \frac{c}{2}\int_0^\infty dk\, \tan^{-1}k\, J_0(k\rho)\, H(1;k) \int_0^1 \frac{d\theta}{\cos^2(a\theta)} \frac{H\left[\frac{\sin(a\theta)}{k}\right]}{\frac{k}{\sin(a\theta)} + 1} . \qquad (7.77)$$

The evaluation of Eqs. (7.64a), (7.71), and (7.76) may be done numerically and are discussed in the next section.

7.E. Results for The Searchlight Problem

The searchlight problem provides the benchmarking community with a case study which is rich in both numerical analysis and mathematical theory. It also provides a benchmark which is three-dimensional. Due to the complexity of the integral formulations which provide the scalar flux, it will be seen that the calculations which evaluate the integrals are numerically and computer intensive.

7.E.1. The Scalar Flux at the Surface.

The numerical evaluation of the scalar flux is relatively easy as the only complication is the evaluation of an *H*-function. As mentioned, the techniques used for the anisotropic line source in an infinite medium will be used here.

7.E.1.a. Numerical Considerations for the Scalar Flux at the Surface. The numerical evaluation of the surface scalar flux resulting from a beam impinging at some angle at the center of a free surface is obtained by using the numerical techniques discussed

thus far. These include iterative Gauss-Legendre integration, Chebyshev integration, transformation of a semi-infinite integral into an infinite series, Euler-Knopp acceleration, and double inversions in Cartesian coordinates. All of these techniques were used in the evaluation of the scalar flux from the anisotropic line source in an infinite medium. The experience gained there with the double Fourier inversion is now used with the additional complications of having to evaluate *H*-functions and Laplace transform inversion in the integrand of the double Fourier inversion.

The surface scalar flux is given by Eq. (7.63). The required inversion contains a double integral, of which the outer integral is over the k variable and the inner integral is over ψ. As noted, it is quite fortunate that the *H*-function is parametrically only a function of k. This allows the *H*-function iteration to be done outside the ψ integral which saves considerably on computational resources. With the converged values of the *H*-function calculated for each k all that must be done inside the ψ integral is one interpolative evaluation of the *H*-function at the particular ψ values associated with U_0. As usual, the k integral, which has a semi-infinite range, is converted into an infinite series of integrals. The intervals of integration for these integrals may be the zeroes of the zeroth order Bessel function or the zeroes of the integrated function. In general, it is seen to be most efficient when the outer integrals use Gauss-Legendre quadrature or Romberg integration and the inner integral uses Chebyshev integration.

Some numerical results are presented in Table 7.2 in the form of an error analysis. The results were generated with a scattering coefficient of $c = 0.9$, an incident angle $\mu_0 = 0.7$, and at $y = 0.1$. The numerical integration parameters include outer integration using variable Gauss-Legendre quadrature with an initial quadrature of 10 and increment 2, and an inner Chebyshev integration with initial quadrature 20 and increment 20. The zeroes of $J_0(k)$ are the endpoints of the finite outer integrals. It may be seen that for each value of the desired error on the final result the numerical values of the scalar flux agree with each other

to the required number of significant digits. It is also seen that the values of the scalar flux are greater at positive values of x than at negative values of x due to the canted beam shining particles into the region of positive x.

Table 7.2. Error Analysis for the Surface Scalar Flux.

x	$err = 10^{-2}$	$err = 10^{-3}$	$err = 10^{-4}$	$err = 10^{-5}$	$err = 10^{-6}$
-2	4.424424E-3	4.425169E-3	4.425259E-3	4.425270E-3	4.425272E-3
-1.5	8.720801E-3	8.721863E-3	8.721989E-3	8.722005E-3	8.722007E-3
-1	1.965904E-2	1.967439E-2	1.967635E-2	1.967637E-2	1.967637E-2
-0.5	6.050579E-2	6.054166E-2	6.054566E-2	6.054619E-2	6.054618E-2
0	6.873938E-1	6.872902E-1	6.872764E-1	6.872741E-1	6.872742E-1
0.5	2.047136E-1	2.047531E-1	2.047594E-1	2.047592E-1	2.047591E-1
1	7.202231E-2	7.204633E-2	7.204537E-2	7.204524E-2	7.204522E-2
1.5	3.322871E-2	3.322389E-2	3.322325E-2	3.322315E-2	3.322315E-2
2	1.730579E-2	1.730218E-2	1.730159E-2	1.730162E-2	1.730162E-2

As mentioned, a check on the numerical results obtained from the standard double-Fourier inversion from (k,ψ) transformed space is to do the inversion in Cartesian coordinates. When this is done, the H-function becomes a parameter of both k_x and k_y; therefore, the iteration must be performed inside the k_y integral. This will significantly increase the computer time.

Table 7.3 contains a comparison of the two inversion methods. In each case c = 0.9, $\mu_0 = 0.5$, $y = 0.5$ and the same integration parameters are used as those for Table 7.2. The (k_x,k_y) inversion integrals used variable Gauss-Legendre quadrature for both inner and outer integrals beginning with a quadrature of 10 and incrementing in steps of 2. Both sets of data have been converged to $err = 10^{-4}$. Note that the computer time required to obtain the scalar fluxes from a Cartesian inversion are approximately 50 times greater than those

from the standard inversion, as expected. However, since the Cartesian inversion is used solely as a check on the results from the standard inversion, it has proven itself effective for its purpose.

Table 7.3. Inversion Method Comparison for the Surface Scalar Flux.

x	Scalar Flux (k,ψ) Inversion	CPU time (s)	Scalar Flux (k_x,k_y) Inversion	CPU time (s)
-2	2.57605E-3	5.5	2.57607E-3	256.3
-1.5	4.96987E-3	5.5	4.96990E-3	260.8
-1	1.05774E-2	5.4	1.05774E-2	290.3
-0.5	2.60357E-2	5.3	2.60357E-2	249.2
0.5	7.35475E-2	5.0	7.35473E-2	234.9
1	4.75558E-2	5.1	4.75557E-2	274.2
1.5	2.72023E-2	5.1	2.72022E-2	245.9
2	1.55150E-2	5.1	1.55149E-2	242.0

7.E.1.b. General Results for the Scalar Flux at the Surface. The surface scalar flux is primarily a function of two spatial variables (x,y) or (ρ,α), and one source parameter, μ_0. As with the anisotropically emitting infinite line in an infinite medium, it is useful to examine the scalar flux on the surface versus angle and source incident angle. Such plots are displayed in Figs. 7.1a and 7.1b. These figures were generated at $c = 0.9$ and the scalar fluxes are converged to 10^{-4}. Figs. 7.1a and 7.1b show the scalar flux as a function of α and μ_0 at $\rho = 0.01$ and $\rho = 1$, respectively.

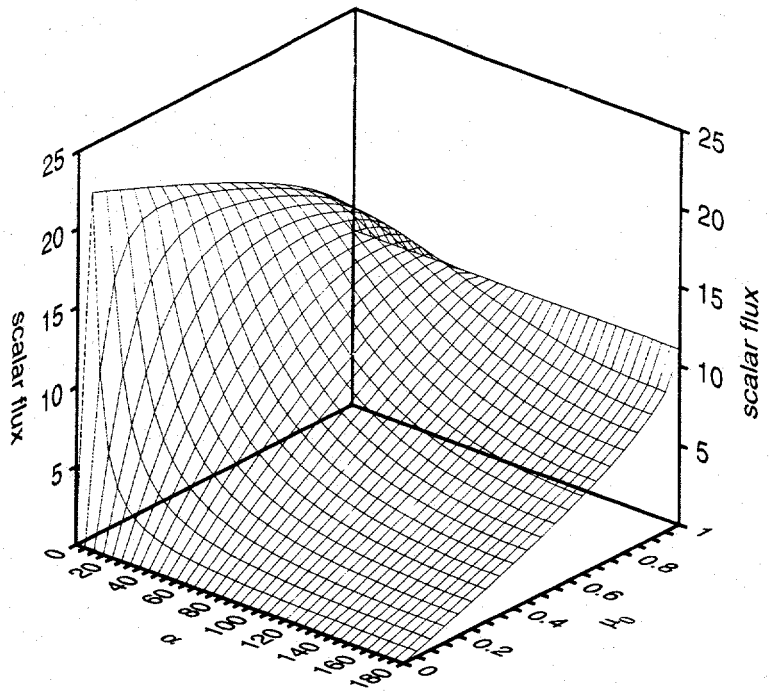

Fig. 7.1a. The surface scalar flux as a function of positional angle (α) and beam incident angle (μ_0) at $\rho = 0.01$ with $c = 0.9$.

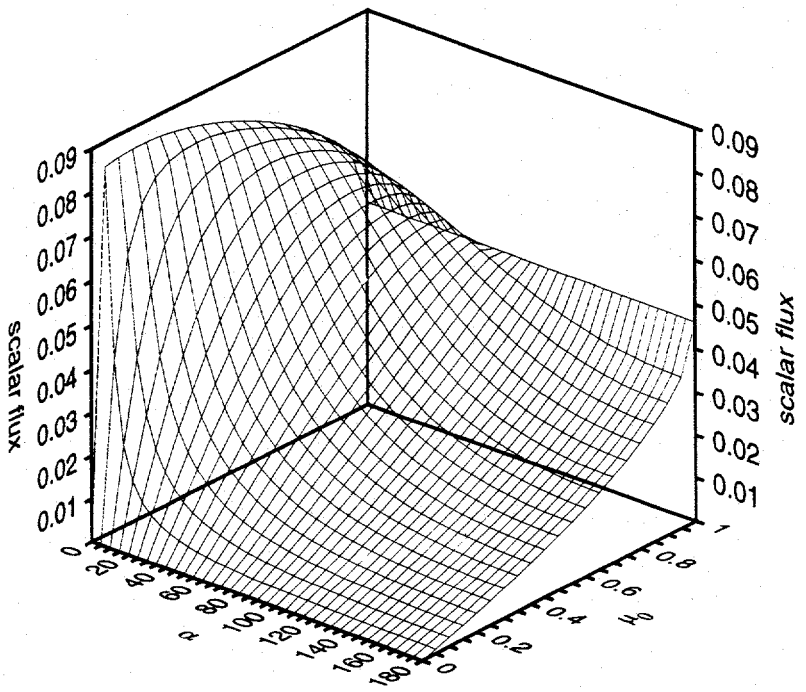

Fig. 7.1b. The surface scalar flux as a function of positional angle (α) and beam incident angle (μ_0) at $\rho = 1$ with $c = 0.9$.

First, it is clearly noted that the values of the scalar fluxes at $\rho = 0.01$ are considerably greater than those at $\rho = 1$. In both figures, when $\mu_0 = 1$ (a normal beam) the scalar flux is independent of angle, as expected, and the value of the scalar flux agrees with that of the two-dimensional version of the searchlight problem [Ganapol, *et al.*, 1994]. When the incident beam is a grazing one ($\mu_0 = 0$), the scalar flux is zero, and as μ_0 approaches zero the scalar flux does likewise. At small angles, the scalar flux begins to increase as μ_0 decreases, peaks, and the decreases to zero. This graphically describes the phenomenon that as the beam is canted more particles are scattered into the areas which have small spatial angular coordinates but that there comes a point where the beam is so canted that the effect of scattering more particles into that region is overcome by either the loss of particles through the surface. At large angles (α near π), when the beam is canted it shines particles in a direction which is increasingly farther from the spatial point and therefore the scalar flux continually decreases.

An analysis of the behavior of the surface scalar flux at various values of the scattering coefficient is provided in Fig. 7.2. A wide range of c values are examined, and both the shape of the scalar fluxes and the magnitudes of the scalar fluxes at the values of c follow expected physical trends.

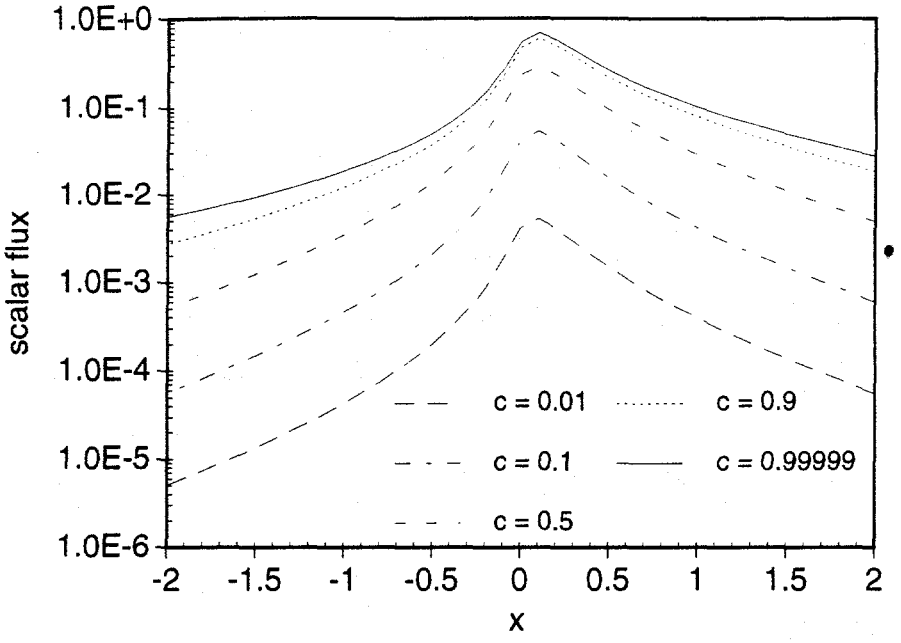

Fig. 7.2. The surface scalar flux as a function of c and x at $y = 0.1$ and $\mu_0 = 0.5$.

The most natural form of general results for the surface scalar flux in the searchlight problem is the scalar flux as a function of position on the surface. Fig. 7.3 contains three such contour plots for three values of the incident angle μ_0. In each case $c = 0.9$ and the scalar flux is plotted in a 4×4 mean-free-path square around the center of the surface. When the beam is very canted (small μ_0) the scalar flux is directed along the x-axis and the magnitude of the scalar flux varies rapidly. As the beam becomes closer to normal to the surface, the scalar flux becomes more symmetric about the center and less variable with distance from the source.

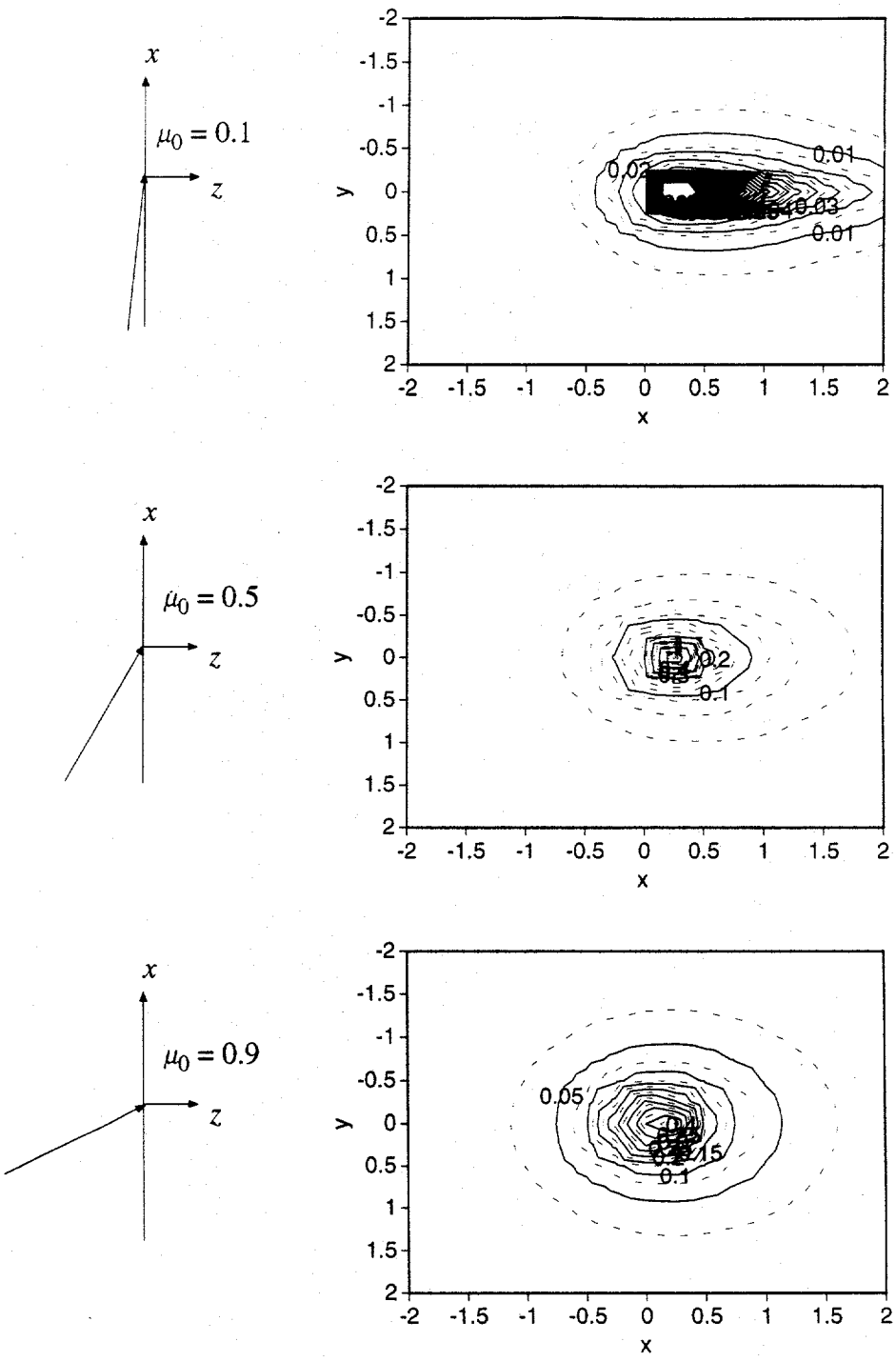

Fig. 7.3. Contour mapping of the surface scalar flux for three values of the incident angle μ_0 with $c = 0.9$.

7.E.2. The Interior Scalar Flux.

As with the scalar flux at the surface of the half-space, evaluation of the interior scalar flux requires evaluation of the *H*-function. However, this is further complicated by the need for a Laplace transform inversion inside the double Fourier inversion.

7.E.2.a. Numerical Considerations for the Interior Scalar Flux. The interior scalar flux is obtained after numerically performing a double-Fourier transform inversion and a Laplace transform inversion. Clearly, this is the most computationally intensive calculation thus far in this work. The "simpler" numerical inversions allowed the use of techniques such as iterative Gauss-Legendre quadrature and iterative Chebyshev quadrature. However, with three embedded integrals to compute it is more efficient to set the calculations so that no iterations are used. Without the confidence in the answer which comes from a solution which has used the iterative processes, some measure must be found to provide confidence in the numerical results of this calculation. This is accomplished primarily by testing the results at various quadrature orders and by occasionally allowing the algorithm to iterate. When this is done, it is seen that the outer integral may be evaluated via Gauss-Legendre quadrature at orders around 10. The Chebyshev integrals generally require quadrature orders around 50 for most problems; however, when c is small higher orders are required.

The Euler-Knopp series accelerator is a crucial part to this numerical evaluation. The k integral is, as usual, converted into an infinite series of integrals. The zeroes of the integrand are determined by bisection (a time consuming process). These zeroes are used as the limits of integration for the integrals which make up the terms of the series. These terms are purely oscillatory, and therefore the series is an excellent candidate for Euler-Knopp acceleration.

One drawback to setting the quadrature orders and not allowing iteration is that the results are limited in their accuracy. It will be seen that the lowest relative error which can

be obtained for most results is 10^{-4}. First, the time required to obtain this error is quite long, and second, the algorithm often becomes unstable if lower errors are requested. This instability arises because the quadrature order of the inner integrals is set, and for large k, as required for evaluations at low relative errors, the quadrature order is not sufficient to provide an accurate determination of the function being integrated. Thus, at sufficiently large k the terms of the series mention previously are no longer accurate, and the acceleration scheme fails. Again, this instability is not inherent in the mathematics of the problem, but arises solely due to the limited computer resources and the consequences thereof.

The computer time required to evaluate the interior scalar flux at a single spatial point is considerably large - on the order of 15 minutes. Thus, it is evident that the searchlight problem is certainly one which could greatly benefit from the use of parallel processing - by giving each processor a spatial point the calculation clock time is decreased according to how many processors can be devoted to the problem. The amount of special programming that would have to be done to parallelize the calculation is minimal as the calculation for each spatial point is independent of all other spatial point calculations.

An error analysis of the results from calculating the interior scalar flux as given in Eq. (7.64a) (where the ψ integral is performed inside the Laplace transform inversion) is provided in Table 7.4. The physical and spatial parameters are $\rho = 1$, $\alpha = 30°$, $c = 0.9$, $\mu_0 = 0.9$. Generally, the inner ψ integral used a Chebyshev quadrature order of 50. It is notable that the values of the error go only as low as 10^{-4}. These calculations take a great amount of time, and an error of 10^{-4} is the lowest one which may be done in a reasonable time and with confidence that the answer is correct. As usual, the results agree with each other to the required number of digits.

Table 7.4. Error Analysis for the Interior Scalar Flux.

z	$err = 10^{-2}$	$err = 10^{-3}$	$err = 10^{-4}$
0.5	1.0828E-1	1.0823E-1	1.0825E-1
1	1.2466E-1	1.2446E-1	1.2445E-1
1.5	1.1289E-1	1.1281E-1	1.1282E-1
2	8.3406E-2	8.3359E-2	8.3361E-2
2.5	5.3373E-2	5.3358E-2	5.3352E-2
3	3.2717E-2	3.2738E-2	3.2741E-2
3.5	2.0357E-2	2.0337E-2	2.0338E-2
4	1.2961E-2	1.2953E-2	1.2952E-2
4.5	8.4463E-3	8.4454E-3	8.4452E-3
5	5.6201E-3	5.6172E-3	5.6167E-3

One of the means of verifying results from the inversions for the surface scalar flux involved inverting in Cartesian coordinates. The calculations for the interior flux take enough time as it is with the H-function iteration occurring outside the Laplace transform inversion and the ψ integral, and if the iteration had to be done inside the ψ integral the calculations may become prohibitively long. Therefore, another simple means of testing the results from the inversions is to perform the inversion integrals in various orders. It was shown earlier that the Laplace transform inversion could be done either inside or outside the ψ integral: Eq. (7.64a) has the ψ integral inside the Laplace transform integral which is inside the k integral, and Eq. (7.71) has the Laplace transform integral inside the ψ integral which is inside the k integral. These two inversion methods are compared in Table 7.5 along with the CPU times required to obtain each result. The scalar fluxes have been converged to 10^{-4}, and y = 1, z = 1, c = 0.9, μ_0 = 0.9. It is clear that the scalar fluxes obtained by each method agree with each other to the required number of significant digits, and the CPU times are comparable. It has been found that the method given in Eq. (7.71) works best for small values of c and the incident angle μ_0.

Table 7.5. Comparison of Two Inversion Methods.

x	dk-$\mathcal{L}_z^{-1}$-$d\psi$ [Eq. (7.64a)] scalar flux	dk-$\mathcal{L}_z^{-1}$-$d\psi$ [Eq. (7.64a)] CPU time (s)	dk-$d\psi$-$\mathcal{L}_z^{-1}$ [Eq. (7.71)] scalar flux	dk-$d\psi$-$\mathcal{L}_z^{-1}$ [Eq. (7.71)] CPU time (s)
-2	1.0248E-2	766.6	1.0247E-2	818.0
-1.5	1.6885E-2	856.6	1.6884E-2	847.7
-1	2.7936E-2	843.5	2.7933E-2	875.5
-0.5	4.4748E-2	1024.9	4.4746E-2	929.3
0	6.3362E-2	984.3	6.3361E-2	980.8
0.5	6.8988E-2	867.6	6.8982E-2	1058.0
1	5.5001E-2	989.7	5.5001E-2	1027.2
1.5	3.6423E-2	979.0	3.6422E-2	970.4
2	2.2746E-2	954.1	2.2745E-2	927.2

7.E.2.b. General Results for the Interior Scalar Flux. The various possible ways one can view the interior scalar flux are infinite because there are three spatial dimensions to be varied along with the physical parameter c and the source parameter μ_0. The fact that it can take 15 minutes to obtain one point (as seen in Table 7.5) makes it even more difficult to use standard methods of display such as three-dimensional graphs or contour plots as these displays require a few hundred points to provide sufficiently smooth curves.

The interior scalar flux results are first analyzed at different values of the scattering properties of the half-space. Table 7.6 contains the interior scalar flux along the z-axis (ρ = 0) resulting from a canted beam with $\mu_0 = 0.9$ at several values of c. The results are generally converged to 10^{-4}; however, at small values of c convergence to 10^{-3} was obtained. For small c, the inversion from Eq. (7.71) is found to converge faster and is more stable than Eq. (7.64a); however, even this method had such difficulty that convergence to only 10^{-3} was attainable for some of the scalar fluxes at $c = 0.1$.

Table 7.6. Interior Scalar Flux as a Function of Position and c.

z	$c = 0.1$	$c = 0.3$	$c = 0.5$	$c = 0.7$	$c = 0.9$	$c = 0.9999$
0.5	3.883E-2*	1.3127E-1	2.4597E-1	3.9313E-1	5.9281E-1	7.3204E-1
1	1.000E-2	3.5903E-2	7.3033E-2	1.2913E-1	2.2346E-1	3.0820E-1
1.5	3.529E-3*	1.3409E-2	2.9320E-2	5.6824E-2	1.1243E-1	1.7514E-1
2	1.443E-3	5.7338E-3	1.3357E-2	2.8201E-2	6.3715E-2	1.1332E-1
2.5	6.308E-4	2.6391E-3	6.5217E-3	1.4943E-2	3.8547E-2	7.9102E-2
3	2.925E-4	1.2739E-3	3.3276E-3	8.2505E-3	2.4311E-2	5.8129E-2
3.5	1.404E-4	6.3574E-4	1.7505E-3	4.6863E-3	1.5784E-2	4.4373E-2
4	6.935E-5*	3.2551E-4	9.4194E-4	2.7175E-3	1.0470E-2	3.4890E-2
4.5	3.504E-5*	1.6992E-4	5.1565E-4	1.6007E-3	7.0614E-3	2.8097E-2
5	1.795E-5	9.0020E-5	2.8608E-4	9.5446E-4	4.8256E-3	2.3080E-2

*Converged to 10^{-3}.

The other parameter which may be varied is the source incidence direction μ_0. Fig. 7.4 displays one possible means of examining the effects of changing μ_0. Three spatial points are fixed [the points are $(x,y,z) = (1,0.5,1)$, $(2,0.5,1)$, and $(3,0.5,1)$] and the scattering property of the medium is described by $c = 0.9$. When $x = 1$ and $z = 1$ the scalar flux should peak when the incident angle is around 45° ($\mu_0 = 0.7071$). The peak actually occurs near $\mu_0 = 0.8$ due to the spatial point of evaluation being offset by one-half of a mean-free-path from the source plane ($y = 0.5$). When $x = 2$ the peak would come at $\mu_0 = 0.4472$ for $y = 0$ and actually occurs near $\mu_0 = 0.55$. A similar physical analysis may also be used for $x = 3$. As on the surface, the scalar flux rises from zero for a grazing beam ($\mu_0 = 0$), peaks at some μ_0 where the beam emits into a direction which passes near to the specified spatial point, and then decreases again as the beam direction moves away from the spatial point until it emits along the z-axis ($\mu_0 = 1$). The final and possibly most useful means of viewing the scalar flux comes as a contour plot which has two spatial dimensions as its axes.

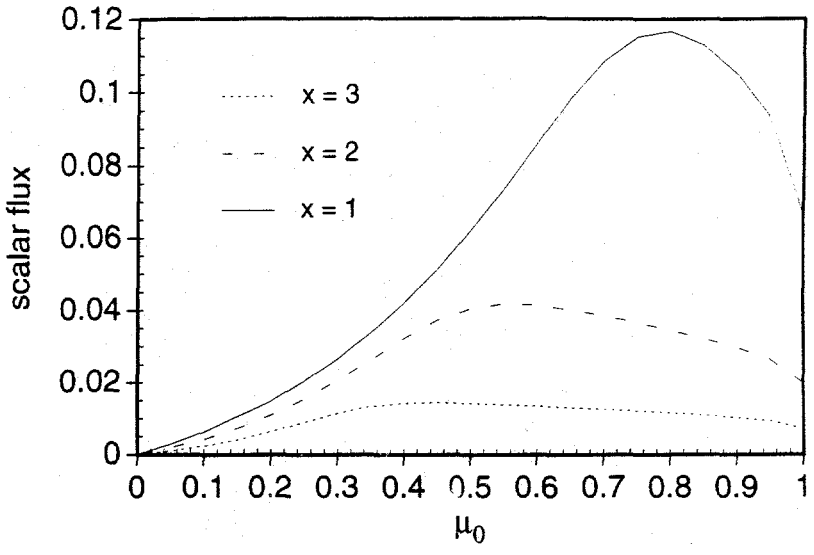

Fig. 7.4. Interior scalar flux as a function of μ_0 for three values of x at $z = 1$, $y = 0.5$, and $c = 0.9$.

When a beam of light illuminates a water surface which has some scattering centers in it (such as dilute milk), one can see a buildup of light intensity just inside the surface where the beam impinges. When the beam is canted the expected result is seen as the buildup simply moves with the direction of the incident beam. It is therefore desirable to obtain some graphical representation of the aforementioned phenomenon.

This graphical representation comes as a contour plot of the scalar flux versus position in the medium. A slice of the medium is taken parallel to the z-axis at a particular position y so that the canted nature of the beam is clearly visible. The variation in z begins at the free surface and extends to some point in the medium. Figs. 7.5a, 7.5b, and 7.5c display contour plots of the scalar flux versus x and z at the positions $y = 0.5$, 1, and 2, respectively. x ranges from [–2, 2] and z ranges from [0,5]. The beam impinges on the free surface of a $c = 0.9$ medium at an angle $\mu_0 = 0.9$ ($\theta_0 = 25.8°$). When the evaluation grid is near the source (Fig. 7.5a), the directed nature of the source is clearly visible. The buildup peak inside the surface is also clearly visible. As the evaluation grid moves farther

from the source the buildup peak moves into the medium and the directed nature of the source becomes less evident. When a point is far enough away from the source, the source should appear as though it emitted particles isotropically.

In each of the three figures, the grid consists of 20×17 points. At the rate of 10 minutes per point for 10^{-3} convergence it takes 2.23 CPU *days* to compile the data needed for each plot. As mentioned previously, this leads to the conclusion that the searchlight problem could benefit greatly by the use of parallel processing techniques.

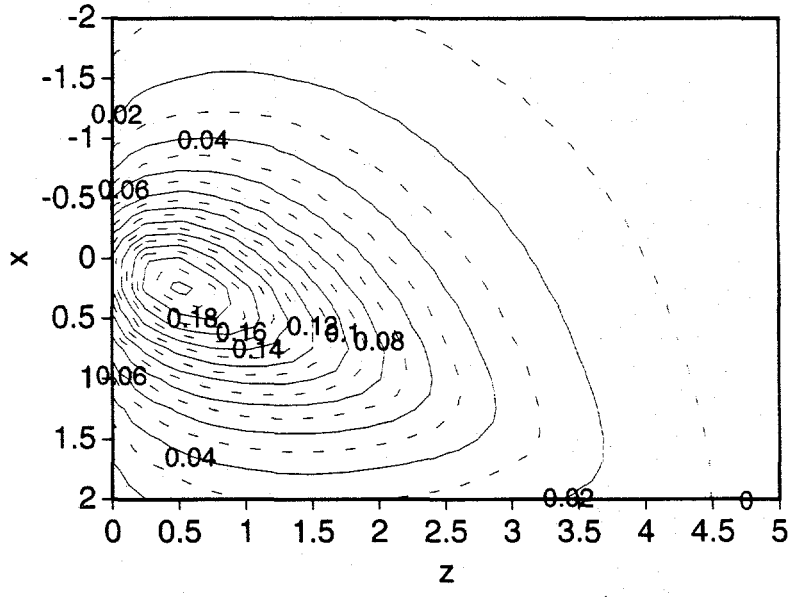

Fig. 7.5a. Contour mapping of the interior scalar flux as a function of x and z for $c = 0.9$, $\mu_0 = 0.9$, and $y = 0.5$.

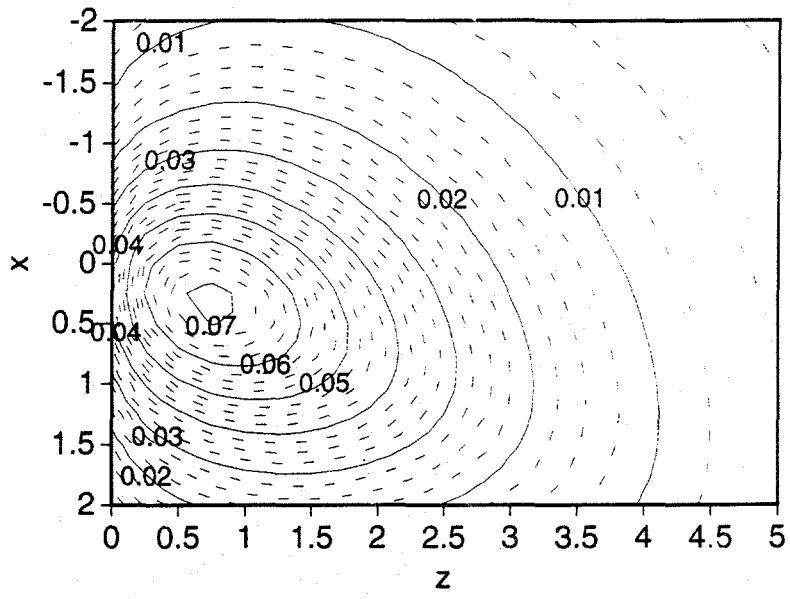

Fig. 7.5b. Contour mapping of the interior scalar flux as a function of x and z for c = 0.9, μ_0 = 0.9, and y = 1.

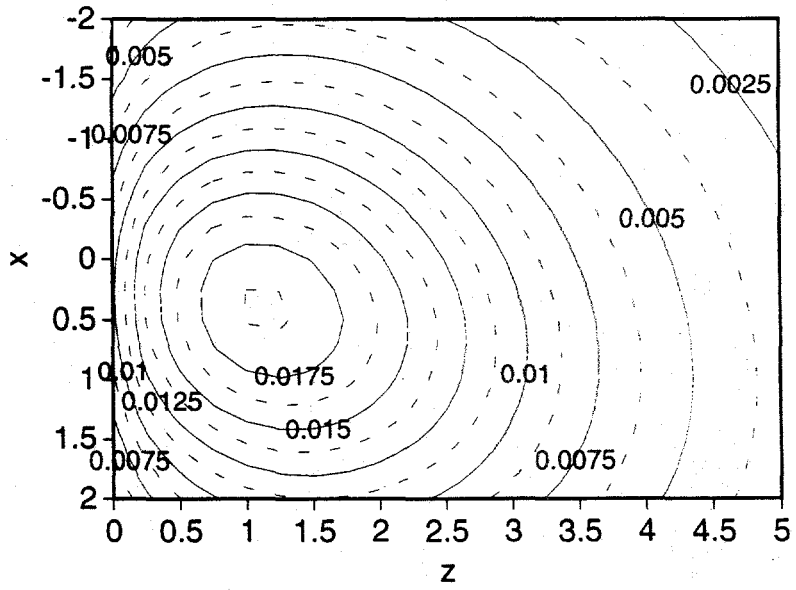

Fig. 7.5c. Contour mapping of the interior scalar flux as a function of x and z for c = 0.9, μ_0 = 0.9, and y = 2.

7.E.3. The Current at the Surface.

7.E.3.a. Numerical Considerations for the Current at the Surface. The current at the surface has been shown to be comprised of two components: a positive component due to the incident source, and a negative component due to the return current from the medium. All results presented will be of this return current, and are the magnitude thereof (i.e. the values of the current are positive, and the negative sign in the derived integral equations indicates the current in the negative z-direction).

The current at the surface of the half-space is obtained by numerically integrating Eq. (7.76). This includes an outer k integral over a semi-infinite range, an inner θ integral over [0,1], and a ψ integral over $[0,\pi]$. The k integral is evaluated, as usual, by converting the integral into an infinite series of integrals where the ranges of integration are the zeroes of $J_0(k)$ or are the zeroes of the integrated function. These integrals are generally evaluated using iterative Gauss-Legendre quadrature as described previously for the scalar flux at the surface. It is also noted that the numerical evaluation of the H-function conveniently results in the H-function evaluated at the arguments used in the second integral in Eq. (7.76). This integral is evaluated using the input Gauss-Legendre order L_m used for the H-function iteration. Therefore, no iterations are done for the θ integral. The innermost ψ integral is evaluated using iterative Chebyshev integration as usual.

The first investigation regarding the numerical aspects of the evaluation of Eq. (7.76) is to determine what values of L_m are necessary for an accurate determination of the current at the surface. Table 7.7 displays the current as a function of x and L_m. The current is evaluated with the following parameters: $c = 0.9$, $\mu_0 = 0.9$, and $y = 0.1$. The outer integral is converged to 10^{-4}.

Table 7.7. Quadrature Order Study for the Surface Current.

x	$L_m = 10$	$L_m = 20$	$L_m = 30$	$L_m = 40$	$L_m = 50$	$L_m = 60$
-2	2.98458E-3	2.98458E-3	2.98458E-3	2.98458E-3	2.98458E-3	2.98458E-3
-1.5	5.67721E-3	5.67722E-3	5.67722E-3	5.67722E-3	5.67722E-3	5.67722E-3
-1	1.23713E-2	1.23712E-2	1.23712E-2	1.23712E-2	1.23712E-2	1.23712E-2
-0.5	3.73657E-2	3.73647E-2	3.73647E-2	3.73647E-2	3.73647E-2	3.73647E-2
0	4.63681E-1	4.59024E-1	4.59166E-1	4.59163E-1	4.59163E-1	4.59163E-1
0.5	7.82324E-2	7.82383E-2	7.82383E-2	7.82383E-2	7.82383E-2	7.82383E 2
1	3.16336E-2	3.16333E-2	3.16333E-2	3.16333E-2	3.16333E-2	3.16333E-2
1.5	1.40507E-2	1.40507E-2	1.40507E-2	1.40507E-2	1.40507E-2	1.40507E-2
2	7.20651E-3	7.20651E-3	7.20651E-3	7.20651E-3	7.20651E-3	7.20651E-3

Note that for values of x far from the source ($x = 0$) the inner integral is converged around $L_m = 10$ or 20. Near the source a greater quadrature order ($L_m = 40$) is required to obtain pure convergence. If the spatial evaluation point is very near the source, successively greater quadrature orders are required for convergence. Table 7.8 contains the value of the surface current for $x = -0.5$, 0, and 0.5 with $y = 0.01$ and the same source and scattering properties as those used for Table 7.7. The interesting point is that for $(x,y) = (0,0.01)$ a quadrature order of 80 or 100 is required to obtain convergence within the desired relative error for the final result (in this case again $err = 10^{-4}$), and quadrature orders up to 200 are required for convergence to all significant figures shown in the table.

Given that proper use of the quadrature order for the θ integral is understood, the next important step is to ensure that the resultant calculation of the current provides benchmark quality results. Therefore an error analysis for the final result is provided in Table 7.7. As with the previous tabular results, the source and scattering properties are $\mu_0 = 0.9$ and $c = 0.9$. The quadrature order for the θ integral is set to 40 and the required error tolerance for the innermost ψ integral is 10^{-6}. Therefore the error analysis is only on the outer integral, which provides the final numerical value for the return current. The

current is given as a function of x with $y = 0.1$. Note that in all cases the results agree to the required number of significant digits.

Table 7.8. Quadrature Order Study for the Surface Current Near the Source.

L_m	x = -0.5	x = 0	x = 0.5
50	3.822076E-2	5.666583E+0	1.027947E-1
60	3.822076E-2	5.574652E+0	1.027947E-1
80	3.822076E-2	5.577080E+0	1.027947E-1
100	3.822076E-2	5.577148E+0	1.027947E-1
120	3.822076E-2	5.577124E+0	1.027947E-1
140	3.822076E-2	5.577122E+0	1.027947E-1
160	3.822076E-2	5.577123E+0	1.027947E-1
180	3.822076E-2	5.577123E+0	1.027947E-1
200	3.822076E-2	5.577123E+0	1.027947E-1

Table 7.9. Error Analysis for the Surface Current.

x	$err = 10^{-2}$	$err = 10^{-3}$	$err = 10^{-4}$	$err = 10^{-5}$	$err = 10^{-6}$
-2	2.98523E-3	2.98465E-3	2.98458E-3	2.98457E-3	2.98457E-3
-1.5	5.67813E-3	5.67731E-3	5.67722E-3	5.67720E-3	5.67720E-3
-1	1.23726E-2	1.23713E-2	1.23712E-2	1.23712E-2	1.23712E-2
-0.5	3.73917E-2	3.73678E-2	3.73647E-2	3.73647E-2	3.73647E-2
0	4.59267E-1	4.59140E-1	4.59163E-1	4.59158E-1	4.59155E-1
0.5	7.82508E-2	7.82399E-2	7.82383E-2	7.82381E-2	7.82381E-2
1	3.16438E-2	3.16346E-2	3.16333E-2	3.16333E-2	3.16333E-2
1.5	1.40588E-2	1.40505E-2	1.40507E-2	1.40507E-2	1.40507E-2
2	7.20578E-3	7.20638E-3	7.20651E-3	7.20650E-3	7.20650E-3

With a good understanding of the numerical requirements for obtaining benchmark quality results the next step is to generate general results which display the physical properties of the return current.

7.E.3.b. General Results for the Current at the Surface. As with the surface scalar flux there are several variables and parameters which may be studied for the return current. The current as a function of angle and source incident angle is the first means of viewing the current and is displayed in Fig. 7.6. The return current looks and behaves very much like the scalar flux at the surface, as expected. Also, for $\mu_0 = 1$ the return current is invariant with respect to the positional angle and agrees with the values obtained from the two-dimensional calculation.

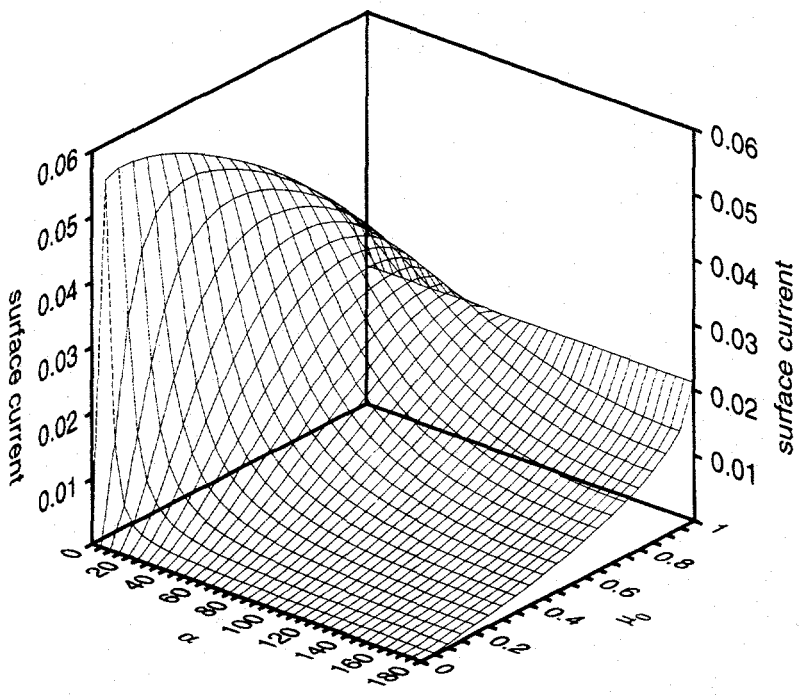

Fig. 7.6. The return current as a function of positional angle (α) and beam incident angle (μ_0) at $\rho = 1$ with $c = 0.9$.

The final display of the surface current is the most obvious means of display - that of current as a function of position on the surface. As with the scalar flux this is done in contour plots as seen in Fig. 7.7. As expected, the sharply canted beams produce lower

valued currents yet more directed contours on the surface. As the beam approaches $\mu_0 = 1$ the contours become more symmetric about the origin. Thus the general results for the surface scalar flux and current look and behave similarly.

It has therefore been demonstrated that the calculation of the scalar flux resulting from a canted beam impinging on the surface of a half-space, which involves integrals related to three inversions, requires a great deal of computational power and time to produce results. Results can be provided to a 10^{-4} accuracy in a reasonable time for problems which are not highly absorbing and for beams which are not severely canted. However, given the nature of the inversions these calculations would have been impossible without the improved speed of computers which are now available in desktop workstations and personal computers.

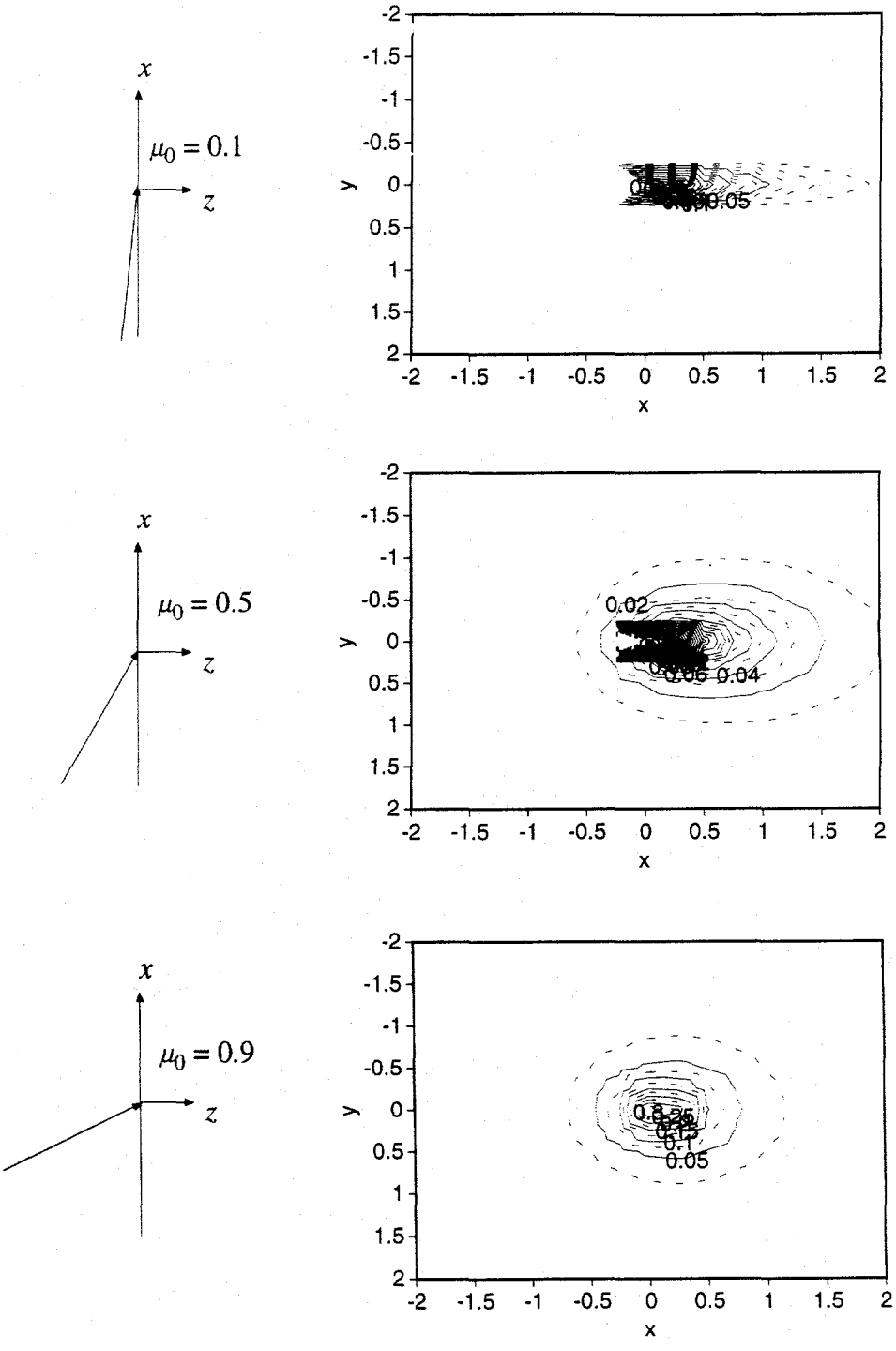

Fig. 7.7. Contour mapping of the return current for three values of the incident angle μ_0 with $c = 0.9$.

CHAPTER 8: CONCLUSIONS AND RECOMMENDATIONS

A wide variety of benchmark-type problems have been investigated. The basic theme of this work was the examination of the suite of infinite medium benchmarks and how they are related to one another, with the ultimate goal of obtaining results for the three-dimensional searchlight problem. Because the searchlight problem is extremely complex with regard to the mathematics and numerics required for solution, the infinite medium problems were investigated to gain experience with benchmarking in general, and to develop numerical methods which would eventually be applied to the three-dimensional searchlight problem.

The study of benchmarks progressed from the fundamental problems in infinite media: the isotropic point, plane, and line sources. The solutions were obtained through Fourier transforms and inversions. The methods to obtain numerical results using the Fourier inversion were thus established, as was the concept of integrating one source to obtain the solution for another. In this light, is was shown that, intuitively, all sources and geometric shapes can be derived from the solution to a point source emitting particles in a specific direction, called the Green's function source. Mathematically, however, all sources and geometric shapes, including the Green's function source, can most conveniently be derived from the solution for the scalar flux from an isotropic point source.

The benchmarks progressed from those which have one-dimensional variation in the scalar flux arising from isotropic sources, to those which have two-dimensional and three-dimensional variation arising from finite isotropic sources. Here, the methods for evaluating multiple embedded integrals was established. This progression of complexity then led to anisotropic sources and the evaluation of the Green's function source.

The final case which was studied for the infinite medium suite of benchmarks was the infinite line source emitting particles in a particular direction. This case was unique in that the scalar flux's spatial variation was two-dimensional in a plane, that is, the variation was according to polar coordinates. This benchmark was considered in order to complete the suite of benchmarks in infinite media and to gain experience with double-Fourier transforms and inversions - the scalar flux in the plane is obtained by a double-Fourier inversion. With this benchmark, the basic suite of problems in infinite homogeneous media was considered complete. Thus, with the infinite medium benchmarks well-characterized, the next step was to progress to semi-infinite media.

There has been much analysis of one-dimensional half-space problems from the astrophysical and radiative transfer communities; however, only recently have the computational platforms been available which allow numerical analysis of problems having two-dimensional variation of the scalar flux in a half-space. In the case of the searchlight problem, two-dimensional Fourier transforms and inversions are used for the transverse plane, and the Laplace transform is used for the longitudinal dimension. The results of such analyses are embedded integrals which contain generalized Chandrasekhar's *H*-functions. It was found that the scalar flux on the surface was relatively easy to evaluate owing to the fact that only a double integral need be evaluated. When the interior scalar flux was considered, much more difficulty was encountered and much more computer resources were required. Very oblique incident angles presented some difficulty, as did small values of c.

One purpose of analyzing these benchmarks is to develop more comprehensive benchmarks so that those who create production-scale codes would have test problems which they may use to benchmark new and more complicated codes. Again, the ultimate goals of this work were to obtain numerical results for the three-dimensional searchlight problem and, secondarily, to provide a compilation of benchmarks in infinite homogenous

media. Both goals were met; however, there are multiple opportunities for further research regarding both infinite medium benchmarks, semi-infinite medium benchmarks, and the searchlight problem, in particular.

Even though the suite of infinite medium benchmarks is considered "well-characterized," it is far from complete. The solutions which may be generated are as varied as the kinds of sources which may be envisioned. As mentioned, shell sources and finite volumetric sources have not been investigated in this work, and are certainly of interest. When considering a radioactive foil for radiation oncology applications, it is understood that a foil has a finite thickness; therefore, obtaining solutions for finite volumetric sources will be important for benchmarking codes which are capable of modeling such sources. It may therefore be desirable to investigate other source geometries like cylinders or helixes, but the solutions will be more difficult when compared to the isotropic surface sources. One possible means of approximating such sources is to construct such sources out of an array of isotropic point sources. For example, the scalar flux from a finite isotropic line source may be approximated as a series of point sources placed in a line. The scalar flux from the finite line source was obtained by mathematically integrating the solution from the isotropic point source, so in the approximate case, the fluxes from the point sources would be used as interpolation points by which a polynomial expression may be produced and integrated. This would then produce an approximate value for the scalar flux from a finite line source. Similarly, the rectangular source could be approximated by a series of line sources or an array of point sources. Such approximations could allow the evaluation of the scalar fluxes from more complex sources.

Construction of a semi-infinite suite of benchmarks would be complementary to the one for infinite media. Past work has been performed regarding plane and point sources on the surface of a half-space, but to date no one has considered the solutions which have isotropic and anisotropic line sources on the surface.

It was seen that the searchlight problem required extensive computational effort to produce results. Further research should be devoted to obtaining quicker and more extensive results from the searchlight problem. This is especially true for small values of c. This may involve better integration techniques, or better use of the ones available. Other acceleration schemes, such as the epsilon algorithm, may also be investigated. It was also noted that convergence to errors below 10^{-4} was difficult due to the required increase in quadrature order to obtain accurate values for the integrands at large k. Methods of mitigating this must be developed in order to obtain numerical results for tighter error requirements. Ultimately, however, the future of analytical benchmarking lies in the use of parallel processing. The formulations are such that a minimal amount of parallel programming would have to be done so that individual processors could be devoted to separate evaluations of the integral expressions based on spatial or source parameters. Accomplishment of these tasks should be a part of a subsequent and consistent effort to provide more complex and realistic benchmarks for the nuclear, medical, astrophysical, and earth sciences communities.

Another area which may be interesting to pursue is that of visualization. With the production of benchmarks which produce a scalar flux as a function of three spatial variables there results a four-dimensional system. Clearly, with graphics as they exist presently, only three-dimensional images may be produced. Development of new and innovative means of visualizing or manipulating three-dimensional data fields (such as shining light on the data field and noting the effect) may be of great benefit regarding the use of these kinds of benchmarks, and may also be very educational.

Finally, the ability to use these benchmarks as pedagogical tools can not be understated. Great insights regarding physical phenomena may be gained by using these simplified problems. The proper use of certain numerical methods may also be a result of using these benchmarks in consideration of the numerical methods used therein. Students

and teachers alike often gain the most knowledge by being familiar with basic problems and their associated physics.

APPENDIX A: SCALAR FLUX EXPANSIONS NEAR VARIOUS SOURCES

It may be useful to have asymptotic forms of solutions for various problems in infinite media. It is usually more difficult to obtain numerical solutions near sources; therefore it is desirable to use asymptotic solutions to check standard numerical results and perhaps as the solution if the desired edit point is sufficiently close to the source so that the asymptotic form is very dominant. Such asymptotic forms are obtained using limiting processes found in Case, DeHoffmann, and Placzek for several source types.

A.1. The Scalar Flux at Small r for an Isotropic Point Source in an Infinite Medium

The scalar flux from an isotropic point source in an infinite homogeneous medium is given by

$$\rho(r) = \frac{1}{2\pi^2 r}\int_0^\infty dk\; k\, f(k)\, \sin(kr) \quad , \tag{A.1}$$

where the function $f(k)$ is given by

$$f(k) \equiv \frac{L(k)}{1 - cL(k)} \; ;$$

$$L(k) = \frac{\tan^{-1}(k)}{k} \quad .$$

In order to determine the behavior of $\rho(r)$ at small r, a simple change of variable is applied to Eq. (A.1) to give

$$\rho(r) = \frac{1}{2\pi^2 r^3}\int_0^\infty dz\; z\, f\left(\frac{z}{r}\right) \sin(z) \quad . \tag{A.2}$$

$$\rho_1(r) = \rho(r) - \frac{1}{4\pi r^2} \; ; \tag{A.5}$$

then from Eq. (A.2)

$$\rho_1(r) = \frac{1}{2\pi^2 r^3} \int_0^\infty dz \; z \, f\left(\frac{z}{r}\right) \sin(z) - \frac{1}{4\pi r^2} \int_0^\infty dz \, \sin(z) \; . \tag{A.6a}$$

Combining integrals yields

$$\rho_1(r) = \frac{1}{2\pi^2 r^2} \int_0^\infty dz \left[\left(\frac{z}{r}\right) f\left(\frac{z}{r}\right) - \frac{\pi}{2} \right] \sin(z) \; . \tag{A.6b}$$

Upon introduction of the definition of $f(k)$, the term in square brackets becomes

$$L_1 = \frac{\tan^{-1}\left(\frac{z}{r}\right)}{1 - \frac{cr}{z}\tan^{-1}\left(\frac{z}{r}\right)} - \frac{\pi}{2} \; . \tag{A.7}$$

The asymptotic expansion for the inverse tangent (for $|x| > 1$) is

$$\tan^{-1} x \; = \; \frac{\pi}{2} + \sum_{j=1}^{\infty} \frac{(-1)^j}{x^{2j-1}\,(2j-1)} = \frac{\pi}{2} - \frac{1}{x} + \frac{1}{3x^3} - \ldots \quad .$$

By approximating the inverse tangent using the first two terms, Eq. (A.7) becomes

$$L_1 = \frac{\frac{\pi}{2} - \frac{r}{z}}{1 - \frac{c\pi r}{2z} + \frac{cr^2}{z^2}} - \frac{\pi}{2} \; , \tag{A.8a}$$

which upon simplification is

$$L_1 = \frac{-\frac{r}{z} + \frac{c\pi^2 r}{4z} - \frac{c\pi r^2}{2z^2}}{1 - \frac{c\pi r}{2z} + \frac{cr^2}{z^2}} \; . \tag{A.8b}$$

For small r L_1 becomes

$$L_1 = \frac{r}{z}\left[\frac{c\pi^2}{4} - 1\right] . \tag{A.8c}$$

Defining α_1 as $\frac{c\pi^2}{4} - 1$ and inserting Eq. (A.8c) into the equation for $\rho_1(r)$ produces

$$\rho_1(r) = \frac{\alpha_1}{2\pi^2 r}\int_0^\infty dz\, \frac{\sin(z)}{z} . \tag{A.9}$$

The integral in Eq. (A.9) has the value of $\pi/2$ [Gradshteyn and Ryzhik]. However, for consistency, Laplace transforms may be used to obtain this value. The following property of Laplace transforms,

$$\mathcal{L}\left\{\frac{f(t)}{t}\right\} = \int_s^\infty ds'\, F(s') , \tag{A.10}$$

is employed. Letting $f(t) = \sin(t)$ and $F(s) = \frac{1}{1 + s^2}$ produces

$$\int_0^\infty dt\, e^{-st}\frac{\sin(t)}{t} = \int_s^\infty \frac{ds'}{1 + s'^2} = \tan^{-1}s'\Big|_s^\infty = \frac{\pi}{2} - \tan^{-1}s = \tan^{-1}(1/s) .$$

Now taking the limit as s approaches zero gives the desired result:

$$\lim_{s\to 0}\int_0^\infty dt\, e^{-st}\frac{\sin(t)}{t} = \int_0^\infty dt\, \frac{\sin(t)}{t} = \frac{\pi}{2} .$$

Inserting this expression into Eq. (A.9) yields the second term for the expansion of the scalar flux from a point source at small r:

$$\rho_1(r) = \frac{\alpha_1}{4\pi r} . \tag{A.11}$$

The next term in the expansion is obtained in a similar fashion. Let

$$\rho_2(r) = \rho(r) - \frac{1}{4\pi r^2} - \frac{\alpha_1}{4\pi r} \quad . \tag{A.12}$$

Introducing the integral forms of the above terms and combining the integrals yields

$$\rho_2(r) = \frac{1}{2\pi^2 r^2} \int_0^\infty dz \left[\left(\frac{z}{r}\right) f\left(\frac{z}{r}\right) - \frac{\pi}{2} - \frac{\alpha_1 \pi r}{2} \right] \sin(z) \quad . \tag{A.13}$$

Again manipulating the term in square brackets and using the first two terms in the expansion of the inverse tangent as above produces

$$L_2 = \frac{\frac{\pi}{2} - \frac{r}{z} - \frac{\pi}{2}\left[1 - \frac{c\pi r}{2z} + \frac{cr^2}{z^2}\right] - \frac{\alpha_1 \pi r}{2}\left[1 - \frac{c\pi r}{2z} + \frac{cr^2}{z^2}\right]}{1 - \frac{c\pi r}{2z} + \frac{cr^2}{z^2}} \quad . \tag{A.14a}$$

To obtain the next term, the denominator is expanded in its Taylor series and the numerator is simplified (with terms of r^3 and greater neglected) as

$$L_2 = \frac{\alpha_1 r}{z} - \frac{c\pi r^2}{2z^2} - \frac{\alpha_1 \pi r}{2} + \frac{\alpha_1 c \pi r^2}{2z^2} \quad . \tag{A.14b}$$

Inserting the definition for α_1 and rearranging terms yields

$$L_2 = \frac{\pi r}{2} - \frac{r}{z} + \frac{c\pi^2 r}{4z} - \frac{c\pi^3 r}{8} - \frac{c\pi r^2}{z^2} + \frac{c^2 \pi^3 r^2}{8z^2} \quad . \tag{A.14c}$$

When Eq. (A.14c) is placed into the equation for $\rho_2(r)$ and the individual integrals are evaluated the first two terms in L_2 cancel, as do the third and fourth terms. When the remaining two terms are placed in the integral there results

$$\rho_2(r) = \frac{1}{2\pi^2}\left[- c\pi + \frac{c^2\pi^3}{8} \right] \int_0^\infty dz \, \frac{\sin(z)}{z^2} \quad . \tag{A.15}$$

Again, the integral in Eq. (A.15) does not have a finite value. However, recall that this expression is the result of a limit as r approaches zero, and the manner in which it diverges may be determined via Laplace transform methods. Letting $f(t) = \sin(t)/t$ and $F(s) = \tan^{-1}(1/s)$ in Eq. (A.10) produces

$$\int_0^\infty dt\, e^{-st}\frac{\sin(t)}{t^2} = \int_s^\infty ds'\, \tan^{-1}(1/s) = s'\tan^{-1}\frac{1}{s'} + \frac{1}{2}\ln\left(1 + s'^2\right)\Big|_s^\infty .$$

Now taking the limit as s approaches zero gives

$$\lim_{s\to 0}\int_0^\infty dt\, e^{-st}\frac{\sin(t)}{t^2} = \int_0^\infty dt\,\frac{\sin(t)}{t^2} = \lim_{s'\to\infty}\left[s'\tan^{-1}\frac{1}{s'} + \frac{1}{2}\ln\left(1 + s'^2\right)\right] ,$$

which can be evaluated as

$$\int_0^\infty dt\,\frac{\sin(t)}{t^2} = 1 + \lim_{s'\to\infty}\ln(s') = 1 - \lim_{s'\to 0}\ln(s') = -\lim_{s'\to 0}\ln(s') \quad . \tag{A.16}$$

Recognizing this logarithmic singularity, Eq. (A.15) can be rewritten as

$$\rho_2(r) = \frac{1}{4\pi}\left[2c - \frac{c^2\pi^2}{4}\right]\ln(r) \quad . \tag{A.17}$$

Successively performing this analysis yields an infinite series of constant terms. Thus, for an isotropic point source in an infinite medium, the scalar flux near the source is given by

$$\rho(r) = \frac{1}{4\pi r^2}\left[1 + \left(\frac{c\pi^2}{4} - 1\right)r + \left(2c - \frac{c^2\pi^2}{4}\right)r^2\ln(r)\right] + O(\text{constant}) \quad . \tag{A.18}$$

A.2. The Scalar Flux at Small r for an Isotropic Planar Source in an Infinite Medium

It was shown that the scalar flux from a plane source in an infinite medium could be expressed as

$$\phi_{plane}(z) = \frac{1}{\pi}\int_0^\infty dk\, f(k)\, \cos(kz) \quad , \tag{A.19a}$$

or upon using the integrated form of a point source solution after a change of variable and contour in the complex plane can also be written as [Case, DeHoffmann, and Placzek]

$$\phi_{plane}(z) = \frac{1}{2k_0}\frac{\partial k_0^2}{\partial c}\, e^{-k_0 z} + \frac{1}{2}\int_0^1 \frac{d\mu}{\mu}\, e^{-z/\mu}\, g(c,\mu) \quad , \tag{A.19b}$$

where

$$g(c,\mu) \equiv \left[\left(1 - c\mu \tanh^{-1}\mu\right)^2 + \left(\frac{\pi}{2}c\mu\right)^2\right]^{-1} \quad , \tag{A.19c}$$

$$\frac{\partial k_0^2}{\partial c} = \frac{2k_0^2(k_0^2 - 1)}{c(1 - c - k_0^2)} \quad , \tag{A.19d}$$

and k_0 satisfies the dispersion relation

$$1 - \frac{c}{k_0}\tanh^{-1}(k_0) = 0 \quad . \tag{A.19e}$$

Subtracting and adding 1 inside the integrand yields

$$\phi_{plane}(z) = \frac{1}{2k_0}\frac{\partial k_0^2}{\partial c}\, e^{-k_0 z} + \frac{1}{2}\int_0^1 \frac{d\mu}{\mu}\, e^{-z/\mu}\, [g(c,\mu) - 1] + \frac{1}{2}E_1(z) \quad . \tag{A.20}$$

By applying the following infinite series expansions for the exponentials and the exponential integral in the above equation

$$e^{-az} = \sum_{n=0}^{\infty} \frac{(-1)^n (az)^n}{n!} = 1 - az + \frac{a^2 z^2}{2!} - \ldots$$

$$E_1(z) = -\ln z - \gamma - \sum_{n=0}^{\infty} \frac{(-1)^n z^n}{n\, n!}$$

the expansion for the scalar flux from a planar source near the source is obtained by truncating the resultant infinite series at an appropriate point. The result is [Case, DeHoffmann, and Placzek]

$$\phi_{plane}(z) = -\frac{1}{2}\ln z + \frac{1}{2}\left[-\gamma + T_{-1}(c) + \frac{1}{k_0}\frac{\partial k_0^2}{\partial c}\right] + \frac{z}{2}\left(1 - \frac{c\pi^2}{4}\right) + O(z^2) \quad , \qquad \text{(A.21a)}$$

where

$$T_{-1}(c) = \int_0^1 \frac{d\mu}{\mu}\,[g(c,\mu) - 1] \qquad \text{(A.21b)}$$

and the fact that

$$\frac{\partial k_0^2}{\partial c} + \int_0^1 \frac{d\mu}{\mu^2}\,[g(c,\mu) - 1] = \frac{c\pi^2}{4} \qquad \text{(A.21c)}$$

has been used [Case, DeHoffmann, and Placzek]. Clearly, as the source plane is approached, the terms containing powers of z become exceedingly small and the remaining asymptotic scalar flux is given by a logarithm plus a constant term.

A.3. The Scalar Flux at Small r for an Isotropic Line Source in an Infinite Medium

The scalar flux from an isotropic line is

$$\phi_{line}(r) = \frac{1}{2\pi}\int_0^{\infty} dk\; k\, f(k)\, J_0(kr) \quad , \qquad \text{(A.22a)}$$

which may also be written as

$$\phi_{line}(r) = \frac{1}{2\pi r^2}\int_0^{\infty} du\; u\, f\left(\frac{u}{r}\right) J_0(u) \quad . \qquad \text{(A.22b)}$$

For small r, the function $f\left(\frac{u}{r}\right)$ may be approximated by $\frac{\pi r}{2u}$, which leaves for the approximate scalar flux

$$\phi_{line}(r) = \frac{1}{4r}\int_0^\infty du\, J_0(u) \quad . \tag{A.23a}$$

The above integral has a value of 1, which can be obtained from Laplace transform arguments as

$$\int_0^\infty dt\, e^{-st} J_0(at) = \frac{1}{\left(s^2 + a^2\right)^{1/2}} \quad , \tag{A.23b}$$

or upon taking the limit as s approaches zero the value of the above integral is obtained. Thus, near the source, the scalar flux from an isotropic line source is

$$\phi_{line}(r) \sim \frac{1}{4r} \quad . \tag{A.23c}$$

Defining $\rho_1(r)$ as

$$\rho_1(r) = \phi_{line}(r) - \frac{1}{4r} \quad , \tag{A.24a}$$

and inserting the expression for $\phi_{line}(r)$ yields

$$\rho_1(r) = \frac{1}{2\pi r}\int_0^\infty du\, J_0(u)\left[\frac{u}{r} f\left(\frac{u}{r}\right) - \frac{\pi}{2}\right] \quad . \tag{A.24b}$$

The term in brackets may be shown to be

$$\frac{u}{r} f\left(\frac{u}{r} - \frac{\pi}{2}\right) \approx \left(\frac{c\pi^2}{4} - 1\right)\frac{r}{u} \quad ,$$

so that

$$\rho_1(r) = \frac{1}{2\pi r}\left(\frac{c\pi^2}{4} - 1\right)\int_0^\infty du\, J_0(u)\, \frac{r}{u} \quad . \tag{A.25}$$

Using the formula for Laplace transforms divided by t as done previously, it is seen that the above integral is logarithmically singular. Thus,

$$\rho_1(r) = \frac{1}{2\pi}\left(\frac{c\pi^2}{4} - 1\right)\lim_{s\to\infty} \ln(s) = -\frac{1}{2\pi}\left(\frac{c\pi^2}{4} - 1\right)\lim_{r\to 0} \ln(r) \ , \tag{A.26}$$

which gives for the approximate flux

$$\phi_{line}(r) = \frac{1}{4r} - \frac{1}{2\pi}\left(\frac{c\pi^2}{4} - 1\right)\ln(r) \ . \tag{A.27}$$

Continuing the singularity subtraction and limiting process results in a series of constants. Therefore, the asymptotic scalar flux near in an infinite line source in an infinite medium is

$$\phi_{line}(r) = \frac{1}{4r} - \frac{1}{2\pi}\left(\frac{c\pi^2}{4} - 1\right)\ln(r) + O(\text{constant}) \ . \tag{A.28}$$

A.4. The Scalar Flux at Small r for Sources Derived from the Isotropic Point Source Solution in an Infinite Medium

Because the isotropic point source in an infinite medium is one of the most basic problems in transport theory, other sources can be constructed by integrating the point source solution over a line, surface, or volume. In this section, the scalar flux near the sources which are derived from the isotropic point source, the finite line source, the finite disk source, and the rectangular source, will be approximated.

A.4.1. The Scalar Flux at Small r for an Isotropic Finite Line Source.

In a fashion similar to that above, the approximate form of the scalar flux near a finite isotropic line source is obtained by integrating the asymptotic form of the isotropic point source solution as

$$\phi_{IFL}(r,z) \approx \int_{-z_0}^{z_0} du\, \rho\left[\left(r^2 + (z-u)^2\right)^{1/2}\right] , \tag{A.29}$$

which becomes

$$\phi_{IFL}(r,z) \approx \frac{1}{4\pi}\left(I_1 + \alpha_0 I_2 + \frac{\alpha_1}{2} I_3\right) , \tag{A.30a}$$

where

$$I_1 = \int_{-z_0}^{z_0} \frac{du}{r^2 + (z-u)^2} , \tag{A.30b}$$

$$I_2 = \int_{-z_0}^{z_0} \frac{du}{\left[r^2 + (z-u)^2\right]^{1/2}} , \tag{A.30c}$$

$$I_3 = \int_{-z_0}^{z_0} du \ln\left[r^2 + (z-u)^2\right] . \tag{A.30d}$$

All three integrals may be evaluated analytically to give for the approximate scalar flux near the finite line source

$$\phi_{IFL}(r,z) \approx \frac{1}{4\pi}\left\{\left[\tan^{-1}\frac{z+z_0}{r} - \tan^{-1}\frac{z-z_0}{r}\right]\left[\frac{1}{r} + \alpha_1 r\right] + \alpha_1 \frac{z+z_0}{2} \ln\left[r^2 + (z+z_0)^2\right] -\right.$$

$$\left. - \alpha_1 \frac{z-z_0}{2} \ln\left[r^2 + (z-z_0)^2\right] + \alpha_0 \ln\left[\frac{\left(r^2 + (z-z_0)^2\right)^{1/2} + z_0 - z}{\left(r^2 + (z+z_0)^2\right)^{1/2} - z_0 - z}\right] - 2\alpha_1 z_0\right\} . \tag{A.31}$$

A.4.2. The Scalar Flux at Small r for an Isotropic Disk Source.

As with the Green's function and the finite line source, the approximate form of the scalar flux near a finite isotropic disk source is obtained by integrating the asymptotic form of the isotropic point source solution over the source disk as

$$\phi_{IFD}(r,z) \approx \int_0^{2\pi} d\theta \int_0^{R_0} du\ \rho(r_s) \ , \tag{A.32}$$

where $r_s^2 = r^2 + z^2 + u^2 - 2\rho u\cos\theta$. Inserting the expression for the asymptotic flux from the isotropic point source yields the usual

$$\phi_{IFD}(r,z) \approx \frac{R_0^2}{4\pi}\left(I_1 + \alpha_0 I_2 + \frac{\alpha_1}{2} I_3\right) , \tag{A.33a}$$

where

$$I_1 = \int_0^{2\pi} d\theta \int_0^1 \frac{du\ u}{r^2 + z^2 + u^2 R_0^2 - 2\rho u R_0 \cos\theta} \ , \tag{A.33b}$$

$$I_2 = \int_0^{2\pi} d\theta \int_0^1 \frac{du\ u}{\left[r^2 + z^2 + u^2 R_0^2 - 2\rho u R_0 \cos\theta\right]^{1/2}} \ , \tag{A.33c}$$

$$I_3 = \int_0^{2\pi} d\theta \int_0^1 du\ \ln\left[r^2 + z^2 + u^2 R_0^2 - 2\rho u R_0 \cos\theta\right] \ . \tag{A.33d}$$

The first integral may be analytically evaluated (see Sec. 3.B) and the last two may be partially evaluated. In the terms of Sec. 3.B, $I_1 = e^z I_{g2z}/R_0^2$, $I_2 = e^z I_z/R_0^2$ (which has the θ integral analytically evaluated), and the θ integral may also be evaluated for I_3 by noting

$$\int_0^{2\pi} d\theta \ln(a - b\cos\theta) = 2\pi \ln\left[\frac{a + (a^2 - b^2)^{1/2}}{2}\right] .$$

Combining all the terms results in the following expression for the approximate scalar flux near a finite isotropic disk source:

$$\phi_{IFD}(r,z) \approx \frac{R_0^2}{4\pi}\left(\frac{e^z I_{g2z}}{R_0^2} + \alpha_0 \frac{e^z I_z}{R_0^2} + \frac{\alpha_1 \pi}{2}\ln 2 + \alpha_1 \pi \int_0^1 du\ u\ \ln p\right) , \tag{A.34}$$

where $p = r^2 + z^2 + u^2R_0^2 + \left[\left(r^2 + z^2 + u^2R_0^2\right)^2 - \left(2\rho uR_0\right)^2\right]^{1/2}$.

A.4.3. The Scalar Flux at Small r for an Isotropic Rectangular Source.

The approximate form of the scalar flux near an isotropic rectangular source is obtained by integrating the asymptotic form of the isotropic point source solution over the source area as

$$\phi_{IFR}(x,y,z) \approx \int_{-a_0}^{a_0} dx' \int_{-b_0}^{b_0} dy'\, \rho\left(r_s\right) \ , \tag{A.35}$$

where $r_s^2 = (x - x')^2 + (y - y')^2 + z^2$. Inserting the expression for the asymptotic flux from the isotropic point source again yields

$$\phi_{IFR}(x,y,z) \approx \frac{a_0 b_0}{\pi}\left(I_1 + \alpha_0\, I_2 + \frac{\alpha_1}{2} I_3\right) , \tag{A.36a}$$

where

$$I_1 = \int_0^1 du \int_0^1 \frac{dv}{(x + a_0 - 2a_0u)^2 + (y + b_0 - 2b_0v)^2 + z^2} \ , \tag{A.36b}$$

$$I_2 = \int_0^1 du \int_0^1 \frac{dv}{\left[(x + a_0 - 2a_0u)^2 + (y + b_0 - 2b_0v)^2 + z^2\right]^{1/2}} \ , \tag{A.36c}$$

$$I_3 = \int_0^1 du \int_0^1 dv\, \ln\left[(x + a_0 - 2a_0u)^2 + (y + b_0 - 2b_0v)^2 + z^2\right] \ . \tag{A.36d}$$

In all three integrals the v integral may be evaluated analytically; the first two are given in Sec. 3.C where it is also seen that $I_1 = I_{g2z}$ and $I_2 = I_z$. The integral over the logarithm is

evaluated by making the change of variable $s = (y + b_0 - 2b_0v)/p$ where $p^2 = (x + a_0 - 2a_0u)^2 + z^2$ to give

$$I_v = 2\ln p - 1 + \frac{p}{2b_0}\left\{\frac{y}{p}\ln\frac{1+q_+^2}{1+q_-^2} + \frac{b_0}{p}\ln(1+q_+^2)(1+q_-^2) + 2(\tan^{-1}q_+ - \tan^{-1}q_-)\right\}$$

where $q_+ = (y + b_0)/p$ and $q_- = (y - b_0)/p$. Integrating this expression over u will yield the third term I_3.

APPENDIX B: MULTIPLE COLLISION ANALYSIS

The basic kernel that appears throughout infinite medium transport theory in the Fourier inversion integrals is

$$f(k) = \frac{1}{1 - cL(k)} \quad , \tag{B.1a}$$

where $L(k) = \frac{\tan^{-1}k}{k}$. Noting that $f(k)$ has the form $(1 - x)^{-1}$ and $cL(k) \leq 1$ (equality occurs only for a conservative system, $c = 1$, and $k = 0$), it may be restated as a Taylor series as

$$f(k) \;=\; 1 + cL(k) + [cL(k)]^2 + [cL(k)]^3 + \ldots = \sum_{n=0}^{\infty}[cL(k)]^n \quad , \tag{B.1b}$$

where the term $c^n L^r(k)$ is denoted upon inversion as the "n-th collided flux." Thus the inversion of the first term [1] is the uncollided flux, or the flux of those particles which have suffered zero collisions, the second term $[cL(k)]$ is the first collided flux, or the flux of those particles which have suffered one collision, etc. The sum of each collided flux will equal the total flux, the kernel of which is appropriately seen in Eq. (B.1b). With this Taylor expansion, it is possible to determine both the scalar flux from particles that have had n collisions and the scalar flux from all the remaining sets of collided fluxes.

Invariably, it is necessary (due to mathematical singularities) to extract the uncollided flux before evaluating the inversion integral(s). When this is done, the remaining flux is the collided flux, or those particles which have suffered at least one collision. In general, it is desirable to define the "N-th+ collided flux" which is the scalar

flux from those particles which have suffered at least N collisions. This is determined by subtracting the kernels of the collided fluxes up to $N-1$ from the total flux kernel as

$$f_N(k) = \sum_{n=0}^{\infty}[cL(k)]^n - f_0(k) - f_1(k) - \ldots - f_{N-1}(k) \ , \tag{B.2a}$$

or

$$f_N(k) = \frac{1}{1 - cL(k)} - 1 - cL(k) - \ldots - c^{N-1}L^{N-1}(k) \ . \tag{B.2b}$$

Placing all terms in the numerator with the appropriate common denominator yields

$$f_N(k) = \frac{1 - [1 - cL(k)] - cL(k)[1 - cL(k)] \ldots - c^{N-1}L^{N-1}(k)[1 - cL(k)]}{1 - cL(k)} \ , \tag{B.3a}$$

which is immediately seen to be

$$f_N(k) = \frac{c^N L^N(k)}{1 - cL(k)} \ . \tag{B.3b}$$

Recalling that when the uncollided flux is extracted, the remaining flux of collided particles has the kernel

$$f_c(k) = \frac{cL(k)}{1 - cL(k)} \ , \tag{B.4}$$

which agrees with the above analysis for $N = 1$. Thus, it is possible to evaluate the scalar flux from particles which have had *only* n collisions by replacing the standard kernel [Eq. (B.1a)] with $c^nL^n(k)$ and it is possible to evaluate the scalar flux from particles which have had *at least* N collisions by replacing the standard kernel with $\frac{c^N L^N(k)}{1 - cL(k)}$.

APPENDIX C: THE TRANSFORMED CURRENT AT THE SURFACE

The transformed current at the surface for the searchlight problem is obtained in the same way as the transformed scalar flux. Integral transport theory, the formation of a kernel, and the pseudo problem are all used in the derivation.

The transformed current is defined as

$$\bar{J}(z;\vec{k}) = \int_{4\pi} d\vec{\Omega}\ \mu\ \bar{\Psi}(z,\vec{\Omega};\vec{k})\ , \tag{C.1}$$

which can be decomposed into regions of positive and negative μ so that

$$\bar{J}(z;\vec{k}) = \int_0^{2\pi} d\phi \int_0^1 d\mu\ \mu\ \bar{\Psi}(z,\vec{\Omega};\vec{k}) - \int_0^{2\pi} d\phi \int_0^1 d\mu\ \mu\ \bar{\Psi}(z,-\vec{\Omega};\vec{k})\ . \tag{C.2a}$$

Inserting the appropriate expressions for the transformed angular flux in the above equation leaves

$$\bar{J}(z;\vec{k}) = \mu_0\, e^{-z/U_0}\, \bar{S}(\vec{k}) + \frac{c}{4\pi} \int_0^z dz'\ \bar{\Psi}(z';\vec{k}) \int_0^1 d\mu \int_0^{2\pi} d\phi\ e^{-(z-z')/U} -$$

$$- \frac{c}{4\pi} \int_z^\infty dz'\ \bar{\Psi}(z';\vec{k}) \int_0^1 d\mu \int_0^{2\pi} d\phi\ e^{-(z'-z)/U}\ . \tag{C.2b}$$

The ϕ integrals may be evaluated by inserting the form of U to give

$$\frac{1}{2\pi} \int_0^{2\pi} d\phi\ e^{-z/U} = e^{-z/\mu}\, J_0\left[\frac{kz}{\mu}(1-\mu^2)^{1/2}\right]\ ,\quad z > 0\ . \tag{C.3}$$

The kernel of the integrals in Eq. (C.2b) is now defined as

$$L(z) \equiv \int_0^1 d\mu \; e^{-z/\mu} \; J_0\left[\frac{kz}{\mu}(1-\mu^2)^{1/2}\right] \quad . \tag{C.4a}$$

Using methods similar to those found in Ch. 4, this kernel may be reformulated as

$$L(z) = \int_0^1 d\mu \; e^{-z(1+k^2\mu^2)^{1/2}/\mu} \quad . \tag{C.4b}$$

Thus, Eq. (C.2b) is seen to be

$$\bar{J}(z;\vec{k}) = \mu_0 \, e^{-z/U_0} \, \bar{S}(\vec{k}) + \frac{c}{2}\int_0^\infty dz' \; \mathrm{sgn}(z-z') \; \bar{\Psi}(z';\vec{k}) \; L(|z-z'|) \quad . \tag{C.5}$$

Applying the same mathematical analysis to the pseudo transport equation yields a similar expression for the pseudo transformed current at the surface:

$$\gamma(z;\mu^*) = \mu^* a(\mu^*) \, e^{-z/\xi^*} + \frac{c}{2}\int_0^\infty dz' \; \mathrm{sgn}(z-z') \; \tilde{\phi}(z';\mu^*) \; L(|z-z'|) \quad , \tag{C.6a}$$

where

$$\gamma(z;\mu^*) = \int_{-1}^1 d\mu \; \mu \; a(\mu) \; \tilde{\phi}(z,\mu;\mu^*) \quad . \tag{C.6b}$$

The equivalence relation between the pseudo current and the actual current is obtained by multiplying Eq. (C.6a) by $\bar{S}(\vec{k})\,(d\xi^*/d\mu^*)\,\delta(\xi^* - U_0)$ and integrating over μ^* to give

$$\tilde{\gamma}(z;\vec{k}) = \bar{S}(\vec{k}) U_0 b[\mu(U_0)] \, e^{-z/U_0} + \frac{c}{2}\int_0^\infty dz' \; \mathrm{sgn}(z-z') \; \bar{\Psi}(z';\vec{k}) \; L(|z-z'|) \quad , \tag{C.7a}$$

where

$$\tilde{\gamma}(z;\vec{k}) \equiv \bar{S}(\vec{k}) \int d\mu^* \, \frac{d\xi^*}{d\mu^*} \, \delta(\xi^* - U_0) \; \gamma(z;\mu^*) \quad , \tag{C.7b}$$

which upon substitution of the initial definition of $\gamma(z;\mu^*)$ yields

$$\tilde{\gamma}(z;\vec{k}) = \bar{S}(\vec{k}) \int_{-1}^1 d\mu \; \mu \; a(\mu) \; \int d\mu^* \, \frac{d\xi^*}{d\mu^*} \, \delta(\xi^* - U_0) \; \tilde{\phi}(z,\mu;\mu^*) \quad . \tag{C.7c}$$

Substitution of the integral term in Eq. (C.7a) into Eq. (C.5) gives the transformed current as

$$\bar{J}(z;\vec{k}) = e^{-z/U_0}\,\bar{S}(\vec{k})\left\{\mu_0 - U_0 b[\mu(U_0)]\right\} + \tilde{\gamma}(z;\vec{k}) \quad . \tag{C.8}$$

Letting $z = 0$ gives the transformed current at the surface of the half-space:

$$\bar{J}(0;\vec{k}) = \bar{S}(\vec{k})\left\{\mu_0 - U_0 b[\mu(U_0)]\right\} + \tilde{\gamma}(0;\vec{k}) \quad . \tag{C.9a}$$

$\tilde{\gamma}(0;\vec{k})$ is evaluated as (with the interchange of integrals and separation of the μ integral into positive and negative portions)

$$\tilde{\gamma}(0;\vec{k}) = -\bar{S}(\vec{k})\int d\mu^* \frac{d\xi^*}{d\mu^*}\,\delta(\xi^* - U_0)\int_0^1 d\mu\;\mu a(\mu)\left[\tilde{\phi}(0,\mu;\mu^*) - \tilde{\phi}(0,-\mu;\mu^*)\right] \quad . \tag{C.9b}$$

It is now recalled that $\tilde{\phi}(0,\mu;\mu^*) = Q_0\,\delta(\mu - \mu^*)$ and

$$\tilde{\phi}(0,-\mu;\mu^*) = \frac{c}{2}\frac{1}{\mu a(\mu)}\frac{\xi^*\xi}{\xi + \xi^*}H(\xi^*;k)H(\xi;k) \quad ,$$

which leaves for $\tilde{\gamma}(0;\vec{k})$

$$\tilde{\gamma}(0;\vec{k}) = \bar{S}(\vec{k})U_0 b[\mu(U_0)] - \frac{c}{2}\bar{S}(\vec{k})\,U_0 H(U_0;k)\int_0^1 d\mu\,\frac{\xi}{\xi + U_0}H(\xi;k) \quad . \tag{C.9c}$$

Combining Eqs. (C.9a) and (C.9c) yields

$$\bar{J}(0;\vec{k}) = \bar{S}(\vec{k})\left\{\mu_0 - \frac{c}{2}U_0 H(U_0;k)\int_0^1 d\mu\,\frac{\xi}{\xi + U_0}H(\xi;k)\right\} \quad , \tag{C.10}$$

which is the final form of the transformed current at the surface of the half-space.

APPENDIX D: *H*-FUNCTION FACTORIZATION FOR A COMPLEX ARGUMENT

It is desirable to obtain some analytical expression to which an evaluation of an *H*-function with a complex argument may be compared. This is done by deriving a type of dispersion relation to provide the analytical expression desired and using the standard factorization of the *H*-function as seen in Busbridge and Chandrasekhar to obtain the numerically evaluated expression.

D.1. *H*-function Calculus: Derivation of the Dispersion Relation

The *H*-function is given by the non-linear integral equation

$$H(\xi;k) = 1 + \frac{c}{2}\xi\, H(\xi;k)\int_0^{(1+k^2)^{-1/2}} \frac{d\xi}{\left(1-k^2\xi'^2\right)^{1/2}}\frac{H(\xi';k)}{\xi+\xi'}\ , \tag{D.1a}$$

where ξ may be complex and $H(\xi;k)$ is analytic in the entire complex ξ plane cut from $-(1+k^2)^{-1/2}$ to 0. Eq. (D.1a) may be rewritten as

$$H(\xi;k) = \left[1 - \frac{c}{2}\xi\int_0^{(1+k^2)^{-1/2}} \frac{d\xi}{\left(1-k^2\xi'^2\right)^{1/2}}\frac{H(\xi';k)}{\xi+\xi'}\right]^{-1}\ . \tag{D.1b}$$

The methods of Chandrasekhar and Busbridge will be followed in this analysis. Eq. (D.1b) is multiplied by the inverse of the right hand side and then multiplied by a similar factor to give (with a change in integration variable and letting $\xi = z$)

$$H(z;k)\left[1 - \frac{cz}{2}\int_0^{(1+k^2)^{-1/2}} \frac{du}{\left(1-k^2u^2\right)^{1/2}}\frac{H(u;k)}{z+u}\right]\left[1 - \frac{cz}{2}\int_0^{(1+k^2)^{-1/2}} \frac{dv}{\left(1-k^2v^2\right)^{1/2}}\frac{H(v;k)}{z-v}\right]$$

$$= \left[1 - \frac{cz}{2} \int_0^{(1+k^2)^{-1/2}} \frac{dv}{\left(1 - k^2 v^2\right)^{1/2}} \frac{H(v;k)}{z - v} \right] . \tag{D.2a}$$

With the following definition

$$\Lambda(z;k) = \left[1 - \frac{cz}{2} \int_0^{(1+k^2)^{-1/2}} \frac{du}{\left(1 - k^2 u^2\right)^{1/2}} \frac{H(u;k)}{z + u} \right] \times$$

$$\times \left[1 - \frac{cz}{2} \int_0^{(1+k^2)^{-1/2}} \frac{dv}{\left(1 - k^2 v^2\right)^{1/2}} \frac{H(v;k)}{z - v} \right] , \tag{D.3}$$

Eq. (D.2a) becomes

$$H(z;k)\, \Lambda(z;k) = \left[1 - \frac{cz}{2} \int_0^{(1+k^2)^{-1/2}} \frac{dv}{\left(1 - k^2 v^2\right)^{1/2}} \frac{H(v;k)}{z - v} \right] , \tag{D.4}$$

where the regions of analyticity for $H(z;k)$ and $\Lambda(z;k)$ are shown in Fig. D.1.

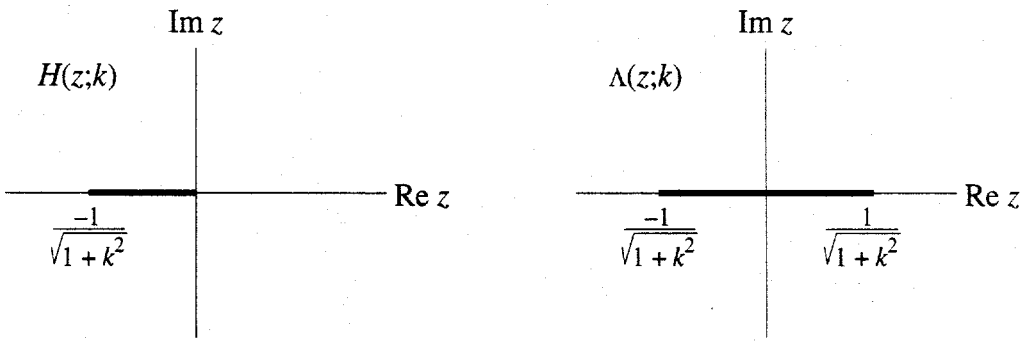

Fig. D.1. Regions of analyticity for $H(z;k)$ and $\Lambda(z;k)$ in the complex plane.

It is desirable to obtain a simpler expression for $\Lambda(z;k)$. Performing the indicated multiplication in Eq. (D.3) produces

$$\Lambda(z;k) = 1 - \frac{cz}{2}\int_0^{(1+k^2)^{-1/2}} \frac{du}{\left(1-k^2u^2\right)^{1/2}} \frac{H(u;k)}{z+u} - \frac{cz}{2}\int_0^{(1+k^2)^{-1/2}} \frac{dv}{\left(1-k^2v^2\right)^{1/2}} \frac{H(v;k)}{z-v} +$$

$$+ \frac{cz}{2}\int_0^{(1+k^2)^{-1/2}} \frac{du\, H(u;k)}{\left(1-k^2u^2\right)^{1/2}} \int_0^{(1+k^2)^{-1/2}} \frac{dv\, H(v;k)}{\left(1-k^2v^2\right)^{1/2}} \frac{c}{2} \frac{z}{(z+u)(z-v)} . \qquad \text{(D.5)}$$

Using the following definition

$$J_1 \equiv \int_0^{(1+k^2)^{-1/2}} \frac{du\, H(u;k)}{\left(1-k^2u^2\right)^{1/2}} \int_0^{(1+k^2)^{-1/2}} \frac{dv\, H(v;k)}{\left(1-k^2v^2\right)^{1/2}} \frac{c}{2} \frac{z}{(z+u)(z-v)} , \qquad \text{(D.6a)}$$

and noting that

$$\frac{z}{(z+u)(z-v)} = \frac{u}{(z+u)(u+v)} + \frac{v}{(z-v)(u+v)}$$

yields

$$J_1 = \int_0^{(1+k^2)^{-1/2}} \frac{du}{\left(1-k^2u^2\right)^{1/2}} \int_0^{(1+k^2)^{-1/2}} \frac{dv}{\left(1-k^2v^2\right)^{1/2}} \times$$

$$\times \frac{c}{2} H(u;k)H(v;k)\left[\frac{u}{(z+u)(u+v)} + \frac{v}{(z-v)(u+v)}\right] , \qquad \text{(D.6b)}$$

or

$$J_1 = \int_0^{(1+k^2)^{-1/2}} \frac{du}{\left(1-k^2u^2\right)^{1/2}} \frac{u}{z+u} \frac{c}{2} H(u;k) \int_0^{(1+k^2)^{-1/2}} \frac{dv}{\left(1-k^2v^2\right)^{1/2}} \frac{H(v;k)}{u+v} +$$

$$+ \int_0^{(1+k^2)^{-1/2}} \frac{dv}{\left(1-k^2v^2\right)^{1/2}} \frac{v}{z-v} \frac{c}{2} H(v;k) \int_0^{(1+k^2)^{-1/2}} \frac{du}{\left(1-k^2u^2\right)^{1/2}} \frac{H(u;k)}{u+v} . \qquad \text{(D.6c)}$$

Upon recollection that

$$H(u;k) - 1 = \frac{cu}{2} H(u;k) \int_0^{(1+k^2)^{-1/2}} \frac{dv}{\left(1-k^2v^2\right)^{1/2}} \frac{H(v;k)}{u+v}$$

J_1 becomes

$$J_1 = \int_0^{(1+k^2)^{-1/2}} \frac{du}{\left(1 - k^2u^2\right)^{1/2}} \frac{H(u;k)-1}{z + u} + \int_0^{(1+k^2)^{-1/2}} \frac{dv}{\left(1 - k^2v^2\right)^{1/2}} \frac{H(v;k)-1}{z - v} \quad . \tag{D.7}$$

Inserting this expression into Eq. (D.5) and canceling like terms yields

$$\Lambda(z;k) = 1 - \frac{cz}{2}\int_0^{(1+k^2)^{-1/2}} \frac{du}{(z + u)\left(1 - k^2u^2\right)^{1/2}} -$$

$$- \frac{cz}{2}\int_0^{(1+k^2)^{-1/2}} \frac{dv}{(z - v)\left(1 - k^2v^2\right)^{1/2}} \quad . \tag{D.8a}$$

Making the changes of variable $u = (\sin\phi)/k$ and $v = (\sin\phi)/k$ in the above integrals produces

$$\Lambda(z;k) = 1 - \frac{cz}{2}\int_0^p \frac{d\phi}{zk + \sin\phi} - \frac{cz}{2}\int_0^p \frac{d\phi}{zk - \sin\phi} \quad , \tag{D.8b}$$

where $p = \sin^{-1}\dfrac{k}{\left(1 + k^2\right)^{1/2}}$. The integrals in Eq. (D.8b) may be evaluated using [Abramowitz and Stegun]

$$\int \frac{dz}{a + b\sin z} = \frac{1}{\left(b^2 - a^2\right)^{1/2}} \ln\left[\frac{a\tan(z/2) + b - \left(b^2 - a^2\right)^{1/2}}{a\tan(z/2) + b + \left(b^2 - a^2\right)^{1/2}}\right] \quad , \quad b^2 > a^2 \quad .$$

Thus in Eq. (D.8b) $a = zk$ and $b = \pm 1$. Evaluating the integrals in Eq. (D.8b) with the limits $[0,p]$ yields (after some simplification)

$$\Lambda(z;k) = 1 - \frac{cz}{2}\frac{1}{\left(1 - z^2k^2\right)^{1/2}} \ln\left[\frac{zk\tan^2(p/2) - 2\tan(p/2)\left(1 - z^2k^2\right)^{1/2} - zk}{zk\tan^2(p/2) + 2\tan(p/2)\left(1 - z^2k^2\right)^{1/2} - zk}\right] \quad . \tag{D.9}$$

Noting that $\tan(p/2) = k\left[1 + \left(1 + k^2\right)^{1/2}\right]^{-1}$, inserting this into Eq. (D.9), collecting like terms, and factoring out the term $\left[1 + \left(1 + k^2\right)^{1/2}\right]$ leads to the final expression for $\Lambda(z;k)$:

$$\Lambda(z;k) = 1 - \frac{cz}{2}\frac{1}{\left(1 - z^2k^2\right)^{1/2}}\ln\left[\frac{z + \left(1 - z^2k^2\right)^{1/2}}{z - \left(1 - z^2k^2\right)^{1/2}}\right] . \qquad \text{(D.10)}$$

Note that in the limit as k approaches zero, Λ approaches the standard dispersion relation given in Chandrasekhar and Busbridge:

$$\Lambda(z;0) = 1 - \frac{cz}{2}\ln\left[\frac{z + 1}{z - 1}\right] . \qquad \text{(D.11)}$$

D.2. *H*-function Calculus: Factorization

With the dispersion relation above, the H-function may now be factored and related to this dispersion relation. From Eq. (D.1b)

$$1 - \frac{1}{H(z;k)} = \frac{cz}{2}\int_0^{(1+k^2)^{-1/2}} \frac{du}{\left(1 - k^2u^2\right)^{1/2}} \frac{H(u;k)}{z + u} . \qquad \text{(D.12a)}$$

Letting $z \to -z$ and $u \to v$

$$1 - \frac{1}{H(-z;k)} = \frac{cz}{2}\int_0^{(1+k^2)^{-1/2}} \frac{dv}{\left(1 - k^2v^2\right)^{1/2}} \frac{H(v;k)}{z - v} . \qquad \text{(D.12b)}$$

Multiplying the left hand side of Eq. (D.12a) by the left hand side of Eq. (D.12b) gives

$$\left[1 - \frac{1}{H(z;k)}\right]\left[1 - \frac{1}{H(-z;k)}\right] = 1 - \frac{1}{H(z;k)} - \frac{1}{H(-z;k)} + \frac{1}{H(z;k)H(-z;k)} = \text{LHS} \ ; \qquad \text{(D.13a)}$$

doing the same for the right hand sides of Eqs. (D.12) gives

$$\text{RHS} = \frac{cz}{2}\int_0^{(1+k^2)^{-1/2}} \frac{du}{\left(1 - k^2u^2\right)^{1/2}} \int_0^{(1+k^2)^{-1/2}} \frac{dv}{\left(1 - k^2v^2\right)^{1/2}} \times$$

$$\times \frac{c}{2} H(u;k)H(v;k) \frac{z}{(z + u)(z - v)} , \qquad \text{(D.13b)}$$

which is also $\frac{cz}{2}J_1$. Using Eqs. (D.5) and (D.6a)

$$\frac{cz}{2}J_1 = \Lambda(z;k) - 1 +$$

$$+\frac{c}{2}z\int_0^{(1+k^2)^{-1/2}} \frac{du}{\left(1-k^2u^2\right)^{1/2}} \frac{H(u;k)}{z+u} - \frac{c}{2}z\int_0^{(1+k^2)^{-1/2}} \frac{dv}{\left(1-k^2v^2\right)^{1/2}} \frac{H(v;k)}{z-v} .$$

Inserting Eqs. (D.12) into the above expression yields

$$\frac{cz}{2}J_1 = \Lambda(z;k) - 1 + \left[1 - \frac{1}{H(z;k)}\right] + \left[1 - \frac{1}{H(-z;k)}\right] ,$$

or

$$\frac{cz}{2}J_1 = \Lambda(z;k) + 1 - \frac{1}{H(z;k)} - \frac{1}{H(-z;k)} . \tag{D.14}$$

Thus, upon equating Eqs. (D.13a) and (D.14) there results the expected formula for the *H*-function factorization:

$$H(z;k)H(-z;k) = \frac{1}{\Lambda(z;k)} . \tag{D.15}$$

Eq. (D.15) provides an excellent check for determining whether or not the algorithm which calculates the *H*-function with a complex argument is accurate. The algorithm would calculate the *H*-functions on the left hand side of Eq. (D.15), and the results may be compared to the analytical expression on the right hand side as given by Eq. (D.10). Note however that this comparison may not be done on the real axis from $-(1 + k^2)^{-1/2}$ to $(1 + k^2)^{-1/2}$, as the analytical expression is singular in this region.

APPENDIX E: THE INVERSION FOR THE SURFACE SCALAR FLUX IN (k_x,k_y) SPACE

In order to provide some check on the numerical results of the double Fourier inversion for the seachlight problem, an alternative inversion method is considered. A transformation of coordinate systems is performed which provides an analytical expression for the scalar flux using a different inversion.

As in Ch. 6, the Jacobian matrix may be formed for the transformed polar (k,ψ) and Cartesian (k_x,k_y) coordinate systems. The ultimate result of such a transformation on Eq. (7.60) is

$$\phi_c(0,x,y) = \frac{1}{(2\pi)^2}\int_{-\infty}^{\infty} dk_x \int_{-\infty}^{\infty} dk_y \, e^{-ik_x} \, e^{-ik_y} \left\{ [H_R(U_0;k) - 1] + i\, H_I(U_0;k) \right\} . \quad \text{(E.1)}$$

and

$$U_0 = \frac{\mu_0}{1 + k_x^2\gamma_0^2} + i\,\frac{\mu_0\gamma_0 k_x}{1 + k_x^2\gamma_0^2} = U_{0R} + i\,U_{0I} . \quad \text{(E.2)}$$

Again separating the H-function into real and imaginary parts as in Eqs. (7.57) and making the change of variable $\xi' = p = \sin(a\theta)/k$, $(a = \tan^{-1}k)$ yields

$$H(\xi;k) = \frac{1}{x - iy} = \frac{x}{x^2 + y^2} + i\,\frac{y}{x^2 + y^2} = H_R(\xi;k) + i\,H_I(\xi;k) , \quad \text{(E.3a)}$$

where $H_R(\xi;k)$, $H_I(\xi;k) \in \Re$ and

$$x = 1 - \frac{c}{2}\frac{a}{(k_x^2 + k_y^2)^{1/2}} \int_0^1 d\theta \, \frac{p\,U_{0R} + U_{0R}^2 + U_{0I}^2}{(p + U_{0R})^2 + U_{0I}^2} H(p;k_x,k_y) , \quad \text{(E.3b)}$$

$$y = \frac{c}{2}\frac{a}{(k_x^2 + k_y^2)^{1/2}}\int_0^1 d\theta \, \frac{pU_{0I}}{(p + U_{0R})^2 + U_{0I}^2} H(p;k_x,k_y) \quad . \tag{E.3c}$$

Examination of Eqs. (E.2) and (E.3) will show that the real part of the H-function is even with respect to both k_x and k_y while the imaginary part of the H-function is even with respect to k_y and odd with respect to k_x. A fair amount of algebra will show that by using even/odd arguments the integral for the imaginary part of the scalar flux is seen to vanish (as it must) and the remaining terms combine to provide the surface scalar flux as

$$\phi_c(0,x,y) = \frac{1}{\pi^2}\int_0^\infty dk_x \int_0^\infty \Big\{ dk_y \cos(k_x x)\cos(k_y y)[H_R(U_0;k_x,k_y) - 1] \quad +$$

$$+ \sin(k_x x)\cos(k_y y)H_I(U_0;k_x,k_y)\Big\} \quad . \tag{E.4}$$

The numerical methods used to evaluate this double integral are the same as those presented in Ch. 6. Note that an iterative evaluation of the H-function is required in the integrand, making this a very inefficient means of evaluating the scalar flux as compared to the inversion in transformed cylindrical coordinates.

APPENDIX F: THE LAPLACE TRANSFORM INVERSION FOR A COMPLEX FUNCTION $f(t)$

It is shown in Ch. 7 that the Laplace transform inversion for a general (possible complex) function $f(t)$ is given by

$$f(t) = \frac{e^{\gamma t}}{2\pi}\int_0^\infty d\omega \left[e^{i\omega t} F(\gamma + i\omega) + e^{-i\omega t} F(\gamma - i\omega)\right] . \tag{F.1}$$

Expanding the exponentials into sines and cosines and collecting terms yields

$$f(t) = \frac{e^{\gamma t}}{2\pi}\int_0^\infty d\omega \cos(\omega t) \left[F(\gamma + i\omega) + F(\gamma - i\omega)\right] +$$

$$+ i\frac{e^{\gamma t}}{2\pi}\int_0^\infty d\omega \sin(\omega t) \left[F(\gamma + i\omega) - F(\gamma - i\omega)\right] . \tag{F.2}$$

Defining the second term as

$$I_2 = \frac{e^{\gamma t}}{2\pi}\int_0^\infty d\omega \sin(\omega t) \left[F(\gamma + i\omega) - F(\gamma - i\omega)\right] , \tag{F.3a}$$

the sine is then converted back into complex exponentials and the terms are rearranged to give

$$I_2 = \frac{e^{\gamma t}}{4\pi}\int_0^\infty d\omega \left[e^{i\omega t}F(\gamma+i\omega) + e^{-i\omega t}F(\gamma-i\omega) - e^{-i\omega t}F(\gamma+i\omega) - e^{i\omega t}F(\gamma-i\omega)\right]$$

which is seen to be

$$I_2 = \frac{1}{2}f(t) - \frac{e^{\gamma t}}{4\pi}\int_0^\infty d\omega \left[e^{-i\omega t} F(\gamma + i\omega) + e^{i\omega t} F(\gamma - i\omega)\right] . \tag{F.3b}$$

Replacing the second term in Eq. (F.2) with this modified term and simplifying yields

$$f(t) = \frac{e^{\gamma t}}{\pi} \int_0^\infty d\omega \cos(\omega t) \left[F(\gamma + i\omega) + F(\gamma - i\omega) \right] -$$

$$- \frac{e^{\gamma t}}{2\pi} \int_0^\infty d\omega \left[e^{-i\omega t} F(\gamma + i\omega) + e^{i\omega t} F(\gamma - i\omega) \right] . \qquad \text{(F.4)}$$

Considering the second integral as

$$I_{2a} = \int_0^\infty d\omega \left[e^{-i\omega t} F(\gamma + i\omega) + e^{i\omega t} F(\gamma - i\omega) \right] =$$

$$= \int_0^\infty d\omega \, e^{-i\omega t} F(\gamma + i\omega) + \int_0^\infty d\omega \, e^{i\omega t} F(\gamma - i\omega)) \quad , \qquad \text{(F.5a)}$$

the change of variable $\omega' = -\omega$ in the second integral is made to give for I_{2a}

$$I_{2a} = \int_{-\infty}^\infty d\omega \, e^{-i\omega t} F(\gamma + i\omega) \quad . \qquad \text{(F.5b)}$$

Determining the value of I_{2a} is made possible by recalling the form of the inverse Laplace transform itself:

$$f(t) = \frac{e^{\gamma t}}{2\pi} \int_{-\infty}^\infty d\omega \, e^{i\omega t} F(\gamma + i\omega) \quad . \qquad \text{(F.6)}$$

In order to obtain Eq. (F.6), the change of variable $s = \gamma + i\omega$ (or $\omega = (s - \gamma)/i$) was made. This can be thought of as two changes of variable: $\omega' = s - \gamma$ and $\omega = (-i)\omega'$. In the original s frame, the Bromwich contour is such that all the singularities of $F(s)$ lie to the left of the contour. The first change of variable has the effect of shifting the Bromwich contour so that it lies along the imaginary axis in the ω' frame. Now all singularities lie in the plane such that their real component is negative. The second change of variable rotates the points in the ω' frame –90° so that the contour lies on the real axis of the ω frame and all singularities lie in the upper half plane. These transformations are shown in Fig. F.1. The

exponential in the integrand ($e^{i\omega t}$) and the fact that $t > 0$ requires that the contour be closed in the upper half ω plane for a convergent integral. This is expected as all the poles lie in this region and the original contour in the s plane was closed to the left. If the contour were closed in the lower half plane, as would be required if the exponential term was $e^{-i\omega t}$, the value of the closed contour integral would be zero. The integral in Eq. (F.5b) is the real line contour of the contour closed in the lower half plane and is therefore zero. Therefore, since $I_{2a} = 0$, the Laplace transform inversion is given by

$$f(t) = \frac{e^{\gamma t}}{\pi} \int_0^\infty d\omega \cos(\omega t) \left[F(\gamma + i\omega) + F(\gamma - i\omega)\right] . \qquad \text{(F.7)}$$

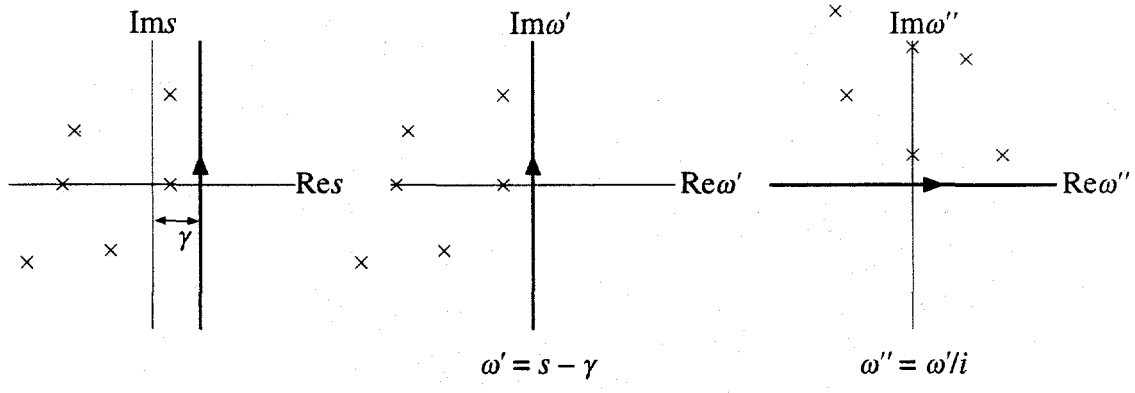

Fig. F.1. Changes of variable to place Bromwich contour onto the real axis.

REFERENCES

Abramowitz, M., and I. Stegun, Eds., *Handbook of Mathematical Functions*, New York: Dover Publications, Inc., 1970.

Bell, G. I., and S. Glasstone, *Nuclear Reactor Theory*, Malabar, Florida: Robert E. Krieger Publishing Co., 1979.

Busbridge, I. W., *The Mathematics of Radiative Transfer*, Cambridge University Press, 1960.

Case, K., F. DeHoffmann, and G. Placzek, *Introduction to the Theory of Neutron Diffusion*, Los Alamos National Laboratory, 1953.

Case, K., and P. Zweifel, *Linear Transport Theory*, Reading, Mass.: Addison-Wesley, 1967.

Chandrasekhar, S., "On the Diffuse Reflection of a Pencil of Radiation by a Plane-Parallel Atmosphere," *Proceedings of the National Academy of Science U. S. A.*, Vol. 44, p. 933 (1958).

Chandrasekhar, S., *Radiative Transfer*, New York: Dover Publications, Inc., 1960.

Crosbie, A. L.. and L. C. Lee, "Relation Between Multidimensional Radiative Transfer in Cylindrical and Rectangular Coordinates with Anisotropic Scattering," *Journal of Quantitative Spectroscopy and Radiative Transfer*, Vol. 38, p. 231 (1987).

Davison, B., *Neutron Transport Theory*, Oxford: Clarendon Press, 1958.

Elliott, J. P., "Milne's Problem with a Point-Source," *Proceedings of the Royal Society (London)*, Vol. A228, p. 424 (1955).

Ganapol, B. D., *The Analytical Benchmark Library for Nuclear Engineering: PC Version*, in press.

Ganapol, B. D., *Proceedings: Transport Theory, Invariant Imbedding, and Integral Equations*, New York: Marcel Dekker, 1989.

Ganapol, B. D., D. E. Kornreich, J. A. Dahl, D. W. Nigg, S. N. Jahshan, and C. A. Wemple, "The Searchlight Problem for Neutrons in a Semi-Infinite Medium," *Nuclear Science and Engineering*, Vol. 118, p. 38, (1994).

Ganapol, B. D., and D. W. Nigg, "Analytical Two-Dimensional Neutron Transport Benchmark: The Searchlight Problem," *Transactions of the American Nuclear Society*, Vol. 64, p. 276 (1991).